Modeling and Analysis of Heterogeneous and Cognitive Cellular Networks

by

Yamuna Dhungana

A thesis submitted in partial fulfillment of the requirements for the degree of

Doctor of Philosophy

in

Communications

Department of Electrical and Computer Engineering
University of Alberta

Abstract

The unprecedented escalation in the data traffic demand due to rapid proliferation of smart phones and tablets cannot be fulfilled with the advancement in radio link technologies only as the radio link efficiency is fast approaching its limit. This problem motivates new paradigms of network deployment and spectrum utilization – *heterogeneous network (HetNet)* and *cognitive radio*. This thesis addresses the coexistence and interference management challenges in HetNets and cognitive radio networks while exploring the capacity and reliability improvement opportunities.

Due to the increasing irregularity in the spatial deployment of the network nodes in HetNets and cognitive radio networks, the stochastic geometry based modeling and analysis is adopted. The idea is to abstract the locations of the network nodes with a suitable point process and then analyze the average behavior of the network using tools from stochastic geometry. With this approach, the cell range expansion (CRE) method of load balancing supported by interference coordination via resource partitioning for the capacity improvement in HetNets is analyzed. In order to accurately model the network interference, the cell-load is also incorporated in this analysis. To understand the coexistence between the multi-antenna techniques and HetNet, and how they complement each other for the network throughput improvement, a tractable framework for modeling and analyzing a multi-antenna HetNet is developed, along with comprehensive performance evaluation of beamforming, multi-user spatial multiplexing and interference nulling techniques in the presence of perfect as well as imperfect channel state information (CSI).

Motivated by the lack of error probability analysis of the cellular networks in the presence of inter-cell interference, a mathematical framework for computing the

average error probability of a typical cellular user is introduced. Uniform approximation (UA) method for the average error probability analysis in Poisson field of interferers is also developed to simplify the analytical complexity of the existing results. To alleviate the spectrum scarcity problem in future cellular networks, an underlay method of cognitive secondary access to television (TV) spectrum is analyzed, and a relay transmission technique to improve the performance of secondary users is proposed.

Preface

Chapter 3 of the thesis has been published as Y. Dhungana and C. Tellambura, "Multi-channel analysis of cell range expansion and resource partitioning in two-tier heterogeneous cellular networks," *IEEE Transactions on Wireless Communications*, vol. 15, no. 3, pp. 2394–2306, March 2016.

Chapter 4 of the thesis has been submitted for possible publication as Y. Dhungana and C. Tellambura, "Performance analysis of SDMA with inter-tier interference nulling in HetNets," *IEEE Transactions on Wireless Communications* in March 2016, and has been accepted for publication in part as Y. Dhungana and C. Tellambura, "Performance analysis of SDMA with inter-tier interference nulling in HetNets," in *Proceedings of the IEEE International Conference on Communications (ICC)*, Kuala Lampur, Malaysia, May 2016.

Chapter 5 of the thesis has been published as Y. Dhungana and C. Tellambura, "Stochastic geometry analysis of error probability in interference limited wireless networks," in *Proceedings of the IEEE International Conference on Communications (ICC)*, London, UK, June 2015, pp. 2857–2862.

Chapter 6 of the thesis has been published as Y. Dhungana and C. Tellambura, "Outage probability of underlay cognitive relay networks with spatially random nodes," in *Proceedings of the IEEE Global Communications Conference (GLOBECOM)*, Austin, TX USA, December 2014, pp. 3597–3602.

For each publication listed above, I carried out the problem formulation, the system model development, the mathematical analysis and computer simulations under the supervision of Dr. Tellambura. While I was responsible for the manuscript composition, Dr. Tellambura contributed to manuscript edits.

Appendix C, which provides the analytical tool used in Chapter 5, has been pub-

lished as Y. Dhungana and C. Tellambura, "Uniform approximations for wireless performance in fading channels, *IEEE Transactions on Communications*, vol. 16, no. 11, pp. 4768–4779, November 2013 and as C. Tellambura, Y. Dhungana, and M. Soysa, "Uniform approximations for wireless performance in fading, noise and interference," in *Proceedings of the IEEE International Conference on Communications (ICC)*, Ottawa, Canada, June 2012, pp. 2410–2415. C. Tellambura formulated the concept. For the conference paper, both C. Tellambura and myself were responsible for the mathematical analysis, the results generation and the manuscript composition. M. Soysa helped with some of the results. For the journal, I was responsible for the additional mathematical analysis/results and the manuscript composition, and C. Tellambura contributed to manuscript edits.

Acknowledgement

I would like to express my sincere gratitude to my supervisor Dr. Chintha Tellambura for his excellent mentorship. He encouraged me to work creatively by giving me complete freedom to formulate and solve research questions, while providing constructive and effective feedback, guidance and advice whenever needed.

I extend my sincere gratitude to my PhD supervisory committee members Dr. Witold Krzymień and Dr. Yindi Jing for their valuable time spent in evaluating my thesis work and providing constructive comments and feedback. I would also like to convey my special thanks to Dr. Halim Yanikomeroglu from Carleton University and Dr. Ehab Elmallah for their valuable suggestions during my final PhD defense. I am thankful to Dr. Alan Lynch for chairing my final PhD defense and to Dr. Majid Khabbazian for chairing my PhD candidacy examination. My humble acknowledgment to Ms. Pinder Bains, the Graduate Student Advisor for her kind support and advice.

I gratefully acknowledge Alberta Innovates Technology Futures (AITF) for offering me Alberta Innovates Doctoral Graduate Student Scholarship to conduct my PhD research. I am also grateful to Mitacs-Accelerate Graduate Research Internship Program for providing me the opportunity to work as a research intern with Ericsson Canada Inc., Ottawa, ON, Canada.

I would like to thank all my fellow lab-mates for productive discussions we had and motivation they provided. I express my sincere appreciation to all my friends, specially Vesh, Sandeep and Sudip for their moral support and for joyous time spent together.

Finally, my heartiest gratitude to my family, specially my mother and my elder sister Indira Dhungana, and my dearest friend Rakesh Kumar Gupta for being my strength during hard times, and comforting my stay away from home with their constant love and care.

Table of Contents

List of Tables

List of Figures

Vectors & Matrices

Notation	Definition
$\mathbf{a} = [a_i]_{1 \leq i \leq n} \in \mathbb{C}^{n \times 1}$	Complex vector $\mathbf{a}$ of dimension $(n \times 1)$ with ith element a_i
$\|\|\mathbf{a}\|\|$	Euclidean norm of vector $\mathbf{a}$
$\mathbf{A} = [\mathbf{b}_j]_{1 \leq j \leq m} \in \mathbb{C}^{n \times m}$	Complex matrix $\mathbf{A}$ of dimension $(n \times m)$ with jth column vector $\mathbf{a}_j$ of dimension $(n \times 1)$
$\mathbf{0}_{n \times 1}$	$(n \times 1)$ zero vector
$\mathbf{I}_n$	$(n \times n)$ identity matrix
$\mathbf{A}^*$	Conjugate transpose of $\mathbf{A}$
$\mathbf{A}^{-1}$	Inverse of $\mathbf{A}$

Probability & Statistics

Notation	Definition
$\mathbb{P}(\cdot)$	Probability measure
$\mathbb{E}[\cdot]$	Statistical expectation
$f_X(\cdot)$	Probability density function (PDF) of X
$f_{X\|Y}(\cdot)$	Conditional PDF of X given Y
$F_X(\cdot)$	Cumulative distribution function (CDF) of X
$F_{X\|Y}(\cdot)$	Conditional CDF of X given Y
$\bar{F}_X(\cdot)$	Complementary cumulative distribution function (CCDF) of X
$\mathcal{N}(m, \sigma^2)$	Gaussian random variable (RV) with mean m and variance σ^2
$\mathcal{CN}(m, \sigma^2)$	Circularly symmetric Gaussian RV with mean m and variance σ^2
$\mathcal{CN}(\mathbf{m}, \mathbf{K})$	Circularly symmetric Gaussian random vector with mean vector $\mathbf{m}$ and variance matrix $\mathbf{K}$
$S(\mu, \beta, \gamma)$	Stable RV with characteristic exponent μ, skew parameter β and dispersion γ
Exp$[\lambda]$	Exponential RV with mean λ^{-1}
Gamma(k, θ)	Gamma RV with shape k and scale θ
$\Psi_X(\omega)$	Characteristic function of X
$M_X(s)$	Moment generating function (MGF) of X
$\mathcal{L}_X(s)$	Laplace transform (LT) of of X
$\mathcal{F}_X(s) = \int x^{s-1} f_B(x) dx$	Mellin transform (MT) of $f_X(x)$

Elementary & Special Functions

Notation	Definition
${}_2F_1[a, b, c, z]$	Gauss Hypergeometric function
${}_pF_q[a_1, \ldots, a_p; b_1, \ldots, b_q; z]$	Generalized Hypergeometric function
$\Gamma(z)$	Gamma function
$\Gamma(a, z)$	Incomplete gamma function
$\Gamma(\alpha, x, b, \beta)$	Extended incomplete gamma function
$\text{Beta}(a, b)$	Beta function
$Q(x)$	Gaussian Q function
$\log_2(x)$	Base 2 logarithm
$\ln(x)$	Natural logarithm

Miscellaneous

Notation	Definition
$\mathbb{R}^d$	d-dimensional Euclidean space
$\mathbb{R}^+$	Positive real line
$\|\|x - y\|\|$	Euclidean distance between two points $x, y \in \mathbb{R}^d$
$\|s\|$	Absolute value of complex quantity s
$(a)_q$	Pochhammer symbol
$x \to a$	x tends to a
$\arg\max_x f(x)$	Value of x which maximizes $f(x)$
$\lim_{x \to a} f(x)$	Limit of function $f(x)$ as x tends to a

List of Abbreviations

3GPP	3rd generation partnership project
4G	4th-generation
5G	5th-generation
ABSF	almost blank subframe
AF	amplify-and-forward
AWGN	additive white Gaussian noise
BER	bit error rate
BPP	binomial point process
BPSK	binary phase shift keying
BS	base-station
CAGR	compound annual growth rate
CCDF	complementary cumulative distribution function
CDF	cumulative distribution function
CDI	channel direction information
CRE	cell range expansion
CS	circularly symmetric
CSI	channel state information
CSMA	carrier sense multiple access
DF	decode-and-forward
EB	exabytes
HCPP	hard core point process
HetNet	heterogeneous network
i.i.d.	independent and identically distributed
INR	interference-to-noise ratio
LT	Laplace transform
LTE	Long Term Evolution
MAC	medium access control
MGF	moment generating function

MIMO	multiple input multiple output
MMSE	minimum mean square error
MRC	maximal ratio combining
MRT	maximal ratio transmission
MT	Mellin transform
OFDM	orthogonal frequency division multiplexing
OFDMA	orthogonal frequency division multiple access
PCP	Poisson cluster process
PDF	probability density function
PGFL	probability generating functional
PMF	probability mass function
PPP	Poisson point process
RB	resource block
RV	random variable
SDMA	space division multiple access
SINR	signal-to-interference-and-noise ratio
SIR	signal-to-interference ratio
SNR	signal-to-noise ratio
STBC	space-time block coding
SU-BF	single user-beamforming
TV	television
UA	uniform approximation
WiFi	Wireless Fidelity
ZF	zero-forcing

Chapter 1

Introduction

Wireless communication has gone through decades of thriving advances. With revolutionary developments such as multiple input multiple output (MIMO), smart antennas, advanced coding and orthogonal frequency division multiplexing (OFDM), it has already evolved to a point where the efficiency of a point-to-point radio link is near optimal, as determined by information theoretic limits.

The ease of connectivity brought about by wireless communication is transforming our society. Over the past few years, the rapid proliferation of smart-phones and tablets, and the bandwidth-intensive usage trends they encourage such as video and audio streaming, online gaming, social networking and cloud computing, have led to an explosion in the demand for data traffic in cellular networks (a.k.a. mobile networks). In 2015, more than half a billion mobile devices were added to the market, most of which were smart-phones, and global mobile data traffic grew by 74% [1]. Following this trend, the global mobile data traffic is expected to grow at a compound annual growth rate (CAGR) of 53% from 2015 to 2020, reaching 30.6 exabytes (EB) per month by 2020 (Figure 1.1), which is nearly an eight-fold increase over 2015 [1]. Consequently, even with advanced radio link technologies, the cellular networks are struggling to keep pace with the user demand. Furthermore, the radio spectrum is a scare resource and cannot be increased at the rate of the escalating data traffic demand. Hence, to meet the evolving needs for higher data rates, the next generation of technology must revolutionize the way the radio spectrum is utilized.

The traditional spectrum allocation method which assigns fixed non-overlapping

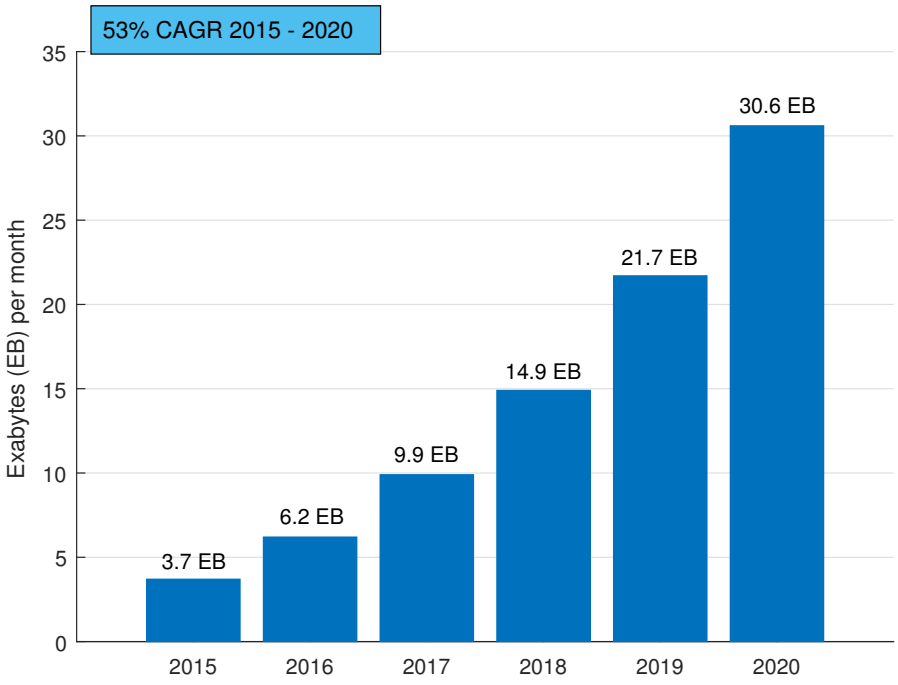

Figure 1.1: Global mobile data traffic [1]

blocks to different services from the available spectrum, and the conventional macro-centric network deployment approach hinder efficient utilization of the resources. This problem motivates the search for a new paradigm of spectrum utilization that will maximize the exploitation of the available resources to the fullest. To this end, (i) *heterogeneous network (HetNet)* deployments and (ii) *cognitive radio* techniques have received significant research interest. Both approaches have tremendous potential to increase the spectral efficiency of wireless access. While HetNet supports aggressive spatial reuse of the spectrum, cognitive radio allows unlicensed users to access underutilized portions of the radio spectrum. These technologies are currently being investigated towards the evolution of the existing 4th-generation (4G) wireless standards such as 3rd generation partnership project (3GPP) Long Term Evolution (LTE)-Advanced [4–6] on the road to 5th-generation (5G) wireless.

1.1 Heterogeneous Cellular Networks

Cellular networks are conventionally homogeneous where an identical set of base-stations (BSs) with similar transmit power levels and similar backhaul links are laid in a planned layout. These BSs, usually referred to as macro BSs, are typically big, high-power tower-mounted transceivers and have service areas called cells of roughly the same size. To meet the increasing data traffic demand, the cellular networks rely on cell splitting by increasing the density of BSs. However, the additional deployment of BSs in the conventional one-size-fits-all approach is very difficult and expensive in dense urban areas due to site-acquisition issues. To resolve this problem, the concept of heterogeneous deployments has recently emerged [4, 7, 8]. The main idea behind a HetNet is to improve spectral efficiency per unit area with the deployment of a diverse set of non-conventional, low-power nodes such as *pico BSs*, *femto BSs* and *relays* within the areas covered by the existing macro cellular infrastructure, over the same frequency spectrum.

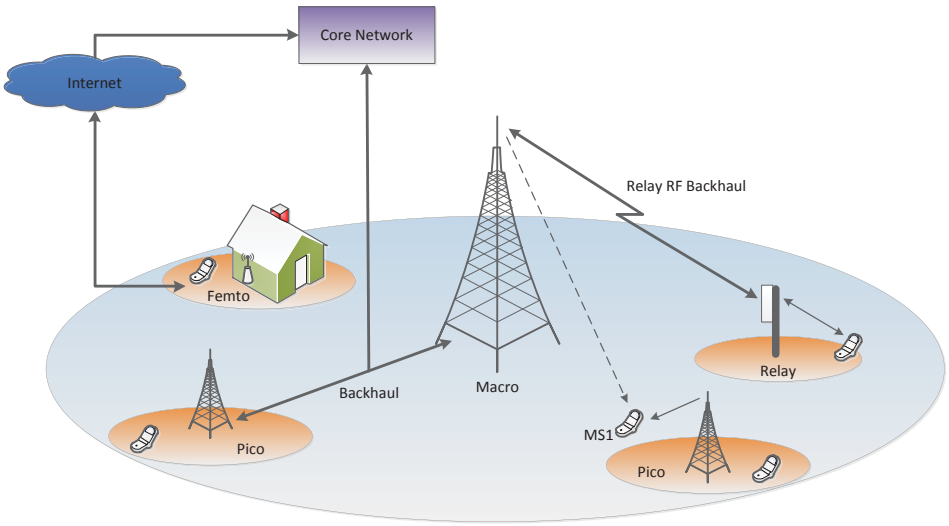

Figure 1.2: Heterogeneous Cellular Network

A typical HetNet is depicted in Figure 1.2. Macro BSs, which are typically deployed in a planned layout to provide basic coverage, transmit at high power levels (5W to 40W). Pico BSs are usually intended for outdoor deployments to alleviate

Table 1.1: Types of Nodes in Heterogeneous Cellular Networks

Node	Transmit power	Features
macro	$5\text{W} - 40\text{W}$	operator deployed, open access, dedicated backhaul
pico	$250\text{mW} - 2\text{W}$	operator deployed, same access and backhaul features as macro
femto	$< 100\text{mW}$	consumer deployed, typically closed access (but can be open or hybrid), backhaul facilitated by consumer's digital subscriber line or cable modem
relay	$250\text{mW} - 2\text{W}$	operator deployed, wireless backhaul

"dead-spots" (no-coverage zones) and "hot-spots" (localities of higher traffic demand), and thus follow relatively unplanned placements. Pico BSs usually have the same access and backhaul features as macro BSs [9], but operate with much lower transmit power, typically 250mW to 2W. Femto BSs, on the other hand, are typically consumer-deployed indoor nodes with transmit power of less than 100mW. Their backhaul connections to the operator's network are typically facilitated by the consumer's digital subscriber line or cable modem. Access to femto BS may be unrestricted, or restricted to the users within a closed subscriber group, or a combination of both with priority to users within the closed subscriber group [10]. These access mechanisms are termed as open, closed and hybrid, respectively. When wired backhaul is not feasible, relay nodes are deployed. Depending on whether the backhaul connection is on the same frequency as the access link or on different frequencies, relays are classified as in-band and out-of-band [11]. A summary of different types of nodes in HetNets is given in the Table 1.1.

HetNets are thus characterized by unplanned/random locations of the network nodes with large disparities in transmit power between the nodes, in contrast to planned layout of the conventional macro-cellular networks with similar transmit power levels of all the nodes. Such differences impose many challenges and require several fundamental changes to the traditional approaches to modeling, analyzing and designing cellular networks. Some of the required changes are discussed below.

1. **Spatial Modeling of the BS-locations**

   A major change in cellular networks is the network topology, which is evolving towards the irregular spatial deployment of nodes. In a conventional cel-

lular network, macro BSs are somewhat evenly spaced as compared to low-power BSs (pico, femto, relays), which follow mainly ad hoc placements in a HetNet. Thus, the locations of BSs have been conventionally modeled as a regular grid, most popularly a hexagonal grid [12, 13]. Their coverage areas, commonly known as cells, are thus simply the hexagons they belong to. Clearly, the traditional grid-based model is not suitable for modeling the spatial distribution of low-power BSs in a HetNet. They are not regularly spaced and their coverage areas are not homogeneous. Even for macro BSs, the grid-based model is highly idealized, as the real deployment is structurally very different. Meanwhile, due to the analytical intractability of the grid-based model, parameter tuning and performance evaluation in cellular networks have relied on simulations. As networks become more complex with the addition of irregularly deployed low-power nodes, even simulations become nontrivial. Thus, stochastic geometry characterization of the spatial distribution of BSs has been adopted [14–22], in which the locations of the BSs are abstracted by a suitable point process. The details on stochastic geometry modeling of wireless networks are given in Section 2.2.

2. **BS-user Association**

   The traditional approach to BS-user association where a mobile user connects to the BS with the strongest downlink received signal may not be appropriate in a HetNet. The large disparities in transmit power between macro and pico/femto BSs imply that the downlink coverage area of a pico/femto BS is potentially much smaller than that of a macro BS. Thus, the strongest signal based association would cause most of the users to be attracted towards macro BSs, with only a few users connected to pico/femto BSs. This situation might cause a macro BS to be severely congested while the resources at the nearby pico/femo BS are not even fully utilized. Thus, even if a user receives the strongest signal from the macro BS, it is desirable to offload the user connection to the nearby lightly-loaded pico/femto cell, which can serve the user with higher data rate by allocating a larger fraction of radio resources.

Such offloading also reduces the macro cellular load, thereby allowing the remaining macro users to be served with improved rates. The optimal BS-user association in a HetNet is the one that can maximize the data rate of all users in the network through balanced distribution of user loads across all tiers of the BSs. But such optimal association is very complex to compute [23]. A rather simple, yet very effective method is cell range expansion (CRE) [7, 8], in which the coverage area of a low-power BS is expanded by virtually increasing its power by an amount known as the *association bias*.

3. **Interference Management**

   Since interference rather than noise is the performance limiting factor in cellular networks, managing interference is a primary concern in any cellular network. However, the interference scenarios in HetNets are more complex than those in conventional cellular networks and require advanced management techniques. For example, as explained above, the users in HetNets are proactively offloaded from macro to small cells for load balancing. If the low-power nodes are deployed in the same frequency band as macro BSs, i.e., if co-channel deployment is used, each offloaded user suffers from severe downlink interference because the macro BS, which should have been the serving BS based on the strongest downlink received signal, now acts as an interferer. Thus, the benefits of load balancing cannot be fully realized unless a suitable interference mitigation technique is employed. Another example of an interference scenario in co-channel deployment occurs when users in the coverage area of a femto BS must be served by the nearest macro BS due to the restricted access to the femto BS. In this case, these users suffer from severe downlink interference from the femto BS. Meanwhile, the femto users are also severely interfered by these users in the uplink. Thus, interference management is critical in HetNet.

1.1.1 Interference Management Techniques in HetNets

An obvious solution to avoid complex interference scenarios between macro and small cell networks is to deploy pico/femto BSs in a different frequency band than the one the macro network is deployed on. However, such deployment results in reduced spectral efficiency, and is not preferred as the whole idea behind HetNets is to improve spectral efficiency. The following are some of the techniques for interference management in HetNets.

1. **Resource Partitioning**

   Interference can be controlled through coordination of time/frequency resource blocks, where an interfering BS sacrifices some of its resources to enable communication to vulnerable users in these interference protected resources. In time-domain resource partitioning, the macro tier is periodically muted on certain fraction of subframes, known as almost blank subframes (ABSFs) [7, 21, 24] so that the offloaded users can be scheduled on these macro interference-free subframes. An approach to frequency-domain resource partitioning is fractional frequency reuse in OFDMA based networks. In this method, the cell-center users are assigned subchannels with universal reuse (i.e., a reuse factor of 1), whereas the subchannels with a higher reuse factor are allocated to cell-edge users [25]. Subchannels allocation in this method, however, becomes very complex for multi-tier HetNets as the number of tiers increases.

2. **Carrier Aggregation**

   Carrier aggregation, a key feature of LTE-Advanced [26], allows multiple component carriers to be used simultaneously to increase the system bandwidth. The component carriers need not be contiguous and not necessarily be in the same frequency band, thereby allowing fragmented chunks of spectrum to be aggregated for higher data rates. The carrier aggregation feature can be exploited for deploying HetNets without creating severe interference scenarios. Consider a macro-pico network in which both tiers use two component

carriers, f_1 and f_2. If the macro BS transmits at its regular power level on both f_1 and f_2, the coverage area of the pico BS will be limited, and thus, the pico resources will not be sufficiently utilized. However, if the macro BS reduces the transmit power on f_2, while continuing to provide regular coverage on f_1, the coverage area of the pico cell on f_2 will be enlarged without incurring severe macro interference. Since both tiers use two carrier frequencies, carrier aggregation capable users can enjoy enhanced data rates. However, this solution may be highly inefficient for users incapable of aggregating carriers, unless each component carrier has ample spectrum.

3. **Coordinated Multipoint Transmission**

   In coordinated multipoint operation, alternatively known as network MIMO or multicell processing or BS coordination, multiple BSs mutually cooperate either to mitigate interference or even to turn interference signals into meaningful signals. Coordinated multipoint transmission is an integral component of LTE-Advanced [27]. The coordination techniques have been broadly classified into the following categories [28, 29].

   - **Joint Transmission**: Multiple coordinating BSs simultaneously transmit data to a user, thereby converting interfering signals into desired signals. The coordinated BSs may jointly or independently encode data to allow coherent or non-coherent combining of the signals at the receiver. With coherent transmission, the available spatial degrees of freedom can be efficiently exploited for diversity/multiplexing gain.
   - **Transmission Point Selection**: User data is available at multiple coordinating BSs, but is transmitted from a single BS, for example, the BS with the highest received signal-to-interference-and-noise ratio (SINR). The selected BS utilizes channel state information (CSI) of the user for transmission in order to improve the received SINR. The remaining BSs in the coordinating set may remain silent to further improve the SINR. The dynamic selection of BS can be changed subframe-to-subframe.

- **Coordinated Scheduling/Beamforming**: User data is always transmitted from the serving BS only, unlike the above two techniques. However, scheduling decisions and beamforming vectors are coordinated among multiple BSs so that the scheduled users within the coordinating cells either do not create mutual interference at all or receive minimum interference. Such coordination requires information such as the CSI of the users and the offered cell-load to be shared among the coordinated BS.

By exploiting the additional spatial degrees of freedom, joint transmission and transmission point selection can provide substantial performance gain. However, they require user data sharing between the coordinating BSs, and such sharing is practically very challenging due to backhaul overhead. For coherent joint transmission based on CSI feedback, the CSI of each user is required at all the coordinating BSs, and such demanding requirement makes CSI estimation and feedback very challenging. Furthermore, precise synchronization between the BSs is needed to fully realize the benefits of coherent joint transmission. Coordinated scheduling/beamforming, on the other hand, has lower complexity and overhead since no user data exchange between the BSs is required, and is thus more appealing in terms of implementation. *Interference nulling* is an example of coordinated beamforming, which has been demonstrated to provide considerable gain at the cost of CSI feedback to the serving and a few neighboring BSs [30, 31].

1.1.2 Multi-antenna Transmissions in HetNets

Multi-antenna transmission has been an integral part of cellular standards such as LTE (3GPP Release 8) [32] and LTE-Advanced (3GPP Release 10) [33]. The additional degrees of freedom in the spatial dimension introduced by multiple antennas on top of the time and frequency dimensions can be used for improving link reliability (e.g., transmit diversity through space-time block coding (STBC) [34, 35]), boosting the spectral efficiency of a radio link (single-user spatial multiplexing

[36]), and spatially separating users (user multiplexing known as space division multiple access (SDMA) or multi-user MIMO [37]). MIMO techniques, particularly multi-user MIMO , which serves multiple users on the same time-frequency resource, can significantly improve the spectral efficiency of cellular networks. Multi-antenna techniques will thus complement HetNets to meet the escalating data traffic demand, and therefore their coexistence in future networks is unavoidable.

1.2 Cognitive Radio

Since 1930s, the radio spectrum is allocated for services via licensing. The regulatory bodies assign licenses for spectral frequency blocks to specific groups or companies. For example, the licensed frequency band for digital television (TV) broadcasting channels $14 - 51$ in the United States is $470 - 698$ MHz. Such a static allocation approach has resulted in almost all frequency bands being already assigned, leaving no room for new wireless services. Out of this spectrum shortage has emerged the idea of cognitive radio, [38–40] which allows the unlicensed (secondary) users to access the licensed (primary) users spectrum with minimal or no impact on the primary system communications.

A cognitive radio network is an intelligent communication system which utilizes the available side information of the primary network to enable primary-secondary spectrum sharing in three different ways: (i) *underlay*, (ii) *overlay*, and (iii) *interweave*. While the interweave method allows secondary users to opportunistically communicate over spectrum holes in time, frequency and/or geographic locations that remain temporarily unused by primary users, the other two modes support primary-secondary concurrent transmissions. In overlay systems, the secondary users must mitigate the interference imposed on the primary receivers by applying sophisticated signal processing [40]. The underlay method, on the other hand, constrains the transmit powers of secondary users to ensure that the resultant interference on each primary user is below a predefined threshold [40]. Unlike the overlay system, where the secondary users require knowledge of the primary users' codebooks and their messages as well, the underlay system only require knowl-

edge of the interference channel gains to primary users. Thus, underlay systems are preferred over overlay systems for implementation simplicity. However, underlay system must operate under stringent interference constraints, which limit the coverage range as well as the data rates of secondary users.

1.2.1 Cognitive Cellular Networks

As data traffic volume continues to grow, cellular networks require more spectrum to serve the users. The spectrum scarcity has made researchers explore millimeter wave frequencies (30 GHz-300 GHz) for possible deployment in future networks. The radio propagation characteristics of millimeter waves are, however, very different and challenging compared to the currently deployed frequencies [41]. For example, millimeter waves are more susceptible to blockage effects, and the channel gains fluctuate very rapidly, in the order of hundreds of microseconds. While millimeter wave communication might be potentially deployed in future networks, the very sparse utilization of some portions of the currently deployed radio spectrum [42] indicates that it can still accommodate more demand if utilized efficiently. Cognitive radio exploits the underutilized spectrum to make room for new demand.

The TV band, which occupies a large amount of spectrum in the order of $300-400$ MHz, is an example of an inefficiently utilized spectrum. This spectrum band is particularly appealing for cellular broadband services due to its favorable propagation characteristic (lower propagation loss) and the simplicity of the TV broadcasting system (static network design, open standards and the public availability of information associated with TV transmitters) [43]. A cognitive radio network in the TV spectrum is illustrated in Figure 1.3.

For cellular and TV broadcasting networks to coexist, cellular communication must not harmfully interfere with TV receivers and should require no modification to their design. Also, primary communication should be the first priority at all times. Due to such stringent requirements, standalone broadband service over the TV spectrum with secondary usage may be questionable, considering the quality-of-service requirements of cellular standards such as LTE-Advanced. However, when deployed together with the regular licensed cellular spectrum, the spectral re-

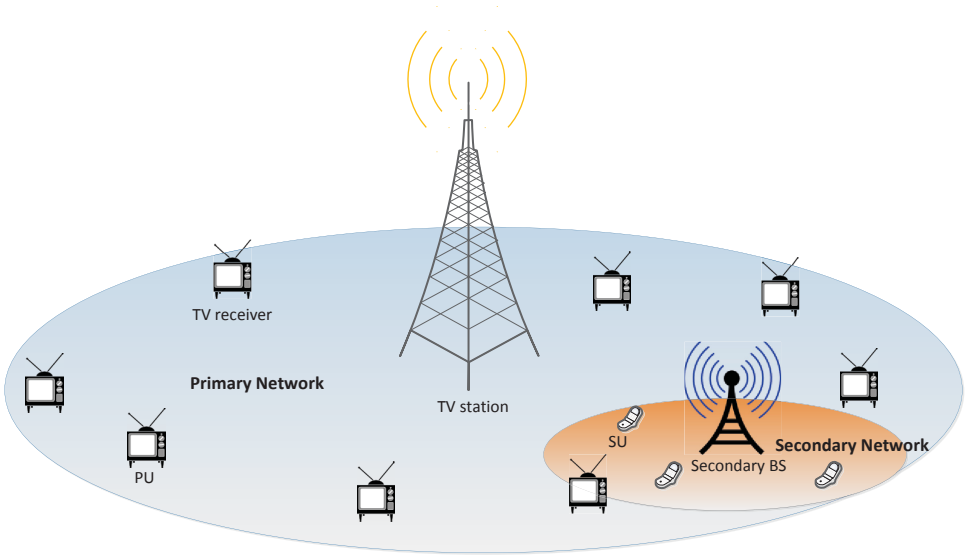

Figure 1.3: Cognitive Radio Network in the TV spectrum

sources of TV networks can be utilized to increase the cellular capacity. With carrier aggregation technology, a cellular network can aggregate the regular licensed and the TV spectrum. By simultaneously transmitting/receiving over carriers in both spectra (of course TV band accessed through cognitive radio), the system capacity can be significantly improved. A similar concept, in which a licensed cellular band and an unlicensed Wireless Fidelity (WiFi) band are aggregated to allow the LTE terminals to opportunistically operate in the WiFi band by using listen-before-talk method, is currently being investigated. This technology is named LTE in unlicensed spectrum [44], or license-assisted access [45].

1.3 Motivation and Objectives

HetNet is a promising concept to meet the traffic demand and performance expectations of future cellular networks. However, with the addition of a wide variety of low-power nodes, each with its own operating characteristics and irregularly deployed in the existing macro-cellular infrastructure, modeling, analyzing and designing HetNets become very challenging. Some of the main challenges were briefly discussed in Section 1.1. To this end, stochastic geometry characterization

of spatial distribution of BSs, the analysis of various BS-user association schemes and interference coordination techniques have been studied [15–18, 21]. However, given that the concept of HetNets has only recently attracted the interest of the research community, the existing studies have many limitations and research gaps regarding analytical modeling, performance metrics, and many other issues. This thesis identifies such limitations and gaps and develops a comprehensive framework for modeling and analyzing HetNets. Despite the potential advantages of HetNet deployments, the growing data traffic volume will create demand for more spectrum in future cellular networks. As a potential solution to this spectrum scarcity problem, cognitive radio communication in the TV spectrum is studied in this thesis. The main objectives of this research are listed as follows.

1. To develop a refined analytical model of the cellular network that comprehensively captures the network heterogeneity in terms of the spatial distribution of different nodes, their transmit powers (and thus, coverage areas), and traffic load.

2. To explore load balancing and interference coordination techniques in HetNets and to devise a framework to evaluate the data rate improvement from such techniques.

3. To investigate multi-antenna transmission techniques in HetNets and offer suggestions for the most suitable technique for optimal performance depending upon the network deployment and user load.

4. To develop a comprehensive mathematical framework for the average error probability analysis in cellular networks.

5. To explore the cognitive radio approach to spectrum sharing between primary TV broadcasting and secondary cellular networks and to develop transmission techniques for the cellular network under such sharing.

1.4 Significance of the Thesis

The deployment of HetNets appears the most pragmatic, scalable and cost-effective approach to meet the ambitious data rate and ubiquitous coverage requirements of next-generation cellular networks and has recently gained much momentum in the industry and research community. The standardization activities for HetNet deployment have already started since 3GPP Release 10 of LTE (known as LTE-Advanced [33]) and is rigorously being investigated [4, 5, 46]. The research outcomes will thus facilitate the standardization of the deployment of HetNets to such wireless standards. The load balancing and interference coordination strategies developed in this research are anticipated to significantly increase the network data rate. With the growing interest in higher frequency bands such as the millimeter wave band, which requires denser deployment of various small cells due to its inherent high signal attenuation, and encourages multiple antenna deployments due to the less stringent antenna spacing constraint, the coexistence of MIMO and HetNets seems almost unavoidable in emerging wireless networks. The thesis results for multi-antenna HetNets confirm the interference mitigation potential of multi-antenna transmission in HetNet deployments and also provide some useful guidelines for selecting the best multi-antenna technique for cellular capacity improvement. The proposed transmission and relay selection scheme for cognitive secondary usage of a TV broadcasting network spectrum will contribute to the development of feasible systems that can leverage the TV spectrum effectively to address the increasing spectrum demand in future cellular networks.

1.5 Thesis Outline and Contributions

This thesis focuses on modeling and analyzing heterogeneous and cognitive cellular networks for spectral efficiency enhancements. The thesis outline is as follows. The theoretical background on wireless channels, stochastic geometry modeling of wireless networks, and other related topics is covered in Chapter 2. The main contributions of this research are presented in Chapter 3 to Chapter 6. Chapter 7 presents the concluding remarks and future research directions.

1.5.1 Novel Contributions of the Thesis

The major contributions of this thesis are summarized as follows.

- Chapter 3 develops an analytical framework for average rate evaluation of the CRE load-balancing technique supported by resource partitioning method of interference coordination in a two-tier (macro-pico) downlink HetNet. The downlink analysis of HetNets usually assumes a time-shared single channel per cell [16, 17, 19, 21, 47]. Thus, only the time-domain method of resource partitioning such as ABSF has been significantly analyzed [21, 24, 47, 48]. In contrast, a multi-channel downlink, for example an orthogonal frequency division multiple access (OFDMA) based LTE downlink, is considered in Chapter 3. Due to the flexibility in subchannel allocation offered by OFDMA, we propose frequency-domain resource partitioning, where the macro tier is restricted from using a fraction of the total subchannels so that they are allocated exclusively to offloaded users. Although the load perceived by a BS is a key factor in determining its interference contribution over the network, most of the analysis in the literature ignores the cell load by considering a fully-loaded network [16, 19, 21, 47]. In Chapter 3, the cell load is properly characterized as a function of user density, association bias and resource partitioning fraction. The results demonstrate that if the bias value and resource partitioning fraction are carefully selected, the rate performance can be highly improved in comparison to the CRE only system (i.e., a system with no resource partitioning), and their jointly tuned optimal combination is strongly dependent on the network load.

- A downlink multi-antenna HetNet with zero-forcing (ZF) precoding based SDMA is modeled and analyzed in Chapter 4. In cellular networks, user distribution determines the number of users in a cell and usually differs from one cell to another. However, the previous analyses of SDMA in multi-antenna HetNet are based on the limiting assumption that the same number of users are simultaneously served on a resource block by every BS of a tier, and the number is chosen arbitrarily. In Chapter 4, the number of simultane-

ously served users in a cell is a function of the total number of users in that cell, with the maximum number of served users limited to $L_{\max}$. Thus, if the number of users in a cell is below the limit, all the users in the cell are simultaneously served; otherwise, only $L_{\max}$ users chosen randomly are simultaneously served. A biased-nearest-distance based BS-user association scheme suitable for a multi-antenna HetNet is proposed, where the bias value can be controlled for load balancing. By exploiting the feasibility of deploying a large number of antennas at a macro BS due to its physical size, an antenna precoding based interference nulling scheme is proposed for interference suppression from the dominating macro BS to the small cell users. The proposed interference nulling scheme is demonstrated to have strong potential for performance improvement, subject to fine tunning of the system parameters. The optimal value of $L_{\max}$ that maximizes the average data rate is numerically evaluated and is shown to have a better performance than single user-beamforming (SU-BF) ($L_{\max} = 1$) and full-SDMA ($L_{\max} = K$), where K is the number of transmit antennas. Antenna precoding requires CSI feedback from the users. The impact of limited feedback, which leads to imperfect CSI, is also analyzed.

- Apart from capacity/throughput and coverage, the effectiveness of a wireless network is also characterized by its reliability, measured by metrics such as error probability, which has been barely analyzed for HetNets. There are only a few studies on error probability analysis of a fixed source-destination link in a Poisson field of interferers [49–51]. However, they are not directly applicable to cellular networks because these studies do not consider BS-user association. Motivated by the lack of error probability analysis of cellular networks in the presence of inter-cell interference, Chapter 5 develops a stochastic geometry based mathematical framework for computing the average error probability of a typical user in a cellular network with maximum received power based BS-user association. As an alternative to the semi-analytical solution in [49] and the complex integral expressions in [50, 51], a highly accurate uniform approximation (UA) method for analyzing average error probability

of an intended communication link with a given transmitter-receiver separation, which is subject to interference from Poisson distributed nodes, is also developed. The error probability UAs for both single-antenna and maximal ratio combining (MRC) receivers are derived.

- Exploitation of the existing TV spectrum for cellular network through cognitive radio techniques is desirable to alleviate the spectrum scarcity problem in cellular networks. For such coexistence to be feasible, the cellular communication must not interfere with the TV receivers and should not require any modification to their design. Thus, the interference generated by a cellular network on TV receivers must be accurately modeled to develop transmission schemes for the cellular network to operate under such interference constraint. In Chapter 6, an underlay approach to such coexistence is analyzed in which the transmit power of a secondary node is controlled to satisfy the interference constraint on the TV receiver to which it generates the maximum interference. This approach ensures that the interference imposed on all the TV receivers is below their tolerable thresholds. However, since this requirement may result in very limited power, and thus, limited coverage of the secondary nodes, cooperative relaying is proposed to achieve adequate radio reception quality at the distant users. A novel relay-selection scheme is developed, which considers not just the source-relay and relay-destination links, but also the stringent interference constraints on all the primary receivers. Closed-form expressions are derived for the outage probabilities of both the relay and direct links, along with their high signal-to-noise ratio (SNR) asymptotics. The random spatial distributions of the TV receivers and secondary relay nodes are taken into consideration for deriving the outage probabilities.

Chapter 2

Background

This chapter reviews the key concepts employed in this thesis. The analysis of any wireless communication system requires proper modeling of the wireless channel. Various channel impairments and their modeling are discussed in Section 2.1. Section 2.2 illustrates the concept of stochastic geometry modeling of wireless networks and introduces popular point processes used to model the wireless networks. Poisson point process (PPP) is used in this thesis for modeling and analyzing HetNets and cognitive radio networks. The special properties of PPP applied in this thesis are thus reviewed in Section 2.3. The accurate characterization of the interference power plays vital role in the analysis and design of interference-limited cellular networks. The probability distribution of total interference in a network with interfering nodes distributed according to a PPP is introduced in Section 2.4. The chapter concludes with a brief overview of multi-antenna and relay communication in Section 2.5 and Section 2.6, respectively.

2.1 Wireless Channel

A radio link between a transmitter and a receiver is referred to as a wireless channel. Radio waves propagate on a wireless channel through diverse mechanisms including reflection, diffraction and scattering. These complex phenomena lead to various impairments in the transmitted radio signal, which can be categorized as *path loss*, *shadowing*, and *multipath fading* [2, 12, 13] (Figure 2.1).

Path Loss

Path loss is signal power attenuation as a function of the distance propagated by the signal. It also depends on the frequency of the transmitted signal, antenna heights and topography. Exact theoretical prediction of the path loss is difficult due to its site-specific behavior. In this thesis, a power-law path loss model is used, in which the signal power attenuates at the rate of $r^{-\alpha}$, where r is the distance from the transmitter. The parameter α is called power loss exponent, which effectively captures the dependence of the path loss on the frequency and topography. The value of the exponent is empirically calculated. It is typically in the range of 1.6 to 6 [12], with $\alpha = 2$ for free space propagation.

Shadowing

Shadowing, also known as large-scale fading, on the other hand, is radio impairment due to large objects such as buildings and hills. Shadowing causes deviation in the average channel power gain anticipated from the path loss. The statistical variation in the channel power gain due to shadowing is most commonly modeled by log-normal distribution [13].

Multipath Fading

In urban cellular communication, a direct line-of-sight between a transmitter and a receiver is rare. Thus, the transmit signal propagates through multiple paths created by reflection, diffraction and scattering. The received multipath signals have different amplitudes and phases, and thus, may combine either constructively or destructively, causing rapid fluctuations in the amplitude as well as the phase of the resultant signal. This phenomenon is known as multipath fading. If all the spectral components of the transmit signal encounter the same amplitude gain and linear phase, the fading is known as frequency flat; otherwise the fading is called frequency selective [13, 52]. While narrowband communications are frequency flat, wideband communications are frequency selective. Although LTE systems are wideband, with OFDM technique, each subchannel communication effectively

becomes narrowband, and thus undergoes flat fading. Flat fading channels are considered in this thesis.

As flat fading has identical effects on each frequency component, this fading can effectively be represented by a single complex channel coefficient $h = |h| \exp(j\psi)$, where $|h|$ is the amplitude gain, and ψ is the phase shift. Ideal coherent modulation assumes phase shifts caused by multipath fading to be perfectly corrected at the receiver. For non-coherent modulation, phase information is not required. Thus, performance analyses usually require knowledge of the fading amplitude statistics only. For communication in a rich scattering environment without a dominant line-of-sight, the fading amplitude is typically modeled by Rayleigh distribution:

$$f_{|h|}(x) = \frac{2x}{\omega} \exp(-\frac{x^2}{\omega}), \quad x \geq 0, \tag{2.1}$$

where $\mathbb{E}[|h|^2] = \omega$. The power gain $|h|^2$ is thus exponentially distributed with mean ω (i.e., $|h|^2 \sim \text{Exp}[\omega]$). The Rayleigh fading model is particularly popular due to its simplicity as it leads to closed-form solutions, thus providing insights into the system performance. A more generalized model is Nakagami-m fading, in which the fading amplitude is distributed as

$$f_{|h|}(x) = \frac{2m^m x^{2m-1}}{\Gamma(m)\omega^m} \exp(-\frac{mx^2}{\omega}), \quad x \geq 0, \tag{2.2}$$

where m determines the severity of fading. The power gain $|h|^2$ is thus Gamma distributed (i.e., $|h|^2 \sim \text{Gamma}(m, \omega)$). Note that the Nakagami-m fading reduces to Rayleigh fading for $m = 1$. When $m \to \infty$, it reduces to the impulse function, which indicates a non-fading, static channel.

With flat multipath fading superimposed on power-law path loss and log-normal shadowing, the channel power gain Ω_{xy} between a pair of nodes at x and y, where $x, y \in \mathbb{R}^d$ are the locations of the transmitter and the receiver respectively, can be modeled as

$$\Omega_{xy} = e^{\sigma g_{xy}} |h_{xy}|^2 ||x - y||^{-\alpha}, \tag{2.3}$$

where $e^{\sigma g_{xy}}$ represents the variation in the channel power gain due to log-normal shadowing with $g_{xy} \sim \mathcal{N}(0, 1)$, and $h_{xy} = |h_{xy}| \exp(j\psi_{xy})$ is the complex multipath fading coefficient with $\mathbb{E}[|h_{xy}|^2] = 1$. σ is the shadowing standard deviation. g_{xy} and h_{xy} are independent random variables (RVs) in (2.3).

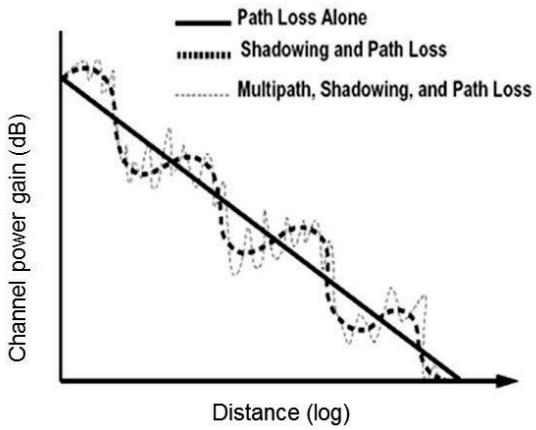

Figure 2.1: Path loss, shadowing and multipath fading effects [2]

2.2 Stochastic Geometry Modeling of Wireless Networks

It is readily evident from (2.3) that the SNR of a receiver, which determines its performance, implicitly depends on the location of the transmitter with respect to the receiver. If other nodes in the network are also transmitting in the same channel, in addition to the desired signal, the test receiver also receives interference signals which depend on the locations of the interfering nodes with respect to the receiver. Therefore, the SINR experienced by a receiver is strongly affected by the *network geometry* and significantly varies from one receiver to another. Unlike traditional wireless networks, where the nodes are deployed in a planned layout, the emerging wireless systems such as HetNets and cognitive radio networks are characterized by unplanned/irregular locations of the nodes. For modeling and analysis of such networks with random topologies, stochastic geometry is a very powerful mathematical tool [53–56]. It allows us to evaluate the average behavior of a network for metrics of interest such as the SINR, outage probability and achievable data rate by averaging over many spatial realizations of the network.

Under stochastic geometry modeling, the spatial distribution of the network nodes is modeled by a suitable point process. A point process is a random sequence of points in the space $\mathbb{R}^d$. Any realization of a point process is a locally

finite subset $\phi = \{x_1, x_2, x_3, \ldots\} \subset \mathbb{R}^d$, where $x_i \neq x_j, \forall i \neq j$ [57]. Some of the popular point processes used to model wireless networks are briefly discussed below. A comprehensive survey on stochastic geometry modeling of cellular and cognitive networks can be found in [58].

1. PPP [57,59]: A point process $\Phi = \{x_1, x_2, x_3, \ldots\} \subset \mathbb{R}^d$ is a PPP of intensity measure Λ if and only if

   (a) the number of points of Φ in a compact set $B \subset \mathbb{R}^d$, denoted by $\Phi(B)$, is a Poisson RV with mean $\Lambda(B) = \int_B \lambda(x)\, dx$, i.e.,

   $$\mathbb{P}(\Phi(B) = k) = \frac{\Lambda(B)^k}{k!} e^{-\Lambda(B)},\ k = 0, 1, 2, \ldots,$$

   (b) the numbers of points in disjoint sets are independent. This property is known as independent scattering.

   If $\lambda(x) = \lambda$, known as intensity or density, is a constant, then Φ is called homogeneous PPP.

   The PPP, suitable for modeling networks with a possibly infinite number of nodes randomly and independently distributed in a finite or infinite area, is the most popular model due to its analytical tractability, and is widely used in modeling and analysis of HetNets and cognitive radio networks. In a multi-tier HetNet, the spatial distribution of the BSs of each tier (macro, pico, and/or femto tiers) are modeled as independent PPPs in [16–21]. It is shown in [15] that for the macro tier, the PPP model provides tight lower bounds for performance measures, as tight as the upper bound results provided by the popular grid model, when compared to the actual 4G network. The PPP based modeling of the locations of primary and secondary users in cognitive radio networks is adopted in [60] to analyze the performance of various medium access control (MAC) protocols and in [61] for aggregate interference analysis of underlay method of spectrum sharing.

2. Binomial point process (BPP) [57]: A point process $\Phi_W^n = \{x_1, x_2, x_3, \ldots x_n\}$ in a compact set $W \subset \mathbb{R}^d$ is a BPP if the number of points in any set $B \subset W$

is a binomial RV with parameters n and $p = \nu_d(B)/\nu_d(W)$, i.e.,

$$\mathbb{P}(\Phi_W^n(B) = k) = \binom{n}{k} p^k (1-p)^k, \quad k = 0, 1, 2, \ldots, n,$$

where $\nu_d(.)$ is a volume measure (e.g., length for $d = 1$, area for $d = 2$). Note that a homogeneous PPP Φ constrained to a compact set W under the condition that $\Phi(W) = n$ yields a BPP. In a wireless network, if the total number of nodes is known and they are independently and uniformly distributed in a finite service area, then BPP is used to model the network [62].

3. Hard core point process (HCPP) [63]: An HCPP is a repulsive point process in which the distance between any two points is at least a predefined hard core parameter $h \geq 0$. It is formed by a dependent thinning operation applied to a homogeneous parent PPP Φ_p of intensity λ_p. The thinning operation retains a point x of Φ_p if a sphere $b(x, h)$ of radius h and centered at x contains no point of Φ_p; otherwise the point x is deleted. This operation is called dependent thinning because the deletion of any point in Φ_p depends on the locations and possible deletions of other points in the process. The resultant HCPP Φ_h is thus given by $\Phi_h = \{x \in \Phi_p; ||x - y|| \geq h, \forall y \in \Phi_p\}$, and its intensity is $\lambda_h = \lambda_p \exp(-\lambda_p \nu_d(b))$, where $\nu_d(b)$ is the volume of $b(x, h)$. The carrier sense multiple access (CSMA) MAC protocol in wireless networks is modeled by HCPP in [64, 65].

4. Poisson cluster process (PCP) [57]: A PCP is constructed from a parent PPP Φ by replacing each point of Φ with a cluster of points.The clusters are of the form $M_{x_i} = M_i + x_i$ for each $x_i \in \Phi$, where M_i is a family of identical, independently distributed point sets, also independent of the parent process. As network operators may deploy more BSs in the areas of higher traffic demand, PCP can be used to abstract such behavior [66]. A special case of PCP is the Neyman-Scott process in which the cluster associated with each x_i is a PPP centered at x_i, and these processes are independent of one another and, of course, independent of the parent process as well.

2.3 Special Properties of the Poisson Point Process

The special properties of and important theorems on PPP used in this thesis are introduced in this section. Further details on these and other properties of PPP can be found in [54, 56, 57, 59].

Superposition

If $\Phi_1, \Phi_2, \ldots, \Phi_k$ are independent PPPs on $\mathbb{R}^d$ with intensity measures $\Lambda_1, \Lambda_2, \ldots \Lambda_k$, respectively, then their superposition $\Phi = \cup_{n=1}^{k} \Phi_n$ is a PPP with intensity measure $\Lambda = \sum_{n=1}^{k} \Lambda_n$. This result follows from the disjointness lemma [59, p. 14], which states that independent PPPs are disjoint with probability 1 in any measurable set. Thus, the number of points of the union set $\Phi = \cup_{n=1}^{k} \Phi_n$ in a compact set B is given by $\Phi(B) = \sum_{n=1}^{k} \Phi_n(B)$. It can then be easily verified that Φ is a PPP with intensity measure Λ.

Independent Thinning

Thinning is an operation that deletes points from a point process to generate a thinned version of the process. Let Φ be a PPP on $\mathbb{R}^d$ with intensity $\lambda(x)$. If a point $x \in \Phi$ is deleted with probability $1 - p(x)$, where $0 \leq p(x) \leq 1$, independent of the location of any other point in the process as well as its possible deletion, the resulting $p(x)$-thinned process Φ_{th} is a PPP with intensity $\lambda_{th}(x) = p(x)\lambda(x)$, where $p(x)$ is the retention probability. Note that the set of deleted or culled points is also a PPP Φ_{cu} with intensity $\lambda_{cu}(x) = (1-p(x))\lambda(x)$, and is independent of Φ_{th}. If Φ is a homogeneous PPP, the p-thinned process Φ_{th} and the corresponding culled process Φ_{cu} are independent PPPs with intensity $p\lambda$ and $(1-p)\lambda$, respectively. The superposition of thinned and culled process recovers the original PPP.

A more generalized form of the property is called the *coloring theorem*. Let each point of Φ belong to exactly one of the k classes, which are referred to as colors. Let the probability of a point $x \in \Phi$ receiving the ith color be $p_i(x)$, independent of the location of any other point and its color. Let Φ_i denote the set of points with ith color. The coloring theorem states that $\Phi_1, \Phi_2, \ldots, \Phi_k$ are independent PPPs with densities $p_1(x)\lambda(x)$, $p_2(x)\lambda(x)$, $\ldots$, $p_k(x)\lambda(x)$, respectively.

The superposition of these independent PPPs is the original PPP with intensity $\sum_{i=1}^{k} p_i(x)\lambda(x) = \lambda(x)$.

Mapping Theorem

According to the mapping theorem, under certain conditions, if the state space $\mathbb{R}^d$ is mapped into another space $\mathbb{R}^s$, a PPP is transformed into another point process, which is again PPP with a different intensity measure. The theorem can be formally stated as follows.

Mapping theorem: Let Φ be a PPP on $\mathbb{R}^d$ with intensity measure Λ, and let $f : \mathbb{R}^d \to \mathbb{R}^s$ be a state space transformation function such that $\Lambda(f^{-1}(x)) = 0$, $\forall x \in \mathbb{R}^s$. If $\mu(B) = \Lambda(f^{-1}(B))$ for every $B \subseteq \mathbb{R}^s$, then $f(\Phi)$ is a PPP on $\mathbb{R}^s$ with intensity measure μ.

Slivnyak's Theorem

Before presenting Slivnyak's theorem, we will first introduce the Palm distribution and reduced Palm distribution. Let the distribution **P** of a point process Φ be determined by the probability $\mathbf{P}(Y) = \mathbb{P}(\Phi \text{ has property} Y)$. For example, the distribution **P** of a homogeneous PPP Φ with density λ is determined by the system of void probabilities

$$\mathbf{P}(\{\phi \in \mathbb{N} : \phi(B) = 0\}) = \mathbb{P}(\Phi(B) = 0) = e^{-\lambda \nu_d(B)}$$

for compact sets $B \subset \mathbb{R}^d$, where $\mathbb{N}$ is the family of all possible realizations ϕ of the PPP Φ. The conditional distribution of Φ given that a point at x belongs to Φ is known as the Palm distribution of **P** at x, denoted by $\mathbf{P}^x$, i.e., $\mathbf{P}^x(Y) = \mathbb{P}(\Phi \text{ has property} Y | x \in \Phi)$. However, if the conditional distribution is defined by excluding x, it is known as the reduced Palm distribution at x, denoted by $\mathbf{P}^{x!}$, i.e., $\mathbf{P}^{x!}(Y) = \mathbb{P}(\Phi \backslash \{x\} \text{ has property} Y | x \in \Phi)$.

To illustrate the Palm and reduced Palm distributions, let us consider the nearest neighbor distance distribution. The complementary cumulative distribution function (CCDF) $\bar{D}(r)$ of the distance l to the nearest neighbor from a typical point

$x \in \Phi$, i.e., $\mathbb{P}(l > r)$ can be expressed in terms of $\mathbf{P}^x$ and $\mathbf{P}^{x!}$ as

$$\begin{aligned}\bar{D}(r) &= \mathbb{P}(\Phi\left(b(x,r)\right) = 1 | x \in \Phi) = \mathbf{P}^x(\{\phi \in \mathbb{N} : \phi(b(x,r)) = 1\}), \\ &= \mathbb{P}(\Phi\left(b(x,r) \backslash \{x\}\right) = 0 | x \in \Phi) = \mathbf{P}^{x!}(\{\phi \in \mathbb{N} : \phi\left(b(x,r)\right) = 0\}). \quad (2.4)\end{aligned}$$

After introducing the Palm and reduced Palm distributions, the Slivnyak's theorem is stated as follows.

Slivnyak's theorem: For a PPP,

$$\mathbf{P}^{x!} = \mathbf{P}, \tag{2.5}$$

i.e., the reduced Palm distribution equals the distribution of the PPP itself. This implies that the properties observed at a point x do not depend on whether x belongs to Φ or not, as long as the point x is not considered if Φ is conditioned to have a point at x. By applying Slivnyak's theorem, the nearest neighbor distance distribution (2.4) for a homogeneous PPP Φ with density λ can be computed as

$$\bar{D}(r) = \mathbb{P}(\Phi\left(b(x,r)\right) = 0) = \exp(-\lambda\, \nu_d(b)).$$

For homogeneous PPP, due to the stationary property $\Phi = \{x_n\}$ has the same distribution as $\Phi_x = \{x_n + x\}$. Thus, $\mathbf{P}^o = \mathbf{P}^x$, and similarly, $\mathbf{P}^{o!} = \mathbf{P}^{x!}$. Hence, the conditional distribution of a homogeneous PPP Φ with respect to any typical point of Φ can be simply defined by the Palm distribution with the respect to the origin without loss of generality.

Probability Generating Functional

The probability generating functional (PGFL) of a point process Φ on $\mathbb{R}^d$ is defined as

$$\mathcal{G}[\nu] = \mathbb{E}\left[\prod_{x \in \Phi} \nu(x)\right] \tag{2.6}$$

for all non-negative functions $\nu(x) : \mathbb{R}^d \to [0,1]$ with $\{x \in \mathbb{R}^d : \nu(x) < 1\}$ bounded. The PGFL of a PPP with intensity function $\lambda(x)$ is given by

$$\mathcal{G}[\nu] = \exp\left(-\int_{\mathbb{R}^d} (1 - \nu(x))\lambda(x)\, dx\right). \tag{2.7}$$

A PGFL is very useful in evaluating the Laplace transform (LT) of the sum $\sum_{x\in\Phi} f(x)$ as follows and is often used in this thesis.

$$\mathbb{E}\left[\exp\left(-s\sum_{x\in\Phi} f(x)\right)\right] = \mathbb{E}\left[\prod_{x\in\Phi}\exp(-sf(x))\right] = \mathcal{G}\left[\exp(-sf(\cdot))\right]. \quad (2.8)$$

2.4 Interference Distribution in Poisson Wireless Networks

Let us consider a network where the nodes are distributed on $\mathbb{R}^2$ as a homogeneous PPP Φ with density λ and each node transmits with power P. Due to Slivnyak's theorem and stationarity of Φ, the aggregate interference power received at a test receiver does not depend on where the receiver is located and whether the receiver location belongs to the process Φ. The test receiver is thus assumed to be located at the origin without loss of generality. The aggregate interference is then given by

$$I = P\sum_{x\in\Phi} Q_x||x||^{-\alpha}, \quad (2.9)$$

where $Q_x = \exp(\sigma g_x)|h_x|^2$ are independent and identically distributed (i.i.d.) RVs. By using tools from stochastic geometry, the interference I can be characterized by its probability distribution function in the form of its LT or equivalently its characteristic function. The LT $\mathcal{L}_I(s) = \mathbb{E}[\exp(-sI)]$ can be computed by applying the PGFL of PPP as in (2.8), and is thus given by [56]

$$\mathcal{L}_I(s) = \exp(-\pi\lambda P^{2/\alpha}\mathbb{E}[\,Q_x^{2/\alpha}]\Gamma(1-2/\alpha)s^{2/\alpha}]). \quad (2.10)$$

Its equivalent characteristic function $\Psi_I(\omega) = \mathbb{E}[\exp(j\omega I)]$ for $\alpha > 2$ is given by [67]

$$\Psi_I(\omega) = \exp\left(-\gamma|\omega|^{\mu}\left[1 - j\beta\text{sign}(\omega)\tan(\pi\mu/2)\right]\right), \quad (2.11)$$

where $\mu = 2/\alpha$, $\beta = 1$, $\gamma = \pi\lambda C_{2/\alpha}^{-1}P^{2/\alpha}\mathbb{E}[Q_x^{2/\alpha}]$ and

$$C_x = \begin{cases} \frac{1-x}{\Gamma(2-x)\cos(\pi x/\alpha)}, & x \neq 1 \\ \frac{2}{\pi}, & x = 1. \end{cases} \quad (2.12)$$

According to the characteristic function given by (2.11), I is a stable RV[1] with characteristic exponent μ, skew parameter β and dispersion γ. Thus,

$$I \sim S\left(\mu = 2/\alpha, \beta = 1, \gamma = \pi\lambda C_{2/\alpha}^{-1} P^{2/\alpha} \mathbb{E}[Q_x^{2/\alpha}]\right). \tag{2.13}$$

2.5 Multi-antenna Communication

The use of multiple antennas at the transmitter and/or receiver enables the spatial dimension to be exploited for diversity gain, array gain, spatial multiplexing gain, and interference mitigation [68, 69].

Diversity Gain

Multiple antennas at the transmitter and/or receiver can be used to achieve diversity against fading by providing multiple independently faded replicas of the transmitted signal to the receiver. The key idea is that if at least one of the copies is not severely faded, the probability of successful reception is high. Well-known multi-antenna transmission technique for diversity gain is STBC [34,35]. A simple way to achieve diversity gain by using multiple receive antennas is selection combining [70], in which the receive antenna branch with the highest SNR is selected.

Technically, diversity gain also known as diversity order is given by the negative of the slope of the average-error-probability/outage-probability versus average-SNR curve on a log-log scale as the average SNR $\rho \to \infty$ [71].

Array Gain

The SNR at the receiver can be improved through coherent combining enabled by either processing at the receive antenna array or precoding at the transmit antenna array or a combination of both. Such spatial filtering techniques are known as beamforming and the resulting gain in SNR is called array gain. Receive-antenna

[1] A real stable RV with characteristic exponent $\mu \in (0, 2]$, skew parameter $\beta \in [-1, 1]$ and dispersion $\gamma \in [0, \infty)$ is denoted by $S(\mu, \beta, \gamma)$, whose characteristic function is given by

$$\Psi(\omega) = \begin{cases} \exp\left(-\gamma|\omega|^{\mu}\left[1 - j\beta \text{sign}(\omega)\tan(\pi\mu/2)\right]\right), & \mu \neq 1 \\ \exp\left(-\gamma|\omega|\left[1 + j2\beta/\pi \text{sign}(\omega)\ln(|\omega|)\right]\right), & \mu = 1. \end{cases}$$

processing, which maximizes the receive SNR is MRC, in which the received signal on each antenna element is weighted by its corresponding complex fading coefficient and then combined [70]. MRC is thus an optimal diversity combining method in the absence of interference. Similarly, on the transmit side, the precoding vector maximizing the receive SNR is eigen beamforming, also known as maximal ratio transmission (MRT) [72].

The average error probability of wireless transmissions over flat fading channels impaired by additive white Gaussian noise (AWGN) at high SNR can be quantified in terms of the diversity gain (diversity order) G_d and array gain G_c as [3, 71]

$$P_e(\rho) \approx (G_c \rho)^{-G_d}, \quad \text{as} \quad \rho \to \infty. \tag{2.14}$$

Spatial Multiplexing Gain

For MIMO systems in a rich scattering environment such that the fading coefficients of the channels between each transmit-receive antenna pair are independent, multiple independent data streams can be simultaneously transmitted over the MIMO channel in the same bandwidth. This technique is known as spatial multiplexing. A MIMO system with N_t transmit and N_r receive antennas can support up to $\min(N_t, N_r)$ data streams [36, 73]. Thus, system capacity can be increased linearly with the number of antennas. Precoding and/or receive-antenna processing techniques, for example those based on ZF and minimum mean square error (MMSE) criteria, are employed to help the receiver decode spatially multiplexed signals [71]. While spatial multiplexing in general implies transmitting multiple data streams to a single user, it can be extended to the case where data streams are intended for different users. This technique is known as SDMA, or multi-user MIMO [37].

Interference Mitigation

The spatial dimension can also be exploited to cancel/suppress interference. In cellular networks, if a BS has N_t transmit antennas, the precoding vector can be designed to create a transmit beam with high attenuation in the directions of M other-cell users, while utilizing the remaining degrees of freedom $N_t - M$ to focus the signal energy towards its served user. The ZF criterion is used to design such

precoder in [30,31]. Similarly, receive antenna weights can be designed to suppress the dominant interfering BSs. A ZF receiver with N_r antennas can suppress up to $N_r - 1$ interferers [74].

2.6 Relay Communication

Although multi-antenna techniques improve per link throughput, they cannot solve the problem of limited coverage due to transmit power constraint. An effective solution to the limited-coverage problem is to use an intermediate node known as relay to assist the communication between a source and a destination by forwarding the information received from the source node towards its destination [75]. In addition to the advantage of coverage extension without increasing the transmit power, another advantage of relay transmission is cooperative diversity [76, 77]. Cooperative relay networks, in which the source and the cooperating relay/relays create distributed antenna array by utilizing the broadcast nature of the wireless communication, have been widely investigated in the literature [78–80].

Among the various relaying protocols studied in the literature, amplify-and-forward (AF) and decode-and-forward (DF) are the two most popular protocols. In AF relaying, the relay node simply scales (amplifies) the signal received from the source node and forwards it to the destination. Whereas, in DF protocol, the relay node first decodes the received signal and retransmits the re-encoded signal to the destination. While amplification of the noise and interference is a major drawback of AF relays, DF relays suffer from error propagation. To mitigate error propagation in DF relaying, the relay nodes may be allowed to retransmit only if their received SNRs are above the required thresholds for error-free decoding [81].

When multiple relay nodes are available, they can efficiently utilize the spatial degrees of freedom by jointly transmitting to the destination for higher data rates. However, the limited resources and the minimum cost implementation requirement make the best relay selection scheme (also known as opportunistic relaying) based on the CSI more desirable over multi-relay scheme. Thus, the opportunistic relaying has been significantly investigated in the literature [82–84].

Chapter 3

Multi-Channel Analysis of Cell Range Expansion and Resource Partitioning in Two-Tier HetNets

The capacity of cellular HetNets can be improved by offloading users from congested macro cells to lightly-loaded small cells through biased association known as CRE. However, the offloaded (range-expanded) users must be protected from macro interference. This chapter[1] develops an analytical framework to evaluate the performance gain due to CRE further supported by resource partitioning in two-tier (macro-pico) networks with multi-channel downlinks, for example, those based on OFDMA. By exploiting the flexibility in subchannel allocation offered by OFDMA, frequency-domain resource partitioning is proposed in which the macro tier is muted on a fraction of the total subchannels, which are allocated exclusively to range-expanded pico users to protect them from macro interference. The load perceived by a BS is a key factor in determining its interference contribution over the network and is directly affected by user offloading and resource allocation. Thus, the analysis of CRE and resource partitioning must incorporate the cell load. In this chapter, the cell load is properly characterized as a function of the user density, association bias and resource partitioning fraction. The performance is then evaluated in terms of the average user data rate over the entire network, and the optimal choice of association bias and resource partitioning fraction for maximizing the average data rate is also investigated.

[1]This chapter has been published in the IEEE Transactions on Wireless Communications [85].

3.1 Introduction

With co-channel deployment of low-power BSs such as picos and femtos within the areas covered by the existing macro cellular infrastructure, the system capacity improves as users get offloaded from the congested macro tier to pico/femto tier. The benefits of user offloading are two-fold. First, the offloaded users get access to a larger fraction of radio resources. Second, the macro cellular load is reduced, which allows the remaining macro users to be served with improved rates. The user offloading, however, may be limited due to transmit power disparities between the macro and pico/femto BSs, thereby limiting the capacity gain.

The macro offloading can be increased by biased association known as CRE [7, 8], in which a user is offloaded to a small cell if the received power from it is less than that from a macro cell by at most some amount known as association bias. Such offloaded users are referred to as range-expanded users. With this technique, the number of offloaded users can be controlled with the bias value to obtain a balanced distribution of user loads across the tiers. However, the load balancing offered by CRE comes at the cost of severe downlink co-channel interference to the range-expanded users from the macro tier and such interference must be mitigated by using interference coordination techniques. The interference coordination can be implemented by resource partitioning [7, 8, 86], in which a certain fraction of time or frequency resources is provided exclusively to small cells by muting the macro-tier transmissions in these resources. The range-expanded users are then served by the small cells in these resources, thereby isolating these users from the macro tier interference.

3.1.1 Motivation and Contributions

Simulation results [87–90] demonstrate that CRE with resource partitioning highly enhances the otherwise limited performance gains from the deployment of small cells. These interdependent techniques, however, must be jointly tuned for optimal system performance. The optimal association bias at the given resource partitioning fraction is investigated for sum capacity and related performance metrics in [91]

through a semi-analytical approach. Analytical approaches to determine the optimal combination of the bias value and resource partitioning fraction are presented in [47] and [21] based on the per user spectral efficiency and downlink rate distribution, respectively. However, both assumed a fully loaded network, i.e., a network with all the BSs simultaneously active all the time.

The full-load assumption is not applicable for small cells unless they are deployed in hot-spots and large biasing towards them is introduced. On the other hand, with very large biasing, macro cells may no longer be fully loaded. Thus, the full-load assumption is not reasonable for studying biasing. The analytical results in [19] show that biasing has a detrimental impact on the average rate of the overall network in the fully loaded condition. The motivation behind biasing is to improve the network rate through load balancing, i.e., relieving the heavily loaded macro cells and better utilizing the resources of the lightly loaded small cells. However, if the macro and small cells are assumed to be always fully loaded, then biasing makes no sense. Thus, the full-load assumption cannot reflect the benefits of biasing. Moreover, the interference from a BS is a direct function of its load. For example, the BSs that receive more load have a higher probability of being active at a given time instant and thus contribute more interference to the network. As the load perceived by a BS is significantly affected by the number of users offloaded to/from and the fraction of resources allocated, the interference to a given user strongly depends on the association bias and resource partitioning fraction. Such effects cannot be captured if the full-load assumption is used. Thus, an analytical framework for the performance evaluation of cellular HetNets with biased association and resource partitioning, while appropriately modeling the cell load, becomes essential, and this chapter aims to fulfill this need.

We focus on the downlink performance analysis of two-tier (macro and pico) HetNets, which can be extended to multi-tier networks. The locations of macro and pico BSs are modeled as independent PPPs, which have recently been popular for modeling cellular HetNets [14, 16, 17, 58]. The downlink analysis of cellular HetNets usually assumes a time-shared single channel per cell [16, 17, 19, 21, 47]. Thus, only the time-domain method of resource partitioning has been significantly

analyzed [21, 24, 47, 48]. In this method, the macro tier is periodically muted on certain fraction of the subframes, known as ABSFs. In contrast, we consider a multi-channel downlink, for example, the one based on OFDMA, in which multiple users are simultaneously served in orthogonal subchannels. In LTE networks, multiple access in the downlink is established by OFDMA. Due to the flexibility in subchannel allocation offered by OFDMA, we propose frequency-domain resource partitioning in which the macro tier is restricted from using a fraction of the total subchannels so that they are allocated exclusively to the range-expanded pico users.

The main contributions of this chapter are summarized as follows:

1. Based on the proposed multi-channel model, we first define the load perceived by a BS as a direct function of the number of associated users and the number of available subchannels. Such characterization effectively captures the effect of the user density, association bias and resource partitioning fraction on the cell load.

2. Next, we evaluate the performance of the proposed system in terms of the average user data rate that can be attained over the entire network, while incorporating the cell load into the analysis.

3. We comprehensively analyze the average rate performance under different bias values and resource partitioning fractions and investigate their optimal combination.

4. We numerically demonstrate that if the bias value and resource partitioning fraction are carefully selected, the rate performance can be highly improved in comparison to the CRE-only system (i.e., a system with no resource partitioning).

5. We show that the optimal combination of the association bias and resource partitioning fraction is strongly dependent on the network load.

We hasten to add that although the stochastic geometry method for multi-channel downlink analysis of cellular HetNets has been considered before, for example

Table 3.1: System Parameters for CRE with resource partitioning

Symbol	Description
$\mathbf{\Phi}_m; \mathbf{\Phi}_p; \mathbf{\Phi}_u$	PPP of macro BSs; PPP of pico BSs; PPP of users
$\lambda_m; \lambda_p; \lambda_u$	Density of macro BSs; density of pico BSs; density of users
$P^m_{\text{max}}; P^p_{\text{max}}$	Maximum allowable transmit power of macro BS; Maximum allowable transmit power of pico BS
$P_m; P_p$	Transmit power per subchannel of macro BS; Transmit power per subchannel of pico BS
B	Association bias for pico CRE
$\alpha_p; \alpha_m$	Path-loss exponent of macro tier; path-loss exponent of pico tier
$\mathbf{\Phi}^m_u; \mathbf{\Phi}^o_u; \mathbf{\Phi}^e_u$	Set of macro users; set of unbiased pico users; set of range-expanded pico users
$U_m; U_o; U_p$	Association probability of a typical user to Φ^m_u; association probability of a typical user to Φ^o_u; association probability of a typical user to Φ^e_u
$N_m; N_o; N_e$	Number of users in a typical macro cell; number of unbiased users in a typical pico cell; number of range expanded users in a typical pico cell
$L; L_r; L_c$	Total number of subchannels; number of subchannels reserved for range-expanded pico users; number of common subchannels shared by macro and pico tier
$\mathcal{S}_r; \mathcal{S}_c$	Set of subchannels reserved for range-expanded pico users; set of common subchannels shared by maro and pico users
$p_m; p_o; p_e$	Probability that a typical macro BS is active on a given subchannel from the set $\mathcal{S}_c$; probability that a typical pico BS is active on a given subchannel from the set $\mathcal{S}_c$ and $\mathcal{S}_r$ respectively
σ^2	Noise variance
$T_m; T_o; T_e$	Average share of resources of a typical macro user; average share of resources of a typical unbiased pico user; average share of resources of a typical range-expanded pico user
$R_m; R_o; R_e$	Average rate of a typical macro user; average rate of a typical unbiased pico user; average rate of a typical range-expanded pico user

in [18, 25], the problem of CRE with resource partitioning in a multi-channel environment, while successfully capturing their impact on cell load is addressed here for the first time.

The chapter is organized as follows. The network model, user association policy and resource partitioning scheme are described in Section 3.2. Section 3.3 utilizes the user association probability and cell load derived in Section 3.2 to derive the average user data rate over the entire network. The special case of no resource partitioning is also analyzed in Section 3.3.1. The analytical results are validated through Monte-Carlo simulation in Section 3.4, along with extensive numerical analysis to assess the impact of biasing and resource partitioning on the user data rate. Section 3.5 finally concludes the chapter.

3.2 System Model

3.2.1 Network and Channel Model

We consider an OFDMA based two-tier downlink cellular HetNet consisting of macro and pico BSs, which are assumed to be spatially distributed on $\mathbb{R}^2$ plane as independent homogeneous PPPs $\mathbf{\Phi}_m$ of density λ_m and $\mathbf{\Phi}_p$ of density λ_p, respectively. For the macro tier, the PPP model provides tight lower bounds for performance measures, as tight as the upper bound results provided by the popular grid model, when compared to the actual 4G network [15]. However, the analytical tractability of the PPP model is a key benefit over the grid model. The adoption of PPP model for the pico tier is justified because randomness is expected in the pico BS locations. Similarly, user locations are modeled as an independent PPP $\mathbf{\Phi}_u$ with density λ_u. The two network tiers share the same spectrum, which is evenly divided into $L > 1$ subchannels[2]. We consider flat transmit power spectrum on the downlink[3] and thus, the power per subchannel is kept constant at P_m and P_p for the macro and pico tiers, respectively. If P^m_{max} and P^p_{max} are the maximum allowable transmit powers of the macro and pico BSs, respectively, then $P_m = P^m_{\text{max}}/L$ and $P_p = P^p_{\text{max}}/L$.

Independent Rayleigh multipath fading with power-law path loss is assumed between any BS-user pair. The channel power gains from the macro BS located at $x_m \in \mathbf{\Phi}_m$ and the pico BS located at $x_p \in \mathbf{\Phi}_p$ to a typical user located, without loss of generality, at the origin, are thus given by $h_{x_m}||x_m||^{-\alpha_m}$ and $h_{x_p}||x_p||^{-\alpha_p}$, respectively, where $h_{x_m} \sim \text{Exp}[1]$ and $h_{x_p} \sim \text{Exp}[1]$ are the corresponding fading powers, and α_m and α_p are the path-loss exponents of the macro and pico tier, respectively.

3.2.2 User Association

The user association scheme is based on biased received power. Thus, each user is associated with the BS offering the maximum biased received power [19, 21]. The

[2]A subchannel may refer to one or multiple resource blocks (RBs) in LTE systems.
[3]This assumption is consistent with LTE downlink power allocation [92].

fading effect is ignored in the association metric to avoid the ping-pong handover effect [93]. If B is the association bias introduced for the pico CRE, a typical user at the origin is associated with the nearest macro BS only if $P_m R_m^{-\alpha_m} \geq P_p B R_p^{-\alpha_p}$, where $R_m = \min_{x_m \in \mathbf{\Phi}_m} \|x_m\|$ and $R_p = \min_{x_m \in \mathbf{\Phi}_p} \|x_p\|$ are the distances from the origin to the nearest macro and pico BSs, respectively. The user is otherwise associated with the nearest pico BS. When associated with the nearest pico BS, the user is registered in its user list as an *unbiased user* if $P_p R_p^{-\alpha_p} \geq P_m R_m^{-\alpha_m}$ and as a *range-expanded user* if $P_p R_p^{-\alpha_p} \leq P_m R_m^{-\alpha_m} < P_p B R_p^{-\alpha_p}$. The nomenclatures for pico users (*unbiased* and *range-expanded*) have been adopted from [21].

For the given user association scheme, if we randomly pick a user, it may turn out to be a macro user, an unbiased pico user, or a range-expanded pico user with certain probabilities. The following lemma expresses these probabilities.

Lemma 1. *Let U_m, U_o, and U_e denote the probabilities that a randomly chosen user is a macro user, unbiased pico user, or range-expanded pico user, respectively, which are given by,*

$$U_m = 2\pi\lambda_m \int_0^\infty r e^{-\pi\lambda_m r^2} \exp\Big(-\pi\lambda_p \Big(\frac{BP_p}{P_m}\Big)^{\frac{2}{\alpha_p}} r^{\frac{2\alpha_m}{\alpha_p}}\Big) \mathrm{d}r \tag{3.1}$$

$$U_o = 2\pi\lambda_p \int_0^\infty r e^{-\pi\lambda_p r^2} \exp\Big(-\pi\lambda_m \Big(\frac{P_m}{P_p}\Big)^{\frac{2}{\alpha_m}} r^{\frac{2\alpha_p}{\alpha_m}}\Big) \mathrm{d}r \tag{3.2}$$

$$U_e = 2\pi\lambda_p \int_0^\infty r e^{-\pi\lambda_p r^2} \Big\{ \exp\Big(-\pi\lambda_m \Big(\frac{P_m}{BP_p}\Big)^{\frac{2}{\alpha_m}} r^{\frac{2\alpha_p}{\alpha_m}}\Big) - \exp\Big(-\pi\lambda_m \Big(\frac{P_m}{P_p}\Big)^{\frac{2}{\alpha_m}} r^{\frac{2\alpha_p}{\alpha_m}}\Big)\Big\} \mathrm{d}r. \tag{3.3}$$

Proof. Since the analysis conducted on a typical user located at the origin is valid for any randomly chosen user according to Slivnyak's theorem (Section 2.3), U_m can be derived as

$$U_m = \mathbb{P}(P_m R_m^{-\alpha_m} \geq P_p B R_p^{-\alpha_p}) = \mathbb{E}_{R_m}\left[\mathbb{P}(R_p \geq \left(P_p/P_m B\right)^{1/\alpha_p} R_m^{\alpha_m/\alpha_p})\right],$$

which can be solved by using the probability distributions of R_m and R_p. We know that $\mathbb{P}(R_l > r)$, $l \in \{m, p\}$, is the probability that no points of $\mathbf{\Phi}_l$ lie within a circle of radius r, centered at the origin. Since $\mathbf{\Phi}_l$ is a PPP with density λ_l, we have $\bar{F}_{R_l}(r) = \mathbb{P}(R_l > r) = \exp(-\pi\lambda_l r^2)$. The probability density function (PDF) of R_l

can then be obtained as $f_{R_l}(r) = -d\bar{F}_{R_l}(r)/dr = 2\pi\lambda_l r \exp(-\pi\lambda_l r^2)$. Similarly, by using these distributions, U_o and U_e can be obtained as $U_o = \mathbb{P}(P_p R_p^{-\alpha_p} \geq P_m R_m^{-\alpha_m})$ and $U_e = \mathbb{P}(P_p R_p^{-\alpha_p} \leq P_m R_m^{-\alpha_m} < P_p B R_p^{-\alpha_p})$. □

For the special case of equal path-loss exponents, i.e., $\alpha_m = \alpha_p = \alpha$, the integrals in (3.1)-(3.3) can be reduced to the following simple closed-form expressions by using $\int_0^\infty r \exp(-\beta r^2) dr = 1/(2\beta)$:

$$U_m = \frac{\lambda_m P_m^{2/\alpha}}{\lambda_m P_m^{2/\alpha} + \lambda_p (B P_p)^{2/\alpha}}, \; U_o = \frac{\lambda_p P_p^{2/\alpha}}{\lambda_m P_m^{2/\alpha} + \lambda_p P_p^{2/\alpha}},$$
$$U_e = \frac{\lambda_p (B P_p)^{2/\alpha}}{\lambda_m P_m^{2/\alpha} + \lambda_p (B P_p)^{2/\alpha}} - \frac{\lambda_p P_p^{2/\alpha}}{\lambda_m P_m^{2/\alpha} + \lambda_p (P_p)^{2/\alpha}}. \tag{3.4}$$

The probabilities (3.1)-(3.4) are also derived in [21] and are given here for the sake of completeness.

As per the given user association scheme, the set of total users in the network $\mathbf{\Phi}_u$ can be divided into three subsets:

1. $\mathbf{\Phi}_u^m$, the set of **macro users**,
2. $\mathbf{\Phi}_u^o$, the set of **unbiased pico users**, and
3. $\mathbf{\Phi}_u^e$, the set of **range-expanded pico users**,

such that $\mathbf{\Phi}_u = \mathbf{\Phi}_u^m \cup \mathbf{\Phi}_u^o \cup \mathbf{\Phi}_u^e$. Since each user in $\mathbf{\Phi}_u$ can belong to exactly one of these three sets, they are disjoint. The probabilities U_m, U_o, and U_e can also be interpreted as the average fraction of users belonging to the sets $\mathbf{\Phi}_u^m$, $\mathbf{\Phi}_u^o$ and $\mathbf{\Phi}_u^e$, respectively. For each user-set, we are interested in the number of users associated with a typical BS to characterize the typical cell load of each tier and the average share of radio resources received by a typical user. The actual locations of users with respect to each other in each $\mathbf{\Phi}_u^l$, $l \in \{m, o, e\}$ are less important to us. Thus, $\mathbf{\Phi}_u^m$, $\mathbf{\Phi}_u^o$ and $\mathbf{\Phi}_u^e$ can be equivalently modeled as independent PPPs with densities $U_m\lambda_u$, $U_o\lambda_u$ and $U_e\lambda_u$, respectively. In other words, they can be modeled as thinned versions of the original process $\mathbf{\Phi}_u$ with retention probabilities U_m, U_o and U_e, respectively, independent of the locations of the users.

Each user in $\mathbf{\Phi}_u^m$ is always associated with the nearest macro BS, and each user in $\mathbf{\Phi}_u^o \cup \mathbf{\Phi}_u^e$ is always associated with the nearest pico BS. The network can thus be viewed as a superposition of two independent Voronoi tessellations of the macro and pico tier, respectively. The Voronoi cells of each tessellation are disjoint, and their sizes are i.i.d. RVs [94]. Hence, together with the independent scattering property of the PPP, which states that the number of points of a PPP in disjoint sets are independent RVs [57, 59], the number of macro users in different macro Voronoi cells are i.i.d RVs, and so are the number of unbiased pico users and the number of range-expanded pico users in different pico Voronoi cells. The following lemma gives their probability mass functions (PMFs), which will be used later in this chapter for calculating the typical cell load of each tier and the average share of radio resources received by a typical user.

Lemma 2. *Let N_m be the number of users associated with a randomly chosen macro BS and N_o and N_e be the number of unbiased and range-expanded users of a randomly chosen pico BS. Their PMFs are given by*

$$\mathbb{P}(N_l = n) = \frac{3.5^{3.5}\Gamma(3.5+n)(U_l\lambda_u/\lambda_{\zeta(l)})^n}{\Gamma(3.5)n!(U_l\lambda_u/\lambda_{\zeta(l)}+3.5)^{n+3.5}},\ n \geq 0,\ \forall l \in \{m, o, e\}, \qquad (3.5)$$

where $\lambda_{\zeta(m)} = \lambda_m$ and $\lambda_{\zeta(o)} = \lambda_{\zeta(e)} = \lambda_p$.

Proof. Since $\mathbf{\Phi}_u^m$ is a PPP of density $U_m\lambda_u$, the number of macro users in a typical macro Voronoi cell of given area A is Poisson distributed with mean $U_m\lambda_u A$. The unconditional PMF of N_m in (3.5) is then obtained by averaging over the distribution of the Voronoi cell area A approximated by the Gamma distribution, $f_A(a) = (3.5\lambda_m)^{3.5}a^{2.5}\exp(-3.5\lambda_m a)/\Gamma(3.5)$ [94]. The PMFs of N_o and N_e can be similarly obtained. □

3.2.3 Resource Allocation and Partitioning

For any range-expanded pico user in $\mathbf{\Phi}_u^e$, the average received power from its nearest macro BS is greater than that from the serving pico BS. The range-expanded users thus need to be protected from high-power macro interference. If each macro BS leaves a set of L_r subchannels unutilized out of the total L subchannels, each

pico BS can serve its range-expanded users in these macro-interference free subchannels. Each macro BS thus allocates $L - L_r = L_c$ number of subchannels to serve its users. The unbiased users in each pico cell are also served in the same set of L_c subchannels since L_r macro-interference free subchannels are reserved exclusively for its range-expanded users.

Let the set of L_r macro-interference free subchannels reserved exclusively for range-expanded users be denoted by $\mathcal{S}_r$ and the set of L_c common subchannels shared by the macro and pico tiers be denoted by $\mathcal{S}_c$. The subchannels in each BS are allocated to individual users according to one subchannel per user and they are uniformly and independently selected from the available set. However, if the number of users associated with a BS is greater than the number of subchannels available, the resources are time-shared equally among the users. This scheduling method is basically frequency- and time-domain round-robin scheduling, which gives an equal share of the resources to all the users. This simple scheduling algorithm leads to analytical tractability and provides important insights into system parameters. Sophisticated scheduling algorithms like max-rate and proportional fair schedulers, which add significant complexities to the analysis, can be considered in future work. The current analysis serves as a lower bound on the performance of these sophisticated algorithms.

We assume that each BS has a saturated downlink transmission queue for each associated user, and thus, each user always has data to receive from its serving BS. While some BSs may have more users than the available subchannels, some may have less. Thus, depending upon the number of users associated with it, a BS, may or may not be active on all of its available subchannels. In the following lemma, we derive the probability that a typical BS of each tier is active on a given subchannel.

Lemma 3. *Let p_m be the probability that a randomly chosen macro BS is active on a given subchannel from the set $\mathcal{S}_c$. Similarly, let p_o and p_e be the probabilities that a randomly chosen pico BS is active on a given subchannel from the set $\mathcal{S}_c$ and $\mathcal{S}_r$,*

respectively. Then,

$$p_l = 1 - \frac{3.5^{3.5}}{\Gamma(3.5)} \frac{1}{L_{\kappa(l)}} \sum_{n=0}^{L_{\kappa(l)}-1} \left[\frac{(L_{\kappa(l)} - n)\Gamma(3.5+n)(U_l\lambda_u/\lambda_{\zeta(l)})^n}{n!(U_l\lambda_u/\lambda_{\zeta(l)} + 3.5)^{3.5+n}} \right], \forall l \in \{m, o, e\} \tag{3.6}$$

where $\lambda_{\zeta(m)} = \lambda_m$, $\lambda_{\zeta(o)} = \lambda_{\zeta(e)} = \lambda_p$, $L_{\kappa(m)} = L_{\kappa(o)} = L_c$ *and* $L_{\kappa(e)} = L_r$.

Proof. If the number of users associated with a typical macro cell is less than L_c (i.e. $N_m < L_c$), the probability that a subchannel of S_c is used in the cell is N_m/L_c. However, if $N_m \geq L_c$, all the subchannels of S_c are used in the cell with probability 1. Thus, p_m can be expressed as

$$\begin{aligned} p_m &= \sum_{n=0}^{L_c-1} \frac{n}{L_c} \mathbb{P}(N_m = n) + \sum_{n=L_c}^{\infty} \mathbb{P}(N_m = n) \\ &= 1 - \sum_{n=0}^{L_c-1} \left(1 - \frac{n}{L_c}\right) \mathbb{P}(N_m = n). \end{aligned} \tag{3.7}$$

The final expression for p_m is then obtained by substituting the PMF of N_m in the above equation. The probabilities p_o and p_e can be similarly obtained. □

Remark. As we explained earlier, the number of users associated with different macro cells are independent. Thus, the probability that any randomly chosen macro BS is active on a given subchannel from the set $\mathcal{S}_c$, which is p_m, is independent of any other macro BS. Similarly, the probabilities p_o and p_e of any arbitrary pico BS are independent of any other pico BS.

We refer to p_m as the load of a typical macro cell. It can also be interpreted as the probability that a typical macro BS is contributing to network interference because a typical user being served on a subchannel receives interference from only those BSs which are active on that particular subchannel. While the authors in [20] used the mean statistic of the number of users associated with a typical BS to approximate this probability by $\min\left(\frac{\text{Average number of users}}{\text{Total number of frequency RBs available}}, 1\right)$, we derive the exact probability in this paper. Similarly, p_o and p_e are referred to as the loads of a typical pico cell in two different groups of frequency resources S_c and S_r, respectively. We can observe that user density, association bias and the degree of resource partitioning directly affect the cell load.

Having derived the cell loads, we can compute the SINR of a typical user u located at the origin when it belongs to $\mathbf{\Phi}_u^l$, denoted by SINR$_l$, for each $l \in \{m, o, e\}$ as

$$\text{SINR}_m = \frac{P_m h_{b_m} D_m^{-\alpha_m}}{P_m \sum\limits_{x_m \in \mathbf{\Psi}_m \setminus b_m} h_{x_m} ||x_m||^{-\alpha_m} + P_p \sum\limits_{x_o \in \mathbf{\Psi}_o} h_{x_o} ||x_o||^{-\alpha_p} + \sigma^2}, \tag{3.8}$$

$$\text{SINR}_o = \frac{P_p h_{b_o} D_o^{-\alpha_p}}{P_m \sum\limits_{x_m \in \mathbf{\Psi}_m} h_{x_m} ||x_m||^{-\alpha_m} + P_p \sum\limits_{x_o \in \mathbf{\Psi}_o \setminus b_o} h_{x_o} ||x_o||^{-\alpha_p} + \sigma^2}, \tag{3.9}$$

$$\text{SINR}_e = \frac{P_p h_{b_e} D_e^{-\alpha_p}}{P_p \sum\limits_{x_e \in \mathbf{\Psi}_e \setminus b_e} h_{x_e} ||x_e||^{-\alpha_p} + \sigma^2}, \tag{3.10}$$

where b_l is the serving BS at a distance D_l from the user u when it belongs to $\mathbf{\Phi}_u^l$ and σ^2 is AWGN power. If the user u is being served on a subchannel from the set S_c (i.e., when the user is either a macro user or an unbiased-pico user), $\mathbf{\Psi}_m$ and $\mathbf{\Psi}_o$ are the sets of the macro and pico BSs, respectively, that are active on that particular subchannel. The sets $\mathbf{\Psi}_m$ and $\mathbf{\Psi}_o$ are independent thinning of the the original PPPs $\mathbf{\Phi}_m$ and $\mathbf{\Phi}_p$, respectively, with retention probabilities p_m and p_o, respectively. Hence, they are independent PPPs with densities $p_m\lambda_m$ and $p_o\lambda_p$, respectively. Similarly, $\mathbf{\Psi}_e$ is the set of active pico BSs on the subchannel the user u being served from the set S_r (i.e., when u is a range-expanded pico user) and is also a PPP with density $p_e\lambda_p$.

3.3 Average User Data Rate

The motivation behind CRE supported by resource partitioning in cellular HetNets is to provide a high data rate to users through load balancing. Thus, the performance metric chosen is the average user data rate that can be attained over the entire network.

Theorem 1. *The average data rate per unit bandwidth of a typical user u is given by*

$$\bar{R} = \sum_{l \in \{m,o,e\}} U_l \, T_l \, \mathbb{E}\left[\log_2(1 + \textit{SINR}_l)\right], \tag{3.11}$$

where $U_l = \mathbb{P}(u \in \mathbf{\Phi}_u^l)$, which is given by Lemma 1, and T_l is the average time share of frequency resources received by the user u when it belongs to $\mathbf{\Phi}_u^l$.

Proof. With an adaptive transmission scheme so that the Shannon bound can be achieved and treating interference as noise [15], the data rate per unit bandwidth of a typical user u, conditioned on u belonging to $\mathbf{\Phi}_u^l$, is given by

$$R_l = t_l \log_2(1 + \text{SINR}_l), \, \forall l \in \{m, o, e\}, \tag{3.12}$$

where t_l is the fraction of time the user u is served on a subchannel. Let N_l' be the number of other users in the cell to which the user u belongs. If the total number of users is no greater than $L_{\kappa(l)}$ (i.e., $N_l' + 1 \leq L_{\kappa(l)}$), where $L_{\kappa(m)} = L_{\kappa(o)} = L_c$ and $L_{\kappa(e)} = L_r$, the user u can exclusively occupy a subchannel without time sharing, and thus, $t_l = 1$. Otherwise, the subchannels are time-shared equally among the total users, and thus, $t_l = L_{\kappa(l)}/(N_l' + 1)$.

The average data rate per unit bandwidth of the user $u \in \mathbf{\Phi}_u^l$ is $\bar{R}_l = \mathbb{E}[R_l] = \mathbb{E}[t_l \log_2(1+\text{SINR}_l)]$. Since the number of users associated with a BS determines its probability of being active on a certain subchannel (Lemma 3), the total interference received by the user u, and thus, its SINR depend on the number of users associated with the cells other than the serving cell in the network. t_l, however, is the function of the number of users in the serving cell. As we discussed in Section 3.2.2, the number of users in different cells are independent, which implies that t_l and SINR_l are independent. Thus, $\mathbb{E}[t_l \log_2(1 + \text{SINR}_l)] = T_l \, \mathbb{E}[\log_2(1 + \text{SINR}_l)]$, where $T_l = \mathbb{E}[t_l]$. According to the law of total expectation, the overall data rate of a typical user u is then given by $\bar{R} = \sum_{l \in \{m,o,e\}} U_l \, \bar{R}_l$. By using Lemma 4 and 5, which derive $T_l = \mathbb{E}[t_l]$ and the average spectral efficiency $\mathbb{E}\left[\log_2(1 + \text{SINR}_l)\right]$, respectively, the final expression for the average user data rate is obtained. □

In the following Lemma, we derive T_l, which is required to compute the average user data rate in (3.11).

Lemma 4. *The average time-share of the frequency resources T_l received by a*

typical user u when $u \in \mathbf{\Phi}_u^l$ is given by

$$T_l = \frac{L_{\kappa(l)}\lambda_{\zeta(l)}}{U_l\lambda_u}\left(1 - \left(1 + 3.5^{-1}U_l\lambda_u/\lambda_{\zeta(l)}\right)^{-3.5}\right) - \frac{3.5^{3.5}}{\Gamma(3.5)}\sum_{n=1}^{L_{\kappa(l)}} \frac{\Gamma(3.5+n)\left(U_l\lambda_u/\lambda_{\zeta(l)}\right)^{n-1}\left(L_{\kappa(l)}-n\right)}{n!\left(U_l\lambda_u/\lambda_{\zeta(l)}+3.5\right)^{3.5+n}} \forall l \in \{m,o,e\}, \quad (3.13)$$

where $\lambda_{\zeta(m)} = \lambda_m$, $\lambda_{\zeta(o)} = \lambda_{\zeta(e)} = \lambda_p$, $L_{\kappa(m)} = L_{\kappa(o)} = L_c$ and $L_{\kappa(e)} = L_r$.

Proof. The proof is given in Appendix A.1. □

To finally compute the average user data rate in (3.11), we now derive the average link spectral efficiency $\mathbb{E}\left[\log_2(1+\text{SINR}_l)\right]$.

Lemma 5. *The average link spectral efficiency $\mathbb{E}\left[\log_2(1+\text{SINR}_l)\right]$ of the user u when it belongs to $\mathbf{\Phi}_u^l$, denoted by C_l is given by*

$$C_l = \frac{1}{\ln 2}\int_0^\infty \frac{\bar{F}_l(t)}{1+t}dt, \; \forall l \in \{m,o,e\}, \quad (3.14)$$

where $\bar{F}_l(t) = \mathbb{P}(\text{SINR}_l \geq t)$ is the conditional CCDF of the SINR of the user u when it belongs to $\mathbf{\Phi}_u^l$. $\bar{F}_l(t)$ for each $l \in \{m,o,e\}$ is given by

$$\bar{F}_m(t) = \frac{2\pi\lambda_m}{U_m}\int_0^\infty r\exp\left\{-\frac{t}{P_m}\sigma^2 r^{\alpha_m} - \pi\lambda_p\left(\frac{P_p}{P_m}\right)^{\frac{2}{\alpha_p}} r^{2\frac{\alpha_m}{\alpha_p}} \times\left(B^{\frac{2}{\alpha_p}} + \frac{2p_o}{(\alpha_p-2)}\frac{B^{\frac{2}{\alpha_p}}}{(1+\frac{B}{t})}\,{}_2F_1\left[1,1,2-\frac{2}{\alpha_p},\frac{1}{(1+\frac{B}{t})}\right]\right) - \pi\lambda_m r^2 \times\left(1+\frac{2p_m}{(\alpha_m-2)}\frac{1}{(1+\frac{1}{t})}\,{}_2F_1\left[1,1,2-\frac{2}{\alpha_m},\frac{1}{(1+\frac{1}{t})}\right]\right)\right\}\mathrm{d}r, \quad (3.15)$$

$$\bar{F}_o(t) = \frac{2\pi\lambda_p}{U_o}\int_0^\infty r\exp\left\{-\frac{t}{P_p}\sigma^2 r^{\alpha_p} - \pi\lambda_m\left(\frac{P_m}{P_p}\right)^{\frac{2}{\alpha_m}} r^{2\frac{\alpha_p}{\alpha_m}} \times\left(1+\frac{2p_m}{(\alpha_m-2)}\frac{1}{(1+\frac{1}{t})}\,{}_2F_1\left[1,1,2-\frac{2}{\alpha_m},\frac{1}{(1+\frac{1}{t})}\right]\right) -\pi\lambda_p r^2\left(1+\frac{2p_o}{(\alpha_p-2)}\frac{1}{(1+\frac{1}{t})}\,{}_2F_1\left[1,1,2-\frac{2}{\alpha_p},\frac{1}{(1+\frac{1}{t})}\right]\right)\right\}\mathrm{d}r, \quad (3.16)$$

$$\bar{F}_e(t) = \frac{2\pi\lambda_p}{U_e}\int_0^\infty r\exp\left\{-\frac{t}{P_p}\sigma^2 r^{\alpha_p} - \pi\lambda_m\left(\frac{P_m}{P_p}\right)^{\frac{2}{\alpha_m}} r^{2\frac{\alpha_p}{\alpha_m}} \right.$$
$$\left. -\pi\lambda_p r^2\left(1+\frac{2p_e}{(\alpha_p-2)}\frac{1}{(1+\frac{1}{t})}\,{}_2F_1\left[1,1,2-\frac{2}{\alpha_p},\frac{1}{(1+\frac{1}{t})}\right]\right)\right\}$$
$$\times\left\{\exp\left(-\pi\lambda_m\left(\frac{P_m}{P_p}\right)^{\frac{2}{\alpha_m}} r^{2\frac{\alpha_p}{\alpha_m}}(B^{-\frac{2}{\alpha_m}}-1)\right)-1\right\}\mathrm{d}r. \qquad (3.17)$$

If the noise is ignored (i.e., if the network is interference-limited) and the path-loss exponents are assumed equal ($\alpha_m = \alpha_p = \alpha$), then $\bar{F}_m(t)$, $\bar{F}_o(t)$ and $\bar{F}_e(t)$ can be simplified as follows:

$$\bar{F}_m(t) = U_m^{-1}\left\{1+\frac{2p_m}{(\alpha-2)}\frac{1}{(1+\frac{1}{t})}\,{}_2F_1\left[1,1,2-\frac{2}{\alpha},\frac{1}{(1+\frac{1}{t})}\right]+\frac{\lambda_p}{\lambda_m}\left(\frac{P_p}{P_m}B\right)^{\frac{2}{\alpha}}\right.$$
$$\left.\times\left(1+\frac{2p_o}{(\alpha-2)}\frac{1}{(1+\frac{B}{t})}\,{}_2F_1\left[1,1,2-\frac{2}{\alpha},\frac{1}{(1+\frac{B}{t})}\right]\right)\right\}^{-1}, \qquad (3.18)$$

$$\bar{F}_o(t) = U_o^{-1}\left\{1+\frac{\lambda_m}{\lambda_p}\left(\frac{P_m}{P_p}\right)^{\frac{2}{\alpha}}+\frac{2}{(\alpha-2)}\frac{1}{(1+\frac{1}{t})}\right.$$
$$\left.\times\,{}_2F_1\left[1,1,2-\frac{2}{\alpha},\frac{1}{(1+\frac{1}{t})}\right]\left(p_o+\frac{\lambda_m p_m}{\lambda_p}\left(\frac{P_m}{P_p}\right)^{\frac{2}{\alpha}}\right)\right\}^{-1}, \qquad (3.19)$$

$$\bar{F}_e(t) = U_e^{-1}\left[\left\{1+\frac{2p_e}{(\alpha-2)}\frac{1}{(1+\frac{1}{t})}\,{}_2F_1\left[1,1,2-\frac{2}{\alpha_p},\frac{1}{(1+\frac{1}{t})}\right]\right.\right.$$
$$\left.+\frac{\lambda_m}{\lambda_p}\left(\frac{P_m}{P_p}\right)^{\frac{2}{\alpha}}\right\}^{-1}-\left\{1+\frac{\lambda_m}{\lambda_p}\left(\frac{P_m}{P_pB}\right)^{\frac{2}{\alpha}}\right.$$
$$\left.\left.+\frac{2p_e}{(\alpha-2)}\frac{1}{(1+\frac{1}{t})}\,{}_2F_1\left[1,1,2-\frac{2}{\alpha_p},\frac{1}{(1+\frac{1}{t})}\right]\right\}^{-1}\right]. \qquad (3.20)$$

Proof. The proof is given in Appendix A.2. □

These conditional SINR distributions can also be interpreted as the conditional coverage probability because $\mathbb{P}(\mathrm{SINR}_l > \tau)$ is the probability that a randomly chosen user can achieve the target SINR τ under the condition that the user belongs to $\mathbf{\Phi}_u^l$.

Unlike the SINR distribution in [21], in this chapter, the distribution is also dependent on the user density and the degree of resource partitioning, apart from

association bias. In the full-load model, the impact of biasing on SINR distribution is only due to the associated users' geometry (i.e., with biased association, only the very good geometry users are served by macro cells while the pico users now also include worse geometry users). In this work, biasing also affects the interference power through the cell load. Thus, the impact of biasing on SINR distribution is better captured than in [21]. The SINR distribution of the unbiased pico users is also dependent on the association bias unlike that in [21] as the interference from the macro tier to the unbiased pico users depends on biasing. These claims will be verified through the numerical results in Figure 3.2.

The special case of no resource partitioning will be addressed next so that the average data rate with resource partitioning can be compared against the no resource partitioning case, subsequently quantifying the gain.

3.3.1 Special Case: CRE without Resource Partitioning

If no resource partitioning is applied, the pico users need not be categorized as unbiased and range-expanded users because they are served from the same pool of total L subchannels in each pico cell. Let U_p denotes the probability that a randomly chosen user is a pico user. Then,

$$U_p = 1 - U_m,$$

where U_m is the probability that a randomly chosen user is a macro user, and is derived in Lemma 1. The total users in the network can thus be divided into two sets: $\mathbf{\Phi}_u^m$, the set of macro users, and $\mathbf{\Phi}_u^p$, the set of pico users. $\mathbf{\Phi}_u^m$ and $\mathbf{\Phi}_u^p$ are independent PPPs of densities $U_m\lambda_u$ and $U_p\lambda_u$, respectively.

With no resource partitioning, each macro BS can access all the available subchannels in the system to serve its users (i.e., a total of L subchannels). Meanwhile, in each pico cell, as explained earlier, the users (either the unbiased or the range-expanded users) are served from the same pool of L subchannels. The cell loads of a typical macro BS and a typical pico BS, denoted by p_m and p_p, respectively, are thus given by

$$p_j = 1 - \frac{3.5^{3.5}}{\Gamma(3.5)} \frac{1}{L} \sum_{n=0}^{L-1} \left[\frac{(L-n)\Gamma(3.5+n)(U_j\lambda_u/\lambda_j)^n}{n!(U_j\lambda_u/\lambda_j + 3.5)^{3.5+n}} \right], \forall j \in \{m, p\}. \quad (3.21)$$

In any macro or pico cell, if the total associated users are less than L, all the users can exclusively occupy a subchannel; otherwise, the subchannels have to be time-shared among the users. The average time shares received by a typical macro user and a typical pico user, denoted by T_m and T_p, respectively, are given by

$$T_j = \frac{L\lambda_j}{U_j\lambda_u}\left(1 - \left(1 + 3.5^{-1}U_j\lambda_u/\lambda_j\right)^{-3.5}\right) - \frac{3.5^{3.5}}{\Gamma(3.5)}\sum_{n=1}^{L}\frac{\Gamma(3.5+n)\left(U_j\lambda_u/\lambda_j\right)^{n-1}(L-n)}{n!\left(U_j\lambda_u/\lambda_j + 3.5\right)^{3.5+n}}, \forall j \in \{m,p\}. \tag{3.22}$$

The average user data rate per unit bandwidth for the case with no resource partitioning can finally be expressed as

$$\bar{R} = U_m T_m C_m + U_p T_p C_p, \tag{3.23}$$

where $C_j = \mathbb{E}\left[\log_2(1 + \text{SINR}_m\right)$, and $C_p = \mathbb{E}\left[\log_2(1 + \text{SINR}_p\right)$ are the spectral efficiencies of a typical user u located at the origin when it belongs to $\mathbf{\Phi}_u^m$ and $\mathbf{\Phi}_u^p$, respectively. The corresponding SINRs are given by

$$\text{SINR}_m = \frac{P_m h_{b_m} D_m^{-\alpha_m}}{P_m \sum\limits_{x_m \in \mathbf{\Psi}_m \setminus b_m} h_{x_m}||x_m||^{-\alpha_m} + P_p \sum\limits_{x_p \in \mathbf{\Psi}_p} h_{x_p}||x_p||^{-\alpha_p} + \sigma^2}, \tag{3.24}$$

$$\text{SINR}_p = \frac{P_p h_{b_p} D_p^{-\alpha_p}}{P_m \sum\limits_{x_m \in \mathbf{\Psi}_m} h_{x_m}||x_m||^{-\alpha_m} + P_p \sum\limits_{x_p \in \mathbf{\Psi}_p \setminus b_p} h_{x_p}||x_p||^{-\alpha_p} + \sigma^2}, \tag{3.25}$$

where b_j is the serving BS at a distance D_j from u when $u \in \mathbf{\Phi}_u^j$, $j \in \{m,p\}$. $\mathbf{\Psi}_m$ and $\mathbf{\Psi}_p$ are the sets of macro and pico BSs respectively, that are active on the subchannel the user u is being served on, and they are PPPs with densities $p_m\lambda_m$ and $p_p\lambda_p$, respectively. As in Lemma 5, the spectral efficiencies can be derived as

$$C_j = \frac{1}{\ln 2}\int_0^\infty \frac{\bar{F}_j(t)}{1+t}dt, \forall j \in \{m,p\}, \tag{3.26}$$

where, $\bar{F}_m(t)$ and $\bar{F}_p(t)$ are given by

$$\bar{F}_m(t) = \frac{2\pi\lambda_m}{U_m}\int_0^\infty r\exp\left\{-\frac{t}{P_m}\sigma^2 r^{\alpha_m} - \pi\lambda_p\left(\frac{P_p}{P_m}\right)^{\frac{2}{\alpha_p}} r^{2\frac{\alpha_m}{\alpha_p}} \times\left(B^{\frac{2}{\alpha_p}} + \frac{2p_p}{(\alpha_p-2)}\frac{B^{\frac{2}{\alpha_p}}}{(1+\frac{B}{t})}\,{}_2F_1\left[1,1,2-\frac{2}{\alpha_p},\frac{1}{(1+\frac{B}{t})}\right]\right) -\pi\lambda_m r^2\left(1+\frac{2p_m}{(\alpha_m-2)}\frac{1}{(1+\frac{1}{t})}\,{}_2F_1\left[1,1,2-\frac{2}{\alpha_m},\frac{1}{(1+\frac{1}{t})}\right]\right)\right\}\mathrm{d}r, \tag{3.27}$$

$$\bar{F}_p(t) = \frac{2\pi\lambda_p}{U_p}\int_0^\infty r\exp\left\{-\frac{t}{P_p}\sigma^2 r^{\alpha_p} - \pi\lambda_m\left(\frac{P_m}{P_p}\right)^{\frac{2}{\alpha_m}} r^{2\frac{\alpha_p}{\alpha_m}} \times\left(B^{-\frac{2}{\alpha_m}} + \frac{2p_m}{(\alpha_m-2)}\frac{B^{-\frac{2}{\alpha_m}}}{(1+\frac{1}{Bt})}\,{}_2F_1\left[1,1,2-\frac{2}{\alpha_m},\frac{1}{1+\frac{1}{Bt}}\right]\right) -\pi\lambda_p r^2\left(1+\frac{2p_p}{(\alpha_p-2)}\frac{1}{(1+\frac{1}{t})}\,{}_2F_1\left[1,1,2-\frac{2}{\alpha_p},\frac{1}{(1+\frac{1}{t})}\right]\right)\right\}\mathrm{d}r. \tag{3.28}$$

If the network is interference limited (i.e., if the noise can be ignored) and $\alpha_m = \alpha_p = \alpha$, simplified expressions for $\bar{F}_m(t)$ and $\bar{F}_p(t)$ can be obtained as follows.

$$\bar{F}_m(t) = U_m^{-1}\left\{1+\frac{2p_m}{(\alpha-2)}\frac{1}{(1+\frac{1}{t})}\,{}_2F_1\left[1,1,2-\frac{2}{\alpha},\frac{1}{1+\frac{1}{t}}\right] + \frac{\lambda_p}{\lambda_m}\left(\frac{P_p}{P_m}B\right)^{2/\alpha} \times\left(1+\frac{2p_p}{(\alpha-2)}\frac{1}{(1+\frac{B}{t})}\,{}_2F_1\left[1,1,2-\frac{2}{\alpha},\frac{1}{1+\frac{B}{t}}\right]\right)\right\}^{-1}, \tag{3.29}$$

$$\bar{F}_p(t) = U_p^{-1}\left\{1+\frac{2p_p}{(\alpha-2)}\frac{1}{(1+\frac{1}{t})}\,{}_2F_1\left[1,1,2-\frac{2}{\alpha},\frac{1}{1+\frac{1}{t}}\right] + \frac{\lambda_m}{\lambda_p}\left(\frac{P_m}{P_pB}\right)^{2/\alpha} \times\left(1+\frac{2p_m}{(\alpha-2)}\frac{1}{(1+\frac{1}{Bt})}\,{}_2F_1\left[1,1,2-\frac{2}{\alpha},\frac{1}{1+\frac{1}{Bt}}\right]\right)\right\}^{-1}. \tag{3.30}$$

Remark: The results for the case of neither biasing nor resource partitioning can be found by substituting $B = 1$ in the above results.

3.4 Simulation and Numerical Results

In this section, we present numerical analysis and validation of our analytical results. Unless otherwise stated, we choose $L = 20$, $\lambda_m = 1\text{BS}/\text{km}^2$, $P^m_{\text{max}} = 46$

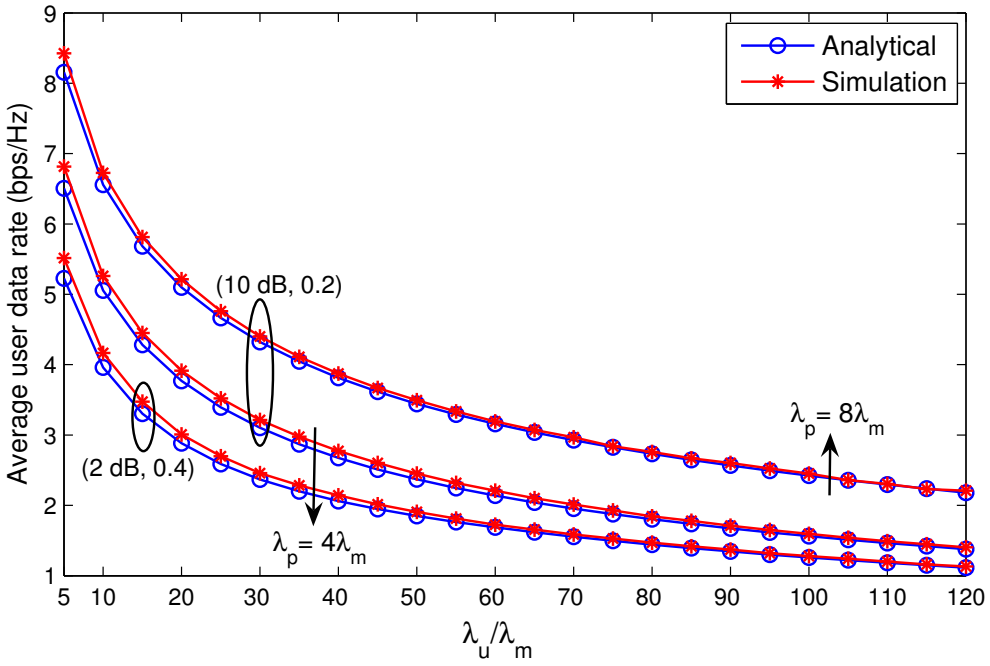

Figure 3.1: Validation of the analytical result for average user data rate (3.11) via Monte Carlo simulations for different values of user density λ_u, pico cell density λ_p, and association bias and resource partitioning fraction (B, μ).

dBm, $P^p_{\text{max}} = 30$ dBm, $\sigma^2 = -109$ dBm, $\alpha_m = 3.5$ and $\alpha_p = 4$. The degree of resource partitioning is expressed by the fraction $\mu = L_r/L$.

The average user data rate (3.11) is validated in Figure 3.1 via Monte Carlo simulations on a square window of $20 \times 20\,\text{km}^2$. This figure reveals that the analytical results match the simulation results quite well. The small gaps are mainly due to the approximation for the cell area distribution.

Before numerically analyzing the average user data rate, we first analyze the conditional coverage probabilities (3.15)-(3.17) so that the data rate trends can be better understood. Figure 3.2 shows that the coverage probability of unbiased pico users increases with the increase in bias because when more macro users are offloaded to the pico tier, the cell load p_m of the macro tier decreases and so does the interference from the macro tier. Similarly, for macro users and range-expanded pico users, apart from the users' geometry, the variation in the coverage probability with bias is mainly due to the change in p_m and p_e. The coverage probability of each user type decreases as the user density increases because more BSs become active

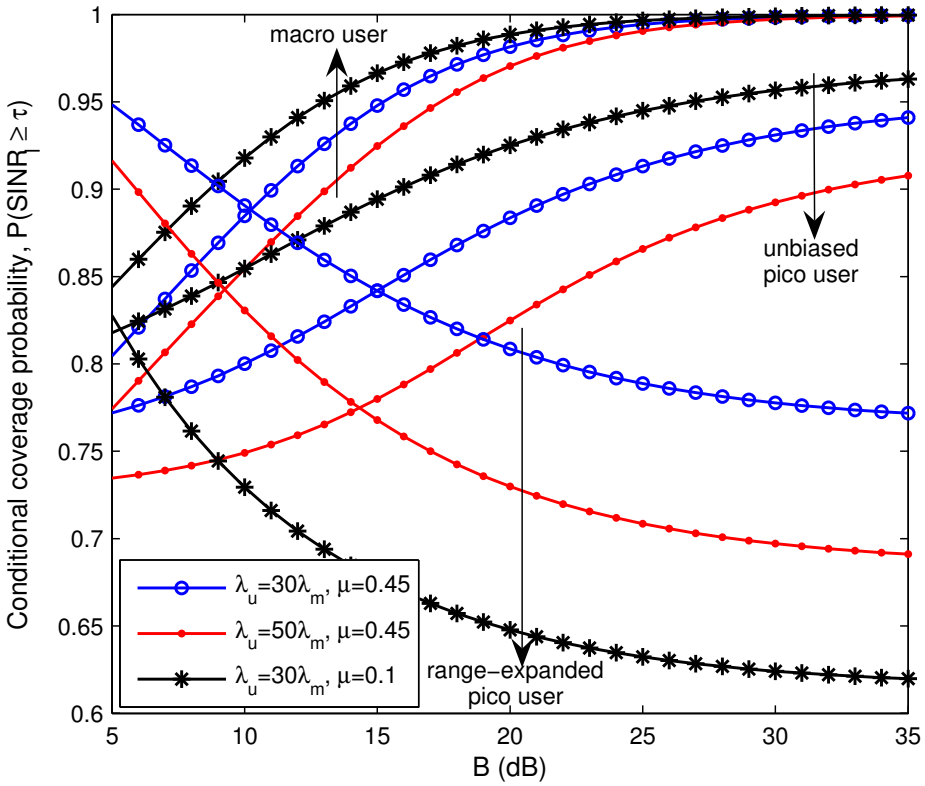

Figure 3.2: Impact of association bias B, user density λ_u and resource partitioning fraction μ on conditional coverage probabilities of macro user and both types of pico user (unbiased and range-expanded): $\lambda_p = 4\lambda_m$, $\tau = 0.5$.

to serve the increased number of users, and the increase in BS activity increases the network interference. We can observe that the resource partitioning fraction μ directly impacts the coverage probability. As μ decreases, more subchannels become available for the macro users and unbiased pico users. As a result, p_m and p_o decreases, consequently increasing the coverage probabilities of macro and unbiased pico users due to the decrease in interference. The coverage probability of range-expanded users, on the other hand, decreases due to the increase in p_e.

In Figure 3.3, the average user data rate of biased association with and without resource partitioning is compared against that of unbiased association with different load conditions. In our model, the network load is directly proportional to the user density. The user data rate decreases with an increasing load due to the increase in interference and the decrease in the users' share of resources. In biased association without resource partitioning, the SINR of the offloaded users degrades.

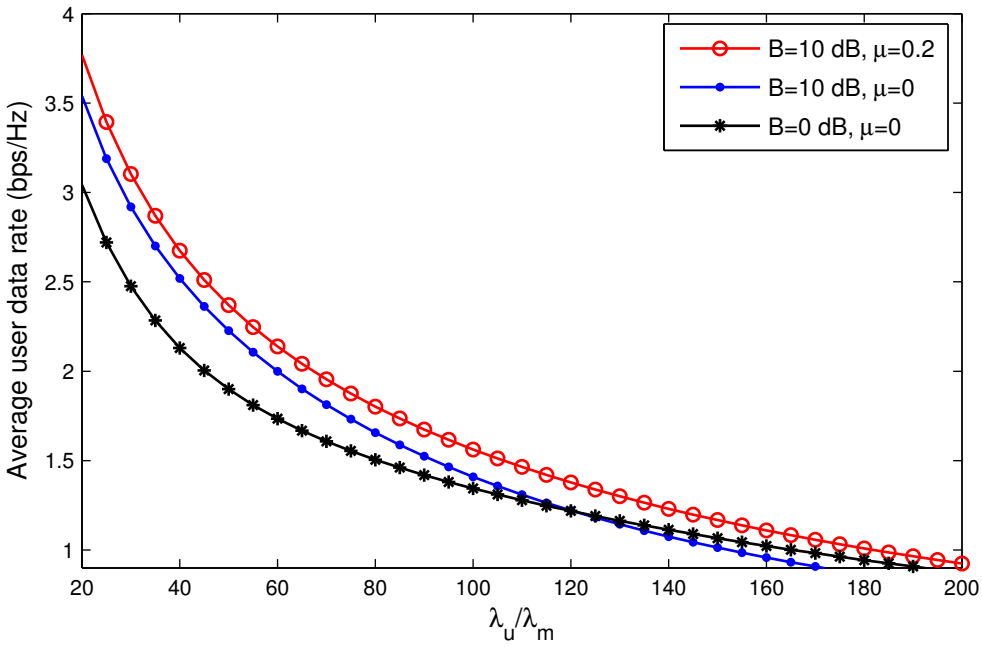

Figure 3.3: Effect of CRE with and without resource partitioning on user data rate, as user density is varied: $\lambda_p = 4\lambda_m$

However, in a lightly loaded network, they are offloaded to BSs offering the higher share of resources, and thus, the user data rate improves compared to that with unbiased association. However, when the network is heavily loaded, the decrease in SINR dominates, and the unbiased association outperforms the biasing. The SINR degradation of the offloaded users can be compensated by resources partitioning. The resource partitioning fraction of 0.2, for example, is shown to outperform no-resource-partitioning scenario in terms of average user data rate in Figure 3.3 in any load condition.

Since resource partitioning costs the macro tier its available resources, the resource partitioning fraction μ must be coordinated within the network for the optimal user data rate. The optimal pair (B, μ) for the given network parameters is investigated in Figure 3.4. The pair is found to be strongly dependent on the user density (i.e., the network load). For $\lambda_u = 30\lambda_m$, the optimal pair is $(29\text{dB}, 0.45)$, while for $\lambda_u = 100\lambda_m$, the optimal pair is $(30\text{dB}, 0.1)$.

With resource partitioning, for the given value of μ, the average link spectral efficiency C_m of a typical macro user increases with the increase in bias because

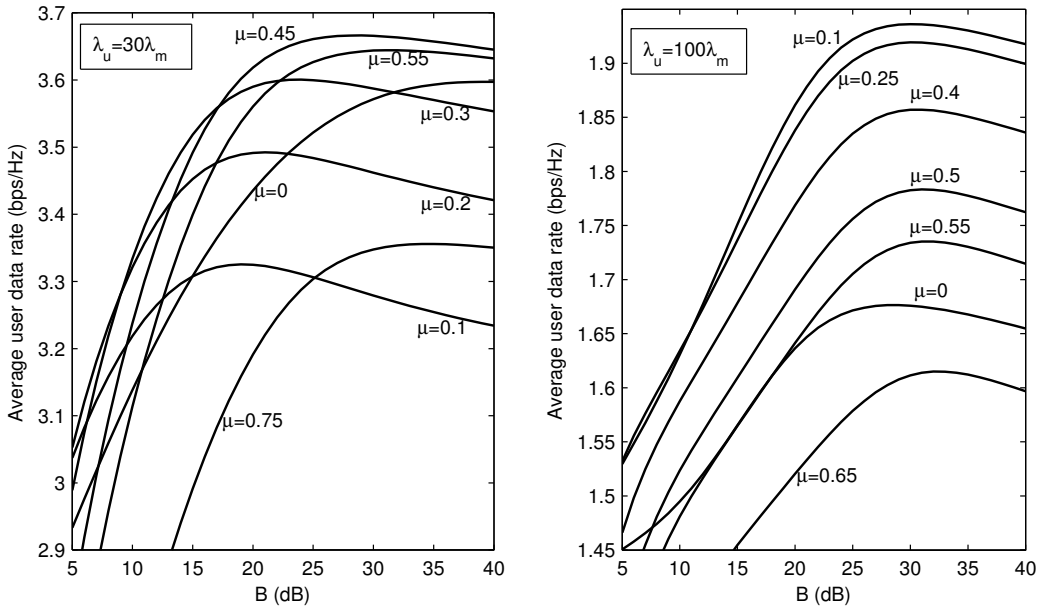

Figure 3.4: Average user data rate vs. association bias B for different values of resource partitioning fraction μ in lightly loaded (left) and heavily loaded (right) network conditions: $\lambda_p = 4\lambda_m$, $\alpha_m = \alpha_p = 4$, $\sigma^2 = 0$.

more macro users with low SINR (the users far from the serving macro BS) are offloaded to pico cells, and the interference from other macro cells also decreases due to the decrease in the macro cell load. Note that the interference from the pico tier is invariant to biasing because the pico cell load in the resource group S_c is independent of bias. Meanwhile, the share of the radio resources received by the macro users also increases. Thus, the contribution of the macro users towards the average data rate increases with the increase in bias. However, after a certain association bias, this contribution eventually decreases due to the decreasing fraction of macro users. Similarly, the contribution from the range-expanded pico users initially increases with an increase in bias due to the increasing fraction of range-expanded users, but eventually decreases after a certain bias due to the decrease in the average link spectral efficiency C_e and the increase in the number of users sharing the resources. The decrease in C_e occurs because more users with low SINR (the users far from the prospective pico BS) are associated with the pico cell, and in the meantime, the interference from other pico cells increases due to the increase in the pico cell load in the resource group S_r. On the other hand, the fraction of unbi-

ased pico users is invariant to biasing and hence, so is the share of radio resources received by the unbiased users. However, with increasing bias, the contribution to the average data rate from these unbiased users significantly increases because of the decreasing macro-tier interference as a result of the decrease in the macro cell load. Overall, the average data rate initially increases with the increase in bias, but decreases beyond a certain association bias, and hence, the optimal bias exists.

Figure 3.5 reveals that for the case with resource partitioning, the optimal bias increases with increasing μ because more resources are reserved for the offloaded users. For $\lambda_u = 30\lambda_m$ (a lightly loaded network), the optimal bias lies in the range of 19 dB and above as μ increases from 0.1, whereas it lies in the range of 30 dB and above for $\lambda_u = 100\lambda_m$ (a heavily loaded network).

With no resource partitioning (i.e., $\mu = 0$), the contribution from the macro users to the average user data rate varies with bias in the same way as in the case of resource partitioning. The contribution from the pico users, however, has a different variation as both the unbiased and range-expanded users are now served from the same pool of L subchannels. The average link spectral efficiency C_p of a randomly selected pico user (either unbiased or range-expanded) initially drops as more users with poor SINR (users with higher average received power from the nearest macro BS as compared to the nearest pico BS) are associated with the pico cell. However, beyond a certain bias, the decreasing macro-tier interference causes C_p to improve. If the increasing fraction of pico users dominates the initial drop in C_p and the decreasing share of radio resources, the contribution from the pico users to the average data rate increases with increasing bias. Otherwise, the contribution may drop initially, but eventually increases as C_p improves. When the number of pico users sharing the resources become large, the contribution towards the average user rate subsequently decreases. The initial drop in the contribution from the pico users towards average user data rate is the reason for the initially low rate of increase in the average user data rate for $\lambda_u = 100\lambda_m$ in Figure 3.5.

The optimal bias values for $\lambda_u = 30\lambda_m$ and $\lambda_u = 100\lambda_m$ are found to be 39 dB and 29 dB, respectively, with $\mu = 0$ in Figure 3.4. Thus, with no resource partitioning, the optimal bias decreases with increasing user density, as large bias

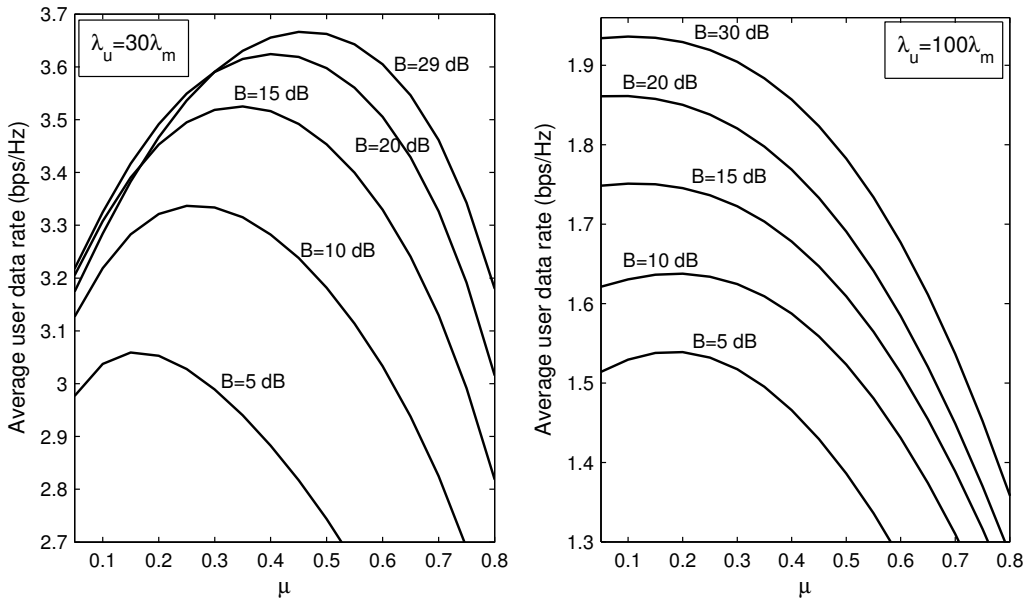

Figure 3.5: Average user data rate vs. resource partitioning fraction μ for different values of association bias B in lightly loaded (left) and heavily loaded (right) network conditions: $\lambda_p = 4\lambda_m$, $\alpha_m = \alpha_p = 4$, $\sigma^2 = 0$.

values will make the pico cells overly congested with poor SINR users in a heavily loaded network.

The variation of the average user data rate with the resource partitioning fraction μ for the given bias value is plotted in Figure 3.5. As previously explained while analyzing the conditional coverage probabilities in Figure 3.2, the cell loads p_m and p_o increase with increasing μ. The average spectral efficiency of a typical macro user thus decreases with increasing μ due to the increasing interference from the macro and pico tiers as a result of the increasing cell load, and so does the average spectral efficiency of a typical unbiased pico user. This effect, together with the decrease in the average share of the radio resources received by the users, causes the average data rate of both the macro and unbiased pico users to decrease with the increasing μ. On the other hand, as more subchannels are available for the range-expanded pico users with increasing μ, their average data rate increases. The net result is the initial increase in the average data rate with increasing μ and the subsequent decrease beyond a certain value of μ. With the full-load assumption, the spectral efficiency would be independent of μ, and the data rate would vary due

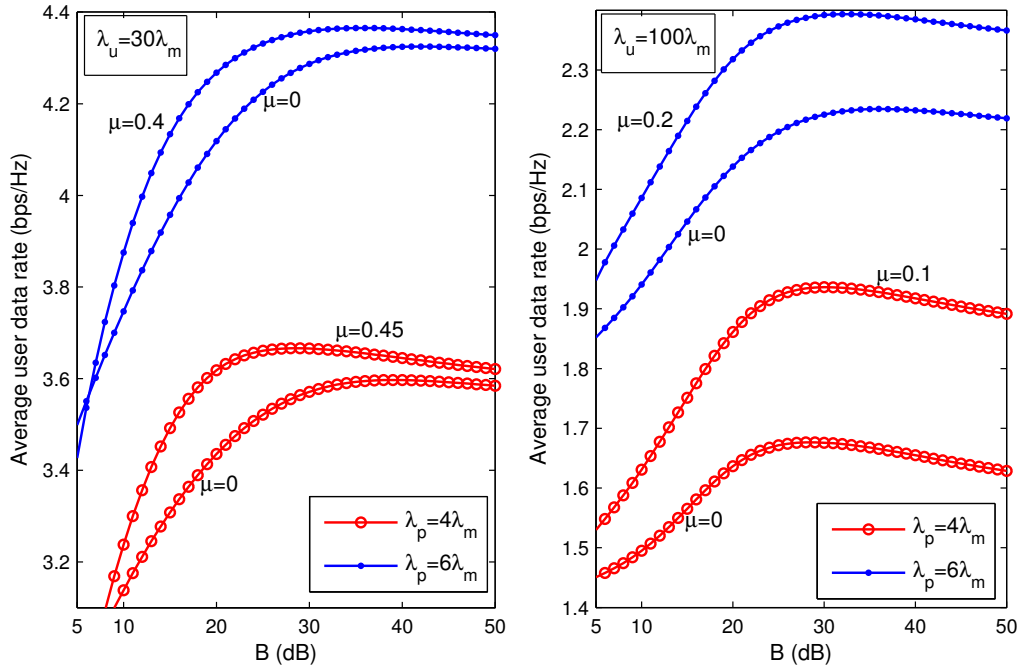

Figure 3.6: Effect of pico cell density λ_p on the optimal choices of association bias B and resource partitioning fraction μ in lightly loaded (left) and heavily loaded (right) network conditions: $\alpha_m = \alpha_p = 4$, $\sigma^2 = 0$.

to only the change in the users' share of the radio resources.

Figure 3.5 shows that in a lightly loaded network ($\lambda_u = 30\lambda_m$), the optimal resource partitioning fraction shifts towards higher values as association bias increases, whereas in a heavily loaded network ($\lambda_u = 100\lambda_m$), it shifts towards lower values. Thus, in a heavily loaded network, when a large number of macro users are offloaded to pico cells, allocating more resources to serve these offloaded users highly degrades the rate of the remaining macro users and unbiased pico users instead of improving the average data rate. Hence, a lower resource partitioning fraction is desirable.

In Figure 3.6, we analyze how small cell density affects the optimal choices of the association bias and resource partitioning fraction. It is clearly visible from the figure that, irrespective of the user density and association bias, the average user data rate always increases with an increase in pico cell density as the number of users served by each BS decreases, and thus, users get access to a larger fraction of resources. With no resource partitioning, whether the network is lightly or heavily

loaded, the optimal bias is found to increase as the pico cell density increases. The optimal bias increased from 39 dB to 42 dB for $\lambda_u = 30\lambda_m$ and 29 dB to 36 dB for $\lambda_u = 100\lambda_m$ when λ_p changed from $4\lambda_m$ to $6\lambda_m$. With resource partitioning, the optimal pair (B, μ) changed from $(29\text{dB}, 0.45)$ to $(36\text{dB}, 0.4)$ for $\lambda_u = 30\lambda_m$ and $(30\text{dB}, 0.1)$ to $(33\text{dB}, 0.2)$ for $\lambda_u = 100\lambda_m$ as λ_p increased from $4\lambda_m$ to $6\lambda_m$. When λ_p further increased to $8\lambda_m$, the optimal pairs for $\lambda_u = 30\lambda_m$ and $\lambda_u = 100\lambda_m$ were found to be $(38\text{dB}, 0.3)$ and $(34\text{dB}, 0.25)$, respectively (not shown in the figure). Thus, as in the case with no resource partitioning, the optimal bias increases with increasing pico cell density in both the lightly and heavily loaded network conditions. The optimal μ, however, decreases with increasing pico cell density in a lightly loaded network.

3.5 Conclusion

We developed an analytical framework to evaluate the downlink performance of cellular HetNets with CRE and resource partitioning in a multi-channel environment, while taking the cell load into account. The incorporated cell load model effectively captured the impact of user offloading and resource partitioning on network interference. The performance was evaluated in terms of the average user data rate that could be achieved over the entire network. We observed that if CRE is supported by resource partitioning, the average user data rate can be highly increased. However, the bias value B and resource partitioning fraction μ must be carefully tuned. With the optimal pair (B, μ), the gain can be as high as 115%. Our analysis showed that the optimal pair must be updated in accordance with the changing network load.

Chapter 4

Performance Analysis of SDMA with Inter-tier Interference Nulling in HetNets

The downlink performance of two-tier (macro/pico) multi-antenna HetNets employing SDMA technique is analyzed in this chapter[1]. The number of users simultaneously served with SDMA by a BS in a resource block depends on the number of active users in its cell, with the maximum served users limited to $L_{\max}$. Due to the feasibility of deploying a large number of antennas at the macro BS because of its physical size, we propose to utilize the excess spatial degrees of freedom for interference nulling to pico users from their corresponding nearest (dominant) macro BSs. The precoding matrix at the macro BS thus, not only considers user multiplexing in its own cell, but also interference nulling to selected pico users. The SINR coverage probability, rate distribution and average data rate of a typical user are then derived. Our results demonstrate that the proposed interference-nulling scheme has strong potential for improving performance. However, the critical system parameters such as the association bias and number of dedicated antennas at the macro BS for serving its own users must be carefully tuned. The optimal $L^*_{\max}$ for both the macro and pico tier which maximize the average data rate is also investigated and is found to outperform both SU-BF and full-SDMA. Finally, the impact of CSI quantization error due to limited feedback is analyzed.

[1] A part of this chapter has been accepted for publication in the proceedings of the IEEE International Conference on Communications (ICC) 2016, Kuala Lampur, Malaysia [95]. A journal version has been submitted to the IEEE Transactions on Wireless Communications [96].

4.1 Introduction and Motivation

In Chapter 3, we analyzed the gain in the average data rate due to the load balancing realized by CRE, together with resource partitioning method of interference coordination in single-antenna HetNets. As multi-antenna techniques are well-known to improve the spectral efficiency of wireless systems, the data rates can be further improved by deploying multiple antennas in HetNets. Multi-antenna communication has been an integral feature of cellular standards LTE (3GPP Release 8) [32] and LTE-Advanced (3GPP Release 10) [33]. BSs equipped with multiple antennas can utilize the additional spatial degrees of freedom for diversity, signal power boosting through beamforming, multiplexing (single-user or multi-user), interference suppression/mitigation or a combination of these.

Multi-antenna techniques in general for isolated links without any interfering source have been extensively studied. Some examples of diversity- and array-gain oriented techniques are space-time coding [34, 35], and SNR maximization through coherent processing at the multi-antenna transmitter/receiver, known as beamforming [97]. The potential of multi-antenna systems to transmit independent data streams simultaneously over spatial sub-channels, a technique known as spatial multiplexing is explored in [36], and the trade-off between the diversity and multiplexing gain is analyzed in [98]. Multi-user spatial multiplexing, also known as SDMA which allows multiple users to be served simultaneously on the same time/frequency resource has also been analyzed [37, 99]. Cellular systems, however, are interference limited. Moreover, the interference scenarios in HetNets are rather complex compared to those in conventional networks. The effectiveness of spatial multiplexing is demonstrated to diminish in the presence of interference in [100]. However, if the available spatial degrees of freedom due to multiple antennas are intelligently utilized to suppress/mitigate interference along with diversity and multiplexing, the performance of HetNets can be improved. The interactions between multi-antennas techniques and HetNets for enhanced data rate have not been sufficiently explored yet, as very few attempts have been made to study their coexistence. In this chapter, we develop a tractable framework for analyzing down-

link multi-antenna HetNets employing ZF precoding for SDMA along with an interference nulling scheme for inter-tier interference coordination. The developed framework considers generic SDMA and thus, allows SU-BF and full-SDMA to be analyzed as special cases.

4.1.1 Previous Related Work and Contributions of the Chapter

The SINR coverage of SU-BF is compared with ZF precoding based closed-loop SDMA under the perfect CSI assumption for a two-tier multi-antenna HetNet in [101] by considering a single fixed-radius circular macro cell with multiple femto cells of fixed radii, distributed according to PPP within the macro cell. However, since BS-user association is not considered and macro-tier interference is ignored, the insights in [101] may not be accurate for practical HetNets. The coverage probability and average link spectral efficiency, spatially averaged over a given cell of known radius and guard region are derived for ZF precoding in multi-antenna HetNet in [102]. Unlike the spatial averaging over a given cell in [102], system-wide spatial averaging is considered in [103] and the upper bounds on coverage probability of ZF SDMA and SU-BF in a multi-tier HetNet are derived. The research in [103] is further extended in [104] to derive the ordering results for the coverage probability and rate per user performance of SDMA, SU-BF and single-antenna transmission by using tools from stochastic orders. While the analyses in [103, 104] are based on maximum instantaneous SINR based BS-user association, which may lead to unnecessary handovers, known as the ping-pong effect, BS-user association rules that are intended to maximize the average receive SINR (and thus, the SINR coverage), and biased association for optimal rate coverage are proposed in [105]. The performance of SDMA, SU-BF and single-antenna transmission are then compared. In all of these works [101–105], each cell of a tier is assumed to be serving the same number of users with SDMA, say L, and it can be any arbitrary integer in the interval $[1, K_i]$, where K_i is the number of antennas at a BS of the ith tier. This assumption is not suitable for cellular networks since the number of users in a cell, which depends on user distribution, is generally different from that in another cell. An open-loop SDMA with each antenna serving an independent data stream to its

user with the limiting requirement that the number of users in each cell must be at least equal to the number of transmit antennas is analyzed in [106] for two-tier cellular HetNets with MMSE receivers.The performance of an open-loop SDMA with ZF and MMSE receivers in single-tier cellular networks with a similar limitation is analyzed in [107]. In this chapter, rather than fixing the number of users served with SDMA to an arbitrary value, we set the limit only on the maximum number of users served, say $L_{\max}$. If the number of users is below the limit, all the users are served; otherwise only $L_{\max}$ users chosen randomly are served.

One of the key challenges in cellular HetNets is inter-cell interference management. Due to the huge disparities in transmit power between macro and small-cell nodes such as picos and femtos, and proactive user offloading from macro to small cells, interference management between the macro and pico/femto tiers is very important because the performance of the small-cell users on the cell edge could be severely degraded. While interference management techniques such as ABSF [21, 24, 47, 48] and frequency-domain resource partitioning [25, 85] can be used, interference can be more efficiently managed without compromising time-frequency resources by using multiple antennas. In this chapter, we analyze a ZF-precoding based *interference-nulling* method for inter-tier interference management. Due to the physical size of macro BSs, it is more feasible to have a larger number of antennas at the macro BS than at the low-power BSs. Thus, the idea is to utilize the extra degrees of freedom at the macro BSs to suppress the interference from the macro tier to small-cell users through nulling. Compared to other multicell processing techniques for interference mitigation such as joint transmission [108] and transmission point selection [109], which require both user data and CSI to be shared between the coordinated BSs, interference nulling requires only CSI to be shared. In [110] interference nulling to U offloaded pico users by each macro BS is analyzed, where the optimal U for maximum rate coverage is also investigated. However, unlike [110] which considers a single served user per resource block in each cell of both the macro and pico tiers, we consider a user-distribution dependent SDMA scheme. SU-BF with interference nulling to a fixed number of neighboring-cells users at each BS of any tier for general multi-tier HetNets is analyzed in [111],

without specifying how these users are selected. SU-BF with interference nulling in single-tier cellular networks is studied in [30, 31]. Although SU-BF with interference nulling has been relatively well analyzed, to the best of our knowledge, this thesis is the first work to analyze a user-distribution dependent SDMA scheme with interference nulling in cellular HetNets. The main contributions of this chapter are summarized as follows.

1. We develop a tractable framework to analyze a user-distribution dependent SDMA scheme in a two-tier (macro/pico) multi-antenna HetNet with a ZF precoding transmission, in which the number of users simultaneously served by a BS in a resource block depends on the number of active users in its cell, with the maximum number of served users limited to L^m_{max} for the macro tier and L^p_{max} for the pico tier. The performance of SU-BF and full-SDMA can be analyzed by taking $L^l_{\text{max}} = 1$ and $L^l_{\text{max}} = K_l$, respectively, for each $l \in \{m, p\}$, where K_m and K_p are the number of antennas at the macro and pico BS, respectively.

2. An interference-nulling scheme for suppressing macro-to-pico interference is investigated, in which a ZF precoder at each active macro BS nulls the interference to at most $K_m - T_{\text{min}}$ active pico users while serving its at most L^m_{max} scheduled users, where T_{min} is the number of dedicated antennas at each macro BS for serving its own users. An active macro BS b receives requests for interference nulling from those active pico users, each of which has b as its nearest interfering macro BS.

3. Unlike most of the previous work, we do not assume all the BSs of each tier to be simultaneously active all the time. In this work, BS activity depends on user distribution.

4. In multi-antenna HetNets, since different BSs employ different precoders, the BS-user association is not as simple as in single-antenna networks. In [110, 111], antenna precoding is ignored in BS-user association by assuming that the reference signal used for association is transmitted from single an-

tenna with full transmit power. Various association rules for coverage probability maximization and load balancing are proposed in [105]. However, they are based on the assumption that a deterministic fixed number of users are served with SDMA in each cell. Hence, these association rules do not apply to our proposed SDMA scheme, and a different biased-nearest-distance based association rule is introduced in this chapter, where the bias value accounts for antenna precoding and transmit power disparities, as well as load balancing.

5. We derive the SINR and rate distributions, as well as the average data rate of a typical user. T_{min} is an important design parameter because it determines the spatial degrees of freedom available for the macro users, and also the probability that the macro interference to a typical pico user is nulled. The optimal value of T_{min} for a given performance metric is thus numerically investigated in this chapter. The numerical results demonstrate that the proposed interference-nulling scheme has strong potential for performance improvement if T_{min} is carefully tuned. The optimal values of L^m_{max} and L^p_{max} which maximize the average data rate are also investigated and are found to outperform both SU-BF and full-SDMA.

6. Finally, the impact of the CSI quantization error due to limited feedback for the special case of $L^m_{\text{max}} = L^p_{\text{max}} = 1$ is also investigated.

The chapter is organized as follows. Section 4.2 presents the network model, user association policy, proposed interference-nulling scheme and precoding matrices. Section 4.3 derives the SINR coverage probability. The rate distribution and average user data rate are derived in Section 4.4. In Section 4.5, the impact of limited feedback is investigated. The analytical results are validated through Monte-Carlo simulations in Section 4.6, along with extensive numerical analysis for assessing the impact of various parameters on network performance. Finally, Section 4.7 concludes the chapter.

4.2 System Model

We consider the downlink of a two-tier multi-antenna HetNet comprising macro and pico BSs spatially distributed on $\mathbb{R}^2$ plane as independent homogeneous PPPs $\mathbf{\Phi}_m$ with density λ_m and $\mathbf{\Phi}_p$ with density λ_p, respectively. The macro BSs are equipped with K_m transmit antennas, and the pico BSs with K_p antennas. Similarly, users are assumed to be distributed according to an independent PPP $\mathbf{\Phi}_u$ with density λ_u, and each has a single receive antenna. The two network tiers share the same spectrum with the universal frequency reuse.

The transmission scheme is SDMA with ZF precoding applied at each BS to serve multiple users simultaneously in each RB. We assume only one RB per time slot. As the BSs and users are independently distributed on the $\mathbb{R}^2$ plane, the number of users in different cells is different. Thus, in our proposed SDMA scheme, a typical active macro cell with $N_m \geq 1$ users serves $M_m = \min(N_m, L^M_{\text{max}})$ users simultaneously in a given time slot, where L^M_{max} is the maximum number of users it can serve. If $N_m > L^M_{\text{max}}$, the BS choses L^M_{max} users for service randomly, else, all N_m users are served. Similarly, $M_p = \min(N_p, L^P_{\text{max}})$ users are simultaneously served by a typical active pico cell in a given time slot, which has $N_p \geq 1$ users, and L^P_{max} is the maximum number the pico cell can serve. The macro and pico BSs transmit to each of their users with power P_m and P_p, respectively.

4.2.1 User Association

According to the user association rule introduced in [105], a typical user at the origin is associated with the nearest pico BS if $P_p\sqrt{\Delta_p\tau_p}X_p^{-\alpha} \geq P_m\sqrt{\Delta_m\tau_m}X_m^{-\alpha}$, and otherwise, is associated with the nearest macro BS, where $X_m = \min\limits_{x_m\in\mathbf{\Phi}_m} \|x_m\|$ and $X_p = \min\limits_{x_m\in\mathbf{\Phi}_p} \|x_p\|$ are the distances from the origin to the nearest macro and pico BSs, respectively. If associated with the macro tier, Δ_m is the average desired channel gain from the nearest macro BS, and τ_p is the average interference channel gain from the nearest pico BS. Similarly, Δ_p and τ_m are the corresponding parameters, if associated with the pico tier. The average gains of the desired and interference channels depend on the number of users served with SDMA. This association rule

is thus not suitable for our proposed SDMA scheme, where the number of users served with SDMA in each cell is a function of the number of users in that cell. The number of users, on the other hand, is determined by the association rule. The above rule however can be equivalently expressed as follows: a user is associated with the pico tier only if

$$X_m \geq \left(\frac{P_m}{P_p}\right)^{\frac{1}{\alpha}} \left(\frac{1}{\eta}\right)^{\frac{1}{\alpha}} X_p \Rightarrow X_m \geq \rho X_p, \tag{4.1}$$

where $\rho = (\frac{P_m}{P_p}\frac{1}{\eta})^{\frac{1}{\alpha}}$, $\eta = \sqrt{\frac{\Delta_p \tau_p}{\Delta_m \tau_m}}$. This rule can be perceived as biased nearest distance association, where the biasing is due to the transmit power disparity between the macro and pico tiers, the difference in average channel gains to a typical user from the nearest macro and pico BSs, and for load balancing as well. We will investigate the optimal value of η for the average data rate in Section Section 4.6. This value, in turn, determines the optimal ρ.

Given that X_m and X_p are Rayleigh RVs with mean $1/(2\sqrt{\lambda_m})$ and $1/(2\sqrt{\lambda_p})$, respectively [57], the probability that a typical user at the origin is associated with the pico tier is

$$A_p = \mathbb{P}(X_m \geq \rho X_p) = \frac{\lambda_p}{\lambda_p + \lambda_m \rho^2}, \tag{4.2}$$

and the probability that this user is associated with the macro tier is $A_m = 1 - A_p$.

These tier association probabilities are also valid for any randomly selected user. As per the given association scheme, the total set of users in the network, $\mathbf{\Phi}_u$ can be divided into two disjoint subsets: $\mathbf{\Phi}_u^m$ and $\mathbf{\Phi}_u^p$, the set of macro and pico users, respectively. A_m and A_p can be interpreted as the average number of users belonging to $\mathbf{\Phi}_u^m$ and $\mathbf{\Phi}_u^p$, respectively. As we are interested in the number of users in a typical cell, rather than the actual locations of users, $\mathbf{\Phi}_u^m$ and $\mathbf{\Phi}_u^p$ can be equivalently modeled as independent PPPs with density $A_m\lambda_m$ and $A_p\lambda_p$ respectively. Since each macro user is always associated with the nearest macro BS and each pico-user with the nearest pico BS, the network can be viewed as a superposition of two independent Voronoi tessellations of macro and pico tiers. The distribution of the number of users associated with a typical macro and pico BS is derived next.

Lemma 6. *Let the number of users in a randomly chosen macro and pico cell be*

denoted by U_m and U_p, respectively. Their PMFs are given by

$$\mathbb{P}(U_l = n) = \frac{3.5^{3.5}\Gamma(3.5+n)(A_l\lambda_u/\lambda_l)^n}{\Gamma(3.5)n!(A_l\lambda_u/\lambda_l+3.5)^{n+3.5}}, n \geq 0, \forall l \in \{m, p\}, \tag{4.3}$$

Proof. Given that the area of a typical macro/pico Voronoi cell is Y, U_l is Poisson distributed with mean $A_l\lambda_u Y$. The PMF of U_l in (4.3) is obtained by integrating the conditional distribution of U_l over the probability density function (PDF) of Y approximated as Gamma$(3.5, (3.5\lambda_l)^{-1})$ [94]. □

A BS without any user associated does not transmit at all and is inactive. The following corollary gives the PMFs of the number of users in a typical cell of macro and pico tiers, under the condition that it is active.

Corollary 1. *The PMFs of the number of users in a randomly chosen active cell of the macro and pico tiers are given by*

$$\mathbb{P}(N_l = n) = \frac{\mathbb{P}(U_l = n)\mathbf{1}(n \geq 1)}{p_l}, \forall l \in \{m, p\}, \tag{4.4}$$

where p_m and p_p are the probabilities that a typical BS of the macro and pico tiers, respectively, is active, and are given by

$$p_l = 1 - \mathbb{P}(U_l = 0) = 1 - \left(1 + 3.5^{-1}\frac{A_l\lambda_u}{\lambda_l}\right)^{-3.5}, \forall l \in \{m, p\}. \tag{4.5}$$

Let the sets of active macro and active pico BSs be denoted by $\mathbf{\Psi}_m$ and $\mathbf{\Psi}_p$, respectively. $\mathbf{\Psi}_m$ and $\mathbf{\Psi}_p$ are thinned versions of the original PPPs $\mathbf{\Phi}_m$ and $\mathbf{\Phi}_p$, respectively, and hence are independent PPPs with densities $p_m\lambda_m$ and $p_p\lambda_p$, respectively.

By using corollary 1, the PMFs of the number of users simultaneously served by a typical active macro BS and a typical active pico BS in a given time slot $M_l = \min(N_l, L^l_{\text{max}})$ for $L^l_{\text{max}} > 1$ can be obtained as

$$\mathbb{P}(M_l = n) = \begin{cases} \mathbb{P}(N_l = n), & 1 \leq n < L^l_{\text{max}} \\ 1 - \sum_{k=1}^{L^l_{\text{max}}-1} \mathbb{P}(N_l = k), & n = L^l_{\text{max}}, \end{cases} \quad \forall l \in \{m, p\}, \tag{4.6}$$

For the special case of $L^l_{\text{max}} = 1, \mathbb{P}(M_l = 1) = 1, \forall l \in \{m, p\}$.

4.2.2 Interference Nulling

We assume that K_m is typically much larger than K_p. By using the interference nulling strategy, the additional spatial degrees of freedom of macro BSs can be utilized to suppress the strong macro interference to pico users. Thus, we propose that each served pico user requests its nearest active macro BS to perform interference nulling. As interference nulling costs macro BSs their available degrees of freedom for their own users, we assume that each macro BS can handle at most $K_m - T_{\text{min}}$ requests only, in order to ensure that a macro BS has at least $T_{\text{min}} \geq L^M_{\text{max}}$ antennas dedicated for serving its own users. Hence, if Q_m requests are received by a typical active macro BS, it will perform interference nulling to $\mathcal{O} = \min(Q_m, K_m - T_{\text{min}})$ pico users. For $Q_m > (K_m - T_{\text{min}})$, the BS will randomly choose $K_m - T_{\text{min}}$ pico users. Hence, not all interference-nulling requests are satisfied.

The number of interference-nulling requests Q_m received by a typical active macro BS is equal to the number of served pico users within a typical Voronoi cell Υ of the tessellation formed by $\mathbf{\Psi}_m$. Although the number of pico users served by a typical active pico BS cannot exceed L^p_{max}, Q_m is unbounded because the number of active pico BSs within Υ is Poisson distributed with mean $p_p\lambda_p/(p_m\lambda_m)$. In order to derive the PMF of Q_m, we first derive $\mathbb{E}[M_p] = A_p\vartheta_p\lambda_u/(p_p\lambda_p)$, where

$$\vartheta_p = \frac{L^p_{\text{max}} p_p\lambda_p}{A_p\lambda_u} - \frac{3.5^{3.5}}{\Gamma(3.5)} \sum_{k=1}^{L^p_{\text{max}}-1} \left[\frac{\Gamma(3.5+n)}{n!} \frac{(A_p\lambda_u/\lambda_p)^{n-1}(L^p_{\text{max}} - k)}{(A_p\lambda_u/\lambda_p + 3.5)^{n+3.5}} \right]. \quad (4.7)$$

Next, we approximate the set of pico users requesting interference coordination $\mathbf{\Psi}^p_u$ as a PPP with density $A_p\vartheta_p\lambda_u$ so that $\mathbb{E}[Q_m] = A_p\vartheta_p\lambda_u/(p_m\lambda_m)$. Note that for $L^p_{\text{max}} = 1$, $\vartheta_p = \frac{p_p\lambda_p}{A_p\lambda_u}$. By using this approximation, the PMF of Q_m is derived below as the number of points of the PPP $\mathbf{\Psi}^p_u$ within a typical Voronoi cell Υ with an average area $(p_m\lambda_m)^{-1}$.

Lemma 7. *The PMF of the number of interference nulling requests received by a typical active macro BS is given by*

$$\mathbb{P}(Q_m = n) = \frac{3.5^{3.5}\Gamma(3.5+n)\left(\frac{A_p\vartheta_p\lambda_u}{p_m\lambda_m}\right)^n}{\Gamma(3.5)n!\left(\frac{A_p\vartheta_p\lambda_u}{p_m\lambda_m} + 3.5\right)^{n+3.5}}, n \geq 0. \quad (4.8)$$

As explained earlier, not all interference nulling requests received by an active macro BS get satisfied because $K_m - T_{\min}$ is the upper limit on the number of requests the BS can handle. Let χ denotes the set of pico users whose interference nulling requests to their corresponding nearest active macro BSs are satisfied. In the following lemma, we derive the probability that a randomly chosen pico user in service belongs to χ.

Lemma 8. *The probability φ that the interference-nulling request made by a randomly chosen pico user to its nearest active macro BS is fulfilled is given by*

$$\varphi = \frac{(K_m - T_{min})p_m\lambda_m}{A_p\vartheta_p\lambda_u}\left(1 - \left(1 + 3.5^{-1}\frac{A_p\vartheta_p\lambda_u}{p_m\lambda_m}\right)^{-3.5}\right) - \frac{3.5^{3.5}}{\Gamma(3.5)}\sum_{n=1}^{K_m - T_{min}} \frac{\Gamma(3.5+n)\left(\frac{A_p\vartheta_p\lambda_u}{p_m\lambda_m}\right)^{n-1}(K_m - T_{min} - n)}{n!\left(\frac{A_p\vartheta_p\lambda_u}{p_m\lambda_m} + 3.5\right)^{n+3.5}} \tag{4.9}$$

Proof. Let Q'_m denotes the number of other requests received by the macro BS, which received nulling request from a randomly chosen pico user. Then, conditioned on Q'_m, $\varphi = 1$ if $Q'_m + 1 \leq K_m - T_{\min}$; otherwise, $\varphi = (K_m - T_{\min})/(Q'_m + 1)$. Thus, φ can be expressed as

$$\begin{aligned}\varphi &= \sum_{n=0}^{K_m - T_{\min} - 1} \mathbb{P}(Q'_m = n) + \sum_{n=K_m - T_{\min}}^{\infty} \frac{K_m - T_{\min}}{n+1}\,\mathbb{P}(Q'_m = n) \\ &= \sum_{n=1}^{\infty} \frac{K_m - T_{\min}}{n}\,\mathbb{P}(Q'_m = n-1) - \sum_{n=1}^{K_m - T_{\min}} \left(\frac{K_m - T_{\min}}{n} - 1\right)\mathbb{P}(Q'_m = n-1).\end{aligned} \tag{4.10}$$

By using the fact that the conditional PDF $f'_Y(y)$ of the area of a Voronoi cell given that a randomly chosen user belongs to it is equal to $cyf_Y(y)$, where $f_Y(y)$ is the unconditional PDF and c is a constant such that $\int_o^\infty f'_Y(y)dy = 1$ [21], the PMF of Q'_m can be derived as $\mathbb{P}(Q'_m = n) = (n+1)\mathbb{P}(Q_m = n+1)/\mathbb{E}[Q_m]$, $n \geq 0$. Eqn. (4.9) then follows by substituting the PMF of Q'_m in (4.10), where the first term is further simplified by using $\sum_{n=1}^{\infty}\mathbb{P}(Q_m = n) = 1 - \mathbb{P}(Q_m = 0)$. □

4.2.3 Channel Model and Precoding Matrices

For independent unit-mean Rayleigh multipath fading between any transmit-receive antenna pair and standard power law path-loss with exponent α, the received signal

z_m at a typical user u located at the origin if $u \in \mathbf{\Phi}_u^m$ is given by

$$z_m = \sqrt{P_m} D_m^{-\frac{\alpha}{2}} \mathbf{h}_{b_m,1}^* \mathbf{W}_{b_m} \mathbf{s}_{b_m} + \sum_{q \in \{m,p\}} \sqrt{P_q} \sum_{x_q \in \mathbf{\Psi}_q \setminus b_m} ||x_q||^{-\frac{\alpha}{2}} \mathbf{g}_{x_q,1}^* \mathbf{W}_{x_q} \mathbf{s}_{x_q} + n_m, \tag{4.11}$$

where b_m is the serving macro BS at a distance D_m, which is serving M'_m other users simultaneously, $\mathbf{h}_{b_m,1} \sim \mathcal{CN}(\mathbf{0}_{K_m \times 1}, \mathbf{I}_{K_m})$ and $\mathbf{g}_{x_q,1} \sim \mathcal{CN}(\mathbf{0}_{K_q \times 1}, \mathbf{I}_{K_q})$ are the desired and interference channel vectors from the tagged BS b_m and the interfering BS at x_q, respectively, $n_m \sim \mathcal{CN}(0, \sigma^2)$ is the AWGN, $\mathbf{s}_{b_m} = [s_{b_m,i}]_{1 \le i \le M'_m+1} \in \mathbb{C}^{(M'_m+1)\times 1}$ is the signal vector transmitted from b_m to its $M'_m + 1$ served users with the symbol $s_{b_m,1}$ intended for u, and $\mathbf{W}_{b_m} = [\mathbf{w}_{b_m,i}]_{1 \le i \le (M'_m+1)} \in \mathbb{C}^{K_m \times (M'_m+1)}$ is the corresponding precoding matrix.

Let the channel vectors from the tagged BS b_m to its M'_m users other than u be represented by $[\mathbf{h}_{b_m,i}]_{2 \le i \le M'_m+1}$, and the interference channel vector from the tagged BS to $\mathcal{O} = \min(Q_m, K_m - T_{\text{min}})$ pico users chosen for interference nulling by $\mathbf{F} = [\mathbf{f}_i]_{1 \le i \le \mathcal{O}} \in \mathbb{C}^{K_m \times \mathcal{O}}$. Under the perfect CSI assumption, ZF precoding vectors $\mathbf{W}_{b_m} = [\mathbf{w}_{b_m,i}]_{1 \le i \le (M'_m+1)}$ are designed such that $|\mathbf{h}_{b_m,j}^* \mathbf{w}_{b_m,j}|^2$ is maximized for each $j = 1, 2, \ldots, M'_m + 1$, while satisfying the orthogonality conditions $\mathbf{h}_{b_m,j}^* \mathbf{w}_{b_m,i} = 0$ for $\forall i \neq j$ and $\mathbf{f}_i^* \mathbf{w}_{b_m,j} = 0, \forall i = 1, 2, \ldots, \mathcal{O}, \forall j = 1, 2, \ldots, M'_m + 1$. It can be achieved by choosing $\mathbf{w}_{b_m,i}$ in the direction of the projection of $\mathbf{h}_{b_m,i}$ on $\text{Null}\big([\mathbf{h}_{b_m,j}]_{1 \le j \le (M'_m+1), j \neq i}, [\mathbf{f}_i]_{1 \le i \le \mathcal{O}}\big)$. The nullspace is $K_m - M'_m - \mathcal{O}$ dimensional. Under Rayleigh fading, the desired channel power $\beta_{b_m} = |\mathbf{h}_{b_m,1}^* \mathbf{w}_{b_m,1}|^2 \sim \text{Gamma}(\Delta_m, 1)$, where $\Delta_m = K_m - M'_m - \mathcal{O}$ [112]. Given that an interfering macro BS at x_m is serving M_m users simultaneously, $\mathbf{W}_{x_m} = [\mathbf{w}_{x_m,i}]_{1 \le i \le M_m} \in \mathbb{C}^{K_m \times M_m}$, and it is calculated independent of $\mathbf{g}_{x_m,1}$. Thus, $\mathbf{g}_{x_m,1}^* \mathbf{w}_{x_m,1}, \mathbf{g}_{x_m,1}^* \mathbf{w}_{x_m,2}, \ldots, \mathbf{g}_{x_m,1}^* \mathbf{w}_{x_m,M_m}$ are i.i.d. complex Gaussian RVs, and their squared norms are i.i.d. exponential RVs. The interference channel power $\zeta_{x_m} = ||\mathbf{g}_{x_m,1}^* \mathbf{W}_{x_m}||^2 \sim \text{Gamma}(M_m, 1)$, as it is a sum of M_m i.i.d. exponential RVs [104].

A possible choice of $\mathbf{W}_{b_m} = [\mathbf{w}_{b_m,i}]_{1 \le i \le (M'_m+1)}$ is the normalized columns of $\tilde{\mathbf{H}}_{b_m} (\tilde{\mathbf{H}}_{b_m}^* \tilde{\mathbf{H}}_{b_m})^{-1}$, which is a pseudo inverse of $\tilde{\mathbf{H}}_{b_m}^*$, where $\tilde{\mathbf{H}}_{b_m} = [\tilde{\mathbf{h}}_{b_m,i}]_{1 \le i \le (M'_m+1)} \in \mathbb{C}^{K_m \times (M'_m+1)}$, $\tilde{\mathbf{h}}_{b_m,i} = (\mathbf{I}_{K_m} - \mathbf{F}(\mathbf{F}^*\mathbf{F})^{-1}\mathbf{F}^*)\mathbf{h}_{b_m,i}$, being the projection of $\mathbf{h}_{b_m,i}$ on

the nullspace of $\mathbf{F} = [\,\mathbf{f}_i\,]_{1\leq i\leq \mathcal{O}}$.

Similarly, the received signal z_p at u when $u \in \mathbf{\Phi}_u^p$ is

$$z_p = \sqrt{P_p} D_p^{-\frac{\alpha}{2}} \mathbf{h}_{b_p,1}^* \mathbf{W}_{b_p} \mathbf{s}_{b_p} + \sum_{q\in\{m,p\}} \sqrt{P_q} \sum_{x_q \in \mathbf{\Psi}_q \setminus \{v_m, b_p\}} ||x_q||^{-\frac{\alpha}{2}} \mathbf{g}_{x_q,1}^* \mathbf{W}_{x_q} \mathbf{s}_{x_q} + \xi + n_p, \tag{4.12}$$

where

$$\xi = \begin{cases} 0, & \text{if } u \in \chi \\ \sqrt{P_m} V_m^{-\frac{\alpha}{2}} \mathbf{g}_{v_m,1}^* \mathbf{W}_{v_m} \mathbf{s}_{v_m}, & \text{if } u \notin \chi; \end{cases} \tag{4.13}$$

b_p is the serving pico BS at a distance D_p, which is serving M_p' other users simultaneously; $n_p \sim \mathcal{CN}(0, \sigma^2)$ is AWGN, v_m is the nearest active macro BS to u at a distance V_m, which receives an interference-nulling request from u. The ZF precoding vectors $\mathbf{W}_{b_p} = [\mathbf{w}_{b_p,i}]_{1\leq i\leq (M_p'+1)}$ are given by the normalized columns of $\mathbf{H}_{b_p}(\mathbf{H}_{b_p}^* \mathbf{H}_{b_p})^{-1}$, where $\mathbf{H}_{b_p} = [\mathbf{h}_{b_p,i}]_{1\leq i\leq (M_p'+1)} \in \mathbb{C}^{K_p \times (M_p'+1)}$ is the channel matrix from the tagged BS b_p to its $M_p' + 1$ served pico users. The desired channel power $\beta_{b_p} = ||\mathbf{h}_{b_p,1}^* \mathbf{W}_{b_p}||^2 = |\mathbf{h}_{b_p,1}^* \mathbf{w}_{b_p,1}|^2 \sim \text{Gamma}(\Delta_p, 1)$, where $\Delta_p = K_m - M_p'$, and the interference channel power $\zeta_{x_p} = ||\mathbf{g}_{x_p,1}^* \mathbf{W}_{x_p}||^2 \sim \text{Gamma}(M_p, 1)$ given that the interfering pico BS at x_p is serving M_p users simultaneously.

4.2.4 Distance to the Serving BS and the BS Receiving Interference Nulling Request

The distance D_l to the serving BS from a typical user $u \in \mathbf{\Phi}_u^l$ is a RV, and the corresponding PDFs for each $l \in \{m, p\}$ are derived in the following lemma.

Lemma 9. *The PDF $f_{D_m}(r)$ of the distance D_m between the serving macro BS and a typical user u when $u \in \mathbf{\Phi}_u^m$ is given by*

$$f_{D_m}(r) = \frac{2\pi\lambda_m}{A_m} r \exp(-\pi(\lambda_m + \lambda_p/\rho^2) r^2), \tag{4.14}$$

and the PDF $f_{D_p}(r)$ of the distance D_p between the serving pico BS and a typical user u when $u \in \mathbf{\Phi}_u^p$ is given by

$$f_{D_p}(r) = \frac{2\pi\lambda_p}{A_p} r \exp(-\pi(\lambda_m \rho^2 + \lambda_p) r^2). \tag{4.15}$$

Proof. Given that $u \in \mathbf{\Phi}_u^m$, D_m is the distance to the nearest macro BS from u. The cumulative distribution function (CDF) $F_{D_m}(r) = \mathbb{P}(D_m \leq r)$ is thus given by

$$F_{D_m}(r) = \mathbb{P}(X_m \leq r | u \in \mathbf{\Phi}_u^m) = \frac{\mathbb{P}(X_m \leq r, u \in \mathbf{\Phi}_m^m)}{\mathbb{P}(u \in \mathbf{\Phi}_u^m)}$$
$$= \frac{1}{A_m} \int_0^r \mathbb{P}\Big(X_p > \frac{y}{\rho}\Big) f_{X_m}(y) dy. \tag{4.16}$$

By differentiating (4.16) with respect to r, we obtain

$$f_{D_m}(r) = \frac{\mathrm{d}F_{D_m}(r)}{\mathrm{d}r} = \frac{1}{A_m} \mathbb{P}\Big(X_p > \frac{r}{\rho}\Big) f_{X_m}(r). \tag{4.17}$$

The final expression of $f_{D_m}(r)$ in (4.14) is obtained by using the probability distributions of X_m and X_p, which are Rayleigh RVs with mean $1/(2\sqrt{\lambda_m})$ and $1/(2\sqrt{\lambda_p})$, respectively. The PDF $f_{D_p}(r)$ in (4.15) is similarly derived. □

Another quantity of interest is the distance V_m between a typical pico user in service and its nearest active macro BS to which it requests interference nulling.

Lemma 10. *The conditional PDF of the distance V_m between a typical user $u \in \mathbf{\Phi}_u^p$ and the macro BS to which it request interference nulling, given that its distance to the serving pico BS is $D_p = r$, is given by*

$$f_{V_m|D_p}(r_1|r) = 2\pi p_m \lambda_m r_1 \exp\left(-\pi p_m \lambda_m (r_1^2 - \rho^2 r^2)\right), \quad r_1 > \rho r. \tag{4.18}$$

Proof. Given that $u \in \mathbf{\Phi}_u^p$, V_m is the distance to the nearest active macro BS. The conditional CCDF of V_m is thus given by

$$\bar{F}_{V_m|D_p}(r_1|r) = \mathbb{P}(X'_m \geq r_1 | u \in \mathbf{\Phi}_u^p, D_p = r) = \mathbb{P}(X'_m \geq r_1 | X_m > \rho r), \tag{4.19}$$

where $X'_m = \min_{x_m \in \mathbf{\Psi}_m} \|x_m\|$ is the distance from the origin to the nearest active macro BS. The condition $X_m > \rho r$ implies that no points of $\mathbf{\Phi}_m$ are within a circle of radius ρr. Thus, no points of $\mathbf{\Psi}_m$ as well are within ρr because $\mathbf{\Psi}_m$ is the thinned version of $\mathbf{\Phi}_m$. Since X'_m is the distance to the nearest active macro BS, $\mathbb{P}(X'_m \geq r_1) = \mathbb{P}(\text{No active macro BS is closer than } r_1)$. Thus, given that no active macro BS is closer than ρr, the probability of no active macro BS closer than r_1 is equal to the probability that no points of $\mathbf{\Psi}_m$ are within an annulus centered at the

origin with inner radius ρr and outer radius r_1. The conditional CCDF $\bar{F}_{V_m|Dp}(r_1|r)$ thus can be expressed as

$$\bar{F}_{V_m|D_p}(r_1|r) = \exp\left(-\pi p_m \lambda_m (r_1^2 - \rho^2 r^2)\right). \tag{4.20}$$

The conditional PDF of V_m in (4.18) is obtained by differentiating (4.20) with respect to r_1. □

4.3 SINR Coverage Analysis

The SINR coverage probability is defined as the probability that the SINR of a typical user is greater than a threshold γ, which is a minimum SINR level required to establish the connection. Mathematically, the SINR coverage is defined as $\mathrm{P}(\gamma) = \mathbb{P}(\text{SINR} > \gamma)$, where the SINR of a typical user is given by $\text{SINR} = \sum_{l\in\{m,p\}} \mathbf{1}(u \in \mathbf{\Phi}_u^l)\, \text{SINR}_l$. From (4.11) and (4.12) and the discussion that follows, the SINR of a typical user u at the origin when it belongs to $\mathbf{\Phi}_u^l$ can be expressed as

$$\text{SINR}_l = \frac{P_l \beta_{b_l} D_l^{-\alpha}}{I_{b_l,m} + I_{b_l,p} + \sigma^2}, \quad \forall l \in \{m,p\}, \tag{4.21}$$

where $I_{b_l,m}$ and $I_{b_l,p}$ are the interference powers from the macro and pico tiers, respectively when $u \in \mathbf{\Phi}_u^l$, $l \in \{m,p\}$, and are given by

$$\begin{aligned}
I_{b_m,m} &= P_m \sum_{x_m \in \mathbf{\Psi}_m \setminus b_m} \zeta_{x_m} ||x_m||^{-\alpha}, \\
I_{b_m,p} &= P_p \sum_{x_p \in \mathbf{\Psi}_p} \zeta_{x_p} ||x_p||^{-\alpha}, \\
I_{b_p,m} &= \begin{cases} P_m \sum\limits_{x_m \in \mathbf{\Psi}_m \setminus v_m} \zeta_{x_m} ||x_m||^{-\alpha} & \text{if } u \in \chi \\ P_m \sum\limits_{x_m \in \mathbf{\Psi}_m} \zeta_{x_m} ||x_m||^{-\alpha} & \text{if } u \notin \chi, \end{cases} \\
I_{b_p,p} &= P_p \sum_{x_p \in \mathbf{\Psi}_p \setminus b_p} \zeta_{x_p} ||x_p||^{-\alpha}.
\end{aligned} \tag{4.22}$$

By using the law of total probability, the SINR coverage probability of a typical user u is

$$\mathrm{P}(\gamma) = \mathrm{P}_m(\gamma) A_m + \mathrm{P}_p(\gamma) A_p, \tag{4.23}$$

where $A_l = \mathbb{P}(u \in \mathbf{\Phi}_u^l)$, $l \in \{m, p\}$ is the tier association probability derived in Section 4.2.1, and $\mathrm{P}_m(\gamma) = \mathbb{P}(\mathrm{SINR}_m > \gamma | u \in \mathbf{\Phi}_u^m)$, and $\mathrm{P}_p(\gamma) = \mathbb{P}(\mathrm{SINR}_p > \gamma | u \in \mathbf{\Phi}_u^p)$ are the conditional coverage probabilities of the user u when associated with the macro and pico tiers, respectively. In order to evaluate the coverage probability, we first derive the LT of the total interference power received by u.

Lemma 11. *The LT $\mathcal{L}_{I_{b_p}}(s)$ of the total interference power $I_{b_p} = I_{b_p,m} + I_{b_p,p}$ received by u when $u \in \mathbf{\Phi}_u^p$ conditional on $D_p = r$ and $V_m = r_1$ is given by*

$$\mathcal{L}_{I_{b_p}}(s) = \left(\varphi \mathcal{L}^1_{I_{b_p,m}}(s) + (1-\varphi)\mathcal{L}^2_{I_{b_p,m}}(s)\right) \mathcal{L}_{I_{b_p,p}}(s), \tag{4.24}$$

where $\mathcal{L}^1_{I_{b_p,m}}(s) = \mathcal{L}_{I_{b_p,m}}(s|u \in \chi)$, and $\mathcal{L}^2_{I_{b_p,m}}(s) = \mathcal{L}_{I_{b_p,m}}(s|u \notin \chi)$ are the LTs of $I_{b_p,m}$ conditional on $u \in \chi$ and $u \notin \chi$, respectively, and $\mathcal{L}_{I_{b_p,p}}(s)$ is the LT of $I_{b_p,p}$. The LTs are given by

$$\begin{aligned}\mathcal{L}^1_{I_{b_p,m}}(s) = \exp\Bigg\{ &- \pi p_m \lambda_m r_1^2 \Bigg(\sum_{i=1}^{L^m_{max}} \mathbb{P}(M_m = i) \\ &\times \ {}_2F_1\Big[i, -\frac{2}{\alpha}, \frac{\alpha-2}{\alpha}, -\frac{P_m s}{r_1^\alpha}\Big] - 1\Bigg)\Bigg\}, \end{aligned} \tag{4.25}$$

$$\begin{aligned}\mathcal{L}^2_{I_{b_p,m}}(s) = \exp\Bigg\{ &- \pi p_m \lambda_m \rho^2 r^2 \Bigg(\sum_{i=1}^{L^m_{max}} \mathbb{P}(M_m = i) \\ &\times \ {}_2F_1\Big[i, -\frac{2}{\alpha}, \frac{\alpha-2}{\alpha}, -\frac{P_m s}{\rho^\alpha r^\alpha}\Big] - 1\Bigg)\Bigg\}, \end{aligned} \tag{4.26}$$

$$\begin{aligned}\mathcal{L}_{I_{b_p,p}}(s) = \exp\Bigg\{ &- \pi p_p \lambda_p r^2 \Bigg(\sum_{i=1}^{L^p_{max}} \mathbb{P}(M_p = i) \\ &\times \ {}_2F_1\Big[i, -\frac{2}{\alpha}, \frac{\alpha-2}{\alpha}, -\frac{P_p s}{r^\alpha}\Big] - 1\Bigg)\Bigg\}, \end{aligned} \tag{4.27}$$

where ${}_2F_1(a, b, c, z)$ is the Gauss Hypergeometric function [113].

Proof. The proof is given in Appendix B.1. □

Similarly, the LT of $I_{b_m} = I_{b_m,m} + I_{b_m,p}$ conditional on $D_m = r$ can be derived as $\mathcal{L}_{I_{b_m}}(s) = \mathcal{L}_{I_{b_m,m}}(s)\mathcal{L}_{I_{b_m,p}}(s)$, where

$$\begin{aligned}\mathcal{L}_{I_{b_m,q}}(s) = \exp\Bigg\{ &- \pi p_q \lambda_q \varpi_{m,q}^2 \Bigg(\sum_{i=1}^{L^q_{\max}} \mathbb{P}(M_q = i) \\ &\times \ {}_2F_1\Big[i, -\frac{2}{\alpha}, \frac{\alpha-2}{\alpha}, -\frac{P_q}{\varpi_{m,q}^\alpha} s\Big] - 1\Bigg)\Bigg\}, \forall q \in \{m, p\}, \end{aligned} \tag{4.28}$$

with $\varpi_{m,m} = r$ and $\varpi_{m,p} = r/\rho$.

Having derived the LTs, we now evaluate the conditional coverage probability when $u \in \mathbf{\Phi}_u^l$, $\mathrm{P}_l(\gamma) = \mathbb{P}\left(\frac{P_l \beta_{b_l} D_l^{-\alpha}}{I_{b_l}+\sigma^2} > \gamma | u \in \mathbf{\Phi}_u^l\right)$, $\forall l \in \{m, p\}$. Conditioned on $D_l = r$, $V_m = r_1$ and $\Delta_l = n$, we have

$$\mathrm{P}_l(\gamma|r, r_1, \Delta_l = n) = \sum_{l=0}^{n-1} \frac{(\gamma r^\alpha / P_l)^l}{l!} \mathbb{E}_{I_{b_l}} \left[(I_{b_l} + \sigma^2)^l \exp\left(-\frac{\gamma r^\alpha}{P_l} (I_{b_l} + \sigma^2) \right) \right] \tag{4.29}$$

$$= \sum_{l=0}^{n-1} \frac{(-s)^l}{l!} \frac{\mathrm{d}^l}{\mathrm{d}s^l} \left(e^{-s\sigma^2} \mathcal{L}_{I_{b_l}}(s) \right) \Big|_{s=\frac{\gamma r^\alpha}{P_l}}, \tag{4.30}$$

where the first equality follows from the distribution Gamma$(n, 1)$ of β_{b_l} for a given $\Delta_l = n$, and the second is obtained by applying the differentiation property of LT. The LTs in (4.25)-(4.28) are composite functions. Thus, (4.30) requires evaluating lth derivatives of composite functions. These derivatives can be computed by using Faà di Bruno's formula. In this paper, Faà di Bruno's formula is expressed in terms of integer partition. Please note that in contrast to set partition version used in [107], the integer partition version greatly reduces the number of summations, thereby reducing the complexity of the numerical computation. Before introducing the formula, we first introduce the required integer partition notations.

4.3.1 Integer Partition and Faà di Bruno's Formula

Integer partition is a partition of a positive integer n as a sum of positive integers. The set of all possible partitions of n is represented by Ω_n, and the number of partitions is denoted by $\mathcal{P}(n)$. For example, the integer 4 can be partitioned in 5 distinct ways,

$$\Omega_4 = \{\{4\}, \{3, 1\}, \{2, 2\}, \{2, 1, 1\}, \{1, 1, 1\}\}.$$

Thus, $\mathcal{P}(4) = 5$. Let ω_i^n denotes the number of elements in the ith partition p_i^n of n. Also, let μ_{ij}^n denotes the number of positive integer $j \in \{1, 2, \ldots, n\}$ in that partition, and a_{ik}^n denotes the kth element ($k \in \{1, 2, \ldots, \omega_i^n\}$).

Example: For the second partition of integer 4 in Ω_4, i.e., $p_2^4 = \{3, 1\}$, we have $\omega_2^4 = 2$, $\mu_{21}^4 = 1$, $\mu_{22}^4 = 0$, $\mu_{23}^4 = 1$, $\mu_{24}^4 = 0$, $a_{21}^4 = 3$, $a_{22}^4 = 1$. For any partition p_i^n, we have the properties $\sum_{j=1}^n j\mu_{ij}^n = n$ and $\sum_{j=1}^n \mu_{ij}^n = \omega_i^n$.

Faà di Bruno's formula for the lth derivative of the composite function $y(t(s))$ in terms of integer partition can be expressed as

$$y_s^{(l)}(t(s)) = \sum_{o=1}^{\mathcal{P}(l)} c_o^l \, y_{t(s)}^{(\omega_o^l)}(t(s)) \prod_{q=1}^{l} \left(t_s^{(q)}(s)\right)^{\mu_{oq}^l}, \tag{4.31}$$

where

$$c_o^l = \frac{l!}{\prod_{k=1}^{\omega_o^l} a_{ok}^l! \prod_{q=1}^{l} \mu_{oq}^l!},$$

and $y_{t(s)}^{(k)}(t(s))$ is the kth derivative of the function $y(t(s))$ with respect to $t(s)$.

Theorem 2. *The coverage probability of a typical pico user u in the interference-limited scenario, i.e., $\sigma^2 = 0$, is given by*

$$\mathrm{P}_p(\gamma) = \varphi \mathrm{T}_1(\gamma) + (1-\varphi)\mathrm{T}_2(\gamma), \tag{4.32}$$

where $\mathrm{T}_1(\gamma) = \mathbb{P}(\textit{SINR}_p > \gamma | u \in \mathbf{\Phi}_u^p, u \in \chi)$ is the conditional coverage probability of a typical pico user u when $u \in \chi$, which can be computed as

$$\begin{aligned}\mathrm{T}_1(\gamma) = 2p_m\lambda_m \frac{\lambda_p}{A_p} \int_{\theta=0}^{\frac{1}{\rho}} \Bigg[& \sum_{k=0}^{L_{max}^p - 1} \mathbb{P}(M_p^{'} = k) \sum_{l=0}^{K_p-k-1} \frac{\gamma^l}{l!} \theta^{\alpha l+1} \sum_{o=1}^{\mathcal{P}(l)} c_o^l (-1)^{\omega_o^l} \\ & \prod_{q=1}^{l} \Big(p_m\lambda_m \delta^q \, \Xi_q^m(\delta,\theta,\gamma) + \frac{p_p\lambda_p}{\theta^{\alpha q-2}} \, \Xi_q^p(1,1,\gamma) \Big)^{\mu_{oq}^l} \\ & \Gamma(\omega_o^l+2) \Big(p_m\lambda_m \, \Xi_0^m(\delta,\theta,\gamma) + p_p\lambda_p\theta^2 \, \Xi_0^p(1,1,\gamma) \\ & + (1-p_m)\lambda_m\rho^2\theta^2 + (1-p_p)\lambda_p\theta^2 \Big)^{-(\omega_o^l+2)} \Bigg] \, \mathrm{d}\theta, \end{aligned} \tag{4.33}$$

and $\mathrm{T}_2(\gamma) = \mathbb{P}(\textit{SINR}_p > \gamma | u \in \mathbf{\Phi}_u^p, u \notin \chi)$, the conditional coverage probability of a typical pico user u when $u \notin \chi$, can be computed as

$$\begin{aligned}\mathrm{T}_2(\gamma) = & \frac{\lambda_p}{A_p} \sum_{k=0}^{L_{max}^p - 1} \mathbb{P}(M_p^{'} = k) \sum_{l=0}^{K_p-k-1} \frac{\gamma^l}{l!} \sum_{o=1}^{P(l)} c_o^l (-1)^{\omega_o^l} \\ & \prod_{q=1}^{l} \left(\frac{p_m\lambda_m\delta^q}{\rho^{\alpha q-2}} \, \Xi_q^m\left(\delta, \frac{1}{\rho}, \gamma\right) + p_p\lambda_p \, \Xi_q^p(1,1,\gamma) \right)^{\mu_{oq}^l} \\ & \Gamma(\omega_o^l+1) \left(p_m\lambda_m\rho^2 \, \Xi_0^m\left(\delta, \frac{1}{\rho}, \gamma\right) + p_p\lambda_p \, \Xi_0^p(1,1,\gamma) \right. \\ & \left. + (1-p_m)\lambda_m\rho^2 + (1-p_p)\lambda_p \right)^{-(\omega_o^l+1)}. \end{aligned} \tag{4.34}$$

The function $\Xi_q^l(\varsigma,\kappa,\varepsilon)$ *in the above equations is defined as*

$$\Xi_q^l(\varsigma,\kappa,\varepsilon)=\sum_{i=1}^{L_{max}^l}\left(\frac{(i)_q(-\frac{2}{\alpha})_q}{(\frac{\alpha-2}{\alpha})_q}\,{}_2F_1\Big[i+q,-\frac{2}{\alpha}+q,\frac{\alpha-2}{\alpha}+q,-\varsigma\kappa^{\alpha}\varepsilon\Big]\mathbb{P}(M_l=i)\right), \tag{4.35}$$

$(a)_q$ *is a Pochhammer symbol, and* $\delta=P_m/P_p$.

Proof. The proof is given in the Appendix B.2. □

Remark 1. *The number of other users served by the BS which is serving the typical user* $u\in\mathbf{\Phi}_u^l$ *is given by* $M_l'=\min(U_l',L_{max}^l-1)$*, where* U_l' *is the number of other users in the Voronoi cell to which the user* u *belongs. The PMF of* U_l' *can be derived in the same way as* Q'_m *in the proof of Lemma 3, and is given by* $\mathbb{P}(U_l'=n)=(n+1)\mathbb{P}(U_l=n+1)/\mathbb{E}[U_l]$*. The PMF of* M_l' *is thus different from* (4.6) *and is given by*

$$\mathbb{P}(M_l'=n)=\begin{cases}\mathbb{P}(U_l'=n), & 0\le n<L_{max}^l-1\\ 1-\sum_{k=1}^{L_{max}^l-2}\mathbb{P}(U_l'=k), & n=L_{max}^l-1,\end{cases}\qquad\forall l\in\{m,p\}. \tag{4.36}$$

For the special case of $L_{max}^l=1$, $\mathbb{P}(M_l'=0)=1,\forall l\in\{m,p\}$.

Theorem 3. *The coverage probability of a typical macro user* $\mathrm{P}_m(\gamma)$ *in the interference-limited scenario is given by*

$$\begin{aligned}\mathrm{P}_m(\gamma)=&\frac{\lambda_m}{A_m}\sum_{k=0}^{L_{max}^m-1}\mathbb{P}(M_m'=k)\sum_{n=T_{min}-k}^{K_m-k}\mathbb{P}(\Delta_m=n|M_m'=k)\sum_{l=0}^{n-1}\frac{\gamma^l}{l!}\\ &\sum_{o=1}^{\mathcal{P}(l)}c_o^l(-1)^{\omega_o^l}\prod_{q=1}^{l}\Big(p_m\lambda_m\Xi_q^m(1,1,\gamma)+p_p\lambda_p\frac{\rho^{\alpha q-2}}{\delta^q}\Xi_q^p\Big(\frac{1}{\delta},\rho,\gamma\Big)\Big)^{\mu_{oq}^l}\\ &\Gamma(\omega_o^l+1)\left(p_m\lambda_m\Xi_0^m(1,1,\gamma)+\frac{p_p\lambda_p}{\rho^2}\Xi_0^p\left(\frac{1}{\delta},\rho,\gamma\right)\right.\\ &\left.+(1-p_m)\lambda_m+(1-p_p)\frac{\lambda_p}{\rho^2}\right)^{-(\omega_o^l+1)},\end{aligned} \tag{4.37}$$

where the conditional PMF of Δ_m *conditioned on* $M_m'=k$ *for* $T_{min}<K_m$ *is given*

by

$$\mathbb{P}(\Delta_m = n|M'_m = k) = \begin{cases} 1 - \sum_{v=0}^{K_m - T_{min} - 1} \mathbb{P}(Q_m = v), & n = T_{min} - k \\ \mathbb{P}(Q_m = K_m - k - n), & T_{min} - k + 1 \leq n \leq K_m - k. \end{cases} \tag{4.38}$$

For the special case of $T_{min} = K_m$ *which implies no interference nulling,* $\Delta_m = K_m - M'_m$*, thus* $\mathbb{P}(\Delta_m = K_m - k|M'_m = k) = 1$.

Proof. $\mathrm{P}_m(\gamma)$ is derived in the same way as $\mathrm{T}_2(\gamma)$. However, since $\Delta_m = K_m - M'_m - \min(Q_m, K_m - T_{\min})$ is a function of the two RVs M'_m and Q_m, deconditioning with respect to Δ_m is achieved in two steps, first averaging over the conditional PMF of Δ_m for the given M'_m, and then averaging over the PMF of M'_m. The conditional PMF of Δ_m is derived as follows:

For $T_{\min} < K_m$,

$$\begin{aligned} \Delta_m &= K_m - M'_m - \min(Q_m, K_m - T_{\min}) \\ &= \max(K_m - M'_m - Q_m, T_{\min} - M'_m) \\ &= \begin{cases} T_{\min} - M'_m & \text{if } Q_m \geq K_m - T_{\min} \\ K_m - M'_m - Q_m & \text{otherwise.} \end{cases} \end{aligned} \tag{4.39}$$

Thus,

$$\mathbb{P}(\Delta_m = n|M'_m = k) = \begin{cases} \mathbb{P}(Q_m \geq K_m - T_{\min}), & n = T_{\min} - k \\ \mathbb{P}(Q_m = K_m - k - n), & 0 \leq (K_m - k - n) < K_m - T_{\min}. \end{cases} \tag{4.40}$$

Further simplification results in (4.38). □

Remark 2. *For the special case of* $L^m_{max} = L^p_{max} = 1$*,*

$$\mathrm{P}_p(\gamma) = \mathrm{P}_p(\gamma|M'_p = 0) = \varphi \mathrm{T}_1(\gamma|M'_p = 0) + (1 - \varphi)\mathrm{T}_2(\gamma|M'_p = 0), \tag{4.41}$$

$$\mathrm{P}_m(\gamma) = \mathrm{P}_m(\gamma|M'_m = 0), \tag{4.42}$$

where for each $l \in \{m, p\}$*,*

$$\Xi^l_q(\varsigma, \kappa, \varepsilon) = \Xi_q(\varsigma, \kappa, \varepsilon) = \frac{(1)_q(-\frac{2}{\alpha})_q}{(\frac{\alpha-2}{\alpha})_q} {}_2F_1\left(1 + q, -\frac{2}{\alpha} + q, \frac{\alpha - 2}{\alpha} + q, -\varsigma\kappa^\alpha\varepsilon\right). \tag{4.43}$$

4.4 Rate Analysis

In this section, we analyze the achievable downlink rate of a typical user. We derive the CCDF of downlink rate, also defined as the rate coverage, and the average rate of a typical user.

With adaptive modulation so that the Shannon limit can be achieved and interference treated as noise, the data rate of a typical user u is given by

$$R = \sum_{l\in\{m,p\}} S_l W \log_2(1+\text{SINR}_l)\mathbf{1}(u \in \mathbf{\Phi}_u^l), \tag{4.44}$$

where S_l is the fraction of resources received by u when $u \in \mathbf{\Phi}_u^l$. For each $l \in \{m,p\}$, given that U_l' is the number of other users in the cell to which the user u belongs, the total users in the tagged cell are $U_l'+1$. We assume one RB per time slot with total bandwidth W, and at most L_{max}^l users served simultaneously in each RB through spatial multiplexing. Thus, if the total number of users in the tagged cell is less than L_{max}^l (i.e., $U_l'+1 < L_{\text{max}}^l$), each user can utilize the entire bandwidth W without sharing; thus, $S_l = 1$. However, if $U_l'+1$ is no less than L_{max}^l (i.e., $U_l'+1 \geq L_{\text{max}}^l$), we assume that the time-frequency resources are shared equally among the total users; thus, $S_l = L_{\text{max}}^l/(U_l'+1)$. Hence, the fraction of resources received by $u \in \mathbf{\Phi}_u^l$ hence can be expressed as

$$S_l = \min\left(\frac{L_{\text{max}}^l}{U_l'+1}, 1\right).$$

Theorem 4. *The CCDF of the downlink rate of a typical user u, $\mathcal{R}(\upsilon) = \mathbb{P}(R > \upsilon)$ can be expressed as $\mathcal{R}(\upsilon) = A_m\mathcal{R}_m(\upsilon) + A_p\mathcal{R}_p$, where $\mathcal{R}_l(\upsilon) = \mathbb{P}(S_l W \log_2(1+\text{SINR}_l) > \upsilon)$ is the rate distribution of $u \in \mathbf{\Phi}_u^l$, and is given by*

$$\begin{aligned}\mathcal{R}_l(\upsilon) = &\sum_{k=0}^{L_{max}^l-2} \mathrm{P}_l\left(2^{\upsilon/W}-1\,|M_l'=k\right)\mathbb{P}(U_l'=k)\\ &+\sum_{k\geq L_{max}^l-1}\mathrm{P}_l\left(2^{\frac{\upsilon}{W}\frac{(k+1)}{L_{max}^l}}-1\,\middle|M_l'=L_{max}^l-1\right)\mathbb{P}(U_l'=k)\end{aligned} \tag{4.45}$$

Proof. By using (4.44), we have

$$\mathbb{P}(R>\upsilon) = \sum_{l\in\{m,p\}}\mathbb{P}(u\in\mathbf{\Phi}_u^l)\mathbb{P}(S_lW\log_2(1+\text{SINR}_l)>\upsilon) = A_m\mathcal{R}_m(\upsilon)+A_p\mathcal{R}_p,$$

where $A_l = \mathbb{P}(u \in \mathbf{\Phi}_u^l)$ and

$$\begin{aligned}\mathcal{R}_l(\upsilon) &= \mathbb{P}(W\log_2(1+\text{SINR}_l) > \upsilon, U_l' \leq L_{\text{max}}^l - 2) \\ &\quad + \mathbb{P}\left(\frac{L_{\text{max}}^l}{U_l'+1} W\log_2(1+\text{SINR}_l) > \upsilon, U_l' \geq L_{\text{max}}^l - 1\right) \\ &= \sum_{k=0}^{L_{\text{max}}^l-2} \mathbb{P}(\text{SINR}_l > 2^{\upsilon/W} - 1 | U_l' = k)\mathbb{P}(U_l' = k) \\ &\quad + \sum_{k \geq L_{\text{max}}^l - 1} \mathbb{P}(\text{SINR}_l > 2^{\frac{\upsilon}{W}\frac{(k+1)}{L_{\text{max}}^l}} - 1 | U_l' = k)\mathbb{P}(U_l' = k). \end{aligned} \tag{4.46}$$

Since $M_l' = \min(U_l', L_{\text{max}}^l - 1)$,

$$\mathbb{P}(\text{SINR}_l > \gamma | U_l' = k) = \begin{cases} \mathbb{P}(\text{SINR}_l > \gamma | M_l' = k), & 0 \leq k \leq L_{\text{max}}^l - 2 \\ \mathbb{P}(\text{SINR}_l > \gamma | M_l' = L_{\text{max}}^l - 1), & k \geq L_{\text{max}}^l - 1. \end{cases}$$

Equation (4.45) then follows immediately where $\mathrm{P}_l(\gamma | M_l' = k) = \mathbb{P}(\text{SINR}_l > \gamma | u \in \mathbf{\Phi}_u^l, M_l' = k)$ is the conditional SINR coverage probability of $u \in \mathbf{\Phi}_u^l$ for given $M_l' = k$. □

For the special case of $L_{\text{max}}^l = 1$, the rate distribution of $u \in \mathbf{\Phi}_u^l$ further simplifies to

$$\mathcal{R}_l(\upsilon) = \sum_{k \geq 0} \mathrm{P}_l\left(2^{\frac{\upsilon}{W}(k+1)} - 1\right) \mathbb{P}(U_l' = k). \tag{4.47}$$

After deriving the rate distribution, which gives us an idea of the average fraction of users in the network with a rate greater than a given threshold at any time, next we derive the average rate that can be achieved by any randomly chosen user.

Theorem 5. *The average data rate $\bar{R} = \mathbb{E}[R]$ of a typical user u is given by $\bar{R} = A_m\bar{R}_m + A_p\bar{R}_p$ where $\bar{R}_l = \mathbb{E}[S_l W\log_2(1+\textit{SINR}_l)]$ is the average data rate of u when it belongs to $\mathbf{\Phi}_u^l$, and is given by*

$$\begin{aligned}\bar{R}_l =& \frac{W}{\ln 2}\int_0^\infty \frac{1}{1+y}\Bigg[\sum_{k=0}^{L_{max}^l-2} \mathrm{P}_l\left(y \,|M_l' = k\right) \mathbb{P}(U_l' = k) \\ &+ O_l\, \mathrm{P}_l\left(y \,\middle|M_l' = L_{max}^l - 1\right)\Bigg] dy,\ \forall l \in \{m, p\}, \end{aligned} \tag{4.48}$$

where

$$O_l = \frac{L^l_{max}\lambda_l}{A_l\lambda_u}\left(1-\left(1+3.5^{-1}A_l\lambda_u/\lambda_l\right)^{-3.5}\right) - \frac{3.5^{3.5}}{\Gamma(3.5)}\sum_{k=1}^{L^l_{max}-1}\frac{\Gamma(3.5+k)\left(\frac{A_l\lambda_u}{\lambda_l}\right)^{k-1}L^l_{max}}{k!(\frac{A_l\lambda_u}{\lambda_l}+3.5)^{3.5+k}}, \quad \forall l\in\{m,p\}. \tag{4.49}$$

Proof. From (4.44), $\mathbb{E}[R] = \sum_{l\in\{m,p\}} \mathbb{P}(u\in\mathbf{\Phi}^l_u)\,\mathbb{E}[S_l W\log_2(1+\text{SINR}_l)] = A_m\bar{R}_m + A_p\bar{R}_p$, where

$$\bar{R}_l = W\sum_{k=0}^{L^l_{\max}-2}\mathbb{E}\left[\log_2(1+\text{SINR}_l)|U'_l=k\right]\mathbb{P}(U'_l=k) + W\sum_{k\geq L^l_{\max}-1}\frac{L^l_{\max}}{k+1}\mathbb{E}\left[\log_2(1+\text{SINR}_l)|U'_l=k\right]\mathbb{P}(U'_l=k) \tag{4.50}$$

$\mathbb{E}[\log_2(1+\text{SINR}_l)]$ can be computed as $1/(\ln 2)\int_0^\infty \mathbb{P}(\text{SINR}_l > y)(1+y)^{-1}\,dy$. Also, we have $M'_l = \min(U'_l, L^l_{\max}-1)$. Thus,

$$\bar{R}_l = \frac{W}{\ln 2}\int_0^\infty \frac{1}{1+y}\Bigg[\sum_{k=0}^{L^l_{\max}-2}\mathbb{P}(\text{SINR}_l>y|M'_l=k)\mathbb{P}(U'_l=k) + \underbrace{\left(\sum_{k\geq L^l_{\max}-1}\frac{L^l_{\max}}{k+1}\mathbb{P}(U'_l=k)\right)}_{O_l}\mathbb{P}(\text{SINR}_l>y|M'_l=L^l_{\max}-1)\Bigg], \tag{4.51}$$

where O_l can be further simplified as

$$O_l = \sum_{k=1}^{\infty}\frac{L^l_{\max}}{k}\mathbb{P}(U'_l=k-1) - \sum_{k=1}^{L^l_{\max}-1}\frac{L^l_{\max}}{k}\mathbb{P}(U'_l=k-1). \tag{4.52}$$

Equation (4.49) is obtained by substituting $\mathbb{P}(U'_l = k) = (k+1)\mathbb{P}(U_l = k+1)/\mathbb{E}[U_l]$, $k\geq 0$, where the first summation is simplified by using $\sum_{k=1}^{\infty}\mathbb{P}(U_l = k) = 1-\mathbb{P}(U_l=0)$. ∎

For the special case of $L^l_{\max} = 1$, the average data rate of $u\in\mathbf{\Phi}^l_u$ further simplifies to

$$\bar{R}_l = O_l\frac{W}{\ln 2}\int_0^\infty \frac{\mathrm{P}_l(y)}{1+y}\,dy. \tag{4.53}$$

4.5 Impact of Limited Feedback on the Performance of Interference Nulling

The results so far have been derived based on the perfect CSI assumption. However, in practical systems, the CSI is never perfectly accurate. In frequency division duplex systems, the downlink CSI is fed back by the users to serving BSs. Due to the limited feedback, the BSs receive quantized CSI. In this section, we analyze the impact of the quantization error due to limited feedback on the performance of interference nulling. As the focus is on interference-nulling performance, we consider $L^m_{\max} = L^p_{\max} = 1$.

4.5.1 Limited Feedback Model for $L^m_{\max} = L^p_{\max} = 1$

The feedback model is similar to the one used in [30, 31], where the quantized channel direction information (CDI) is fed back by using a quantization codebook of 2^B unit norm vectors, where B is the number of feedback bits. The codebook is known at both the transmitter and the receiver. Each user feeds back the index of the codeword closest to its channel direction, measured by the inner product. For example, a typical user, when it belongs to the macro tier, uses the codebook $\mathcal{C}_m = \{\mathbf{c}_{m,j} : j = 1, 2, \ldots, 2^{B_m}\}$ of size 2^{B_m} to quantize the channel direction $\tilde{\mathbf{h}}_{b_m,1} = \frac{\mathbf{h}_{b_m,1}}{||\mathbf{h}_{b_m,1}||}$ from its serving maco BS b_m. The quantized channel direction is

$$\hat{\mathbf{h}}_{b_m,1} = \arg \max_{\mathbf{c}_{m,j} \in \mathcal{C}_m} \left| \tilde{\mathbf{h}}^*_{b_m,1} \mathbf{c}_{m,j} \right|.$$

Similarly, the typical user, when it belongs to the pico tier, uses the codebook $\mathcal{C}_p = \{\mathbf{c}_{p,j} : j = 1, 2, \ldots, 2^{B_p}\}$ of size 2^{B_p} to quantize the channel direction from its serving pico BS b_p, and the codebook $\mathcal{C}_m = \{\mathbf{c}_{m,j} : j = 1, 2, \ldots, 2^{B_m}\}$ to quantize the channel direction from its nearest active macro BS v_m. Other pico users which request v_m for interference nulling, as well as the user served by v_m, also employ codebooks of size 2^{B_m}, but the codebooks differ from user to user to avoid the possibility of receiving the same quantization vector index from different users. The codebooks are generated by using random vector quantization [114], where each vector $\mathbf{c}_{m,j}$ is independently chosen from the isotropic distribution on the K_m-

dimensional unit sphere, and each vector $\mathbf{c}_{p,j}$ from the isotropic distribution on the K_p- dimensional unit sphere.

Since the precoding vectors are now based on quantized CDIs, for the typical user $u \in \mathbf{\Phi}_u^m$ served by the macro BS b_m, the desired channel power gain $\hat{\beta}_{b_m} \sim \text{Gamma}(\Delta_m, \kappa_m)$, where $\Delta_m = K_m - \min(Q_m, K_m - T_{\min})$, $\kappa_m = 1 - 2^{B_m}\text{Beta}(2^{B_m}, \frac{K_m}{K_m-1})$ [30]. However, as the precoding vector of the interfering BS at $x_q \in \mathbf{\Psi}_q \backslash b_m, q \in \{m, p\}$ is independent of the channel to the typical user u, the interference channel power gain $\hat{\zeta}_{x_q}$ is still distributed as Gamma$(1, 1)$, i.e., Exp$[1]$. Similarly, for the typical user $u \in \mathbf{\Phi}_u^p$ served by the pico BS b_p, the desired channel power gain $\hat{\beta}_{b_p} \sim \text{Gamma}(\Delta_p, \kappa_p)$, where $\Delta_p = K_p$, $\kappa_p = 1 - 2^{B_p}\text{Beta}(2^{B_p}, \frac{K_p}{K_p-1})$. The interference channel power gain from each interfering BS other than v_m is distributed as Exp$[1]$. If v_m does not apply interference nulling, the interference channel power gain from v_m, $\hat{\zeta}_{v_m}$ is also distributed as Exp$[1]$. However, if v_m applies nulling, unlike the perfect CDI case, where the interference from v_m is completely nulled, there will be residual interference due to the quantization error. The interference channel power gain in this case is approximated as an exponential RV with mean $\kappa_I = 2^{-\frac{B_m}{K_m-1}}$ [30]. Thus,

$$\hat{\zeta}_{v_m} \sim \begin{cases} \text{Exp}[1/\kappa_I], & \text{if } u \in \chi \\ \text{Exp}[1], & \text{if } u \notin \chi. \end{cases}.$$

The SINR of the typical user u can be expressed as

$$\text{SINR}_l = \frac{P_l \hat{\beta}_{b_l} D_l^{-\alpha}}{\hat{I}_{b_l,m} + \hat{I}_{b_l,p} + \sigma^2}, \quad \forall l \in \{m, p\}, \tag{4.54}$$

where

$$\hat{I}_{b_l,m} = P_m \sum_{x_m \in \mathbf{\Psi}_m \backslash b_l} \hat{\zeta}_{x_m} ||x_m||^{-\alpha}, \quad \hat{I}_{b_l,p} = P_p \sum_{x_p \in \mathbf{\Psi}_p \backslash b_l} \hat{\zeta}_{x_p} ||x_p||^{-\alpha}. \tag{4.55}$$

Theorem 6. *With limited feedback, the coverage probability of a typical pico user u in the interference-limited scenario, i.e., $\sigma^2 = 0$ is given by*

$$\text{P}_{p,LF}(\gamma) = \text{T}_{1,LF}(\gamma)\varphi + \text{T}_{2,LF}(\gamma)(1 - \varphi), \tag{4.56}$$

where $\text{T}_{1,LF}(\gamma)$ is the coverage probability of a typical pico user u with limited

feedback when $u \in \chi$, given by

$$\begin{aligned}\mathrm{T}_{1,LF}(\gamma) =& 2p_m\lambda_m\frac{\lambda_p}{A_p}\int_{\theta=0}^{\frac{1}{\rho}}\sum_{l=0}^{K_p-1}\left(\frac{\gamma}{\kappa_p}\right)^l\theta^{\alpha l+1}\sum_{v=0}^{l}\frac{(\delta\kappa_I)^{l-v}}{v!(1+\delta\kappa_I\gamma/\kappa_p\theta^\alpha)^{l-v+1}}\\ &\sum_{o=1}^{\mathcal{P}(v)}c_o^v(-1)^{\omega_o^v}\prod_{q=1}^{l}\left(p_m\lambda_m\delta^q\Xi_q\left(\delta,\theta,\frac{\gamma}{\kappa_p}\right)+\frac{p_p\lambda_p}{\theta^{\alpha q-2}}\Xi_q\left(1,1,\frac{\gamma}{\kappa_p}\right)\right)^{\mu_{oq}^v}\\ &\Gamma(\omega_o^v+2)\left(p_m\lambda_m\Xi_0\left(\delta,\theta,\frac{\gamma}{\kappa_p}\right)+p_p\lambda_p\theta^2\Xi_0\left(1,1,\frac{\gamma}{\kappa_p}\right)\right.\\ &\left.+(1-p_m)\lambda_m\rho^2\theta^2+(1-p_p)\lambda_p\theta^2\right)^{-(\omega_o^v+2)}\,\mathrm{d}\theta, \qquad (4.57)\end{aligned}$$

and $\mathrm{T}_{2,LF}(\gamma)=\mathrm{T}_2\left(\gamma/\kappa_p\right)$ is the coverage probability of a typical pico user u with limited feedback when $u \notin \chi$, expressed in terms of the corresponding probability for perfect CSI, $\mathrm{T}_2(\cdot)$. Similarly, with limited feedback, the coverage probability of a typical macro user u in the interference-limited scenario is given $\mathrm{P}_{m,LF}(\gamma)=\mathrm{P}_m\left(\gamma/\kappa_m\right)$ where $\mathrm{P}_m(\cdot)$ is the corresponding probability for perfect CSI.

Proof. The proof is given in Appendix B.3. □

Note that $\mathrm{T}_{2,LF}(\gamma)$ and $\mathrm{P}_{m,LF}(\gamma)$ reduce to $\mathrm{T}_2(\gamma)$ and $\mathrm{P}_m(\gamma)$, respectively, i.e., the perfect CSI case if $\kappa_m=\kappa_p=1$. Similarly, if $\kappa_p=1$ and $\kappa_I=0$, by using $0^0=1$, $\mathrm{T}_{1,LF}(\gamma)$ also reduces to $\mathrm{T}_1(\gamma)$.

After deriving the coverage probabilities for limited feedback, the rate coverage and average rate can be obtained by using Theorem 3 and 4, respectively, with $P_l(\cdot)$ replaced by $P_{l,LF}(\cdot)$.

4.6 Simulation and Numerical Results

In this section, we first validate our analytical results via Monte Carlo simulations on a square window of 20×20 Km^2. After validation, we present some numerical analysis to provide insights on the optimal performance. Unless otherwise stated, we set $\delta=P_m/P_p=100$, $\lambda_m=1\mathrm{BS/Km}^2$ and $W=1$ MHz. We focus on the interference-limited scenario, and hence ignore noise (i.e., $\sigma^2=0$).

In Figure 4.1, the average data rate from Theorem 5 is validated for different system configurations. We assumed perfect CSI in this case. The analytical and

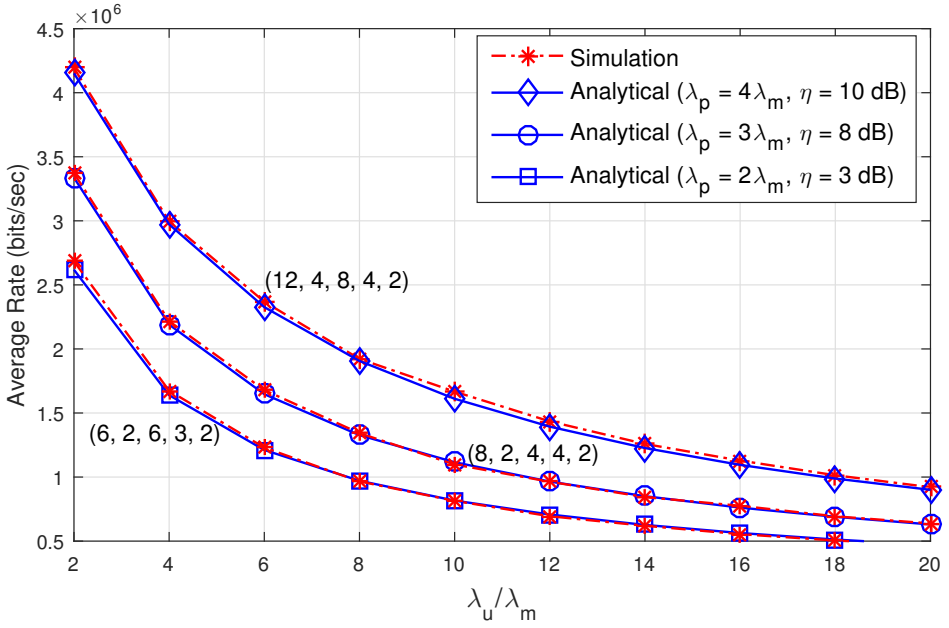

Figure 4.1: Validation of the average user data rate (Theorem 5) for perfect CSI via Monte Carlo simulations for different values of λ_p, η and $(K_m, L^m_{\max}, T_{\min}, K_p, L^p_{\max})$.

simulation results match with each other quite well in the figure. Note that the validation of Theorem 4 for perfect CSI naturally validates the conditional SINR distributions derived in Theorem 2 and 3. In Figure 4.1, the average data rate decreases with an increase in user density λ_u because of the increase in interference and the decrease in users' share of resources. The interference power increases with an increase in user density because more BSs become active, and the average channel power gain from an interfering BS, which is a function of the number of users simultaneously served in a given time slot, also increases as this BS has to serve more users, until the number of users exceeds $L^l_{\max}$.

We next validate the data rate distribution from Theorem 4 in Figure 4.2 for both the perfect CSI and limited feedback scenarios, thereby validating the SINR distribution for limited feedback in Theorem 6 as well. The impact of limited feedback on the performance will be discussed later.

In Figure 4.3, we analyze the impact of interference nulling on the SINR coverage probability of a typical user, where $T_{\min} = K_m$ implies no interference nulling employed. The figure reveals that with properly chosen $T_{\min}$, the SINR coverage

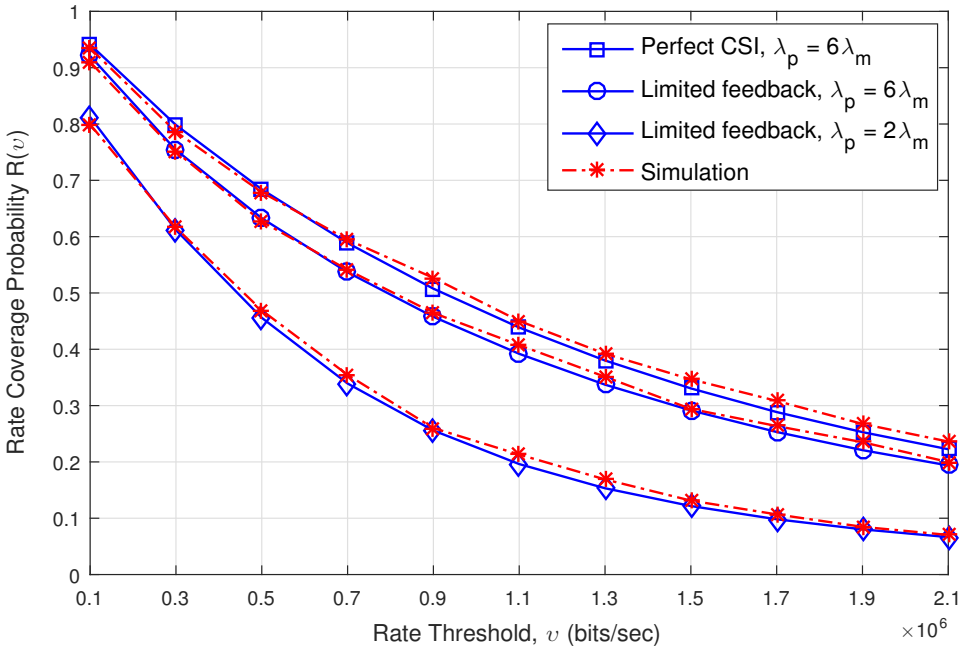

Figure 4.2: Validation of rate coverage probability (Theorem 4) for both perfect CSI and limited feedback via Monte Carlo simulations: $K_m = 12$, $K_p = 4$, $L^m_{\max} = L^p_{\max} = 1$, $T_{\min} = 2$, $\lambda_u = 10\lambda_m$, $\alpha = 3.5$, $\eta = 15$dB.

can be improved with interference nulling. For example, if the required SINR level for a typical user to be under coverage is 0 dB, the average fraction of users under coverage improves from 61% to 70% with interference nulling for the $\lambda_u = 6\lambda_m$, $\eta = 15$ dB case in Figure 4.3. The performance gain, however, decreases with an increasing threshold. At smaller values of thresholds, as interference nulling improves the SINRs of poor cell-edge pico users lacking coverage due to strong interference from their corresponding nearest active macro BSs, the coverage probability of the pico users significantly improves. On the other hand, we know that the SINR of a typical macro user degrades due to interference nulling as it costs the user its available degree of freedom. At lower values of SINR thresholds, the degradation in SINR is, however, not significant enough to impact its coverage probability. Thus, the overall gain in coverage probability is high at smaller threshold levels. However, at larger threshold values, the users under coverage are basically those in the cell interior. Thus, interference nulling may not significantly improve the al-

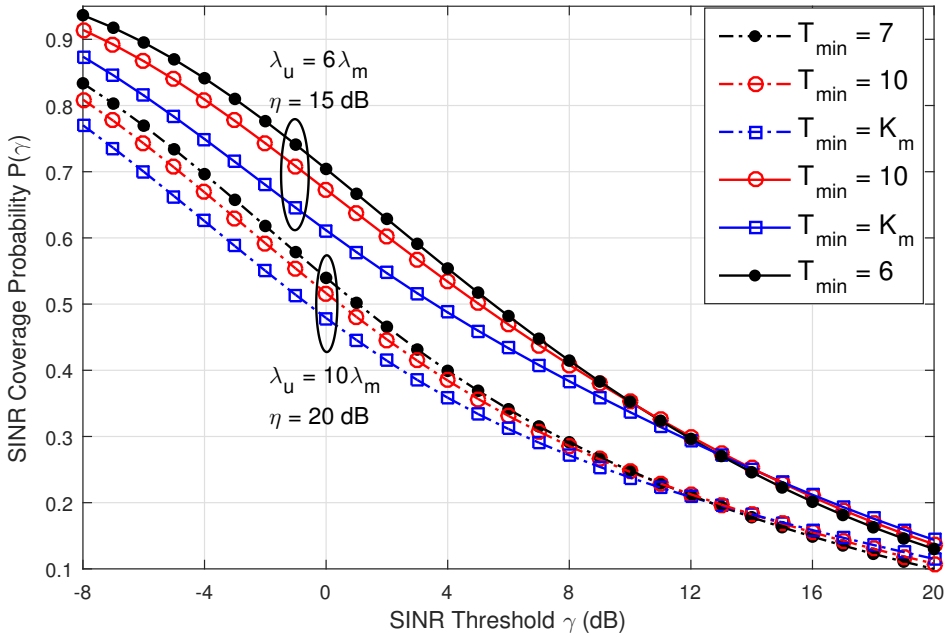

Figure 4.3: Impact of T_{min} on coverage probability: $K_m = 14, L^m_{\text{max}} = 4, K_p = 6, L^p_{\text{max}} = 4, \lambda_p = 6\lambda_m, \alpha = 3.5$.

ready high SINR of cell-interior pico users, resulting in very minimal improvement in pico coverage probability. The SINR degradation of macro users due to interference nulling, which do not have any significance on macro coverage probability at lower thresholds eventually causes the coverage probability to degrade after certain level. This degradation further reduces the overall gain in coverage probability due to interference nulling.

To further clarify the above discussion, the coverage probability of a typical pico user, which always has the interference from its nearest active macro BS nulled, $\mathrm{T}_1(\gamma)$ is compared against that of a pico user without any nulling at all, $\mathrm{T}_2(\gamma)$ in Figure 4.4. It is clearly visible that the gain in pico coverage probability due to interference nulling decreases with an increasing threshold value. In Figure 4.3, as compared to the case with $\lambda_u = 6\lambda_m$, $\eta = 15$ dB, the performance gain in the overall coverage probability for $\lambda_u = 10\lambda_m$, $\eta = 25$ dB is relatively low. However, in Figure 4.4, both cases have similar gains in pico coverage probability due to interference nulling given that the nulling is performed for each pico user. Thus, the reason for the lower performance gain for higher user density λ_u and higher η is

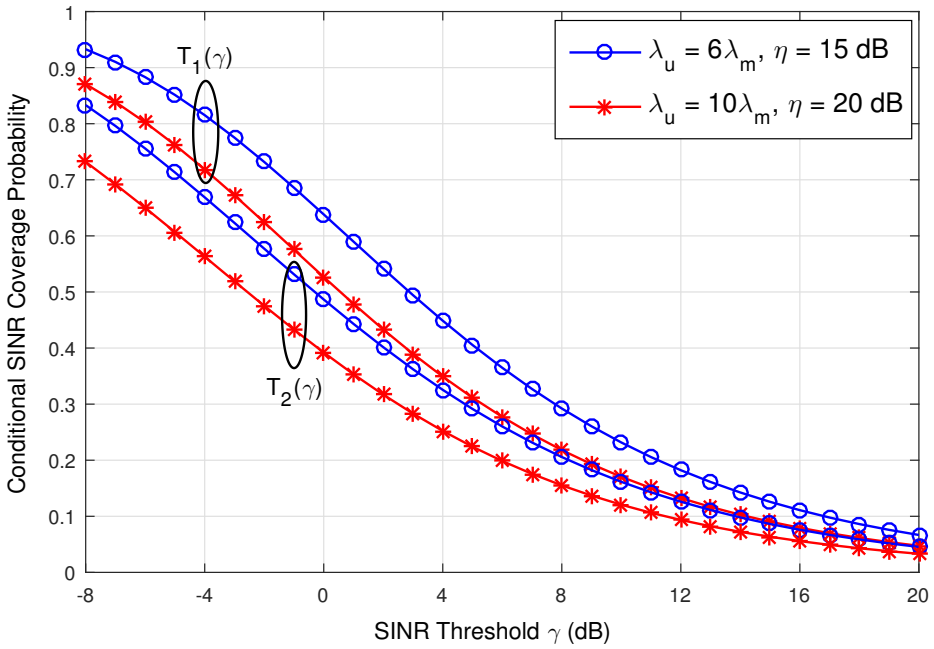

Figure 4.4: Impact of interference nulling on SINR coverage of a typical pico user: $K_m = 14, L^m_{\text{max}} = 4, K_p = 6, L^p_{\text{max}} = 4, \lambda_p = 6\lambda_m, \alpha = 3.5$

the lack of sufficient resources for interference nulling. For $\lambda_u = 6\lambda_m$ and $\eta = 15$ dB, with $T_{\text{min}} = 6$, 83% of the pico users have interference from their corresponding nearest active macro BSs nulled. In contrast, for higher user density of $\lambda_u = 10\lambda_m$ and higher η of 20 dB, with $T_{\text{min}} = 7$, the fraction of interference nulled pico users reduces to 53%.

Next, we investigate the optimal value of η to maximize the average user data rate. η controls the number of users offloaded from the macro to the pico tier to obtain a balanced distribution of the user load across tiers for the optimal user data rate by better utilizing the radio resources in each tier. Meanwhile, since T_{min} determines the spatial degrees of freedom available for serving the macro users, as well as the number of interference-nulled pico users, T_{min} must be tuned according to user offloading. Thus, η and T_{min} must be jointly tuned to maximize the average user data rate. The optimal pair (η, T_{min}) for the given network configuration is investigated in Figure 4.5. The optimal pair is found to be $(10\,\text{dB}, 8)$ and $(11\,\text{dB}, 6)$ for pico density $\lambda_p = 4\lambda_m$ and $\lambda_p = 6\lambda_m$, respectively.

Figure 4.5 shows that the optimal T_{min} decreases with the increase in pico den-

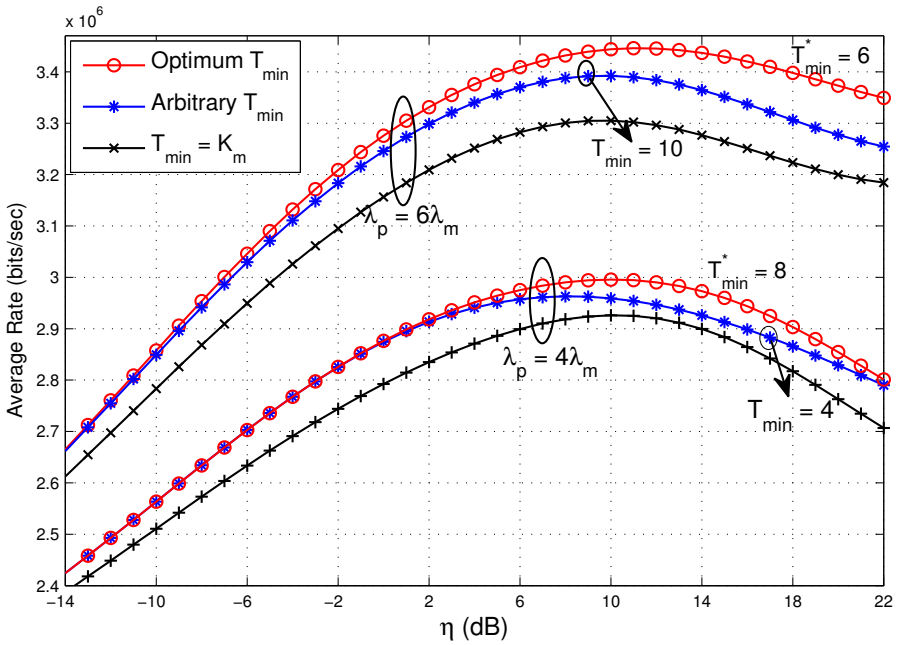

Figure 4.5: Effect of pico cell density λ_p on the optimal choices of T_{min} and η: $\lambda_u = 6\lambda_m$, $K_m = 12$, $L^m_{\text{max}} = 4$, $K_p = 4$, $L^p_{\text{max}} = 4$, $\alpha = 4$.

sity for the given user density. Since the number of interference-nulling requests received by a typical active macro BS is equal to the number of served pico users within a typical Voronoi cell of active macro BSs, for the given user density the number increases with the increase in the pico cell density. To ensure the resources $K_m - T_{\text{min}}$ are sufficient for increased requests without degrading the average user rate, T_{min} is reduced by the required amount.

The variation in the average rate with T_{min} for the given value of η is plotted in Figure 4.6. The average rate of the macro users increases with an increasing T_{min} because the spatial degrees of freedom available at each macro BS for serving its own users increase with an increasing T_{min}. In contrast, the average pico rate decreases with an increasing T_{min} because the number of pico users which get the interference from their corresponding nearest active macro BSs nulled decreases with an increasing T_{min}. The net result is the initial increase in the average rate with an increasing T_{min} and the subsequent decrease beyond a certain value of T_{min}. As we can observe, the optimum T_{min} shifts towards lower values as the value of η increases. For example, for $\eta = 3$ dB, the optimum T_{min} is 7, which decreases

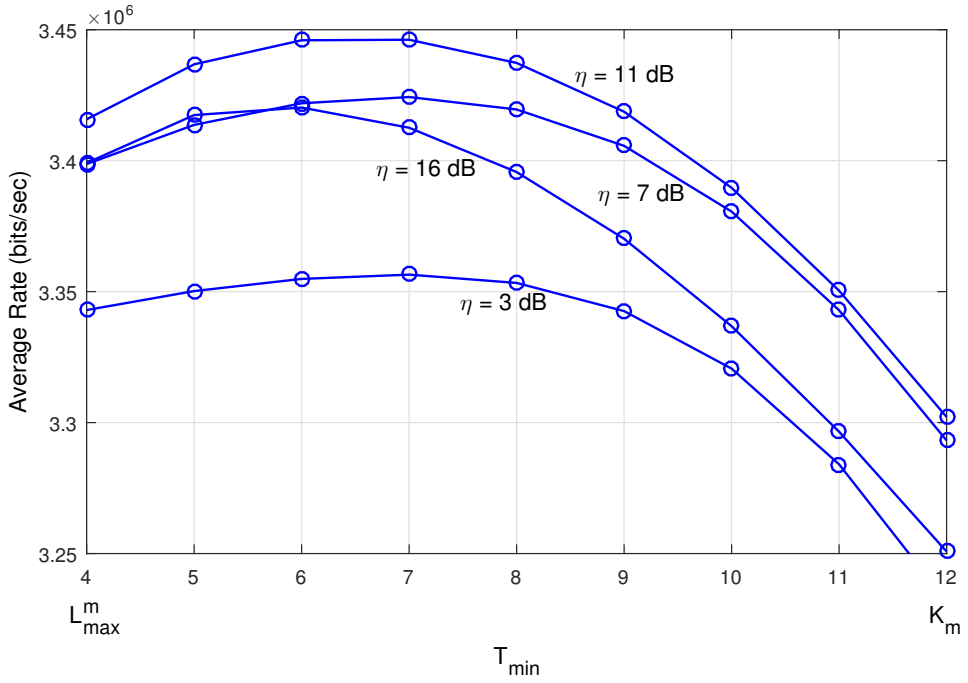

Figure 4.6: Average rate vs. T_{min} for different values of η: $\lambda_u = 6\lambda_m$, $\lambda_p = 6\lambda_m$, $K_m = 12$, $L^m_{\text{max}} = 4$, $K_p = 4$, $L^p_{\text{max}} = 4$, $\alpha = 4$.

to 6 for $\eta = 11$ dB and to 5 for $\eta = 16$ dB. With an increasing η, more users are offloaded to the pico tier. Thus, allocating more antenna resources for interference nulling is desirable.

In Figure 4.7, the CCDF of the data rate of a typical user corresponding to the optimal pair (η, T_{min}) which maximized the average data rate in Figure 4.5 for $\lambda_p = 4\lambda_m$ and $\lambda_p = 6\lambda_m$ is plotted. Let the 5th percentile rate R_{95}, which corresponds to the 5th percentile of the users with rate less than R_{95} (i.e., $\mathcal{R}(R_{95}) = 0.95$), be considered as the cell edge data rate. For $\lambda_p = 4\lambda_m$ and $\eta = 10$ dB, $T_{\text{min}} = 8$, which maximized the average data rate is found to improve the cell edge data rate from 7.2×10^4 bits/sec to 1.12×10^5 bits/sec as compared to that without interference nulling. Similarly, for $\lambda_p = 6\lambda_m$, the cell edge data rate improves from 9.6×10^4 bits/sec to 1.68×10^5 bits/sec if interference nulling with $T_{\text{min}} = 6$ is employed corresponding to $\eta = 11$ dB.

In Figure 4.8, the average data rate is assessed for different values of L^m_{max} and L^p_{max} with and without interference nulling employed. The curve corresponding

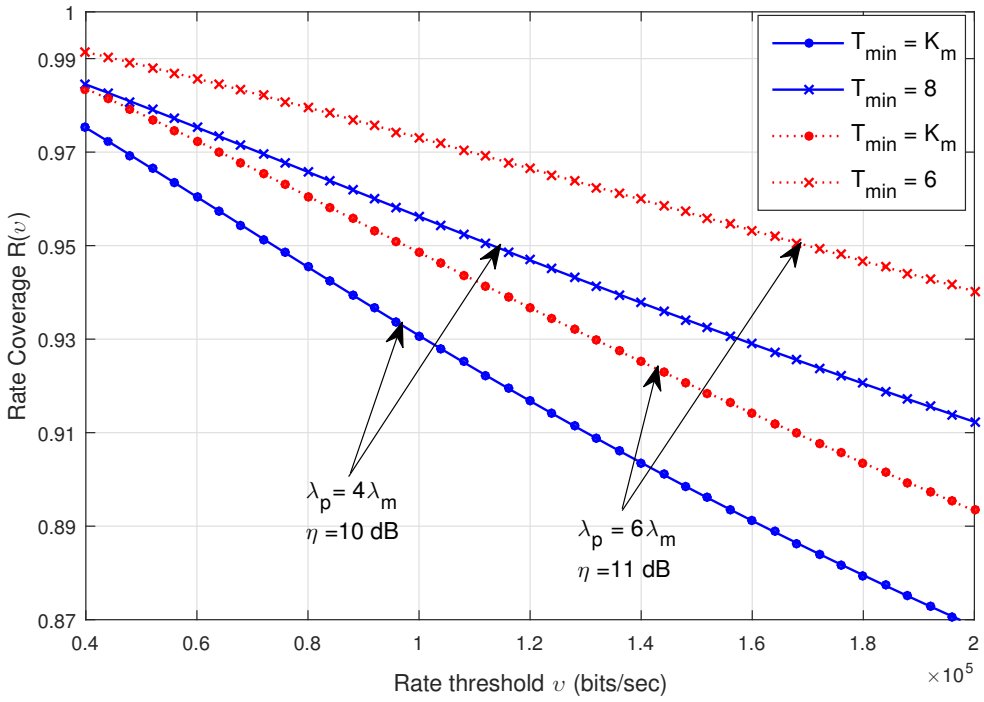

Figure 4.7: Effect of interference nulling on cell edge data rate: $\lambda_p = 6\lambda_m$, $K_m = 12$, $L^m_{\max} = 4$, $K_p = 4$, $L^p_{\max} = 4$, $\alpha = 4$.

to the interference nulling employed is plotted by computing the average rate with optimum $T_{\min}$ for each corresponding value of $L^m_{\max}$ and $L^p_{\max}$. Note that if $L^l_{\max} = 1$, each active BS in the tier $l \in \{m, p\}$ serves a single user chosen randomly in each time-slot, and this multi-antenna technique is known as SU-BF. On the other end, if $L^l_{\max} = K_l$, each active BS serves a maximum of K_l users using K_l antennas, which can be referred to as full-SDMA. Although full-SDMA in general means serving K_l users with K_l antennas, in our case, the number of served users $\min(N_l, K_l)$ can be less than K_l.

As Figure 4.9 reveals, the average data rate in the network can be significantly improved by selecting a proper value of $L^m_{\max}$ compared to either SU-BF or full-SDMA, and similarly a proper value of $L^p_{\max}$. For the case with no interference nulling employed, in which all the antennas at each macro BS are used for serving its own users, the variation of $L^m_{\max}$ has little or no impact on the average rate from $L^m_{\max} = 7$ to $L^m_{\max} = 12$. This result can be observed for each given value of $L^p_{\max}$ because beyond $L^m_{\max} = 7$, the number of macro users simultaneously served

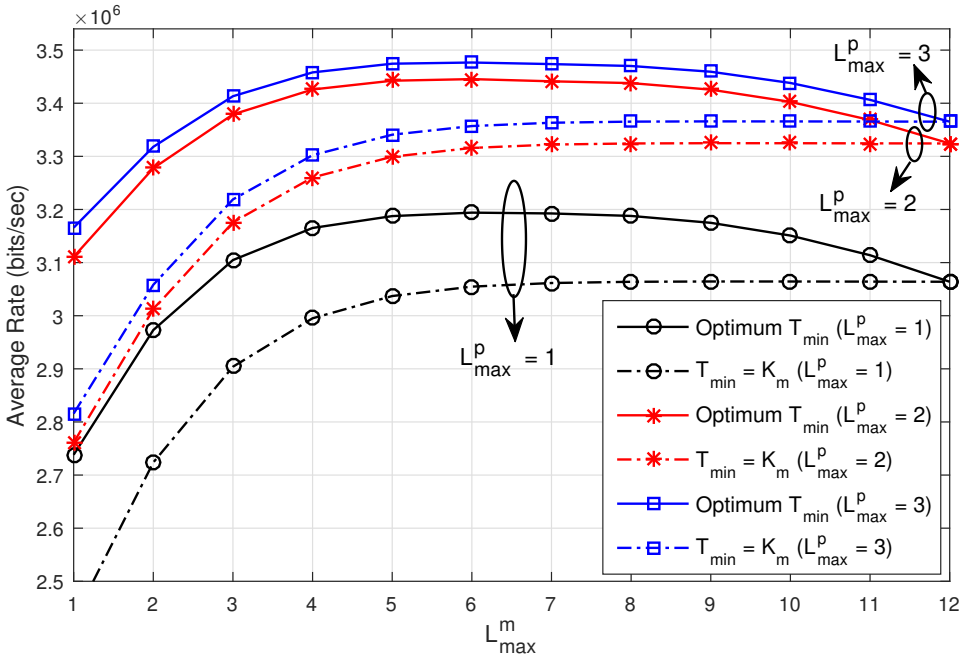

Figure 4.8: Average rate vs. $L^m_{\max}$ for different values of $L^p_{\max}$ with optimum $T_{\min}$ and no interference nulling: $\lambda_p = 6\lambda_m$, $\lambda_u = 6\lambda_m$, $K_m = 12$, $K_p = 4$, $\eta = 12$ dB, $\alpha = 4$.

by a macro BS in each time-slot is limited by the number of users in that cell, rather than $L^m_{\max}$. This explanation is further corroborated by the fact that with interference nulling employed, the optimum $T_{\min}$ beyond $L^m_{\max} = 7$ is found to be the corresponding $L^m_{\max}$ itself, which is the minimum possible value of $T_{\min}$. Since beyond $L^m_{\max} = 7$, the number of macro users in a cell is typically less than $L^m_{\max}$, allocating antenna resources more than $L^m_{\max}$ for macro users would waste resources as the performance can be improved through interference nulling by utilizing those surplus resources.

For each possible value of $L^p_{\max}$, the optimal pair $(L^m_{\max}, T_{\min})$ which maximizes the average data rate is found to be $(6, 7)$. Since the average rate slightly degrades for $L^p_{\max} = 4$ as compared to $L^p_{\max} = 3$ (not shown in the figure), overall the optimal values of $L^m_{\max}$,$T_{\min}$, and $L^p_{\max}$ are 6, 7, and 3, respectively.

After numerically analyzing the proposed SDMA scheme with interference nulling for the perfect CSI, we now investigate the impact of limited feedback on the performance. As explained in Section 4.5, each macro user feeds back B_m CSI bits

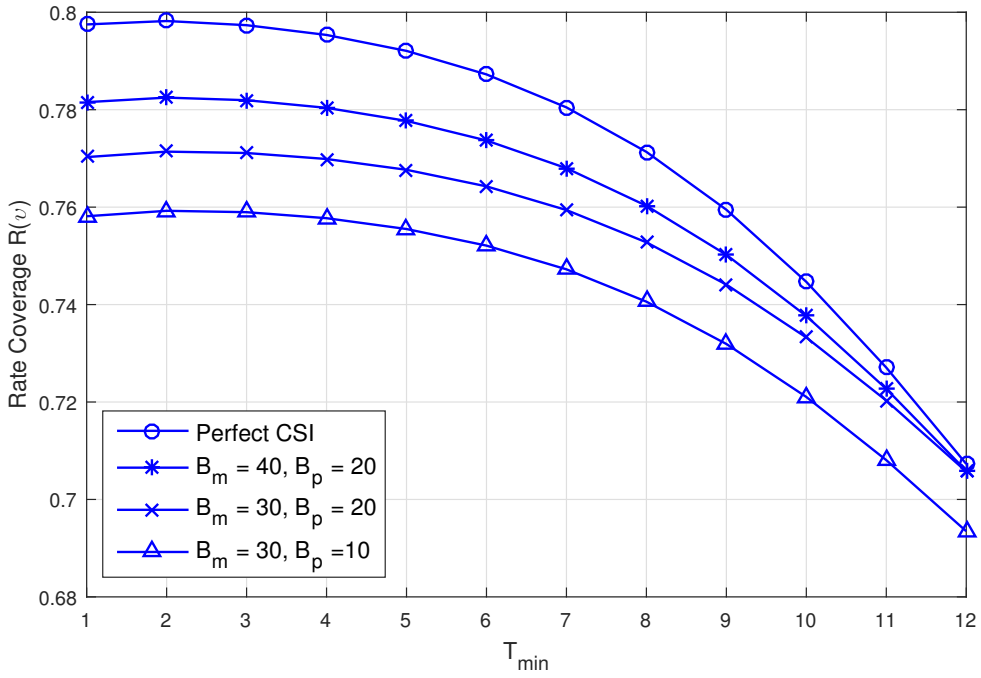

Figure 4.9: Rate Coverage vs. T_{min} for perfect CSI and limited feedback:$\lambda_p = 6\lambda_m$, $\lambda_u = 10\lambda_m$, $K_m = 12$, $K_p = 4$, $L^m_{\text{max}} = L^p_{\text{max}} = 1$, $\eta = 15$ dB, $\alpha = 3.5$.

to its home BS. In contrast, each pico user feeds back B_p CSI bits to its home BS and B_m CSI bits to its nearest active macro BS if the BS is performing interference nulling to the user. In Figure 4.9, the rate coverage performance for SU-BF with interference nulling is plotted against T_{min} for perfect CSI and limited feedback. Irrespective of the value of B_p, the performance loss due to limited feedback bits B_m decreases with an increasing T_{min} because the number of interference nulled pico users decreases with increasing T_{min}, where $T_{\text{min}} = K_m$ implies zero interference nulled users. Thus, the performance loss due to the residual interference resulting from CSI imperfection also decreases. The consistent gap between the performance curves for $B_p = 20$ and $B_p = 10$ with B_m kept constant at 30 throughout the T_{min} axis in Figure 4.9 indicates that the performance loss due to the limited number of B_p does not depend on T_{min}. This result makes sense as B_p is the number of bits fed back by a pico user to its serving pico BS, and thus, has nothing to do with T_{min}.

In Figure 4.10, the impact of the number of feedback bits B_m and B_p on the rate coverage performance with and without interference nulling is investigated. As the

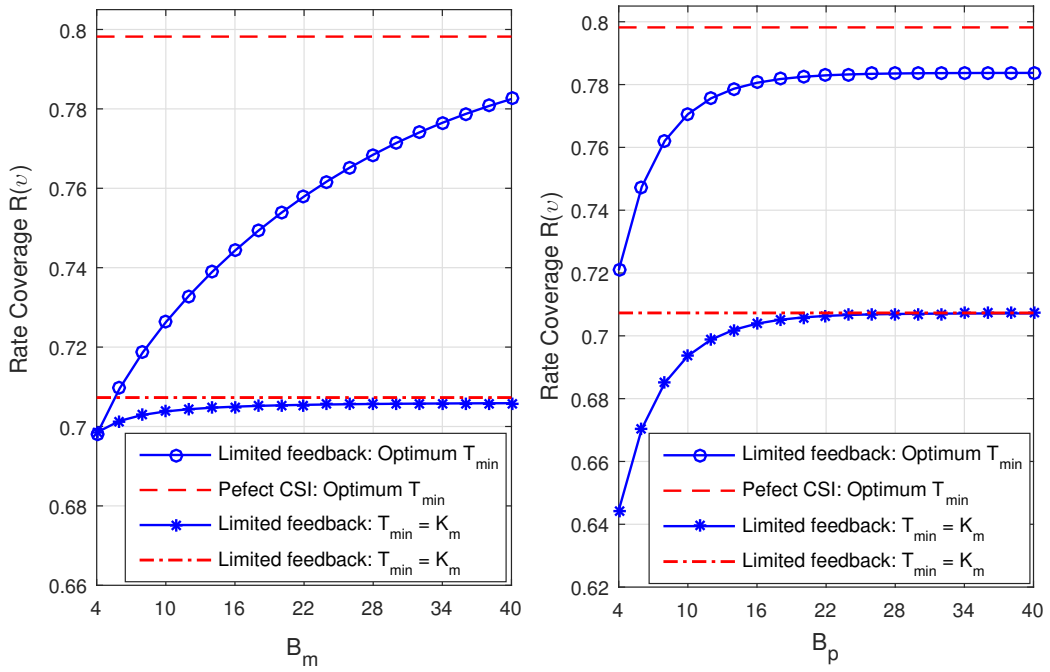

Figure 4.10: Impact of number of feedback bits on the rate coverage performance: $\lambda_p = 6\lambda_m$, $\lambda_u = 10\lambda_m$, $K_m = 12$, $K_p = 4$, $L^m_{\text{max}} = L^p_{\text{max}} = 1$, $\eta = 15$ dB, $\alpha = 3.5$.

number of feedback bits increases, the performance approaches the one with the perfect CSI. Clearly, the impact of limited feedback bits B_m on the performance is very high for the interference-nulling scenario as compared to the one without nulling. $B_m > 16$, which is more than sufficient for the non-coordination case, appears to be insufficient for interference nulling case to reap the full benefits of nulling. Nevertheless, nulling does improve even with limited feedback as compared to the non-coordination case. With no interference nulling employed, the feedback bits B_m are only required for signal power boosting to the single user being served in the cell and such processing is found to be less sensitive to CSI errors as compared to interference nulling. If we observe the rate coverage curve against B_p for the non-coordination case, $B_p > 20$ is near perfect. However, we can observe a performance gap for interference nulling case even beyond $B_p = 20$ because of the limitation in B_m, which is considered to be 40 in this case.

4.7 Conclusion

The downlink performance of multi-antenna HetNets with SDMA was analyzed, in which the ZF precoding matrix at macro BS also considered interference nulling to certain pico users. Further, the number of users served with SDMA in each cell was a function of user distribution. Our results showed that the SINR and rate coverage of victim pico users (those suffering strong interference from macro BS) can be significantly improved with the proposed interference nulling scheme if T_{min} is carefully chosen. The optimal choice of T_{min} was found to be coupled with association bias as T_{min} determines the antenna resources available for serving macro and interference nulling to pico users. The optimal $(T_{\text{min}}, \eta,)$ for the average data rate performance metric was thus investigated. The optimal values of L^m_{max} and L^p_{max} which maximize the average data rate was also investigated and were found to outperform both SU-BF and full-SDMA. The impact of CSI quantization error on the performance of interference nulling due to limited feedback was also analyzed. It was observed that interference nulling is highly sensitive to CSI errors as the residual interference due to CSI imperfection significantly degrades the performance. However, depending on the degree of CSI imperfection, the performance may still be better than that without interference nulling.

Chapter 5

Analysis of Error Probability in Interference Limited Wireless Networks

In this chapter[1], we present mathematical frameworks for error performance analysis in interference-limited networks such as cellular networks. Due to the increasing irregularity in the spatial deployment of nodes in the emerging HetNets, we employ the stochastic geometry approach by abstracting the node locations as a homogeneous PPP. First, we characterize the average error probability of an intended communication link with a given transmitter-receiver separation, which is subject to interference from these Poisson distributed nodes. More specifically, we develop uniform approximation (UA) for average error probability analysis, which is highly accurate over the whole range of the signal-to-interference ratio (SIR). Error probability UAs for both single-antenna and MRC receivers are derived in this chapter. Next, we evaluate the average error probability of any typical user in the network, which is served by the node providing the maximum received power. The Mellin transform (MT) based method is proposed in this case, which often yields a closed-form solution. An example of binary phase shift keying (BPSK) modulation is shown.

[1]This chapter has been published in the proceedings of the IEEE International Conference on Communications (ICC) 2015 [115].

5.1 Introduction

In large wireless networks with numerous nodes spatially distributed over very large areas, such as cellular networks, the performance limiting factor is interference rather than noise. The interference is a direct function of the spatial configuration of the network on which the wireless propagation characteristics such as path loss, shadowing and multipath fading are dependent upon. As cellular networks emerge towards heterogeneous deployments, which are characterized by unplanned/random locations of the nodes, the interference scenario becomes more complex, and computation of the spatially averaged performance metrics becomes critical to derive useful design insights. In Chapter 3 and Chapter 4, we analyzed the coverage and achievable data rate of single- and multi-antenna HetNets for different BS-user association and interference coordination schemes by using tools from stochastic geometry and point process theory. Apart from the coverage and rate, the effectiveness of a wireless network is also characterized by its reliability, measured with metrics such as error probability.

While coverage and rate performance of HetNets have been extensively analyzed [16–19, 48], the average error performance of such networks in the presence of co-tier and cross-tier interference is barely analyzed. There are only few important work towards error probability analysis in the presence of interference from randomly located network nodes [49–51, 67]. The authors in [49, 67] developed a comprehensive framework to characterize the error performance of a given transmitter-receiver link subject to interference from network nodes distributed according to a homogeneous PPP. However, the computation requires Monte-Carlo simulations to average over the network interference which is shown to be a stable RV. This requirement is eliminated in [50] where the authors derived a single-integral expression for the average error probability. Since no closed-form solution is available for the integral, it has to be evaluated numerically. It was further extended to multi-antenna receivers in [51], where the results were obtained in the form of two-fold integral that reduces to a single integral only under special cases.

As an alternative to these semi-analytical solution and complex integral expres-

sions, in this chapter, we develop a UA approach to average error probability analysis of the desired link in the Poisson field of interferers. In cellular networks with frequency reuse 1, which is the main characteristic of next-generation wireless standards such as LTE-Advanced for higher spectral efficiency, the performance is limited by interference, rather than noise. We thus focus on interference-limited scenarios and derive error probability UAs for both single-antenna and MRC receivers. The approximation is named "uniform" to reflect its excellent accuracy over the whole range of SIR. We originally proposed the concept of UA for wireless performance analysis in [116, 117].

After deriving UA for the average error probability of a given link with a deterministic transmitter-receiver distance r_0 in Section 5.2, we next evaluate the average error probability of any typical user in a downlink cellular network with maximum received power based BS-user association in Section 5.3. In this case, the transmitter-receiver distance is no longer deterministic. The error performance of downlink cellular networks for the shortest-distance based BS-user association is analyzed in [118]. The mathematical framework we develop in this chapter for interference-limited scenario is, however, more simple and easily provides insights on important system parameters.

5.2 Uniform Approximation for Average Error Probability in Poisson Field of Interferers

5.2.1 System and Channel Model

We consider a 2-dimensional network in which a transmitter S (located at $x_s \in \mathbb{R}^2$) intends to communicate with a receiver D (located at the origin o without loss of generality). The distance between S and D is fixed at $||x_s - o|| = r_0$. Other nodes in the network which are transmitting in the same channel as S and thus, interfering with $S - D$ communication, are spatially distributed according to a homogeneous PPP $\Phi = \{x_1, x_2, x_3, \ldots\}$ with density λ, where $x_i \in \mathbb{R}^2$ is the location of the ith interferer. For simplicity of analytical expressions, we assume that the transmissions from the interfering nodes are synchronized. The results for asynchronous

case can be easily derived and will be briefly discussed.

We first consider the case where each node in the network including S and D has a single antenna. With multipath fading superimposed on power-law path loss and shadowing, the channel power gain between a transmitter at $x \in \mathbb{R}^2$ and the receiver D at the origin can be modeled as

$$\Omega_x = e^{\sigma g_x} |h_x|^2 ||x - o||^{-\alpha}, \tag{5.1}$$

where $e^{\sigma g_x}$ captures the shadowing effect modeled by log-normal distribution with $g_x \sim \mathcal{N}(0,1)$, σ is the shadowing standard deviation, $h_x = |h_x| \exp(j\psi_x)$ is the complex multipath fading coefficient with $\mathbb{E}[|h_x|^2] = 1$, and α is the power loss exponent. In (5.1), g_x and h_x are independent RVs.

If the source S transmits with power P_0 and each interfering node with power P_I, then according to the channel model (5.1), the complex received signal at D is given by

$$Y = \sqrt{P_0} \frac{e^{\frac{\sigma}{2} g_{x_s}} h_{x_s}}{r_0^{\alpha/2}} s_0 + Z + W, \tag{5.2}$$

where

$$Z = \sqrt{P_I} \sum_{x_i \in \Phi} \frac{e^{\frac{\sigma}{2} g_{x_i}} h_{x_i}}{r_i^{\alpha/2}} s_i \tag{5.3}$$

is the aggregate interference signal, $r_i = ||x_i - o||$ is the distance between the ith interferer at x_i and the receiver D, $W \sim \mathcal{CN}(0, N_0)$ is complex AWGN noise, and $s_0 = a_0 \exp(j\theta_0)$, $s_i = a_i \exp(j\theta_i)$ are the complex modulated symbols transmitted from S and the ith interferer, respectively with $\mathbb{E}[|s_0|^2] = \mathbb{E}[|s_i|^2] = 1$. While all the interfering nodes are assumed to be using the same linear modulation scheme, the transmitter S employs an arbitrary linear modulation. We assume the sequences $\{g_{x_i}\}, \{h_{x_i}\}$ and $\{s_i\}$ are i.i.d.. If the phase ψ_{x_i} of multipath fading coefficient h_{x_i} is uniformly distributed in $(0, 2\pi)$, then, as shown in [49], Z is a CS complex stable RV whose distribution is given by

$$Z \sim \mathcal{S}_c \left(\mu_z = \frac{4}{\alpha}, \beta_z = 0, \eta_z \right)^{2} \tag{5.4}$$

[2]The real and imaginary components of a CS complex stable RV $\mathcal{S}_c(\mu, \beta = 0, \eta)$ are both $\mathcal{S}(\mu, \beta = 0, \eta)$.

for $\alpha > 2$, where $\eta_z = \pi\lambda C_{4/\alpha}^{-1} e^{2\sigma^2/\alpha^2} P_I^{2/\alpha} \mathbb{E}\left[|\,\xi_i|^{4/\alpha}\right]$,

$$C_x = \begin{cases} \frac{1-x}{\Gamma(2-x)\cos(\pi x/2)}, & x \neq 1 \\ \frac{2}{\pi}, & x = 1, \end{cases}$$

and $\xi_i = |h_{x_i}| a_i \cos(\theta_i + \psi_{x_i})$. If the interfering nodes transmit asynchronously, each with an independent random delay $t_i \sim \mathcal{U}(0,T)$ relative to S, then ξ_i is given by $\xi_i = |h_{x_i}| \left[a_i \frac{t_i}{T} \cos(\theta_i + \psi_{x_i}) + a_i'(1 - \frac{t_i}{T}) \cos(\theta_i' + \psi_{x_i})\right]$ [49], where $a_i \exp(j\theta_i)$ and $a_i' \exp(j\theta_i')$ are the successive symbols transmitted from the ith interferer during $[0,T]$.

The CS complex stable RV Z in (5.4) can be decomposed as [49]

$$Z = \sqrt{B} G, \tag{5.5}$$

where

$$B \sim \mathcal{S}\left(\mu_B = \frac{2}{\alpha}, \beta_B = 1, \eta_B = \cos\left(\frac{\pi}{\alpha}\right)\right), \tag{5.6}$$

$$G \sim \mathcal{CN}(0, P_I \nu), \;\; \nu = 4e^{\sigma^2/\alpha} \left(\pi\lambda C_{4/\alpha}^{-1} \mathbb{E}\left[|\,\xi_i|^{4/\alpha}\right]\right)^{\alpha/2}. \tag{5.7}$$

Thus, conditioned on B, $Z + W \sim \mathcal{CN}(0, P_I \nu B + N_0)$. For the particular case of $h_{x_i} \sim \mathcal{CN}(0,1)$, i.e., Rayleigh fading, $\mathbb{E}\left[|\,\xi_i|^{4/\alpha}\right]$ can be easily computed. Since conditioned on s_i, $\xi_i = [|h_{x_i}| a_i \cos(\theta_i + \psi_{x_i})] \sim \mathcal{N}(0, a_i^2/2)$, we have,

$$\mathbb{E}\left[|\,\xi_i|^{4/\alpha}\right] = \frac{\Gamma(1/2 + 2/\alpha)}{\sqrt{\pi}} \mathbb{E}[a_i^{4/\alpha}]. \tag{5.8}$$

In the presence of the CSI of the $S - D$ link only, the receiver employs simple coherent demodulation. The conditional error probability is thus given by the error expression for coherent detection in AWGN noise, denoted by $h(\gamma)$ (for example, $h(\gamma) = Q(\sqrt{2\gamma})$ for BPSK modulation) with

$$\gamma = \frac{\bar{P}_0 e^{\sigma g_{x_s}} |h_{x_s}|^2 r_0^{-\alpha}}{\bar{P}_I \nu B + 1}, \tag{5.9}$$

where $\bar{P}_0 = P_0/N_0$ and $\bar{P}_I = P_I/N_0$ are the noise normalized transmit powers of the node S and the interfering nodes, respectively. $\bar{P}_0$ and $\bar{P}_I$ are referred to as the SNR and interference-to-noise ratio (INR), respectively. In interference-limited scenario, γ can be expressed as $\gamma = \rho X$, where $\rho = \bar{P}_0 e^{\sigma g_{x_s}} r_0^{-\alpha} / (\bar{P}_I \nu)$ is a non-random quantity, referred to as SIR, and $X = |h_{x_s}|^2 / B$ is a RV. Note that for the fixed $S - D$ link, the shadowing coefficient g_{x_s} is assumed to remain constant.

5.2.2 Average Error Probability

The average probability of error can be expressed as (C.2). Since the unavailability of the PDF $f_X(x)$ in closed form is the main obstacle in deriving the closed-form expression for (C.2), we exploit the MT information of $h(\gamma)$ and $f_X(x)$ to derive UA for (C.2). UA is a rational function that matches the asymptotics of $P_e(\rho)$ as $\rho \to 0$ and $\rho \to \infty$, simultaneously (see Appendix C.3).

The MT of $f_X(x)$ is given by

$$\mathcal{F}_X(s) = \mathcal{F}_{|h_{x_d}|^2}(s)\mathcal{F}_B(2-s), \tag{5.10}$$

where $\mathcal{F}_{|h_{x_d}|^2}(s)$ and $\mathcal{F}_B(s)$ are the MTs of the PDFs of $|h_{x_d}|^2$ and B, respectively. The MT of the stable RV B with parameters given in (5.6) is given by [119]

$$\mathcal{F}_B(s) = \frac{\Gamma(1+\frac{\alpha}{2}-\frac{\alpha}{2}s)}{\Gamma(2-s)}. \tag{5.11}$$

If the MTs $\mathcal{F}_{|h_0|^2}(s)$ and $\mathcal{H}(s)$ are known and have only first-order poles, the UA can be easily derived by using (C.10) for any linear modulation and any fading model with the required coefficients computed according to Proposition 1 in Appendix C.2.

Performance with BPSK Modulation in Rayleigh Fading

In the following example, we consider the case where the transmitter S employs BPSK modulation, and the $S-D$ link is Rayleigh faded. In this case, $\mathcal{F}_X(1-s) = \Gamma(1-\frac{\alpha}{2}s)$ and $\mathcal{H}(s) = \frac{\Gamma(s+1/2)}{2s\sqrt{\pi}}$. Thus, $F_X(1-s)$ has poles at $s = 2/\alpha, 4/\alpha, 6/\alpha, \ldots$, while $\mathcal{H}(s)$ has poles at $s = 0, -1/2, -3/2, \ldots$. The first positive pole at $s = 2/\alpha$ indicates that the diversity order is $2/\alpha$. The diversity order, thus, depends on the power loss exponent α. The coefficients $b(0)$ and $c(l)$ required to compute the UA can be obtained by using Proposition 1 in Appendix C.2.

Example: For $\alpha = 4$, we have $\tau = 1/2$, $\delta = 1$, and the required coefficients $b(0)$ and $c(l)$ are given by

$$b(0) = \frac{1}{2\sqrt{\pi}}, \quad c(l) = \begin{cases} \frac{1}{2} & l = 0 \\ \dfrac{(-1)^{(l+1)/2}\Gamma\left[l\right]}{\sqrt{\pi}\Gamma\left[(l+1)/2\right]} & l = 1, 3, \ldots \\ 0 & \text{otherwise.} \end{cases} \tag{5.12}$$

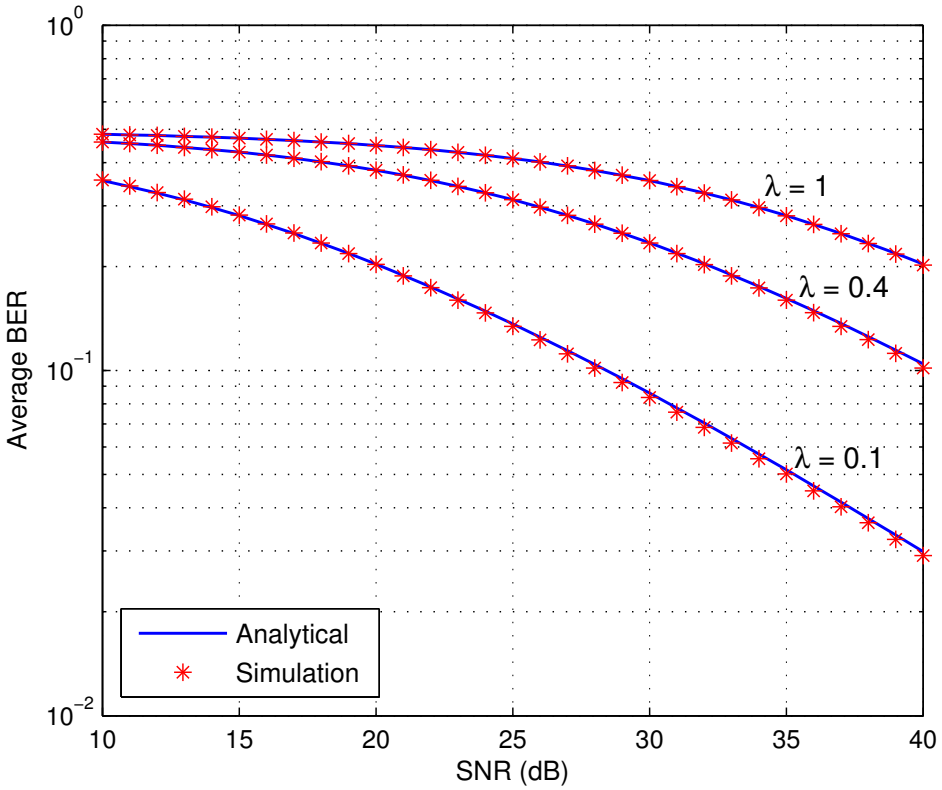

Figure 5.1: Average BER of $S - D$ link with BPSK modulation for different densities of interfering nodes ($\alpha = 4$, $r_0 = 1$ Km, $g_{x_d} = 0$ INR $= 20$ dB, $\sigma_{\text{dB}} = 10$)

The UA can be readily computed by using (C.10).

The average bit error rate (BER) of the $S - D$ link when S as well as all the interfering nodes employ BPSK modulation, and all the links (desired and interfering) undergo independent Rayleigh fading, is depicted in Figure 5.1 for different densities of interfering nodes, 0.1Km^{-2}, 0.4Km^{-2} and 1Km^{-2}. Both the UA and Monte Carlo simulation results are plotted against the SNR. The parameters used are $\alpha = 4$, $r_0 = 1$ Km, $g_{x_s} = 0$ (no shadowing on the desired link), INR $= 20$ dB, $\sigma_{\text{dB}} = 10$, i.e., $\sigma = \ln 10$. Note that noise is not ignored in the simulation results. The excellent match between the UAs and the simulated results shows thats the error performance can be accurately evaluated with the UA method in interference-limited scenario. The Figure 5.1 shows that the error performance improves with the decrease in node density due to the decrease in total interference power.

Performance with N_r-branch MRC Receiver in all Rayleigh Fading

Let the receiver D be equipped with N_r antennas and employ MRC. If $\{h_{x_s,l} = |h_{x_s,l}| \exp(j\psi_{x_s,l}), l = 1, 2, \ldots, N_r\}$ are i.i.d. fading coefficients from S to each receive antenna of D, and similarly, $\{h_{x_i,l} = |h_{x_i,l}| \exp(j\psi_{x_i,l}), l = 1, 2, \ldots, N_r\}$ are i.i.d. fading coefficients from ith interferer, the resultant signal after combining the received signals at each antenna can be expressed as

$$Y = \sqrt{P_0} \frac{e^{\frac{\sigma}{2} g_{x_s}} \sum_{l=1}^{N_r} |h_{x_s,l}|^2}{r_0^{\alpha/2}} s_0 + Z + W, \tag{5.13}$$

where

$$Z = \sqrt{P_I} \sum_{x_i \in \Phi} \frac{e^{\frac{\sigma}{2} g_{x_i}} \sum_{l=1}^{N_r} h_{x_s,l}^* h_{x_i,l}}{r_i^{\alpha/2}} s_i \tag{5.14}$$

is the resultant interference, and $W = \sum_{l=1}^{N_r} h_{x_s,l}^* n_l$ is the resultant noise. Since $\{n_l \sim \mathcal{CN}(0, N_0), l = 1, 2, \ldots, N_r\}$ are i.i.d. complex Gaussian noise, conditioned on $\{h_{x_s,l}\}$, $W \sim \mathcal{CN}(0, N_0 \sum_{l=1}^{N_r} |h_{x_d,l}|^2)$. Z can again be shown to be a circularly symmetric (CS) complex stable RV, which can be decomposed according to (5.5) with B and G given by (5.6) and (5.7), respectively. However, ξ_i in this case is given by

$$\xi_i = \sum_{l=1}^{N_r} |h_{x_s,l}||h_{x_i,l}| a_i \cos(\theta_i + \psi_{x_i,l} - \psi_{x_d,l}). \tag{5.15}$$

Thus, conditioned on B and $\{h_{x_s,l}\}$, $Z + W \sim \mathcal{CN}(0, P_I \nu B + N_0 \sum_{l=1}^{N_r} |h_{x_s,l}|^2)$.

If the interference links are Rayleigh faded, then conditioned on $\{h_{x_s,l}\}$,

$$\mathbb{E}\left[|\xi_i|^{4/\alpha}\right] = \frac{\Gamma(1/2 + 2/\alpha)}{\sqrt{\pi}} \mathbb{E}[a_i^{4/\alpha}] \sum_{l=1}^{N_r} |h_{x_s,l}|^2. \tag{5.16}$$

In the interference-limited scenario, γ can again be expressed as $\gamma = \rho X$, where

$$\rho = \frac{\bar{P}_0 e^{\sigma g_{x_s}} r_0^{-\alpha}}{\bar{P}_I \kappa}, \; X = \frac{\sum_{l=1}^{N_r} |h_{x_s,l}|^2}{B},$$

$\kappa = 4e^{\sigma^2/\alpha} \left(\sqrt{\pi} \lambda C_{4/\alpha}^{-1} \Gamma\left(\frac{1}{2} + \frac{2}{\alpha}\right) \mathbb{E}\left[a_i^{4/\alpha}\right]\right)^{\alpha/2}$. The error probability UA can be similarly obtained as in the single-antenna receiver case with the help of the MT information of $h(\gamma)$ and $f_X(x)$.

If $\{h_{x_s,l}, l = 1, 2, \ldots, N_r\}$ undergo i.i.d. Rayleigh fading, then

$$\mathcal{F}_X(1-s) = \frac{\Gamma(N_r - s)\Gamma(1 - \frac{\alpha}{2}s)}{(N_r - 1)!\Gamma(1-s)},$$

which have poles at $s = 2/\alpha, 4/\alpha, 6/\alpha, \ldots$, and at $s = N_r, N_r + 1, N_r + 2, \ldots$, along with zeros at $s = 1, 2, 3, \ldots$. For exponentially decaying $h(\gamma)$ as $\gamma \to \infty$, $\mathcal{H}(s)$ has only negative poles. The first positive pole at $s = 2/\alpha$ thus indicates that the diversity order is given by $2/\alpha$, irrespective of the number of antennas at the receiver D.

The required parameters to compute UA for the average error probability of BPSK modulation for $\alpha = 4$ are $\tau = 1/2$, $\delta = 1$ and

$$b(0) = \frac{\Gamma(N_r - 1/2)}{2\pi\Gamma(N_r)},$$

$$c(l) = \begin{cases} \frac{1}{2} & l = 0 \\ \dfrac{(-1)^{(l+1)/2}\Gamma(N_r + l/2)\Gamma(l)}{\sqrt{\pi}\Gamma\big((l+1)/2\big)\Gamma(N_r)\Gamma(l/2+1)} & l = 1, 3, \ldots \\ 0 & \text{otherwise.} \end{cases} \tag{5.17}$$

Note that when $\alpha = 4$, the poles at $s = 1, 2, 3, \ldots$ are canceled by the zeros and the effective poles of $\mathcal{F}_X(1-s)$ are $s = 1/2, 3/2, \ldots$ and $s = N_r, N_r + 1, N_r + 2, \ldots$.

The UA and simulation results for the average BER in all-Rayleigh-fading scenario with BPSK modulation at each node are plotted against SNR in Figure 5.2 for different values of N_r. Figure 5.2 clearly reveals that the diversity order of the system is the same for each value of N_r. However, the error performance improves by having more receive antennas.

5.3 Average Error Probability of Downlink Cellular Networks

While the above analysis is suitable for evaluating the average error probability of a particular user whose distance from the serving node is known, in this section, we are interested in evaluating the average error probability of any randomly selected user in a cellular network. We consider a single-tier downlink cellular network with frequency reuse 1.

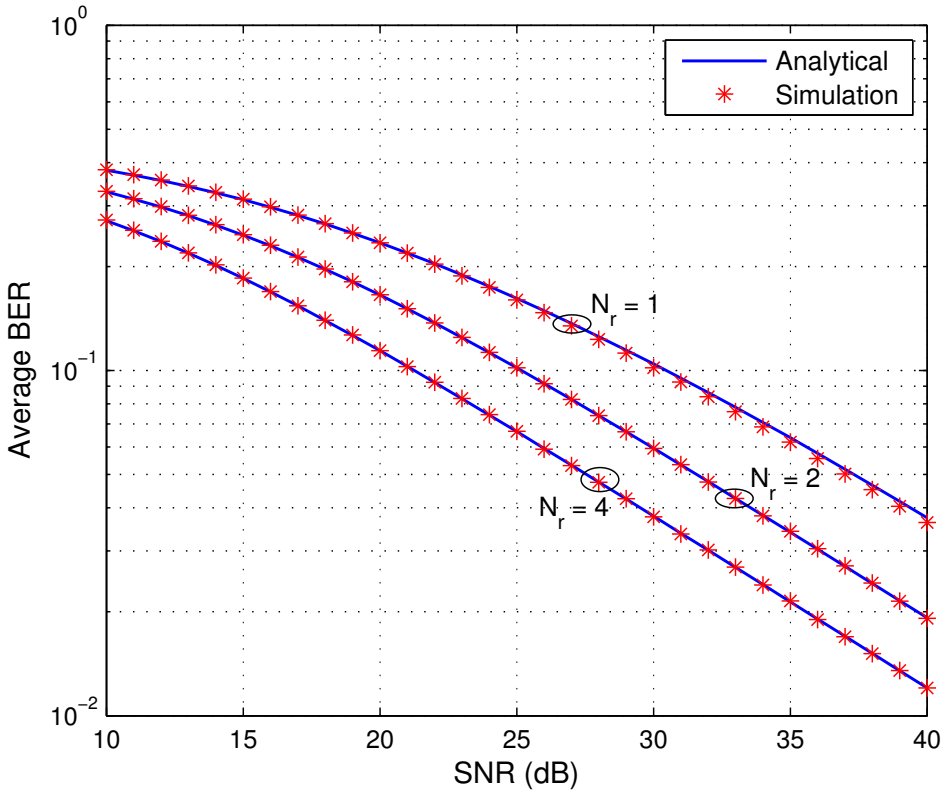

Figure 5.2: Average BER of BPSK modulation with N_r-branch MRC receiver in Rayleigh fading ($\alpha = 4$, $r_0 = 1$ Km, $g_{x_d} = 0$, $\lambda = 0.4\,\text{Km}^{-2}$, INR $= 10$ dB, $\sigma_{\text{dB}} = 10$)

5.3.1 System Model and Error Probability Analysis

The BSs are spatially distributed according to a homogeneous PPP $\Phi = \{x_1, x_2, x_3, \ldots\}$ on $\mathbb{R}^2$ of intensity λ, each employing the same modulation scheme and transmitting with the same power P. Rayleigh fading with power law path loss is assumed between any transmitter-receiver pair. Each user in the network is associated with the BS offering the maximum received power. A typical user o at the origin is thus associated with a BS located at $x_b = \arg\max_{x_i \in \Phi} |h_{x_i}|^2 r_i^{-\alpha}$, where $r_i = ||x_i - o||$ is the distance from o to ith BS and h_{x_i} is the fading coefficient of the channel between o and the ith BS. The BSs other than x_b is the set of interfering nodes for the user o, and is still a homogeneous PPP of intensity λ because for a homogeneous PPP, the reduced Palm distribution is equal to the distribution of PPP itself [57].

We consider the interference-limited scenario and analyze the error probability

at the user o. The error probability is valid for any randomly chosen user according to Slivnyak's theorem (Section 2.3). By using the mathematical framework outlined in Section 5.2.1, the conditional error probability is given by $h(\gamma)$ with

$$\gamma = \frac{1}{\nu} \frac{\max\limits_{i \in \Phi} |h_i|^2 r_i^{-\alpha}}{B}, \tag{5.18}$$

where $\nu = 4\left(\sqrt{\pi}\lambda C_{4/\alpha}^{-1} \Gamma\left(\frac{1}{2} + \frac{2}{\alpha}\right) \mathbb{E}\left[a_i^{4/\alpha}\right]\right)^{\alpha/2}$, and the RV B is given by (5.6). Let $V = \max\limits_{x_i \in \Phi} |h_{x_i}|^2 r_i^{-\alpha}$. The cumulative distribution function (CDF) of V can be derived as

$$\begin{aligned} F_V(v) &= \mathbb{P}\left(\max_{x_i \in \Phi} h_{x_i} r_i^{-\alpha} < v\right) \\ &= \mathbb{E}_\Phi\left[\prod_{x_i \in \Phi} \left(1 - \exp(-v r_i^{\alpha})\right)\right]. \end{aligned} \tag{5.19}$$

By using the PGFL of PPP given by (2.7), we have

$$\begin{aligned} F_V(v) &= \exp\left(-2\pi\lambda \int_0^\infty \exp(-v r^{\alpha}) r \, dr\right) \\ &= \exp\left(-\frac{\pi\lambda}{v^{2/\alpha}} \Gamma\left(\frac{2}{\alpha} + 1\right)\right). \end{aligned} \tag{5.20}$$

The corresponding PDF of V can thus be obtained as

$$f_V(v) = \frac{2\pi\lambda}{\alpha} \Gamma\left(\frac{2}{\alpha} + 1\right) v^{-2/\alpha - 1} e^{-\pi\lambda\Gamma\left(\frac{2}{\alpha}+1\right) v^{-2/\alpha}}. \tag{5.21}$$

The RV V can be expressed as $V = (\pi\lambda\Gamma(2/\alpha + 1))^{\alpha/2} U$, where the PDF of U is given by $f_U(u) = \frac{2}{\alpha} u^{-2/\alpha - 1} \exp(-u^{-2/\alpha})$. γ can finally be expressed as $\gamma = \rho X$, where $\rho = \frac{1}{4}\left[\frac{\sqrt{\pi}\Gamma(\frac{2}{\alpha}+1)}{C_{4/\alpha}^{-1}\Gamma\left(\frac{1}{2}+\frac{2}{\alpha}\right)\mathbb{E}\left[a_i^{4/\alpha}\right]}\right]^{\alpha/2}$ and $X = \frac{U}{B}$.

The average error probability is then given by (C.2). If we closely observe ρ and X, we can see that in interference-limited cellular networks, the average error probability is independent of the BS density λ and the SNR $\bar{P} = P/N_0$. Thus, the error probability cannot be improved by increasing SNR because doing so would increase the interference power as well. On the other hand, if we increase λ, the gain in the desired received signal power due to closer distance between the user and the serving BS is counter-balanced by the increase in interference power. However, by increasing λ, more users can be simultaneously served, and the network capacity naturally improves without affecting the error performance of the network.

Unlike in Section 5.2, ρ is now the function of α and a_i only. For the typical values of α in the range $2 < \alpha \leq 6$ and $\mathbb{E}[a_i^2] = 1$, the range of ρ is much more limited than the range $0 < \rho < \infty$ in Section 5.2. Thus, the use of the UA approach, which basically matches the high-SIR ($\rho \to \infty$) and low-SIR ($\rho \to 0$) asymptotics, may not make much sense in this case. However, one can still use the MT information of $f_X(x)$ and $h(\gamma)$ to evaluate (C.2).

Equation (C.2) can be transformed via the Parseval formula (C.6), where c lies in the fundamental strip of both $\mathcal{H}(s)$ and $\mathcal{F}_X(1-s)$. The MT $\mathcal{F}_X(s)$ is given by $\mathcal{F}_X(s) = \mathcal{F}_U(s)\mathcal{F}_B(2-s)$, where $\mathcal{F}_U(s)$ can be derived as

$$\mathcal{F}_U(s) = \int_0^\infty u^{s-1} f_U(u) du = \Gamma\left(-\frac{\alpha}{2}s + \frac{\alpha}{2} + 1\right), \tag{5.22}$$

and $\mathcal{F}_B(s)$ is given by (5.11). We can apply the residue theorem to obtain a series representation of (C.6), which can often be expressed in terms of the generalized Hypergeometric function ${}_pF_q[a_1, \ldots, a_p; b_1, \ldots, b_q; z]$ [113], thus yielding a closed-form expression.

5.3.2 Average Error Probability in BPSK Modulation

For BPSK modulation, (C.6) can be expressed as

$$P_e = \frac{1}{2\pi j} \int_{c-j\infty}^{c+j\infty} \frac{\Gamma(s+1/2)}{2s\sqrt{\pi}} \frac{\Gamma\left(\frac{\alpha}{2}s+1\right)\Gamma(1-\frac{\alpha}{2}s)}{\Gamma(1-s)} \rho^{-s} ds. \tag{5.23}$$

The poles to the left of the contour $\mathcal{R}(s) = c$ are $s = 0, -(k+1/2), -2(k+1)/\alpha$, where $k = 0, 1, 2, \ldots$. For $\alpha \neq 4$ in the range $2 < \alpha \leq 6$, the poles are simple. Thus, by closing the contour to the left, and then applying the residue theorem, we have

$$\begin{aligned}
P_e &= \frac{1}{2} + \sum_{k=0}^{\infty} \frac{(-1)^{k+1}}{2\sqrt{\pi}} \frac{\Gamma(-\frac{\alpha}{2}k - \frac{\alpha}{4} + 1)\Gamma(1 + \frac{\alpha}{2}k + \frac{\alpha}{4})}{k!(k+\frac{1}{2})\Gamma(k+\frac{3}{2})} \rho^{k+\frac{1}{2}} \\
&\quad + \sum_{k=0}^{\infty} \frac{(-1)^{k+1}}{2\sqrt{\pi}} \frac{\Gamma(-\frac{2}{\alpha}k - \frac{2}{\alpha} + \frac{1}{2})\Gamma(k+2)}{k!(k+1)\Gamma(1 + \frac{2}{\alpha}k + \frac{2}{\alpha})} \rho^{\frac{2(k+1)}{\alpha}} \\
&= \frac{1}{2} + \sum_{k=1}^{\infty} \frac{(-1)^{k}\alpha}{4\sqrt{\pi}} \frac{\Gamma(-\frac{\alpha}{2}k + \frac{\alpha}{4} + 1)\Gamma(\frac{\alpha}{2}k - \frac{\alpha}{4})}{\Gamma(k)\Gamma(k+\frac{1}{2})} \rho^{k-\frac{1}{2}} \\
&\quad + \sum_{k=1}^{\infty} \frac{(-1)^{k}}{2\sqrt{\pi}} \frac{\Gamma(-\frac{2}{\alpha}k + \frac{1}{2})}{\Gamma(\frac{2}{\alpha}k+1)} \rho^{\frac{2k}{\alpha}}
\end{aligned} \tag{5.24}$$

for $\alpha \neq 4$. Both the infinite series in (5.24) can be expressed as a finite sum of generalized Hypergeometric functions. Let the first infinite series in (5.24) be denoted by T_1. Let $\alpha/2 = c/d$, where c and d are integers. For example, $c = 7$ and $d = 5$ for $\alpha = 2.8$. The positive integer k is then partitioned as $k = dp - q$, where $q = 0, 1, \ldots, d-1$ and $p = 1, 2, \ldots$. T_1 then can be expressed as

$$\begin{aligned} T_1 &= \sum_{q=0}^{d-1}\sum_{p=1}^{\infty} \frac{(-1)^{dp-q}}{2\sqrt{\pi}} \frac{c}{d} \frac{\Gamma(-cp+\frac{c}{d}q+\frac{c}{2d}+1)\Gamma(cp-\frac{c}{d}q-\frac{c}{2d})}{\Gamma(dp-q)\Gamma(dp-q+\frac{1}{2})} \rho^{dp-q-\frac{1}{2}} \\ &= \sum_{q=0}^{d-1}\sum_{p=0}^{\infty} \frac{(-1)^{dp+d-q}}{2\sqrt{\pi}} \frac{c}{d} \frac{\Gamma[-c(p+\frac{2(d-q)-1}{2d}-\frac{1}{c})]\Gamma[c(p+\frac{2(d-q)-1}{2d})]}{\Gamma[d(p+\frac{d-q}{d})]\Gamma[d(p+\frac{d-q+1/2}{d})]} \rho^{dp+d-q-\frac{1}{2}} \\ &= \sum_{r=1}^{d}\sum_{p=0}^{\infty} \frac{(-1)^{dp+r}}{2\sqrt{\pi}} \frac{c}{d} \frac{\Gamma[-c(p+\frac{2r-1}{2d}-\frac{1}{c})]\Gamma[c(p+\frac{2r-1}{2d})]}{\Gamma[d(p+\frac{r}{d})]\Gamma[d(p+\frac{r+1/2}{d})]} \rho^{dp+r-\frac{1}{2}}, \end{aligned} \tag{5.25}$$

where the last equality is obtained by setting $d-q = r$, and then reversing the order of summation. Applying eqn. (2.3) and eqn. (2.5) of [120], and further simplifying, we obtain

$$\begin{aligned} T_1 = \sum_{r=1}^{d} \frac{(-1)^r}{2\sqrt{\pi}} \frac{c}{d} \rho^{r-\frac{1}{2}} \frac{\Gamma[-\frac{c(2r-1)}{2d}+1]\Gamma[-\frac{c(2r-1)}{2d}]}{\Gamma(r)\Gamma(r+\frac{1}{2})} \sum_{p=0}^{\infty} \frac{[(-1)^{c+d}]^p(\rho^d)^p}{(d^{2d})^p p!} \\ \times \frac{(1)_p}{(\frac{r}{d})_p(\frac{r}{d}+\frac{1}{d})_p \ldots (\frac{r}{d}+\frac{d-1}{d})_p (\frac{r+1/2}{d})_p (\frac{r+1/2}{d}+\frac{1}{d})_p \ldots (\frac{r+1/2}{d}+\frac{d-1}{d})_p}. \end{aligned} \tag{5.26}$$

According to the definition of generalized Hypergeometric function [113, 9.141], the infinite series in p can be expressed as the Hypergeometric function ${}_1F_{2d}(\cdot;\cdot;\cdot)$. The second infinite series in (5.24) can be similarly reduced to a finite sum of generalized Hypergeometric functions. The average error rate of BPSK modulation for $\alpha \neq 4$ can finally be expressed as

$$\begin{aligned} P_e = \frac{1}{2} + \sum_{r=1}^{d} \frac{(-1)^r \alpha}{4\sqrt{\pi}} \frac{\Gamma(-\frac{\alpha}{4}(2r-1)+1)\Gamma(\frac{\alpha}{4}(2r-1))}{\Gamma(r)\Gamma(r+\frac{1}{2})} \rho^{r-\frac{1}{2}} \\ \times {}_1F_{2d}\Bigg[1; \frac{r+1/2}{d}, \frac{r+1/2}{d}+\frac{1}{d}, \ldots, \frac{r+1/2}{d}+\frac{d-1}{d}, \\ \frac{r}{d}, \frac{r}{d}+\frac{1}{d}, \ldots, \frac{r}{d}+\frac{d-1}{d}; \frac{(-1)^{(c+d)}\rho^d}{d^{2d}}\Bigg] \\ + \sum_{r=1}^{c} \frac{(-1)^r}{2\sqrt{\pi}} \frac{\Gamma(-\frac{2}{\alpha}r+\frac{1}{2})}{\Gamma(\frac{2}{\alpha}r+1)} \rho^{\frac{2}{\alpha}} {}_1F_{2d}\Bigg[1; \frac{r}{c}+\frac{1}{d}, \ldots, \frac{r}{c}+\frac{d}{d}, \\ \frac{r}{c}-\frac{1}{2d}+\frac{1}{d}, \ldots, \frac{r}{c}-\frac{1}{2d}+\frac{d}{d}; \frac{(-1)^{(c+d)}\rho^d}{d^{2d}}\Bigg], \end{aligned} \tag{5.27}$$

For $\alpha = 4$, (5.23) has double poles at $s = -1/2, -3/2, -5/2, \ldots$ to the left of the contour $\mathcal{R}(s) = c$. In order to avoid residue computation with double poles, (5.23) is expressed as follows for $\alpha = 4$ by substituting $s = -s$ and utilizing the properties of the Gamma function [113]:

$$P_e = -\frac{1}{2\pi j}\int_{-c-j\infty}^{-c+j\infty} \frac{\Gamma\left(-s+\frac{1}{2}\right)\Gamma(-2s+1)\Gamma\left(s+\frac{1}{2}\right)}{2^{1-2s}\pi s}\rho^s ds, \tag{5.28}$$

which then has simple poles at $s = -1/2, -3/2, -5/2, \ldots$ to the left of the contour $\mathcal{R}(s) = -c$. Again by applying the residue theorem, followed by reducing the infinite series to a single generalized Hypergeometric function, the average error rate for $\alpha = 4$ can finally be expressed as

$$P_e = \frac{1}{2\pi\sqrt{\rho}}\,{}_3F_0\left[1, 1, \frac{1}{2}; -\frac{1}{\rho}\right]. \tag{5.29}$$

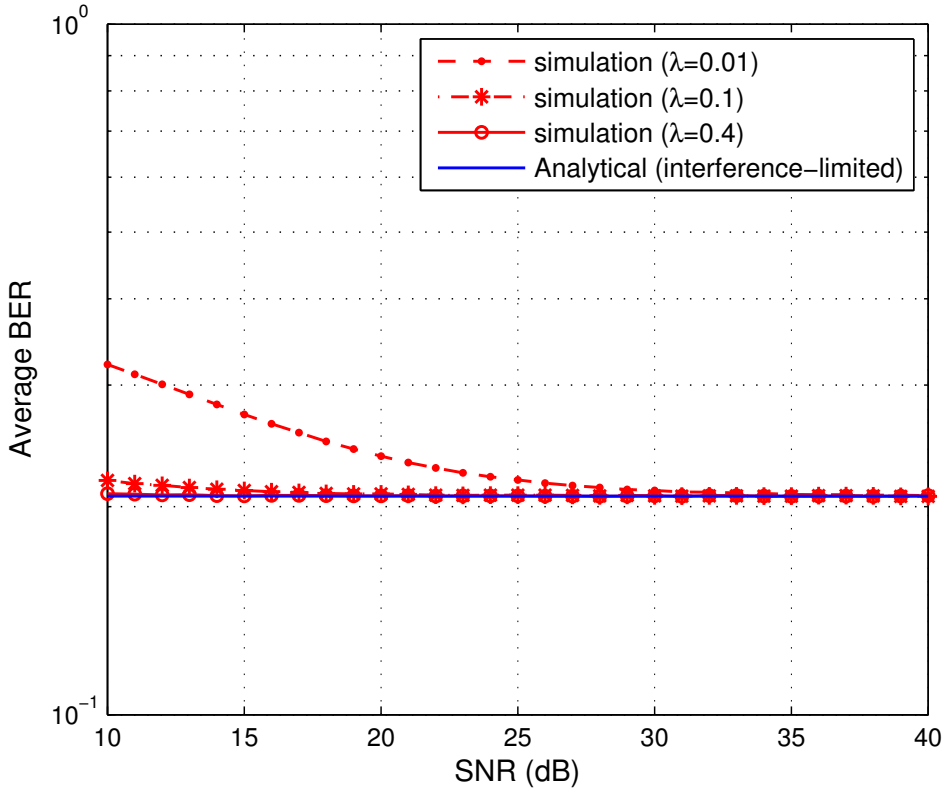

Figure 5.3: Average BER of a typical user in a downlink cellular network with BPSK modulation ($\alpha = 3$).

In Figure 5.3, the simulated BER of a typical user is plotted against SNR without ignoring the impact of noise for three different BS densities $0.01\,\text{BS/Km}^2$, $0.1\,\text{BS/Km}^2$ and $0.4\,\text{BS/Km}^2$. Our analytical result based on the interference-limited assumption is also plotted in the figure, where the result is independent of both λ and SNR. The figure reveals that the simulation and analytical results converge once the network becomes interference limited. If the value of λ is large, as is expected in future networks for higher capacity, the network becomes interference limited even at smaller values of SNR.

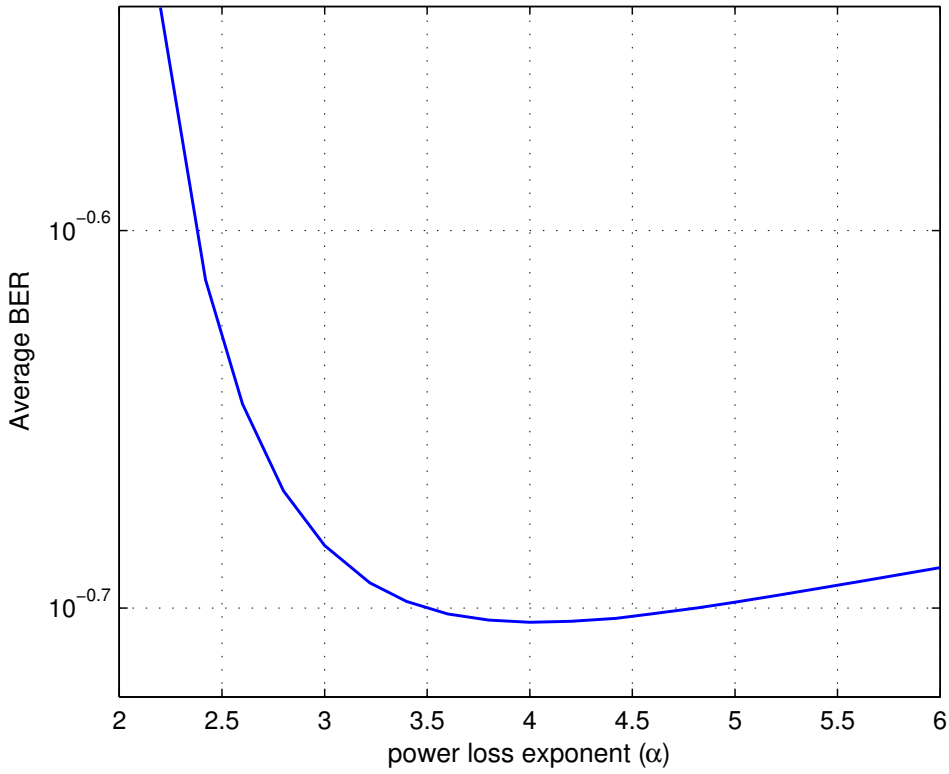

Figure 5.4: Average BER versus power loss exponent (α) in downlink cellular network.

The impact of the power loss exponent, α in the average BER of a downlink cellular network is assessed in Figure 5.4. The error rate initially drops with the increase in α due to the decrease in the aggregate interference power received at a typical user. However, the received power from the serving BS also decreases

at the same time. Eventually, when the decrease in the desired signal power due to the increase in α becomes more significant than the decrease in the aggregate interference power, the error rate starts increasing.

5.4 Conclusion

The contributions of the chapter are two-fold:

1. We developed UA for the error probability of an intended link subject to interference from the surrounding nodes distributed according to a PPP. Both single-antenna and MRC receivers were analyzed. The diversity order of the system is found to be $2/\alpha$, independent of the number of receive antennas.

2. We introduced the MT based approach to error probability analysis of a typical user served by the BS providing the maximum received power in a cellular network. The BS locations were modeled as a PPP. A closed-form expression for the average BER of BPSK modulation in Rayleigh fading was derived. The average error probability is found to be independent of SNR and BS density.

Chapter 6

Outage Probability of Underlay Cognitive Relay Networks with Spatially Random Nodes

This chapter[1] considers an underlay cognitive relay network coexisting with a primary digital TV broadcasting network, in which the secondary user transmissions are power constrained to limit the interference on any primary receiver in the network. The primary receivers and secondary relays are randomly located due to irregular deployments and/or mobility and thus, their spatial distributions are modeled by two independent PPPs. We analyze an opportunistic relaying scenario and develop a relay-selection scheme by considering the interference constraints on all the primary receivers in the network. We then analytically evaluate the relaying performance in terms of the outage probability by using tools from stochastic geometry and point process theory, and finally compare the performance against that of direct communication. Closed-form expressions are derived for the outage probabilities of both the relay and direct links, along with their high SNR asymptotics.

6.1 Introduction

Deployment of HetNets has emerged as the most cost-effective approach to cope with the exponential growth in cellular data traffic. However, despite the tremendous improvement in the spectral efficiency offered by HetNets, more radio spec-

[1]This chapter has been published in the proceedings of the IEEE Global Communications Conference (GLOBECOM) 2014, Austin, Texas [121].

trum than currently available will be needed to accommodate the unrelenting demand for mobile data in future cellular networks. It has been shown in [42] that a large portion of the currently deployed spectrum is sparsely utilized. Cognitive radio is an emerging technique that can potentially alleviate the spectrum-scarcity problem by exploiting the underutilized portions of the radio spectrum. Cognitive radio allows the unlicensed (secondary) users to access the licensed (primary) users spectrum with minimal or no impact on primary user communications. The VHF/UHF TV spectrum is the most promising candidate for cognitive access due to its lower propagation loss and the availability of large amount of underutilized spectrum [122]. A cellular network operating in its regular licensed spectrum can utilize the TV spectrum for additional capacity through cognitive secondary usage.

Among the various approaches to primary-secondary spectrum sharing– *interweave*, *overlay* and *underlay* [40], underlay method is appealing for its low implementation complexity. It supports primary-secondary concurrent transmissions only at the cost of the knowledge of the interference channel gains to primary users, unlike the overlay system, which requires knowledge of primary users' codebooks and their messages as well [40]. In this chapter, we analyze the underlay approach to secondary usage of underutilized TV spectrum. Since the underlay system must operate under strict transmit power constraints to ensure that the resultant interference on each primary receiver is below a predefined threshold, the coverage range is limited. Cooperative relaying, in this case, is a natural choice to achieve the adequate radio-reception quality at distant users. We propose a novel cooperative relay transmission scheme with interference constraints and then evaluate the gain in outage probability (the commonly used measure for quality of reception in wireless communications).

In particular, we consider opportunistic relaying by idle users in underlay cognitive radio networks. Generally, in practical networks, the users are expected to be highly mobile and their locations vary with time. The secondary relays are thus assumed to be randomly and independently located in the network area, and are thus spatially modeled by a PPP. The PPP is a widely used spatial model for networks with a possibly infinite number of nodes randomly and independently distributed in

a finite or infinite area [58]. The PPP-based modeling of the locations of primary and secondary users is adopted in [61] to evaluate the aggregate interference caused by the secondary users on the primary system in underlay cognitive radio networks, and in [60] to analyze the performance of different cognitive radio MAC protocols.

The coexisting primary system is a digital TV broadcasting network. Different standards have been developed for digital TV broadcasting such as European Digital Video Broadcasting (DVB-T for terrestrial and DVB-H for handhelds), the North American Advanced Television Systems Committee (ATSC) and Integrated Services Digital Broadcasting-Terrestrial (ISDB-T), most of which are based on OFDM for robustness against multipath distortion [123]. Due to the broadcast nature, any underlay secondary transmission must satisfy the interference constraints on all the TV receivers in the network. We assume that the TV receivers, either fixed or mobil,e take unplanned/unknown positions, and their spatial distribution is modeled by a PPP.

6.1.1 Previous Work and Contributions of the Chapter

Substantial research work on underlay cognitive relay networks has been reported in the literature [124–127]. The outage probability of a cognitive single-relay network, in which the transmit power is constrained according to the interference threshold at the primary receiver, is analyzed in [124] under Nakagami-m fading. Optimal power allocation schemes, which maximize the overall rate of a cognitive single-relay network are investigated in [125], while adhering to the interference power constraint on the primary receiver. The conventional relay selection schemes are redefined in [126] and [127] for a cognitive multiple-relay network to incorporate the interference constraint in terms of the required outage probability of the primary transmission and the maximum tolerable interference power at the primary receiver, respectively. Joint relay selection and power allocation to maximize the system throughput under interference constraint is investigated in [128]. However, these studies consider a fixed number of relay nodes and either ignore the effect of path loss and thus the spatial configuration of the relays or assume the relay locations to be deterministic (known a priori). These assumptions are not suitable for

analyzing cognitive radio networks with inherent mobility of the secondary users. Further, in these work, no two primary receivers have the same transmitter and thus, any secondary transmission needs to satisfy the interference constraint at only one primary receiver. In contrast to these work, we focus on the following aspects in this chapter.

1. Considering the multicasting primary network, we take into account the spatial distribution of primary receivers and derive the outage probability of the direct link between an underlay secondary source node and its destination, while satisfying the interference constraints on all the primary receivers.

2. We next consider the opportunistic relaying between the source-destination pair and derive the outage probability of the relay link, while taking into account the spatial distribution of the relays.

3. The relay-selection scheme is designed by considering not only the source-relay and relay-destination links, but also the stringent interference constraints on all the primary receivers.

4. We finally compare the outage probability of the relay link with that of the direct link.

The rest of the chapter is organized as follows. The system model and the relaying scheme are presented in Section 6.2. In Section 6.4, the outage probabilities of the direct link and the relay link are derived in closed forms along with their high SNR asymptotics. The analytical results are verified through Monte Carlo simulations in Section 6.5. Finally, some concluding remarks are presented in Section 6.6

6.2 System Model

We consider a cognitive radio system consisting of primary and secondary networks. The multicasting primary network consists of a primary transmitter and a number of primary receivers, which are spatially distributed according to a homogeneous PPP $\Phi_p = \{y_1, y_2, y_3 \ldots\}$ on $\mathbb{R}^2$ with density λ_p, where y_i is the location

of the ith receiver. The wireless communication between a secondary source node S (located at the origin o without loss of generality) and a secondary destination node D (located at $l_d \in \mathbb{R}^2$) is considered, where the distance between S and D, $||o - l_d||$ is fixed at L. The $S - D$ communication occurs either directly or through opportunistic relaying by a set of idle users in the secondary network. The spatial distribution of the idle users on $\mathbb{R}^2$ is denoted by $\Phi_s = \{x_1, x_2, x_3, \ldots\}$, where x_i is the location of the ith user. Φ_s is assumed to be a homogeneous PPP with density λ_s. A realization of the primary receivers and secondary relays spatially distributed according to independent PPPs is shown in Figure 6.1. From the definition of PPP [57, 59], the number of primary receivers N_p and the number of secondary relays N_s in a given area A are independent Poisson random variables (RVs) with mean $A\lambda_p$ and $A\lambda_s$, respectively. Also, the numbers of primary receivers in disjoint areas are independent, and so are the numbers of secondary relays.

The primary multicast network is assumed to be based on OFDM, and thus, each primary receiver occupies a number of frequency channels called subcarriers. A secondary transmission uses a frequency channel from the primary spectra. Each frequency channel undergoes independent flat fading. We assume that all the primary and secondary nodes have a single antenna for transmission and reception. The single antenna model leads to simple analytical results with insights into important system parameters. The extension to various multiple antenna techniques to analyze their impact on the performance could be an important direction for future research.

6.3 Channel Model and Transmission Schemes

Independent Rayleigh multipath fading is assumed between any pair of nodes and across frequency channels. A general power-law path loss model with loss exponent α is also considered in which the signal power decays at the rate of $r^{-\alpha}$ with distance r from the transmitter. Consequently, the channel power gain of the jth frequency channel between a pair of nodes at x and y is given by $h^j_{xy}||x - y||^{-\alpha}$, where h^j_{xy} is the fading power gain, which is exponentially distributed with unit

mean. The value of α is typically in the range of 1.6 to 6 [12], where $\alpha = 2$ is for free space propagation.

6.3.1 Direct Mode

Let the direct $S-D$ communication occur over frequency channel n. The source S, while transmitting, must ensure that the interference imposed on each primary receiver is below a predefined threshold $\bar{I}$. If this constraint is satisfied for the primary receiver to which it generates the largest interference power, then the constraint is satisfied for all other receivers. Let $H_{S_n} = \max_{y \in \Phi_p} h^n_{oy} \, ||o - y||^{-\alpha}$ be the largest interference channel gain associated with S on the nth frequency channel. Then, the transmit power of S on this frequency channel is constrained as $P_{S_n} \leq \bar{I}/H_{S_n}$. The information about the largest interference channel can be acquired through primary receiver detection algorithms [129] or through beacons [130]. If S transmits with the maximum allowable power, the received SNR at the destination D is

$$\text{SNR}_{SD}(o, l_d) = \frac{\bar{I}}{N_0 H_{S_n}} h^n_{ol_d} \, L^{-\alpha}, \tag{6.1}$$

where N_0 is the noise variance. The interference signal from the primary transmitter is treated as Gaussian noise [40].

6.3.2 Relaying Mode

In the relaying mode, the $S - D$ pair communicate through an intermediate node selected from the set of available idle secondary users. The relaying protocol used is decode-and-forward (DF), with the assumption that there is no decoding error if the received SNR is greater than the threshold γ_{th}. Although all the idle users distributed over $\mathbb{R}^2$ are considered as the candidate relays for the selection of the best relay in our analysis, this method is equivalent to considering only the idle nodes within a circle of radius $R >> L$ as the candidate relays. As the path loss becomes more pronounced than fading when the relays move away from the $S - D$ link, the nodes beyond R are less likely to be chosen. The relays operate in the half-duplex mode, and hence, the information transmission from S to D requires two time-slots. We assume that each candidate relay uses a different frequency channel

among the primary spectra [127]. Relay selection, thus, involves the selection of the primary spectrum as well, and the system also gains from multispectrum diversity [131]. If the source S transmits with the maximum allowable power $P_{S_j\max} = \bar{I}/H_{S_j}$ on the jth frequency channel used by the candidate relay R_j at $x \in \Phi_s$, the received SNR at R_j in the first time-slot is given by

$$\text{SNR}_{SR_j}(o,x) = \frac{\bar{I}}{N_0 H_{S_j}} h_{ox}^j \, ||o-x||^{-\alpha}. \tag{6.2}$$

The source S can successfully transmit information to any candidate relay at which the received SNR is greater than the threshold γ_{th}. These nodes are the potential relays (represented by the triangles in Figure 6.1) to retransmit the successfully decoded message to the destination D in the second time-slot. Let $\hat{\Phi}_s$ denote the set of potential relays, i.e.,

$$\hat{\Phi}_s = \{x \in \Phi_s, \text{SNR}_{SR_j}(o,x) \geq \gamma_{th}\}. \tag{6.3}$$

The transmit power of a potential relay R_j at $x \in \hat{\Phi}_s$ is constrained as $P_{R_j} \leq \bar{I}/H_{R_j}$, where $H_{R_j} = \max\limits_{y \in \Phi_p} h_{xy}^j \, ||x-y||^{-\alpha}$ is the largest interference channel gain associated with R_j. Under the proposed relaying scheme, the best node from the set $\hat{\Phi}_s$ is selected. While in a conventional relay network, the relay that has the best channel to the destination would be selected, our selection criterion considers the interference constraint as well. We denote the location of the selected relay by ζ, i.e.,

$$\zeta = \arg\max_{x \in \hat{\Phi}_s} \frac{h_{xl_d}^j ||x-l_d||^{-\alpha}}{H_{R_j}}. \tag{6.4}$$

The corresponding received SNR at the destination D from the relay link when the selected relay transmitted with the maximum allowable power is

$$\text{SNR}_{R_J D}(\zeta, l_d) = \frac{\bar{I}}{N_0 H_{R_J}} h_{\zeta l_d}^J \, ||\zeta - l_d||^{-\alpha}, \tag{6.5}$$

where J is the index of the selected relay.

6.4 Performance Analysis

The outage probability is chosen as the performance metric for the given system. To derive the outage probabilities of both the relay and the direct links, we first

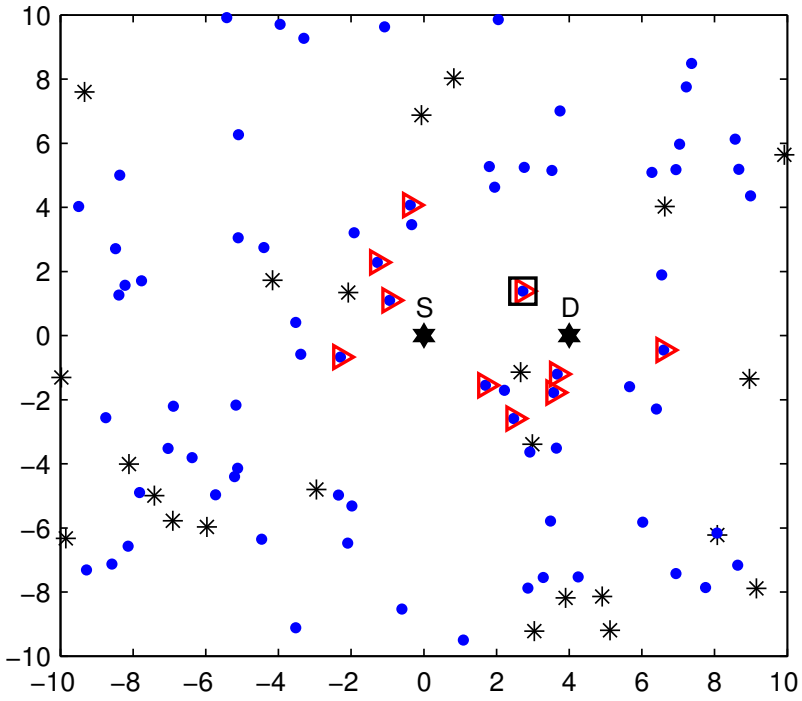

Figure 6.1: Spatial distribution of the primary receivers and the secondary relays according to independent PPPs. The asterisks are the primary receivers ($\lambda_p = 0.15/\pi$); the dots are the idle secondary users which serve as candidate relays ($\lambda_s = 0.5/\pi$); the triangles are the potential relays, i.e., the relays at which the received SNRs are greater than $\gamma_{th} = 5$ dB; and the square is the selected relay as per the proposed scheme. The $S - D$ distance $L = 4$, the path-loss exponent $\alpha = 4$ and the noise normalized interference threshold $\bar{I} = 10$ dB.

derive the distribution of $Z = \max\limits_{y \in \Phi} h_{cy} \, ||c - y||^{-\alpha}$, where $c \in \mathbb{R}^2$, $\{y \in \Phi\}$ are the points of a homogeneous PPP Φ on $\mathbb{R}^2$ with density λ, and $\{h_{cy}; y \in \Phi\}$ are independent exponentially distributed RVs with unit mean. We can observe that Z does not depend on the exact coordinates of the points $y \in \Phi$, but rather on their distances from c. Let us define $\Phi_l \triangleq \{l = ||c - y||; y \in \Phi\}$ as the transformed points of Φ by mapping the 2-D space into a positive real line with a function f such that $f(b(c, l)) = [0, l]$ (i.e., each point of a closed disc $b(c, l)$ on $\mathbb{R}^2$ of radius l and center c is mapped into the closed interval $[0, l]$ on $\mathbb{R}^+$). From the mapping theorem (Section 2.3), Φ_l is also a PPP of density $\lambda(l)$ given by $\int_{[0,l]} \lambda(l) \, dl = \int_{b(c,l)} \lambda \, dx$. Thus, $\lambda(l) = 2\pi\lambda l$.

Probability Distribution of Z

The probability distribution of $Z = \max_{y\in\Phi} h_{cy}\,||c-y||^{-\alpha}$ can be derived as follows:

$$\begin{aligned} F_Z(z) &= \mathbb{P}\left(\max_{y\in\Phi} h_{cy}\,||c-y||^{-\alpha} < z\right) \\ &= \mathbb{E}_{\Phi}\left[\prod_{y\in\Phi} \mathbb{P}\left(h_{cy}\,||c-y||^{-\alpha} < z|y\right)\right] \\ &= \mathbb{E}_{\Phi_l}\left[\prod_{l\in\Phi_l} (1-\exp(-zl^{\alpha}))\right], \end{aligned} \tag{6.6}$$

where the second equality follows from the independence of RVs $\{h_{cy}; y\in\Phi\}$ and (6.6) from the fact that $h_{cy} \sim \text{Exp}[1]$ and the transformation of Φ to Φ_l. Now, by using the PGFL of PPP given by (2.7), we have

$$\begin{aligned} F_Z(z) &= \exp\left(-2\pi\lambda\int_0^{\infty}\exp(-zl^{\alpha})l\,dl\right) \\ &= \exp\left(-\frac{\pi\lambda}{z^{2/\alpha}}\Gamma\left(\frac{2}{\alpha}+1\right)\right), \end{aligned} \tag{6.7}$$

where (6.7) results from the definition of the Gamma function [113, 8.310]. Equation (6.7) reveals that the distribution of Z is independent of c. In the following section, we use the notation $\mathcal{Z}(\lambda,\alpha)$ to denote the distribution of $\max_{y\in\Phi} h_{cy}\,||c-y||^{-\alpha}$, $c\in\mathbb{R}^2$.

The transmit power of any secondary node k given by $P_k = \bar{I}/H_k$, where $H_k \sim \mathcal{Z}(\lambda_p,\alpha)$ is, thus, independent of the location of the node. The average transmit power of a secondary node can be obtained as

$$\bar{P} = \int_0^{\infty}\frac{\bar{I}}{z}\,dF_{H_k}(z) = \bar{I}\frac{\Gamma(\alpha/2+1)}{(\pi\lambda_p\Gamma(2/\alpha+1))^{\alpha/2}}. \tag{6.8}$$

6.4.1 Outage Probability of the Direct Mode

The outage probability of the direct $S-D$ link, $P_d = \mathbb{P}(\text{SNR}_{SD}(o,l_d) < \gamma_{th})$ can be obtained by using the SNR expression (6.1) as follows:

$$\begin{aligned} P_d &= \mathbb{P}\left(\frac{\bar{I}h_{ol_d}^n\,L^{-\alpha}}{N_0 H_{S_n}} < \gamma_{th}\right) \\ &= \mathbb{E}_{h_{ol_d}^n}\left[\mathbb{P}\left(H_{S_n} > \frac{\bar{I}h_{ol_d}^n}{N_0\gamma_{th}L^{\alpha}}\middle| h_{ol_d}^n\right)\right], \end{aligned} \tag{6.9}$$

where $H_{S_n} = \max_{y \in \Phi_p} h_{oy}^n \, ||o-y||^{-\alpha} \sim \mathcal{Z}(\lambda_p, \alpha)$. By applying the CDF derived in (6.7), followed by the expectation over $h_{ol_d}^n \sim \text{Exp}[1]$, P_d can be simplified as

$$\begin{aligned} P_d &= 1 - \int_0^\infty \exp\left(-\beta \, L^2 u^{-2/\alpha}\right) e^{-u} \, du \\ &= 1 - \Gamma\left(1, 0, \beta \, L^2, \frac{2}{\alpha}\right), \end{aligned} \tag{6.10}$$

where $\Gamma(\cdot,\cdot,\cdot,\cdot)$ is the extended incomplete Gamma function [132, Eq. 6.2], $\beta = \left(\Gamma(\alpha/2+1)\gamma_{th}/\rho\right)^{2/\alpha}$, and $\rho = \bar{P}/N_0$ is the average transmit SNR. The asymptotic performance as SNR $\to \infty$, thus, can be analyzed with the asymptotic $\beta \to 0$. By using $\exp(-x) = 1 - x$ as $x \to 0$, the asymptotic outage probability of the direct link is given by

$$P_d \sim b \, L^2 \left(\gamma_{th}/\rho\right)^{2/\alpha} + O(\rho^{-4/\alpha}) \quad \text{as} \quad \rho \to \infty, \tag{6.11}$$

where $b = \Gamma\left(-2/\alpha + 1\right)\left(\Gamma\left(\alpha/2+1\right)\right)^{2/\alpha}$.

6.4.2 Outage Probability of the Relaying Mode

The analysis of the outage probability of the relay link given by $P_r = \mathbb{P}(\text{SNR}_{R_J D} < \gamma_{th})$ involves Euclidean distances from the randomly located relays to the source and the destination. Therefore, it is mathematically convenient to use a polar coordinate system, where $x \in \mathbb{R}^2$ is represented as $x = (r, \theta)$. We take the coordinate axes to be oriented such that $l_d = (L, 0)$. The corresponding distances from the relay located at x to the source and the destination are then given by $d_S(x) = ||o - x|| = r$ and $d_D(x) = ||x - l_d|| = \sqrt{r^2 + L^2 - 2rL\cos\theta}$, respectively. According to (6.4) and (6.5), the relay link outage probability can be expressed as

$$\begin{aligned} P_r &= \mathbb{P}\left(\frac{\bar{I}}{N_0 H_{R_J}} h_{\zeta l_d}^J \, ||\zeta - l_d||^{-\alpha} < \gamma_{th}\right) \\ P_r &= \mathbb{P}\left(\max_{x \in \hat{\Phi}_s} \frac{h_{x l_d}^j d_D^{-\alpha}(x)}{H_{R_j}} < \frac{\gamma_{th} N_0}{\bar{I}}\right). \end{aligned} \tag{6.12}$$

By utilizing the independence of RVs $\{H_{R_j}; x \in \hat{\Phi}_s\}$, we have

$$\begin{aligned} P_r &= \mathbb{E}_{\hat{\Phi}_s}\left[\prod_{x \in \hat{\Phi}_s} \mathbb{E}_{h_{x l_d}^j}\left(\mathbb{P}\left(H_{R_j} > \frac{\bar{I} h_{x l_d}^j}{N_0 \gamma_{th} \, d_D^\alpha(x)} \middle| h_{x l_d}^j, x\right)\right)\right] \\ &= \mathbb{E}_{\hat{\Phi}_s}\left[\prod_{x \in \hat{\Phi}_s} \left(1 - \int_0^\infty \exp\left(-\beta d_D^2(x) v^{-2/\alpha}\right) e^{-v} \, dv\right)\right], \end{aligned} \tag{6.13}$$

where (6.13) follows from the fact that $H_{R_j} \sim \mathcal{Z}(\lambda_p, \alpha)$ and $h^j_{xl_d} \sim$ Exp[1]. In order to compute P_r, we need to first identify the properties of the set of potential relays $\hat{\Phi}_s$. Since the SNRs at the candidate relays (6.2) are independent, the set $\hat{\Phi}_s$ in (6.3) is formed by independent thinning of the original process Φ_s, i.e., by selecting a point x of the process Φ_s with probability $p = \mathbb{P}(\text{SNR}_{SR_j}(o,x) \geq \gamma_{th})$ independently of the other points in the process. Since Φ_s is a PPP, the thinned process $\hat{\Phi}_s$ is also a PPP [57] with density $\hat{\lambda}_s(x)$ given by

$$\begin{aligned}\hat{\lambda}_s(x) &= \lambda_s \mathbb{P}(\text{SNR}_{SR_j}(o,x) \geq \gamma_{th}) \\ &= \lambda_s \int_0^\infty \exp\left(-\beta\, r^2 u^{-2/\alpha}\right) e^{-u}\, du \\ &= \lambda_s \Gamma\left(1, 0, \beta\, r^2, \frac{2}{\alpha}\right), \end{aligned} \tag{6.14}$$

where (6.14) is derived by using the fact that $\mathbb{P}(\text{SNR}_{SR_j}(o,x) \geq \gamma_{th}) = 1 - P_d$ with the receiver location $l_d = x$. The average number of potential relays can be obtained as

$$\begin{aligned}\hat{\Lambda}_s &= \int_0^{2\pi} \int_0^\infty \hat{\lambda}_s\, r dr\, d\theta \\ &= \lambda_s \int_0^\infty e^{-v} \int_0^{2\pi} \int_0^\infty \exp\left(-\beta r^2 u^{-2/\alpha}\right)\, r dr\, d\theta\, du \\ &= \frac{\pi \lambda_s}{\beta} \Gamma\left(\frac{2}{\alpha} + 1\right), \end{aligned} \tag{6.15}$$

where the second equality is obtained by substituting the integral expression for $\hat{\lambda}_s(x)$, followed by the change in the order of integration. Since $\hat{\Phi}_s$ is a PPP of intensity $\lambda_s(x)$, by using the PGFL of a PPP, the P_r in (6.13) can be simplified as

$$\begin{aligned}P_r &= \exp\left(-\int_{\mathbb{R}^2} \hat{\lambda}_s(x) \int_0^\infty \exp\left(-\beta d_D^2(x) v^{-\frac{2}{\alpha}}\right) e^{-v}\, dv\, dx\right) \\ &= \exp\left(-\lambda_s \Upsilon(\beta)\right), \end{aligned} \tag{6.16}$$

where

$$\begin{aligned}\Upsilon(\beta) = &\int_{u=0}^\infty e^{-u} \int_{v=0}^\infty e^{-v} \exp\left(-\beta L^2 v^{-\frac{2}{\alpha}}\right) \\ &\times \int_{r=0}^\infty r \exp\left(-\beta (v^{-\frac{2}{\alpha}} + u^{-\frac{2}{\alpha}}) r^2\right) \\ &\times \int_{\theta=0}^{2\pi} \exp\left(2\,\beta\, L v^{-\frac{2}{\alpha}} r \cos\theta\right)\, d\theta\, dr\, dv\, du. \end{aligned} \tag{6.17}$$

Equation (6.16) is obtained by substituting the integral expression for $\lambda_s(x)$, followed by the conversion of Cartesian to polar coordinates and the change in the order of integration. The integral with respect to θ in (6.17) can be solved by using [113, Eq. 8.431.3] as follows:

$$\begin{aligned}\Upsilon(\beta) = \pi \int_{u=0}^{\infty} e^{-u} \int_{v=0}^{\infty} e^{-v} \exp\left(-\beta L^2 v^{-\frac{2}{\alpha}}\right) \\ \times \int_{r=0}^{\infty} 2\,r\, \exp\left(-\beta(v^{-\frac{2}{\alpha}} + u^{-\frac{2}{\alpha}})r^2\right) \\ \times I_0\left(2\beta L v^{-\frac{2}{\alpha}} r\right) dr\, dv\, du, \end{aligned} \tag{6.18}$$

where $I_0(\cdot)$ is the zeroth order modified Bessel function of the first kind. The integral with respect to r can be reduced to the form $\mathcal{I} = \int_0^{\infty} \frac{2r}{2\sigma^2} \exp\left(-\frac{r^2+s^2}{2\sigma^2}\right) I_0\left(\frac{s}{\sigma^2} r\right) dr$ by substituting $2\beta L v^{-2/\alpha} = s/\sigma^2$ and $\beta(v^{-2/\alpha} + u^{-2/\alpha}) = 1/(2\sigma^2)$ so that $\mathcal{I}$ integrates to unity. $\Upsilon(\beta)$ can then be simplfied as

$$\begin{aligned}\Upsilon(\beta) = \frac{\pi}{\beta} \int_{u=0}^{\infty} e^{-u} \int_{v=0}^{\infty} \frac{e^{-v}}{(v^{-2/\alpha} + u^{-2/\alpha})} \\ \times \exp\left(-\frac{\beta L^2}{v^{2/\alpha} + u^{2/\alpha}}\right) dv\, du, \end{aligned} \tag{6.19}$$

which can be accurately approximated by using the Gauss-Laguerre quadrature rule [133, Eq. 25.4.45]. The outage probability of the relay link can finally be expressed as

$$P_r \approx \exp\left(-\frac{\lambda_s \pi}{\beta} \sum_{i=1}^{n} \sum_{j=1}^{n} w_i w_j \frac{\exp\left(-\frac{\beta L^2}{\vartheta_j^{2/\alpha} + \vartheta_i^{2/\alpha}}\right)}{(\vartheta_j^{-2/\alpha} + \vartheta_i^{-2/\alpha})}\right), \tag{6.20}$$

where $\vartheta_i (i = 1, 2, \ldots, n)$ are the nodes of Gauss-Laguerre quadrature and $w_i (i = 1, 2, \ldots, n)$ are the corresponding weights. The exponential decrease in the outage probability of the relay link with the increasing density λ_s of the relay nodes can be observed. The asymptotic outage probability of the relay link can be obtained as follows by using $\exp(-x) = 1 - x$ as $x \to 0$ for the last exponential in (6.19):

$$\begin{aligned} P_r \sim & A \exp\left(-\lambda_s \pi \mathcal{I}_1 \left(\Gamma(\alpha/2+1)\right)^{-2/\alpha} (\rho/\gamma_{th})^{2/\alpha}\right) \\ & \times \left(1 + O(\rho^{-2/\alpha})\right) \quad \text{as} \quad \rho \to \infty, \end{aligned} \tag{6.21}$$

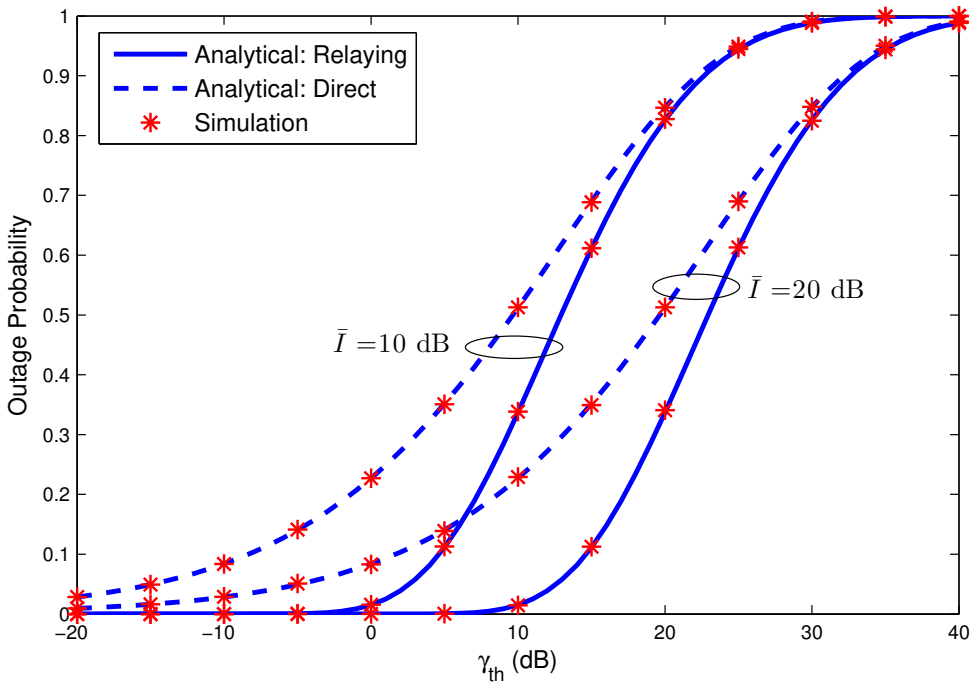

Figure 6.2: The outage probability versus threshold γ_{th} for different levels of interference threshold $\bar{I}$ when $\Lambda_s = 0.5$ and $L = 2$.

where $A = \exp\left(\lambda_s \pi L^2 \mathcal{I}_2\right)$ and $\mathcal{I}_1, \mathcal{I}_2$ are given by

$$\mathcal{I}_1 = \int_{u=0}^{\infty} e^{-u} \int_{v=0}^{\infty} \frac{e^{-v}}{v^{-2/\alpha} + u^{-2/\alpha}} dv\, du, \tag{6.22}$$

$$\mathcal{I}_2 = \int_{u=0}^{\infty} e^{-u} \int_{v=0}^{\infty} \frac{e^{-v}}{(v^{-2/\alpha} + u^{-2/\alpha})(v^{2/\alpha} + u^{2/\alpha})} dv\, du, \tag{6.23}$$

which can be readily computed for the given value of α.

6.5 Numerical and Simulation Results

In this section, we validate our analytical results through Monte Carlo simulations and assess the impact of various parameters on the performance of the proposed system. The path loss exponent α is assumed to be 4. The interference threshold $\bar{I}$ is normalized by the noise power N_0. We define Λ_p and Λ_s as the average number of primary receivers and candidate relays, respectively, within a circle of unit radius, i.e., $\Lambda_p = \pi\lambda_p, \Lambda_s = \pi\lambda_s$. Unless stated otherwise, Λ_p is set to 0.15. To compute the analytical outage probability of the relay link by using (6.20), we choose $n = 30$.

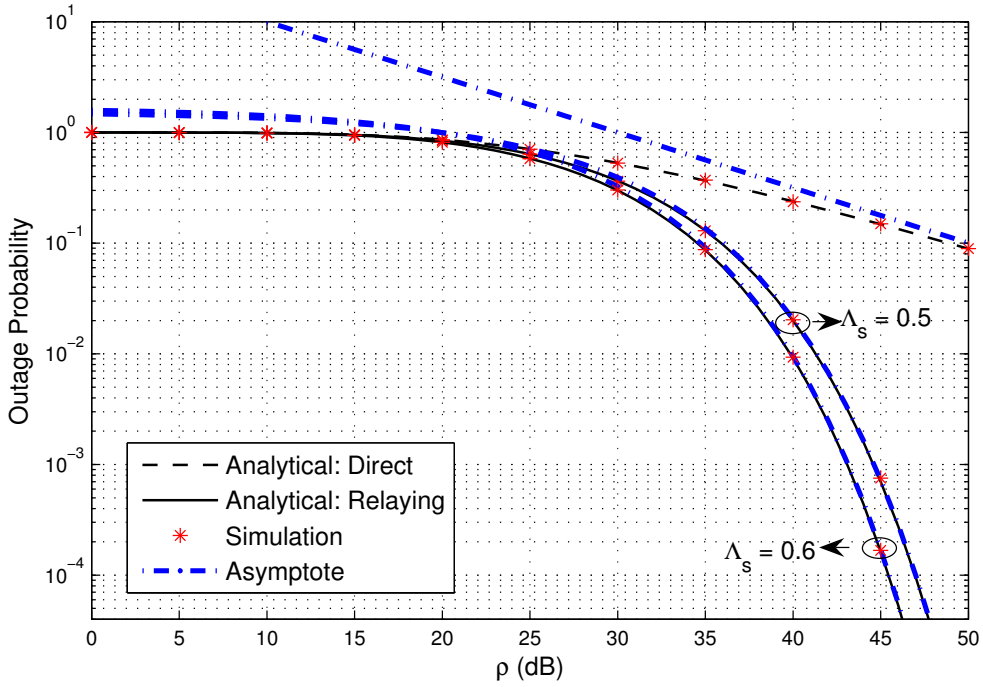

Figure 6.3: The outage probability versus average transmit SNR ρ when $\gamma_{th} = 10$ dB and $L = 2$.

The outage probability versus the threshold γ_{th} is plotted in Figure 6.2 for both the direct and relaying modes. The figure shows an excellent match between the analytical and simulation results. Significant improvement in the outage performance by using the relaying mode over direct transmission is clearly visible. If the primary receivers can tolerate more interference, the secondary nodes can transmit with higher power, and the outage performance naturally improves. Thus, the outage probability at a given value of γ_{th} is lower for $\bar{I} = 20$ dB than that for $\bar{I} = 10$ dB.

The outage probability as a function of the average transmit SNR ρ is presented in Figure 6.3. The high-SNR asymptotes derived in (6.11) and (6.21) for the direct link and the relay link, respectively, are plotted in the figure along with the analytical and simulation curves. At $\rho = 40$ dB, the gain in using the relaying mode over the direct mode, $G = P_d/P_r$, is about 10.6 dB for $\Lambda_s = 0.5$ and 14 dB for $\Lambda_s = 0.6$.

Figure 6.4 assesses the impact of the $S - D$ distance L on the outage performance. As expected, the outage performance of both the direct and relaying modes improves when the $S - D$ distance shrinks. When the density of relays is small

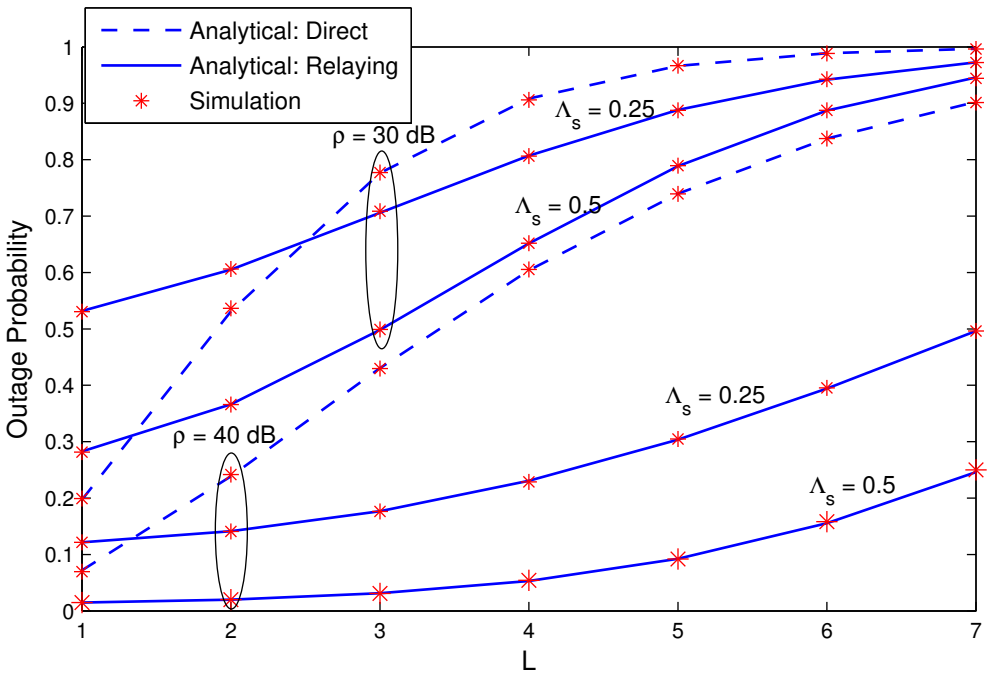

Figure 6.4: The outage probability as a function of the $S-D$ distance L for different levels of average transmit SNR ρ and average density of relay nodes Λ_s when γ_{th}=10 dB.

and the average transmit SNR is low as well, the source may not have any potential relay node available for retransmission. In this case, the outage performance of the direct mode is better than that of the relaying mode. However, if the density of the relays is sufficient, the relaying mode outperforms the direct transmission.

Figure 6.5 shows the required average density of the relay nodes Λ_s as the function of the average density of the primary receivers Λ_p to maintain a given outage probability of the relaying mode. Equation (6.8) shows that the average transmit power of the secondary node is inversely proportional to Λ_p. As the transmit power of the secondary node decreases with the increasing Λ_p, the outage probability tends to increase. However, one can maintain the desired outage probability by increasing Λ_s.

6.6 Conclusion

In this chapter, we analyzed the outage in a dual-hop underlay secondary network coexisting with the primary TV broadcasting network. The spatial distributions

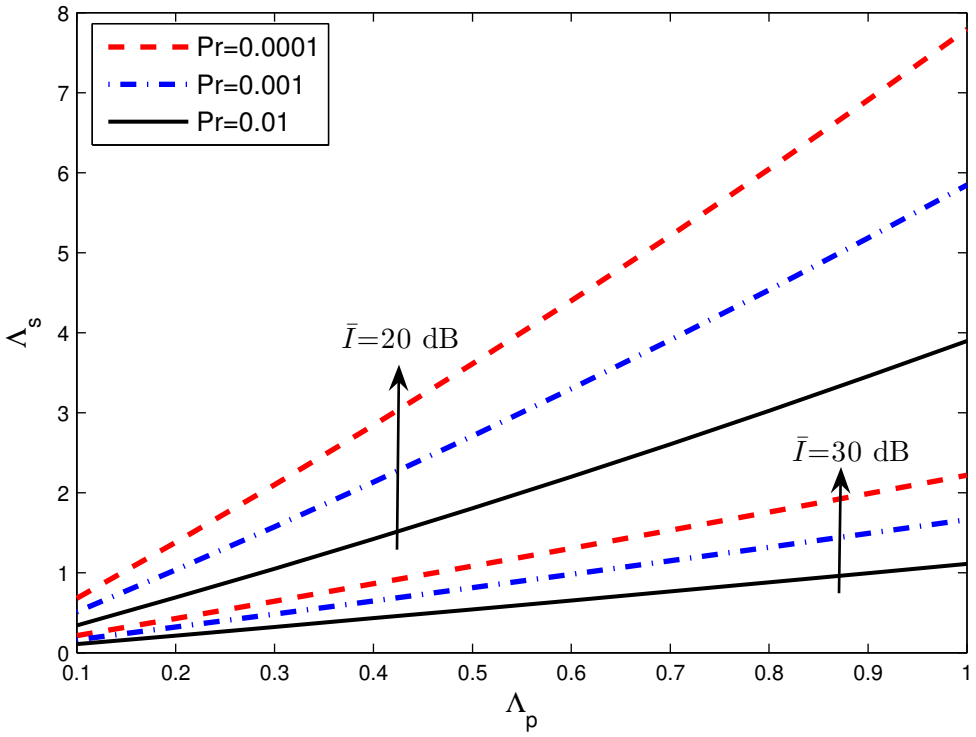

Figure 6.5: The required average density of relay nodes Λ_s as a function of average density of primary receivers Λ_p for different levels of outage probability when $\gamma_{th} = 10$ dB and $L = 1$.

of the secondary relays and primary receivers were modeled as independent PPPs. An opportunistic relaying scenario with a relay selection scheme that satisfies the interference constraint on any primary receiver was investigated. The impact of various parameters on the outage performance was analyzed. We found that the gain in using the relay transmission over the direct mode increases with the density of the relay nodes. The required density of the relay nodes for the desired outage probability increases with the density of the primary receivers. The required density of the relay nodes however, decreases if the primary receivers can tolerate more interference.

Chapter 7

Conclusion and Future Work

7.1 Summary of Contributions and Concluding Remarks

- Chapter 3 presented a refined analytical modeling of HetNets by incorporating a proper notion of the cell load, which effectively captured the impact of the user density and available resources on network interference. The biased-received-power based BS-user association scheme (popularly known as CRE) for load balancing complemented by the resource partitioning method of interference coordination was analyzed for multi-channel downlink. The performance gain due to the load balancing and interference coordination was evaluated in terms of the average user data rate. It was observed that if the bias value and resource partitioning fraction are carefully tuned, the gain can be as high as 115%. However, the parameter tuning must be updated in accordance with the changing network load.

- Chapter 4 analyzed the downlink performance of multi-antenna HetNets with SDMA, in which the number of users simultaneously served with SDMA in each cell is a function of the user distribution. The ZF precoding matrix at each macro BS was designed such that while enabling user multiplexing in its own cell, the interference nulling to certain pico users was also considered. The results indicated that the SINR as well as the rate coverage of the victim pico users (those suffering strong interference from macro BS) can be significantly improved with the proposed interference nulling scheme. However,

since interference nulling costs the macro BS its available degrees of freedom for serving its own users, the number of antennas dedicated for serving its own users, T_{min} must be carefully chosen. The optimal choice of T_{min} was found to be coupled with the association bias. The optimal combination of T_{min} and association bias for average data rate performance metric was thus numerically investigated in this chapter. The optimal L^*_{max} for both macro and pico tier which maximize the average data rate were also investigated. L^*_{max} was found to outperform both the SU-BF ($L_{\text{max}} = 1$) and full-SDMA ($L_{\text{max}} = K$) techniques in terms of the average data rate. The impact of imperfect CSI on the performance was also analyzed. It was observed that the detrimental impact due to CSI imperfection is stronger for the interference nulling scheme as compared to the SNR maximization beamforming scheme.

- Chapter 5 introduced the UA approach to error probability analysis of an intended radio link subjected to interference from surrounding nodes which are distributed according to a PPP. UAs for both single-antenna and MRC receivers were developed. For MRC receivers, the diversity order of the system was found to be $2/\alpha$, independent of the number of receive antennas, where α is the path-loss exponent. An MT based approach for error probability analysis of a typical user served by the BS providing the maximum received power in cellular network was also presented in this chapter. The closed-form expression for the average BER of BPSK modulation in Rayleigh fading was derived. The average error probability was found to be independent of the SNR and BS density.

- Chapter 6 analyzed an underlay cognitive relay network coexisting with TV broadcasting network. An opportunistic relaying scheme in which the selected relay satisfies the interference constraint on any TV receiver was investigated and the impact of various parameters on the outage performance was analyzed. It was concluded from the analysis that the gain in using the relay transmission over the direct mode increases with the density of the relay nodes. Their required density for the desired outage probability increases

with the density of the primary receivers. The required density, however, decreases if the primary receivers can tolerate more interference.

7.2 Future Research Directions

- Due to the inherent irregularity in the spatial distribution of BSs in HetNets, the BS locations can be modeled as spatial point process. The most popular model for this purpose has been the homogeneous PPP, as it provides useful insights due to its analytical tractability. However, this model may not accurately characterize different deployment scenarios. For example, the operators may deploy more BSs in the areas of higher traffic-demand/population-density. Also, although the BSs may be randomly deployed, two BSs may not be arbitrarily close to each other. Thus, the spatial modeling of BSs needs to be refined. While repulsive point processes are suitable for the second scenario mentioned above [134, 135], the first deployment scenario can be modeled as a clustered process [136].

  Along with the refinement in spatial modeling of BSs, the analytical model must accurately capture other important network characteristics such as cell load. Most of the analysis in the literature ignores cell load by considering a fully-loaded network (e.g. [16,19,21,47]). We got rid of fully loaded assumption and characterized cell load as the function of user density and available resources. We modeled user distribution as a homogeneous PPP, which may not accurately captures network performance for scenarios where users could be concentrated at areas of social attractions such as shopping malls. To accommodate such scenarios, spatial user distribution modeling with adjustable statistical properties has been recently investigated in [137]. While refining the spatial modeling of BSs as well as the user distribution, the researchers must be careful not to completely lose the analytical tractability.

- In Chapter 4, we considered multi-antenna BSs with single-antenna receivers. Future work could consider multi-antenna receivers performing receive combining and/or interference cancellation. The impact of imperfect CSI for the

special case of $L^m_{\text{max}} = L^p_{\text{max}} = 1$ could be extended to general L^m_{max} and L^p_{max}.

- The analytical framework presented in Chapter 5 for the average error probability analysis of the downlink communication of a typical user considered a single-tier cellular network with maximum-received-power based BS-user association. An important extension of this work would be to consider multi-tier HetNets with various BS-user association and interference coordination schemes. Even the error probability analysis requires the proper characterization of the cell load because the interference from a BS is a direct function of its load.

Bibliography

[1] Cisco, "Cisco visual networking index: Global mobile data traffic forecast update, 2015–2020," 2015. [Online]. Available: http://www.cisco.com/c/en/us/solutions/collateral/service-provider/visual-networking-index-vni/mobile-white-paper-c11-520862.pdf

[2] A. Goldsmith, *Wireless Communications*. Cambridge University Press, 2005.

[3] Z. Wang and G. Giannakis, "A simple and general parameterization quantifying performance in fading channels," *IEEE Trans. Commun.*, vol. 51, no. 8, pp. 1389 – 1398, Aug. 2003.

[4] Qualcomm Incorporated, "LTE Advanced: Heterogeneous networks," white paper, Jan. 2011.

[5] T. Hu, J. Pang, and H.-J. Su, "LTE-Advanced heterogeneous networks: Release 10 and beyond," in *Proc. IEEE Int. Conf. Commun. (ICC)*, Ottawa, Canada, Jun. 2012, pp. 6999 – 7003.

[6] V. Osa, C. Herranz, J. F. Monserrat, and X. Gelabert, "Implementing opportunistic spectrum access in LTE-Advanced," *EURASIP J. Wireless Commun. Netw.*, pp. 1–17, Mar. 2012.

[7] A. Damnjanovic, J. Montojo, Y. Wei, T. Ji, T. Luo, M. Vajapeyam, T. Yoo, O. Song, and D. Malladi, "A survey on 3GPP heterogeneous networks," *IEEE Wireless Commun. Mag.*, vol. 18, no. 3, pp. 10–21, Jun. 2011.

[8] D. Lopez-Perez, I. Guvenc, G. de la Roche, M. Kountouris, T. Quek, and J. Zhang, "Enhanced intercell interference coordination challenges in heterogeneous networks," *IEEE Wireless Commun. Mag.*, vol. 18, no. 3, pp. 22 – 30, Jun. 2011.

[9] S. Landstrom, H. Murai, and A. Simonsson, "Deployment aspects of LTE pico nodes," in *Proc. IEEE Int. Conf. Commun. Workshops (ICC)*, Kyoto, Japan, Jun. 2011, pp. 1–5.

[10] G. de la Roche, A. Valcarce, D. L*ó*pez-P*é*rez, and J. Zhang, "Access control mechanisms for femtocells," *IEEE Commun. Mag.*, vol. 48, no. 1, pp. 33–39, Jan. 2010.

[11] J. Gora and S. Redana, "In-band and out-band relaying configurations for dual-carrier LTE-Advanced system," in *Proc. IEEE Int. symposium Personal, Indoor and Mobile Radio Commun. (PIMRC)*, Toronto, ON, Sep. 2011, pp. 1820–1824.

[12] T. S. Rappaport, *Wireless Communications: Principles and Practice*, 2nd ed. New Jersey: Prentice Hall, 2001.

[13] G. L. Stuber, *Principles of Mobile Communications*. Norwell, MA: Kluwer, 1996.

[14] A. Ghosh, N. Mangalvedhe, R. Ratasuk, B. Mondal, M. Cudak, E. Visotsky, T. A. Thomas, J. G. Andrews, P. Xia, H.-S. Jo, H. S. Dhillon, and T. D. Novlan, "Heterogeneous cellular networks: From theory to practice," *IEEE Commun. Mag.*, vol. 50, no. 6, pp. 54–64, 2012.

[15] J. G. Andrews, F. Baccelli, and R. K. Ganti, "A tractable approach to coverage and rate in cellular networks," *IEEE Trans. Commun.*, vol. 59, no. 11, pp. 3122–3134, Nov. 2011.

[16] H. S. Dhillon, R. K. Ganti, F. Baccelli, and J. G. Andrews, "Modeling and analysis of k-tier downlink heterogeneous cellular networks," *IEEE J. Select. Areas Commun.*, vol. 30, no. 3, pp. 550–560, Apr. 2012.

[17] S. Mukherjee, "Distribution of downlink SINR in heterogeneous cellular networks," *IEEE J. Select. Areas Commun.*, vol. 30, no. 3, pp. 54–64, Apr. 2012.

[18] H. ElSawy and E. Hossain, "Two-tier HetNets with cognitive femtocells: Downlink performance modeling and analysis in a multichannel environment," *IEEE Trans. Mobile Comput.*, vol. 13, no. 3, pp. 649–663, Mar. 2014.

[19] H.-S. Jo, Y. J. Sang, P. Xia, and J. G. Andrews, "Heterogeneous cellular networks with flexible cell association: A comprehensive downlink SINR analysis," *IEEE Trans. Wireless Commun.*, vol. 11, no. 10, pp. 3484–3495, Oct. 2012.

[20] X. Lin, J. G. Andrews, and A. Ghosh, "Modeling, analysis and design for carrier aggregation in heterogeneous cellular networks," *IEEE Trans. Commun.*, vol. 61, no. 9, pp. 4002–4015, 2013.

[21] S. Singh and J. Andrews, "Joint resource partitioning and offloading in heterogeneous cellular networks," *IEEE Trans. Wireless Commun.*, vol. 13, no. 2, pp. 888 – 901, Feb. 2014.

[22] Y. Zhong and W. Zhang, "Multi-channel hybrid access femtocells: A stochastic geometric analysis," *IEEE Trans. Commun.*, vol. 61, no. 7, pp. 3016–3026, Jul. 2013.

[23] Q. Ye, B. Rong, Y. Chen, M. Al-Shalash, C. Caramanis, and J. G. Andrews, "User association for load balancing in heterogeneous cellular networks," *IEEE Trans. Wireless Commun.*, vol. 12, no. 6, Jun. 2013.

[24] M. Cierny, H. Wang, R. Wichman, Z. Ding, and C. Wijting, "On number of almost blank subframes in heterogeneous cellular networks," *IEEE Trans. Wireless Commun.*, vol. 12, no. 10, pp. 5061–5073, Oct. 2013.

[25] T. D. Novlan, R. K. Ganti, A. Ghosh, and J. G. Andrews, "Analytical evaluation of fractional frequency reuse for heterogeneous cellular networks," *IEEE Trans. Commun.*, vol. 60, no. 7, pp. 2029–2039, 2012.

[26] 3GPP TSG RAN, *Evolved Universal Terrestrial Radio Access (E-UTRA); Carrier Aggregation; Base station radio transmission and reception, Release 10, V.10.1.0.* 3GPP TR 36.808, 2013.

[27] ——, *Evolved Universal Terrestrial Radio Access (E-UTRA); Coordinated multi-point operation for LTE physical layer aspects, Release 11, V.11.2.0.* 3GPP TR 36.819, 2013.

[28] M. Sawahashi, Y. Kishiyama, A. Morimoto, D. Nishikawa, and M. Tanno, "Coordinated multipoint transmission/reception techniques for LTE-advanced," *IEEE Wireless Commun.*, vol. 17, no. 3, pp. 26–34, Jun. 2010.

[29] D. Lee, H. Seo, E. Clerckx, B.and Hardouin, D. Mazzarese, S. Nagata, and K. Sayana, "Coordinated multipoint transmission and reception in LTE-advanced: deployment scenarios and operational challenges," *IEEE Commun. Mag.*, vol. 50, no. 2, pp. 148–155, Feb. 2012.

[30] J. Zhang and J. G. Andrews, "Adaptive spatial intercell interference cancellation in multicell wireless networks," *IEEE J. Select. Areas Commun.*, vol. 28, no. 9, pp. 1455–1468, Dec. 2010.

[31] C. Li, J. Zhang, M. Haenggi, and K. B. Letaief, "User-centric intercell interference nulling for downlink small cell networks," *IEEE Trans. Commun.*, vol. 63, no. 4, pp. 1419–1430, Apr. 2015.

[32] LTE, *Evolved Universal Terrestrial Radio Access (E-UTRA); Physical Layer Procedures, Release 8, V.8.8.0.* 3GPP TS 36.213, 2009.

[33] ——, *Evolved Universal Terrestrial Radio Access (E-UTRA); Physical Layer Procedures, Release 10, V.10.1.0.* 3GPP TS 36.213, 2011.

[34] S. M. Alamouti, "A simple transmit diversity technique for wireless communications," *IEEE J. Select. Areas Commun.*, vol. 16, no. 8, pp. 1451–1458, Oct. 1998.

[35] H. Jafarkhani, *Space-time Coding: Theory and Practice*. Cambridge. U.K.: Cambridge Univ. Press, 2005.

[36] G. J. Foschini, "Layered space-time architecture for wireless communication in a fading environment when using multi-element antennas," *Bell Labs Technical Journal*, vol. 5, no. 2, pp. 41–59, 1996.

[37] D. Gesbert, M. Kountouris, R. W. Heath, C.-B. Chae, and T. Salzer, "From single user to multiuser communications: shifting the MIMO paradigm," *IEEE Signal Process. Mag.*, vol. 24, no. 5, pp. 36–46, Sep. 2007.

[38] J. Mitola and G. Q. Maguire, "Cognitive radio: Making software radios more personal," *IEEE Pers. Commun.*, vol. 6, no. 4, pp. 13–18, Aug. 1999.

[39] S. Haykin, "Cognitive radio: Brain-empowered wireless communications," *IEEE J. Sel. Areas Commun.*, vol. 23, no. 2, pp. 201–220, Feb. 2005.

[40] A. Goldsmith, S. A. Jafar, I. Maric, and S. Srinivasa, "Breaking spectrum gridlock with cognitive radios: An information theoretic perspective," *Proc. IEEE*, vol. 97, no. 5, pp. 894–914, May 2009.

[41] S. Rangan, T. S. Rappaport, and E. Erkip, "Millimeter wave cellular wireless networks: Potentials and challenges," *Proc. IEEE*, vol. 102, no. 3, pp. 36–46, Mar. 2014.

[42] Federal Communications Commission, "Spectrum policy task force," ep. ET Docket no. 02-135, Nov. 2002.

[43] J. Sachs, I. Maric, and A. Goldsmith, "Cognitive cellular systems within the TV spectrum," in *Proc. IEEE Symposium on New Frontiers in Dynamic spectrum*, Singapore, Apr. 2010.

[44] Nokia Networks, "LTE for unlicensed spectrum," white paper.

[45] Ericsson, "LTE license assisted access," http://www.ericsson.com/res/thecompany/docs/press/media_kits/ericsson-license-assisted-access-laa-january-2015.pdf, Jan. 2015.

[46] S. Landstrm, A. Furuskr, K. Johansson, L. Falconetti, and F. Kronestedt, "Heterogeneous networks-increasing cellular capacity," Ericsson Review, 2011. [Online]. Available: http://www.ericsson.com/res/thecompany/docs/publications/ericsson_review/2011/heterogeneous_networks.pdf

[47] S. Mukherjee and I. Guvenc, "Effects of range expansion and interference coordination on capacity and fairness in heterogeneous networks," in *Proc. IEEE Asilomar Conf. Signals, Syst., Comput.*, Pacific Grove, CA, Nov. 2011, pp. 1855 – 1859.

[48] Y. Jin and L. Qiu, "Joint user association and interference coordination in heterogeneous cellular networks," *IEEE Commun. Lett.*, vol. 17, no. 12, pp. 2296–2299, Dec. 2013.

[49] P. C. Pinto and M. Z. Win, "Communication in a Poisson field of interferers–part i: Interference distribution and error probability," *IEEE Trans. Wireless Commun.*, vol. 9, no. 7, pp. 2176–2186, Jul. 2010.

[50] C. Merola, A. Guidotti, M. Di Renzo, F. Santucci, and G. Corazza, "Average symbol error probability in the presence of network interference and noise," in *Proc. IEEE Int. Conf. Commun. (ICC)*, Ottawa, Canada, Jun. 2012, pp. 2613–2618.

[51] M. D. Renzo, C. Merola, A. Guidotti, F. Santucci, and G. E. Corazza, "Error performance of multi-antenna receivers in a Poisson field of interferers: A stochastic geometry approach," *IEEE Trans. Commun.*, vol. 61, no. 5, pp. 2025–2047, May 2013.

[52] D. Tse and P. Viswanath, *Fundamentals of Wireless Communication*. Cambridge University Press, Jun. 2005.

[53] M. Haenggi, J. G. Andrews, F. Baccelli, O. Dousse, and M. Franceschetti, "Stochastic geometry and random graphs for the analysis and design of wireless networks," *IEEE J. Sel. Areas Commun.*, vol. 27, no. 7, Sep. 2009.

[54] F. Baccelli and B. Blaszczyszyn, *Stochastic Geometry and Wireless Networks*. NOW: Foundations and Trends in Networking, 2010.

[55] M. Haenggi, *Stochastic Geometry for Wireless Networks*. Cambridge University Press, 2013.

[56] M. Haenggi and R. K. Ganti, *Interference in Large Wireless Networks*. NOW: Foundations and Trends in Networking, 2009.

[57] S. N. Chiu, D. Stoyan, W. S. Kendall, and J. Mecke, *Stochastic Geometry and its Applications*, 3rd ed. John Wiley and Sons, 2013.

[58] H. ElSawy, E. Hossain, and M. Haenggi, "Stochastic geometry for modeling, analysis, and design of multi-tier and cognitive cellular wireless networks: A survey," *IEEE Commun. Surveys Tuts.*, vol. 15, no. 3, pp. 996–1019, Jul. 2013.

[59] J. Kingman, *Poisson Processes*. Oxford University Press Inc., 1993.

[60] T. V. Nguyen and F. Baccelli, "A stochastic geometry model for cognitive radio networks," *The Computer Journal*, vol. 55, no. 5, pp. 534–552, May 2012.

[61] C. Lee and M. Haenggi, "Interference and outage in Poisson cognitive networks," *IEEE Trans. Wireless Commun.*, vol. 11, no. 4, pp. 1392–1401, Apr. 2012.

[62] S. Srinivasa and M. Haenggi, "Distance distributions in finite uniformly random networks: Theory and applications," *IEEE Trans. Veh. Technol.*, vol. 59, no. 2, pp. 940–949, Feb. 2010.

[63] B. Matern, *Spatial Variation*, 2nd ed. Springer Lecture Notes in Statistics, 1986.

[64] G. Alfano, M. Garetto, and E. Leonardi, "New insights into the stochastic geometry analysis of dense CSMA networks," in *Proc. IEEE INFOCOM'11*, Shanghai, China, Apr. 2011, pp. 2642–2650.

[65] H. ElSawy and E. Hossain, "A modified hard core point process for analysis of random CSMA wireless networks in general fading environments," *IEEE Trans. Commun.*, vol. 61, no. 4, pp. 1520–1534, Apr. 2013.

[66] K. Gulati, B. L. Evans, J. G. Andrews, and K. R. Tinsley, "Statistics of co-channel interference in a field of Poisson and Poisson-Poisson clustered interferers," *IEEE Trans. Signal Process.*, vol. 58, no. 12, pp. 6207–6222, Dec. 2010.

[67] M. Z. Win, P. C. Pinto, and L. A. Shepp, "A mathematical theory of network interference and its applications," *IEEE Proc.*, vol. 97, no. 2, pp. 205–230, Feb. 2009.

[68] E. Biglieri, R. Calderbank, A. Constantinides, A. Goldsmith, A. Paulraj, and H. V. Poor, *MIMO Wireless Communications*. New York, NY, USA: Cambridge University Press, 2007.

[69] J. Mietzner, R. Schober, L. Lampe, W. H. Gerstacker, and P. A. Hoeher, "Multiple-antenna techniques for wireless communications - a comprehensive literature survey," *IEEE Commun. Surveys Tuts.*, vol. 11, no. 2, pp. 87–105, Apr. 2009.

[70] M. K. Simon and M.-S. Alouini, *Digital Communication over Fading Channels* , 2nd ed. Wiley-IEEE Press, Dec. 2004.

[71] J. G. Proakis, *Digital Communications*, 4th ed. McGraw-Hill, 2001.

[72] T. K. Y. Lo, "Maximum ratio transmission," *IEEE Trans. Commun.*, vol. 47, no. 10, pp. 1458–1461, Oct. 1999.

[73] I. E. Telatar, "Capacity of multi-antenna Gaussian channels," Bell Laboratories, Lucent Technologies, Tech. Rep., Oct. 1995.

[74] K. Huang, J. Andrews, D. Guo, R. Heath, and R. Berry, "Spatial interference cancellation for multi-antenna mobile ad hoc networks," *IEEE Trans. Inf. Theory*, vol. 58, no. 3, pp. 1660–1676, Mar. 2012.

[75] M. O. Hasna and M.-S. Alouini, "End-to-end performance of transmission systems with relays over Rayleigh-fading channels," *IEEE Trans. Wireless Commun.*, vol. 2, no. 6, pp. 1126–1131, Nov. 2003.

[76] J. N. Laneman, D. N. C. Tse, and G. W. Wornell, "Cooperative diversity in wireless networks: Efficient protocols and outage behavior," *IEEE Trans. Inf. Theory*, vol. 50, no. 12, pp. 3062–3080, Dec. 2004.

[77] A. Sendonaris, E. Erkip, and B. Aazhang, "User cooperation diversity. part I: System description," *IEEE Trans. Commun.*, vol. 51, no. 11, pp. 1927–1938, Nov. 2003.

[78] Y. Jing and B. Hassibi, "Distributed space-time coding in wireless relay networks," *IEEE Trans. Wireless Commun.*, vol. 5, no. 12, pp. 3524–3536, Dec. 2006.

[79] A. Talebi and W. A. Krzymien, "Multiple-antenna multiple-relay cooperative communication system with beamforming," in *Proc. IEEE Veh. Technol. Conf. (VTC) Spring*, Singapore, May 2008, pp. 2350– 2354.

[80] G. Amarasuriya, M. Ardakani, and C. Tellambura, "Output-threshold multiple-relay-selection scheme for cooperative wireless networks," *IEEE Trans. Veh. Technol.*, vol. 59, no. 6, pp. 3091–3097, Jul. 2010.

[81] F. A. Onat, Y. Fan, H. Yanikomeroglu, and V. Poor, "Threshold-based relay selection for detect-and-forward relaying in cooperative wireless networks," *EURASIP J. Wireless Commun. Netw.*, vol. 2010, pp. 1–9, Apr. 2010.

[82] S. Atapattu, Y. Jing, H. Jiang, and C. Tellambura, "Opportunistic relaying in two-way networks," in *Proc. 5th Int. ICST Conf. Commun. Netw. China (CHINACOM)*, Beijing, Aug. 2010, pp. 1–8.

[83] A. Adinoyi, Y. Fan, H. Yanikomeroglu, H. V. Poor, and F. Al-Shaalan, "Performance of selection relaying and cooperative diversity," *IEEE Trans. Wireless Commun.*, vol. 8, no. 12, pp. 5790–5795, Dec. 2009.

[84] I. Krikidis, J. S. Thompson, S. McLaughlin, and N. Goert, "Max-min relay selection for legacy amplify-and-forward systems with interference," *IEEE Trans. Wireless Commun.*, vol. 8, no. 6, pp. 3016–3027, Jun. 2009.

[85] Y. Dhungana and C. Tellambura, "Multi-channel analysis of cell range expansion and resource partitioning in two-tier heterogeneous cellular networks," *IEEE Trans. Wireless Commun.*, vol. 15, no. 3, pp. 2394–2306, Mar. 2016.

[86] R. Madan, J. Borran, A. Sampath, N. Bhushan, A. Khandekar, and T. Ji, "Cell association and interference coordination in heterogeneous LTE-A cellular networks," *IEEE J. Select. Areas Commun.*, vol. 28, no. 9, pp. 1479–1489, Dec. 2010.

[87] K. Balachandran, J. Kang, K. Karakayali, and K. Rege, "Cell selection with downlink resource partitioning in heterogeneous networks," in *Proc. IEEE Int. Conf. on Commun. Workshops (ICC)*, Kyoto, Japan, Jun. 2011, pp. 1–6.

[88] M. Vajapeyam, A. Damnjanovic, J. Montojo, T. Ji, Y. Wei, and D. Malladi, "Downlink FTP performance of heterogeneous networks for LTE-Advanced," in *Proc. IEEE Int. Conf. Commun. Workshops (ICC)*, Kyoto, Japan, Jun. 2011, pp. 1–5.

[89] S. Strzyz, K. Pedersen, J. Lachowski, and F. Frederiksen, "Performance optimization of pico node deployment in LTE macro cells," in *Proc. Future Network and Mobile Summit*, Warsaw, Poland, Jun. 2011, pp. 1–9.

[90] C.-H. Huang and C.-Y. Liao, "An interference management scheme for heterogeneous network with cell range extension," in *Proc. Asia-Pacific Network Operations and Management Symposium (APNOMS)*, Taipei, Taiwan, Sep. 2011, pp. 1–5.

[91] I. Guvenc, "Capacity and fairness analysis of heterogeneous networks with range expansion and interference coordination," *IEEE Commun. Lett.*, vol. 15, no. 10, pp. 1084 – 1087, Oct. 2011.

[92] D. Colombi, B. Thors, N.Wiren, L.-E. Larsson, and C. Tornevik, "Measurements of downlink power level distributions in LTE networks," in *Proc. IEEE Int. Conf. Electromagn. Adv. Appl. (ICEAA)*, Portland, Oregon, Sep. 2013, pp. 98–101.

[93] L. Barolli, F. Xhafa, A. Durresi, and A. Koyama, "A fuzzy-based handover system for avoiding ping-pong effect in wireless cellular networks." in *Proc. IEEE Int. Conf. Parallel Process. Workshops (ICPP-W)*, Portland, Oregon, Sep. 2008, pp. 135–142.

[94] J.-S. Ferenc and Z. Neda, "On the size distribution of Poisson-Voronoi cells," *Physica A-Stat. Mech. Appl.*, vol. 385, no. 2, pp. 518–526, 2007.

[95] Y. Dhungana and C. Tellambura, "Performance analysis of SDMA with inter-tier interference nulling in HetNets," in *Proc. IEEE Int. Conf. Commun. (ICC)*, Kuala Lampur, Malaysia, accepted Jan. 30, 2016.

[96] ——, "Performance analysis of SDMA with inter-tier interference nulling in HetNets," *IEEE Trans. Wireless Commun.*, submitted March 2016.

[97] M. Kang and M.-S. Alouini, "Largest eigenvalue of complex Wishart matrices and performance analysis of MIMO MRC systems," *IEEE J. Select. Areas Commun.*, vol. 21, no. 3, pp. 418 – 426, Apr. 2003.

[98] L. Zheng and D. Tse, "Diversity and multiplexing: a fundamental tradeoff in multiple-antenna channels," *IEEE Trans. Inform. Theory*, vol. 49, no. 5, pp. 1073 – 1096, May 2003.

[99] Q. H. Spencer, A. L. Swindlehurst, and M. Haardt, "Zero-forcing methods for downlink spatial multiplexing in multiuser MIMO channels," *IEEE Trans. Signal Process.*, vol. 52, no. 2, pp. 461–471, Feb. 2004.

[100] J. G. Andrews, W. Choi, and R. W. Heath, "Overcoming interference in spatial multiplexing MIMO cellular networks," *IEEE Wireless Commun. Mag.*, pp. 95–104, Dec. 2007.

[101] V. Chandrasekhar, M. Kountouris, and J. G. Andrews, "Coverage in multi-antenna two-tier networks," *IEEE Trans. Wireless Commun.*, vol. 8, no. 10, pp. 5314–5327, Oct. 2009.

[102] R. W. Heath, M. Kountouris, and T. Bai, "Modeling heterogeneous network interference with using Poisson point processes," *IEEE Trans. Signal Process.*, vol. 61, no. 16, pp. 4114–4126, Aug. 2013.

[103] H. S. Dhillon, M. Kountouris, and J. G. Andrews, "Downlink coverage probability in MIMO HetNets," in *Proc. IEEE ASILOMAR*, Pasific Grove, CA, USA, Nov. 2012, pp. 683–687.

[104] H. Dhillon and J. Kountouris, M.and Andrews, "Downlink MIMO HetNets: Modeling, ordering results and performance analysis," *IEEE Trans. Wireless Commun.*, vol. 12, no. 10, pp. 5208–5222, Oct. 2013.

[105] A. Gupta, H. Dhillon, S. Vishwanath, and J. Andrews, "Downlink multi-antenna heterogeneous cellular network with load balancing," *IEEE Trans. Commun.*, vol. 62, no. 11, pp. 4052–4067, Nov. 2014.

[106] S. Veetil, K. Kuchi, and R. Ganti, "Spatial multiplexing in heterogeneous networks with MMSE receiver," in *Proc. IEEE Global Commun. Conf. (GLOBECOM)*, Austin, TX, Dec. 2014, pp. 3684–3689.

[107] S. T. Veetil, K. Kuchi, and R. K. Ganti, "Performance of PZF and MMSE receivers in cellular networks with multi-user spatial multiplexing," *IEEE Trans. Wireless Commun.*, vol. 14, no. 9, pp. 4867–4878, Sep. 2015.

[108] J. Zhang, R. Chen, J. Andrews, A. Ghosh, and R. Heath, "Networked MIMO with clustered linear precoding," *IEEE Trans. Wireless Commun.*, vol. 8, no. 4, pp. 1910–1921, Apr. 2009.

[109] M. Feng, X. She, L. Chen, and Y. Kishiyama, "Enhanced dynamic cell selection with muting scheme for DL CoMP in LTE-A," in *Proc. IEEE Veh. Technol. Conf. (VTC) Spring*, Taipei, May 2010, pp. 1–5.

[110] Y. Wu, Y. Cui, and B. Clerckx, "Analysis and optimization of inter-tier interference coordination in downlink multi-antenna HetNets with offloading," *IEEE Trans. Wireless Commun.*, vol. 14, no. 12, pp. 6550–6564, Dec. 2015.

[111] P. Xia, C.-H. Liu, and J. G. Andrews, "Downlink coordinated multi-point with overhead modeling in heterogeneous cellular networks," *IEEE Trans. Wireless Commun.*, vol. 12, no. 8, pp. 4025–4037, Aug. 2013.

[112] N. Jindal, J. G. Andrews, and S. Weber, "Rethinking MIMO for wireless networks: Linear throughput increases with multiple receive antennas," in *Proc. IEEE Int. Conf. Commun. (ICC)*, Dresden, Dec. 2009, pp. 1–6.

[113] I. S. Gradshteyn and I. M. Ryzhik, *Table of Integrals, Series, and Products*, 7th ed. Academic Press, Inc., 2007.

[114] N. Jindal, "MIMO broadcast channels with finite rate feedback," *IEEE Trans. Inf. Theory*, vol. 52, no. 11, pp. 5045–5060, Nov. 2006.

[115] Y. Dhungana and C. Tellambura, "Stochastic geometry analysis of error probability in interference limited wireless networks," in *Proc. IEEE Int. Conf. Commun. (ICC)*, London, UK, Jun. 2015, pp. 2857 – 2862.

[116] C. Tellambura, Y. Dhungana, and M. Soysa, "Uniform approximations for wireless performance in fading, noise and interference," in *Proc. IEEE Int. Conf. on Commun. (ICC)*, Ottawa, Canada, Jun. 2012, pp. 2410–2415.

[117] Y. Dhungana and C. Tellambura, "Uniform approximations for wireless performance in fading channels," *IEEE Trans. Commun.*, vol. 16, no. 11, pp. 4768–4779, Nov. 2013.

[118] P. Guan and M. D. Renzo, "Stochastic geometry analysis of the average error probability of downlink cellular networks," in *Proc. IEEE Int. Conf. Comput., Netw. Commun. (ICNC))*, Honolulu, HI, Feb. 2014, pp. 649–655.

[119] V. M. Zolotarev, *One-dimensional stable distributions*, ser. Translations of mathematical monographs. Providence, Rhode Island: American Mathematical Society, 1986.

[120] A. R. Miller and I. S. Moskowitz, "Reduction of a class of Fox-Wright Psi functions for certain rational parameters," *Computers and Mathematics with Applications*, vol. 30, no. 11, pp. 73–82, Dec. 1995.

[121] Y. Dhungana and C. Tellambura, "Outage probability of underlay cognitive relay networks with spatially random nodes," in *Proc. IEEE Global Commun. Conf. (GLOBECOM) 2014*, Austin, TX USA, Dec. 2014, pp. 3597–3602.

[122] M. Nekovee, "A survey of cognitive radio access to TV white spaces," *Int. J. Digital Multimedia Broadcasting*, vol. 2010, pp. 1–11, Apr. 2010.

[123] M. El-Hajjar and L. Hanzo, "A survey of digital television broadcast transmission techniques," *IEEE Commun. Surveys Tuts.*, vol. 15, no. 4, pp. 1924–1941, Apr. 2013.

[124] C. Zhong, T. Ratnarajah, and K.-K. Wong, "Outage analysis of decode-and-forward cognitive dual-hop systems with the interference constraint in Nakagami-m fading channels," *IEEE Trans. Veh. Technol.*, vol. 60, no. 6, pp. 2875–2879, Jul. 2011.

[125] L. Lu, G. Y. Li, and G. Wu, "Optimal power allocation for CR networks with direct and relay-aided transmissions," *IEEE Trans. Wireless Commun.*, vol. 12, no. 4, pp. 1832–1842, Apr. 2013.

[126] Y. Zou, J. Zhu, B. Zheng, and Y.-D. Yao, "An adaptive cooperation diversity scheme with best-relay selection in cognitive radio networks," *IEEE Trans. Signal Process.*, vol. 58, no. 10, pp. 5438–5445, Oct. 2010.

[127] J. Lee, H. Wang, J. G. Andrews, and D. Hong, "Outage probability of cognitive relay networks with interference constraints," *IEEE Trans. Wireless Commun.*, vol. 10, no. 2, pp. 390–395, Feb. 2011.

[128] L. Li, X. Zhou, H. Xu, G. Y. Li, D. Wang, and A. Soong, "Simplified relay selection and power allocation in cooperative cognitive radio systems," *IEEE Trans. Wireless Commun.*, vol. 10, no. 1, pp. 33–36, Jan. 2011.

[129] B. Wild and K. Ramchandran, "Detecting primary receivers for cognitive radio applications," in *Proc. IEEE Int. Symp. New Frontiers in Dynamic Spectrum Access Networks (DySPAN)*, Baltimore, USA, Nov. 2005, pp. 124–130.

[130] A. P. Hulbert, "Spectrum sharing through beacons," in *Proc. IEEE Int. Symposium on Personal, Indoor and Mobile Radio Commun. (PIMRC)*, Berlin, Sep. 2005, pp. 989–993.

[131] H. Wang, J. Lee, S. Kim, and D. Hong, "Capacity of secondary users exploiting multispectrum and multiuser diversity in spectrum-sharing environments," *IEEE Trans. Veh. Technol.*, vol. 59, no. 2, pp. 1030–1036, Feb. 2010.

[132] M. A. Chaudhry and S. M. Zubair, *On a Class of Incomplete Gamma Functions with Applications*. CRC Press, 2002.

[133] M. Abramowitz and I. A. Stegun, *Handbook of Mathematical Functions with Formulas, Graphs, and Mathematical Tables*. New York: Dover, 1972.

[134] A. M. Ibrahim, T. ElBatt, and A. El-Keyi, "Coverage probability analysis for wireless networks using repulsive point processes," in *Proc. IEEE Int. Symposium on Personal, Indoor, and Mobile Radio Commun. (PIMRC)*, London, Sep. 2013, pp. 1002–1007.

[135] F. Lagum, S. Szyszkowicz, and H. Yanikomeroglu, "CoV-based metrics to quantify the regularity of hard-core point processes for modeling the locations of base stations," *IEEE Wireless Commun. Lett.*, Mar. 2016.

[136] Y. J. Chun, M. O. Hasna, and A. Ghrayeb, "Modeling and analysis of HetNet interference using poisson cluster processes," in *Proc. IEEE Int. Symposium on Personal, Indoor, and Mobile Radio Commun. (PIMRC)*, Washington DC, Sep. 2014, pp. 681–686.

[137] M. Mirahsan, R. Schoenen, and H. Yanikomeroglu, "HetHetNets: Heterogeneous traffic distributionin heterogeneous wireless cellular networks," *IEEE J. Sel. Areas Commun.*, vol. 33, no. 10, pp. 2252–2265, Oct. 2015.

[138] A. Nasri, R. Schober, and Y. Ma, "Unified asymptotic analysis of linearly modulated signals in fading, non-Gaussian noise, and interference," *IEEE Trans. Commun.*, vol. 56, no. 6, pp. 980 –990, Jun. 2008.

[139] Y. Dhungana and C. Tellambura, "New simple approximations for error probability and outage in fading," *IEEE Commun. Lett.*, vol. 16, no. 11, pp. 1760–1763, 2012.

[140] ——, "Rational Gauss-Chebyshev quadratures for wireless performance analysis," *IEEE Wireless Commun. Lett.*, vol. 2, no. 2, pp. 215–218, May 2013.

[141] G. K. Karagiannidis, "Moments-based approach to the performance analysis of equal gain diversity in Nakagami-m fading," *IEEE Trans. Commun.*, vol. 52, no. 5, pp. 685–690, 2004.

[142] P. Flajolet, X. Gourdon, and P. Dumas, "Mellin transforms and asymptotics: Harmonic sums," *Theoretical Comput. Sci.*, vol. 144, no. 1-2, pp. 3–58, 1995.

[143] N. Cressie and M. Borkent, "The moment generating function has its moments," *J. Statistical Planning and Inference*, vol. 13, no. 3, pp. 337–344, 1986.

[144] I. Gradshteyn and I. Ryzhik, *Table of Integrals, Series and Products*, 7th ed. San Diego, California: Academic Press, 2007.

[145] J. H. McCabe, "A formal extension of the padé table to include two point padé quotients," *IMA Journal of Applied Mathematics*, vol. 15, no. 3, pp. 363–372, 1975. [Online]. Available: http://imamat.oxfordjournals.org/content/15/3/363.abstract

[146] A. Shah and A. Haimovich, "Performance analysis of maximal ratio combining and comparison with optimum combining for mobile radio communications with cochannel interference," *IEEE Trans. Veh. Technol.*, vol. 49, no. 4, pp. 1454 –1463, Jul. 2000.

Appendix A

Proofs for Chapter 3

A.1 Proof of Lemma 4

We have

$$t_l = \begin{cases} 1 & \text{if } N_l' + 1 \leq L_{\kappa(l)} \\ \frac{L_{\kappa(l)}}{(N_l'+1)} & \text{otherwise.} \end{cases} \tag{A.1}$$

Thus, $T_l = \mathbb{E}\left[t_l\right]$ can be derived as

$$\begin{aligned} T_l &= \sum_{n=0}^{L_{\kappa(l)}-1} \mathbb{P}(N_l' = n) + \sum_{n=L_{\kappa(l)}}^{\infty} \frac{L_{\kappa(l)}}{n+1}\mathbb{P}(N_l' = n) \\ &= \sum_{n=1}^{\infty} \frac{L_{\kappa(l)}}{n}\mathbb{P}(N_l' = n-1) - \sum_{n=1}^{L_{\kappa(l)}} \left(\frac{L_{\kappa(l)}}{n} - 1\right)\mathbb{P}(N_l' = n-1). \end{aligned} \tag{A.2}$$

We know, the probability that a typical user belongs to a given cell is directly proportional to the area of the cell. Thus, the conditional PDF of the area of a Voronoi cell given that a typical user belongs to it is given by $f_{A'}(a) = caf_A(a)$, where $f_A(a)$ is the unconditional PDF, and c is a constant such that $\int_0^\infty f_{A'}(a)da = 1$. The PMF of N_l' can then be similarly derived as in Lemma 2 as

$$\mathbb{P}(N_l' = n) = \frac{3.5^{3.5}\Gamma(4.5+n)(U_l\lambda_u/\lambda_{\zeta(l)})^n}{\Gamma(3.5)n!(U_l\lambda_u/\lambda_{\zeta(l)} + 3.5)^{n+4.5}},\ n \geq 0,\ \forall l \in \{m, o, e\}, \tag{A.3}$$

where $\lambda_{\zeta(m)} = \lambda_m$ and $\lambda_{\zeta(o)} = \lambda_{\zeta(e)} = \lambda_p$. The final expression for t_l in (3.13) is obtained by substituting the PMF of N_l' in (A.2), where the first term is further simplified by using $\mathbb{P}(N_l' = n-1)/n = \lambda_{\zeta(l)}/(U_l\lambda_u)\mathbb{P}(N_l = n)$, followed by $\sum_{n=0}^{\infty}\mathbb{P}(N_l = n) = 1$.

A.2 Proof of Lemma 5

The average link spectral efficiency C_l of the user u when $u \in \mathbf{\Phi}_u^l$ can be expressed as

$$\begin{aligned} C_l &= \frac{1}{\ln 2}\int_0^\infty \ln(1+t) f_l(t) dt \\ &= -\frac{1}{\ln 2}\int_0^\infty \ln(1+t) d\bar{F}_l(t), \end{aligned}$$

where $f_l(t)$ is the conditional PDF of the SINR of the user u, given that $u \in \mathbf{\Phi}_u^l$. The second equality is obtained by expressing $f_l(t)$ in terms of CCDF $\bar{F}_l(t) = \mathbb{P}(\text{SINR}_l > t)$ as $f_l(t) = -\frac{d\bar{F}_l(t)}{dt}$. Equation (3.14) is then obtained by using integration by parts.

By using the SINR expression (3.8), the SINR distribution of the typical user u conditioned on $u \in \mathbf{\Phi}_u^m$ can be derived as follows:

$$\bar{F}_m(t) = \mathbb{P}\left(\frac{P_m h_{b_m} D_m^{-\alpha_m}}{I_{b_m,m} + I_{b_m,o} + \sigma^2} > t\right), \tag{A.4}$$

where $I_{b_m,m} = P_m \sum_{x_m \in \mathbf{\Psi}_m \setminus b_m} h_{x_m} ||x_m||^{-\alpha_m}$ and $I_{b_m,o} = P_p \sum_{x_o \in \mathbf{\Psi}_o} h_{x_o} ||x_o||^{-\alpha_p}$. By utilizing the fact that $h_{b_m} \sim \text{Exp}(1)$ and the independence between $I_{b_m,m}$ and $I_{b_m,o}$, $\bar{F}_m(t)$ can be further expressed as

$$\bar{F}_m(t) = \int_0^\infty \exp\left(-\frac{t\sigma^2}{P_m} r^{\alpha_m}\right) \mathcal{L}_{I_{b_m,m}}\left(\frac{t}{P_m} r^{\alpha_m}\right) \mathcal{L}_{I_{b_m,o}}\left(\frac{t}{P_m} r^{\alpha_m}\right) f_{D_m}(r) dr, \tag{A.5}$$

where $\mathcal{L}_{I_{b_m,m}}(\cdot)$ and $\mathcal{L}_{I_{b_m,o}}(\cdot)$ are the Laplace transforms of $I_{b_m,m}$ and $I_{b_m,o}$, respectively, and $f_{D_m}(r)$ is the PDF of the distance D_m between the user u and the serving BS b_m. The cumulative distribution function (CDF) of D_m, $F_{D_m}(r) = \mathbb{P}(D_m \le r)$ can be expressed as

$$\begin{aligned} F_{D_m}(r) =& \mathbb{P}(R_m \le r | u \in \mathbf{\Phi}_u^m) = \frac{\mathbb{P}(R_m \le r, u \in \mathbf{\Phi}_u^m)}{\mathbb{P}(u \in \mathbf{\Phi}_u^m)} \\ =& \frac{1}{U_m}\int_0^r \mathbb{P}\left(R_p \ge \left(BP_p/P_m\right)^{1/\alpha_p} R_m^{\alpha_m/\alpha_p} | R_m = y\right) f_{R_m}(y) dy. \end{aligned} \tag{A.6}$$

After using the distributions of R_p and R_m, which are derived in the proof of Lemma 1, the required PDF $f_{D_m}(r)$ can be obtained as

$$f_{D_m}(r) = \frac{dF_{D_m}(r)}{dr} = \frac{2\pi\lambda_m}{U_m} r e^{-\pi\lambda_m r^2} \exp\Big(-\pi\lambda_p \Big(\frac{BP_p}{P_m}\Big)^{\frac{2}{\alpha_p}} r^{\frac{2\alpha_m}{\alpha_p}}\Big). \tag{A.7}$$

The Laplace transform $\mathcal{L}_{I_{b_m,l}}(s) = \mathbb{E}\left[\exp(-sI_{b_m,l})\right], \forall l \in \{m,o\}$ at $s = t/P_m r^{\alpha_m}$ can be derived as

$$\mathcal{L}_{I_{b_m,l}}\left(\frac{t}{P_m}r^{\alpha_m}\right) = \mathbb{E}_{\,\mathbf{\Psi}_l}\left[\prod_{x_l \in \mathbf{\Psi}_l \setminus b_m} \mathbb{E}_{h_{x_l}}\left[\exp\left(-t\frac{P_{\zeta(l)}}{P_m}r^{\alpha_m}h_{x_l}||x_l||^{-\alpha_{\zeta(l)}}\right)\right]\right], \quad \forall l \in \{m,o\}, \quad \text{(A.8)}$$

where $P_{\zeta(m)} = P_m$, $P_{\zeta(o)} = P_p$, $\alpha_{\zeta(m)} = \alpha_m$, and $\alpha_{\zeta(o)} = \alpha_p$. By using the PGFL of PPP $\mathbf{\Psi}_l$ with density $p_l\lambda_{\zeta(l)}$, followed by the expectation with respect to exponential RV h_{x_l}, we have

$$\mathcal{L}_{I_{b_m,l}}\left(\frac{t}{P_m}r^{\alpha_m}\right) = \exp\left(-\int_{\eta_l}^{\infty}\left(1 - \frac{1}{1+t\frac{P_{\zeta(l)}}{P_m}r^{\alpha_m}y^{-\alpha_{\zeta(l)}}}\right)2\pi p_l\lambda_{\zeta(l)}y\,dy\right), \quad \forall l \in \{m,o\}, \quad \text{(A.9)}$$

where $\lambda_{\zeta(m)} = \lambda_m$ and $\lambda_{\zeta(o)} = \lambda_p$; η_m and η_o are the distances from the user u to the closest interferer in the macro and pico tiers, respectively, given that the user u is served by the macro BS b_m at a distance $D_m = r$. Thus, $\eta_m = r$ and $\eta_o = (BP_p/P_m)^{1/\alpha_p}r^{\alpha_m/\alpha_p}$. Now, with the change in variables $(tP_m^{-1}P_{\zeta(l)}r^{\alpha_m})^{-2/\alpha_{\zeta(l)}}y^2 = u$ and further simplification, we get

$$\mathcal{L}_{I_{b_m,l}}\left(\frac{t}{P_m}r^{\alpha_m}\right) = \exp\left(-\pi p_l\lambda_{\zeta(l)}(tP_m^{-1}P_{\zeta(l)}r^{\alpha_m})^{2/\alpha_{\zeta(l)}}\int_{\nu_l}^{\infty}\frac{1}{1+u^{\alpha_{\zeta(l)}/2}}\,du\right), \quad \forall l \in \{m,o\}, \quad \text{(A.10)}$$

where $\nu_m = t^{-2/\alpha_m}$ and $\nu_p = (t/B)^{-2/\alpha_p}$. The integral in the above equation can be solved in terms of the Gauss Hypergeometric function as [17, eqn. (24)]

$$\int_{\nu_l}^{\infty}\frac{1}{1+u^{\alpha_{\zeta(l)}/2}} = \frac{2}{(\alpha_{\zeta(l)}-2)}\frac{\nu_l}{(1+\nu_l^{\alpha_{\zeta(l)}/2})}\,{}_2F_1\left[1,1,2-\frac{2}{\alpha_{\zeta(l)}},\frac{1}{1+\nu_l^{\alpha_{\zeta(l)}/2}}\right] \quad \text{(A.11)}$$

The final expression for $\bar{F}_m(t)$ in (3.15) is obtained by substituting (A.7) and (A.10) into (A.5). The conditional SINR distribution for a typical unbiased and range-expanded pico user, (3.16)-(3.17), can be similarly derived.

The simplified expressions for $\bar{F}_m(t)$, $\bar{F}_o(t)$ and $\bar{F}_e(t)$ in (3.18)-(3.20) can be obtained by substituting $\sigma^2 = 0$, $\alpha_m = \alpha_p = \alpha$ in (3.15)-(3.17), and then solving the integrals as $\int_0^{\infty} r\exp(-\beta r^2)dr = 1/(2\beta)$.

Appendix B

Proofs for Chapter 4

B.1 Proof of Lemma 6

The LT of $I_{b_p} = I_{b_p,m} + I_{b_p,p}$ is given by $\mathcal{L}_{I_{b_p}}(s) = \mathbb{E}[e^{-sI_{b_p}}] = \mathcal{L}_{I_{b_p,m}}(s)\mathcal{L}_{I_{b_p,p}}(s)$, where the LT $\mathcal{L}_{I_{b_p,q}}(s) = \mathbb{E}\left[e^{-sI_{b_p,q}}\right], \forall q \in \{m,p\}$ can be derived as

$$\mathcal{L}_{I_{b_p,q}}(s) = \mathbb{E}_{\hat{\mathbf{\Psi}}_q} \prod_{x_l \in \hat{\mathbf{\Psi}}_q} \mathbb{E}_{\zeta_{x_q}}\Big[\exp(-sP_q\zeta_{x_q}||x_q||^{-\alpha})\Big], \tag{B.1}$$

where $\hat{\mathbf{\Psi}}_p = \mathbf{\Psi}_p \backslash b_p$, $\hat{\mathbf{\Psi}}_m = \mathbf{\Psi}_m \backslash v_m$ if $u \in \chi$, else $\hat{\mathbf{\Psi}}_m = \mathbf{\Psi}_m$. Given M_q, $\zeta_{x_q} \sim$ Gamma$(M_q, 1)$. By performing the expectation over this conditional distribution, followed by the PGFL of PPP with density $p_q\lambda_q$, and finally the expectation over the PMF of M_q, we have

$$\mathcal{L}_{I_{b_p,q}}(s) = \exp\left\{-\pi p_q \lambda_q \varpi_{p,q}^2 \left(\sum_{i=1}^{L_{\max}^q} {}_2F_1\Big[i, -\frac{2}{\alpha}, \frac{\alpha-2}{\alpha}, -\frac{P_q}{\varpi_{p,q}^{\alpha}} s\Big] \mathbb{P}(M_q = i) - 1 \right) \right\}, \tag{B.2}$$

where $\varpi_{p,q}$ is the lower bound on the distance to the closest interferer from u in the tier $q \in \{m,p\}$. Thus, $\varpi_{p,p} = r$, and $\varpi_{p,m} = r_1$ if $u \in \chi$; otherwise, $\varpi_{p,m} = \rho r$. By using the law of total expectation, $\mathcal{L}_{I_{b_p,m}}(s) = \varphi \mathcal{L}_{I_{b_p,m}}(s|u \in \chi) + (1 - \varphi)\mathcal{L}_{I_{b_p,m}}(s|u \notin \chi)$.

B.2 Proof of Theorem 2

By substituting (4.24) into (4.30), followed by $\Delta_p = K_p - M_p'$, and then averaging over the joint PDF $f_{D_p,V_m}(r, r_1)$ of D_p and V_m expressed as $f_{V_m|D_p}(r_1) f_{D_p}(r)$, we

get

$$\mathrm{P}_p(\gamma|M'_p=k)=\varphi\mathrm{T}_1(\gamma|M'_p=k)+(1-\varphi)\mathrm{T}_2(\gamma|M'_p=k), \tag{B.3}$$

where

$$\mathrm{T}_1(\gamma|M'_p=k)=\int_{r=0}^{\infty}\int_{r_1=\rho r}^{\infty}\sum_{l=0}^{K_p-k-1}\frac{(-s)^l}{l!}\frac{\mathrm{d}^l}{\mathrm{d}s^l}\left(\mathcal{L}^1_{I_{b_p,m}}(s)\mathcal{L}_{I_{b_p,p}}(s)\right)\Big|_{s=\frac{\gamma r^\alpha}{P_p}} \times f_{V_m|D_p}(r_1|r)f_{D_p}(r)\,dr_1\,dr, \tag{B.4}$$

and $\mathrm{T}_2(\gamma|M'_p=k)$ is given by a similar expression with $\mathcal{L}^1_{I_{b_p,m}}(s)$ replaced by $\mathcal{L}^2_{I_{b_p,m}}(s)$. However, since the LT in $\mathrm{T}_2(\gamma|M'_p=k)$ is not a function of r_1, averaging over the PDF of D_p only is required. We thus derive $\mathrm{T}_1(\gamma)$ first, as $\mathrm{T}_2(\gamma)$ then follows immediately. Let $y(s)=e^{-\pi s}$, and $t(s)=p_m\lambda_m r_1^2\,\Xi_0^m\left(1,1,\frac{P_m}{r_1^\alpha}s\right)+p_p\lambda_p r^2\,\Xi_0^p\left(1,1,\frac{P_p}{r^\alpha}s\right)$. The LT in (B.4) can be expressed as $\mathcal{L}^1_{I_{b_p,m}}(s)\mathcal{L}_{I_{b_p,p}}(s)=e^{\pi\left(p_m\lambda_m r_1^2+p_p\lambda_p r^2\right)}y(t(s))$, the lth derivative of which can be evaluated by applying Faà di Bruno's formula (4.31). By using $y^{(\omega_o^l)}_{t(s)}(t(s))=(-\pi)^{\omega_o^l}\exp(-\pi t(s))$;

$$\frac{\mathrm{d}^q}{ds^q}\Xi_0^l\left(1,1,\frac{P_l}{\varpi_l^\alpha}s\right)=\left(-\frac{P_l}{\varpi_l^\alpha}\right)^q\Xi_q^l\left(1,1,\frac{P_l}{\varpi_l^\alpha}s\right), \tag{B.5}$$

which follows from the property of the Gauss Hypergeometric function; and the properties of integer partition $\sum_{q=1}^l q\mu_{oq}^l=l$ and $\sum_{q=1}^l\mu_{oq}^l=\omega_o^l$, we have

$$\begin{aligned}
&\frac{\mathrm{d}^l}{\mathrm{d}s^l}\left(\mathcal{L}^1_{I_{b_p,m}}(s)\mathcal{L}_{I_{b_p,p}}(s)\right)\Big|_{s=\frac{\gamma r^\alpha}{P_p}}\\
&=\sum_{o=1}^{\mathcal{P}(l)}c_o^l(-\pi)^{\omega_o^l}(-P_p)^l r_1^{2\omega_o^l-\alpha l}\exp\left\{\pi r_1^2\left(p_m\lambda_m+p_p\lambda_p\left(\frac{r}{r_1}\right)^2\right)\right\}\\
&\times\exp\left\{-\pi r_1^2\left(p_m\lambda_m\,\Xi_0^m\left(\delta,\frac{r}{r_1},\gamma\right)+p_p\lambda_p\left(\frac{r}{r_1}\right)^2\Xi_0^p\left(1,1,\gamma\right)\right)\right\}\\
&\times\prod_{q=1}^{l}\left(p_m\lambda_m\delta^q\Xi_q^m\left(\delta,\frac{r}{r_1},\gamma\right)+p_p\lambda_p\left(\frac{r}{r_1}\right)^{-\alpha q+2}\Xi_q^p\left(1,1,\gamma\right)\right)^{\mu_{oq}^l}.
\end{aligned} \tag{B.6}$$

The final expression for $\mathrm{T}_1(\gamma)$ in (4.33) is obtained by changing the order of integration, followed by substituting $\frac{r}{r_1}\to\theta$, $r_1\to r_1$, then integrating with respect to r_1, and finally averaging over the PMF of M'_p.

For $\mathrm{T}_2(\gamma)$, the lth derivative is the same as (B.6) with r_1 replaced by ρr. After evaluating the derivative, we simply integrate with respect to r, followed by averaging over the PMF of M'_p to obtain the final expression for $\mathrm{T}_2(\gamma)$ in (4.34).

B.3 Proof of Theorem 6

Due to limited feedback, even when a typical pico user u belongs to χ, it receives residual interference $Y = P_m \hat{\zeta}_m V_m^{-\alpha}$ from its nearest active macro BS, where $\hat{\zeta}_m \sim \text{Exp}[1/\kappa_I]$. Thus, the LT of total macro tier interference when $u \in \chi$ is given by

$$\mathcal{L}_{\hat{I}_{b_p,m}}(s|u \in \chi) = \mathcal{L}^1_{I_{b_p,m}}(s)\mathbb{E}[e^{-sY}] = \mathcal{L}^1_{I_{b_p,m}}(s)(1 + sP_m\kappa_I r_1^{-\alpha})^{-1}, \tag{B.7}$$

where $\mathcal{L}^1_{I_{b_p,m}}(s)$ is the LT of total macro tier interference with perfect CSI, given by (4.25). The LT of total pico tier interference $\mathcal{L}_{\hat{I}_{b_p,p}}(s)$ is equal to $\mathcal{L}_{I_{b_p,p}}$ in (4.27). Since $\hat{\beta}_{b_p} \sim \text{Gamma}(K_p, \kappa_p)$,

$$\begin{aligned}
\mathrm{T}_{1,LF}(\gamma|r, r_1) &= \sum_{l=0}^{K_p-1} \frac{(-s)^l}{l!} \frac{\mathrm{d}^l}{\mathrm{d}s^l} \left(\mathcal{L}^1_{I_{b_p,m}}(s)\mathcal{L}_{I_{b_p,p}}(s)(1 + sP_m\kappa_I r_1^{-\alpha})^{-1} \right) \Big|_{s=\frac{\gamma r^\alpha}{\kappa_p P_p}} \\
&= \sum_{l=0}^{K_p-1} \frac{(-s)^l}{l!} \sum_{v=0}^{l} \binom{l}{v} \frac{\mathrm{d}^v}{\mathrm{d}s^v} \left(\mathcal{L}^1_{I_{b_p,m}}(s)\mathcal{L}_{I_{b_p,p}}(s) \right) \\
&\quad \times \frac{\mathrm{d}^{l-v}}{\mathrm{d}s^{l-v}} (1 + sP_m\kappa_I r_1^{-\alpha})^{-1} \Big|_{s=\frac{\gamma r^\alpha}{\kappa_p P_p}} ,
\end{aligned} \tag{B.8}$$

where the second equality follows from Leibnitz's theorem for differentiation of product [133, p. 12]. The vth derivative of $\mathcal{L}^1_{I_{b_p,m}}(s)\mathcal{L}_{I_{b_p,p}}(s)$ at $s = \frac{\gamma r^\alpha}{\kappa_p P_p}$ is given by (B.6) with l replaced by v and γ replaced by γ/κ_p. The $(l-v)$th derivative of $(1 + sP_m\kappa_I r_1^{-\alpha})^{-1}$ can be obtained as

$$\frac{\mathrm{d}^{l-v}}{\mathrm{d}s^{l-v}} (1 + sP_m\kappa_I r_1^{-\alpha})^{-1} \Big|_{s=\frac{\gamma r^\alpha}{\kappa_p P_p}} = \frac{(-P_m\kappa_I r_1^{-\alpha})^{l-v}(l-v)!}{(1 + \frac{\gamma P_m \kappa_I}{\kappa_p P_p}(\frac{r}{r_1})^\alpha)^{l-v+1}}. \tag{B.9}$$

After substituting the derivatives, the final expression of $\mathrm{T}_{1,LF}(\gamma)$ in (4.57) is obtained in the same way as $\mathrm{T}_1(\gamma)$ in Theorem 2 by averaging over the joint PDF of $f_{D_p,V_m}(r, r_1)$.

$\mathrm{T}_{2,LF}(\gamma)$ and $\mathrm{P}_{m,LF}(\gamma)$ can be derived in the same was as $\mathrm{T}_2(\gamma)$ and $\mathrm{P}_m(\gamma)$ for perfect CSI in Theorem 2 and 3, respectively, because the LTs of interference powers are the same as those of perfect CSI case. The only differences that should be taken care of are the probability distributions of $\hat{\beta}_{b_p}$ and $\hat{\beta}_{b_m}$. With limited feedback, $\hat{\beta}_{b_p} \sim \text{Gamma}(\Delta_p, \kappa_p)$ and $\hat{\beta}_{b_m} \sim \text{Gamma}(\Delta_m, \kappa_m)$. Since $\hat{\beta}_{b_p}$ and $\hat{\beta}_{b_m}$ can be expressed as $\hat{\beta}_{b_p} = \kappa_p \beta_{b_p}$ and $\hat{\beta}_{b_m} = \kappa_m \beta_{b_m}$, where $\beta_{b_p} \sim \text{Gamma}(\Delta_p, 1)$

and $\beta_{b_m} \sim$ Gamma$(\Delta_m, 1)$ are the corresponding channel power gains with perfect CSI, $\mathrm{T}_{2,LF}(\gamma)$ is given by (4.34) with γ replaced by γ/κ_p, and similarly $\mathrm{P}_{m,LF}(\gamma)$ by (4.37), with γ replaced by γ/κ_m.

Appendix C

Uniform Approximations for Error Probability Performance in fading, noise and interference

In this appendix[1], the concept of **uniform approximation** (UA) for average error performance analysis of wireless communications is introduced. The average performance analysis of wireless communications impaired by fading, noise and interference typically requires averaging the performance metric $h(\gamma)$ over the statistical distribution of the instantaneous SNR/SINR γ. However, the exact closed-form solution may not always be possible due to analytical intractability. Sometimes, although analytically tractable, the solution may be very complex to provide any useful insight into system performance. Thus, simple approximation which serves as an alternative to exact solution and provides important insights into critical system parameters is highly desirable. Various approximations have thus been developed in the literature [3, 138–141]. In contrast to these approximations, the beauty of the UA is its excellent accuracy over the whole range of SNR/SIR.

A very generalized result for the error probability UA of wireless transmissions over flat fading channels is developed in this appendix, which can be applied for the following typical scenarios in wireless communications.

- The additive impairment is AWGN.

[1]Contents of this appendix have been published in the IEEE Transactions on Communications [117] and also in the proceedings of the IEEE International Conference on Communications (ICC) 2012 [116].

- The additive impairment is dominated by interference.

Theoretically, the UA is valid for any transmission scheme, any modulation, and any fading channel as long as the following assumptions are valid.

AS1) The instantaneous SNR/SIR at the receiver can be expressed as $\gamma = \rho X$, where ρ is a deterministic quantity, and X is a nonnegative RV which depends on the desired and interference channel gains, and the transmission/reception techniques.

AS2) The PDF $f_X(x)$ accepts a polynomial expansion[2] $f_X(x) = \sum_{k=0}^{K-1} a(k)x^{k+t} + O\left(\beta^{K+t+1}\right)$ as $x \to 0^+$, where $a(0) > 0$, and t is the polynomial growth rate of $f_X(x)$ at 0. In [3], the authors approximated the PDF with a monomial term $f_X(x) = a(0)x^t + O(x^{t+1})$ as $x \to 0^+$ to quantify the high-SNR ($\rho \to \infty$) average error probability of wireless transmissions impaired by fading and AWGN in terms of the array gain and diversity gain as (2.14).

AS3) The conditional error probability function denoted by $h(\gamma)$ decays exponentially as $\gamma \to \infty$ and admits a polynomial expansion as $\gamma \to 0^+$. From (C.1), such decay implies that the MT $\mathcal{H}(s)$ has poles in the left half-plane only. This phenomenon shows up in common $h(\gamma)$ including $Q(\sqrt{\kappa\gamma}) = \int_{\sqrt{\kappa\gamma}}^{\infty} \frac{1}{2\pi} e^{-u^2/2} du$, which represents the error probability of various coherent digital modulation and demodulation schemes. Similarly, $h(\gamma) = pe^{-q\gamma}$ or exponential sums/integrals represent the error probability of non-coherent demodulation schemes [70, 71].

Before deriving the error probability UA, we first need to lay the necessary groundwork, which includes mainly the asymptotics of error probability as $\rho \to 0^+$ and $\rho \to \infty$. The asymptotics are derived in Proposition 1 by using the MT-based method. The basics of MT are thus introduced first in Appendix C.1, followed by Proposition 1 in Appendix C.2 and finally, our main result for error probability UA in Appendix C.3.

[2]If $g(x) = \sum_{n=0}^{\infty} a_n x^n$ as $x \to 0^+$, we write $g(x) = S_N(x) + O(x^{N+1})$ as $x \to 0^+$, where $S_N(x) = \sum_{n=0}^{N} a_n x^n$, to express that the difference $|g(x) - S_N(x)|$ is smaller than $C|x^{N+1}|$ for some constant C as $x \to 0^+$. Thus, the partial sum $S_N(x)$ is an **asymptotic** of $f(x)$ with an error term $O(x^{N+1})$ as $x \to 0^+$. Similar series of x^{-n} forms an asymptotic expansion as $x \to \infty$.

C.1 Basics of Mellin Transform

Let $g(y)$ be a function defined on the positive real axis $0 \leq y < \infty$. The MT of $g(y)$ on the complex plane is

$$\mathcal{M}[g(y); s] = \mathcal{G}(s) = \int_0^\infty y^{s-1} g(y)\, \mathrm{d}y, \tag{C.1}$$

for some complex s [142]. $\mathcal{G}(s)$ is holomorphic (a function that is complex differentiable in a neighborhood of every point in its domain) in a vertical strip called the fundamental strip. For example, for $\mathcal{M}[\exp(-y); s] = \Gamma(s)$, the fundamental strip is $0 \leq \Re(s) < \infty$. More generally, if $g(y) = O(y^{-u})$ as $y \to 0^+$ and $O(y^{-v})$ as $y \to \infty$ with $u < v$, the fundamental strip is $u \leq \Re(s) < v$.

Crucially, the MT maps the asymptotic expansions of $g(y)$ at $y = 0$ and ∞ to the poles of $\mathcal{G}(s)$. In order to understand this result, suppose $g(y)$ decays rapidly as $y \to \infty$, and $g(y) = \sum_{n=0}^{N-1} d_n y^n + O(y^N)$ as $y \to 0^+$. The MT is then given by

$$\begin{aligned}\mathcal{G}(s) &= \int_0^1 y^{s-1}\left(g(y) - \sum_{n=0}^{N-1} a_n y^n\right)\mathrm{d}y + \int_0^1 y^{s-1} \sum_{n=0}^{N-1} d_n y^n\, \mathrm{d}y + \int_1^\infty y^{s-1} g(y)\, \mathrm{d}y \\ &= \int_0^1 y^{s-1}\left(g(y) - \sum_{n=0}^{N-1} d_n y^n\right)\mathrm{d}y + \sum_{n=0}^{N-1} \frac{d_n}{s+n} + \int_1^\infty y^{s-1} g(y)\, \mathrm{d}y.\end{aligned}$$

The first integral converges in the larger half-plane $\Re(s) > -N$ and the second for all complex s. Thus, we see that $\mathcal{G}(s)$ is singularity-free for all $\Re(s) > 0$ with simple poles of residue d_n at $s = -n$ $(n = 0, \ldots, N-1)$ and no other singularities.

C.2 Error Probability Asymptotics from Mellin Transforms

The average probability of error can be expressed as

$$P_e(\rho) = \int_0^\infty h\left(\rho x\right) f_X(x)\, \mathrm{d}x, \tag{C.2}$$

where $f_X(x)$ is the PDF of X, and $h(x)$ is a conditional error expression that requires averaging over noise, fading and other effects. Generically, the asymptotic of $P_e(\rho)$ as $\rho \to \infty$ is given by $P_e(\rho) = \sum_{n \geq 0} d_n \rho^{-v_n}$ where d_n and v_n are real number sequences, with v_n positive and increasing. Similarly, as $\rho \to 0^+$,

$P_e(\rho) = \sum_{n\geq 0} d'_n \rho^{u_n}$ where d'_n and u_n are real number sequences, with u_n positive and increasing. For coherent modulations, u_n is not an integer sequence because the conditional error is a function of $\sqrt{\rho}$. In contrast, for non-coherent and differential modulations, u_n is an integer sequence. To treat all such cases in a unified way, we use the following definition.

Definition 1. The asymptotics of $P_e(\rho)$ (C.2) as $\rho \to 0^+$ and $\rho \to \infty$ can be expressed as

$$P_e(\rho) = \begin{cases} \displaystyle\sum_{l=0}^{M_1} c(l) y^l + O(y^{M_1+1}) & \text{as} \quad y \to 0^+ \\ \displaystyle\sum_{l=0}^{M_2} \frac{b(l)}{y^{\delta+l}} + O(y^{-(\delta+M_2+1)}) & \text{as} \quad y \to \infty \end{cases} \tag{C.3}$$

where $y = \rho^\tau$ for a positive real number τ such that both expansions have integer powers of y, whereas the series in terms of ρ may not necessarily have integer powers.

MT is a natural tool for the study of asymptotics. We consider the MT of a general $h(\gamma)$ expressed as a sum of either a finite or an infinite number of terms derived from a common base function. For example, with base function $Q(\sqrt{\gamma})$, we consider $h(\gamma) = \sum_{n\geq 0} \vartheta_n Q(\sqrt{\kappa_n \gamma})$, which is powerful enough to cover all coherent linear modulations, union bound on block and convolutional coded systems and others. With suitable base functions, differential and non-coherent modulation can also be treated. With this generalized $h(\gamma)$, we next show how the asymptotics of $P_e(\rho)$ as $\rho \to 0^+$ and $\rho \to \infty$ can be obtained from the left- and right-sided poles of the MT product $\mathcal{H}(s)\mathcal{F}_X(1-s)$ with respect to its fundamental strip.

Proposition 1. *Consider a generalized conditional error probability given by the sum*

$$h(\gamma) = \sum_n \vartheta_n g(\kappa_n \gamma), \tag{C.4}$$

where $g(\gamma)$ is a general base function. If $\mathcal{G}(s)$ and $\mathcal{F}_X(s)$ are the MTs of $g(\gamma)$ and the PDF $f_X(x)$, respectively, let $\Pi(s) = \mathcal{G}(s)\mathcal{F}_X(1-s)\sum_n \vartheta_n \kappa_n^{-s}$ has an increasing sequence of right-sided poles $\tilde{p}_0, \tilde{p}_1, \ldots$ and a decreasing sequence of

left-sided poles $\tilde{q}_0, \tilde{q}_1, \ldots$ with respect to the fundamental strip. All the poles are assumed to be first-order ones. Then, the asymptotics of $P_e(\rho)$ can be expressed as (C.3)*, where $\delta = \tilde{p}_0/\tau$ and the non-zero coefficients are given by*

$$\begin{Bmatrix} c\left(|\,\tilde{q}_l|\,/\tau\right) \\ b\left((\tilde{p}_l - \tilde{p}_0)/\tau\right) \end{Bmatrix} = \left\{ \begin{bmatrix} \lim\limits_{s\to\tilde{q}_l} \left[(s-\tilde{q}_l)\mathcal{G}(s)\mathcal{F}_X(1-s) \sum\limits_n \vartheta_n \kappa_n^{-s} \right] \\ \lim\limits_{s\to\tilde{p}_l} \left[(\tilde{p}_l - s)\mathcal{G}(s)\mathcal{F}_X(1-s) \sum\limits_n \vartheta_n \kappa_n^{-s} \right] \end{bmatrix} \right\}. \tag{C.5}$$

Otherwise, the coefficients are zero.

Proof. The error probability (C.2) is a type of convolution and thus can be transformed via the Parseval formula [142] as

$$P_e(\rho) = \frac{1}{2\pi\imath} \int_{c-\imath\infty}^{c+\imath\infty} \frac{1}{\rho^s} \mathcal{H}(s)\mathcal{F}_X(1-s)\, ds, \tag{C.6}$$

where the parameter c is chosen to be in the fundamental strip $\langle u, v\rangle$ where both $\mathcal{H}(s)$ and $\mathcal{F}(1-s)$ are holomorphic. For $h(\gamma)$ given in (C.4), the MT $\mathcal{H}(s) = \mathcal{G}(s)\sum \vartheta_n \kappa_n^{-s}$.

To find the asymptotic of (C.6) as $\rho \to 0^+$, we may consider a large rectangular contour to the left of the fundamental strip with sides $\Re(s) = c$ and $\Re(s) = -M$ for $-M < u$. Given that the functions $\mathcal{G}(s)$ and $\mathcal{F}_X(1-s)$ decrease faster than any negative power of $|s|$, and that the series $\sum a_k \vartheta_k^{-s}$ is of, at most, polynomial growth in the extended strip $\langle -M, u\rangle$ as $|s| \to \infty$, the integrand in (C.6) when evaluated along the top and bottom lines of the rectangle has a negligible contribution. In contrast, the integral along the vertical line $\Re(s) = -M$ is bounded by $O(\rho^M)$ [142]. By applying the residue theorem,

$$P_e(\rho) = \sum_{s\in H_M} \text{Res}\left\{ \frac{1}{\rho^s} \mathcal{G}(s)\mathcal{F}_X(1-s) \sum \vartheta_n \kappa_n^{-s} \right\} + O(\rho^M),$$

where H_M is the set of poles enclosed by the rectangular contour, and M is as large as we want it to be.

One can similarly consider a large rectangular contour to the right of the fundamental strip with sides $\Re(s) = c$ and $\Re(s) = M$ for $M > v$ to get the asymptotic expansion as $\rho \to \infty$. However, there is an additional negative sign due to the contour being clockwise. By assuming first-order poles, we get the (C.5) and this completes the proof. □

Remarks:

1. Since $\mathcal{H}(s) = \mathcal{G}(s)\sum \vartheta_n \kappa_n^{-s}$, and the term $\sum \vartheta_n \kappa_n^{-s}$ does not have any poles, the poles of $\mathcal{H}(s)$ are simply those of the base function. For example, consider an error bound for a digital modulation given by $h(\gamma) = \sum \vartheta_n Q(\sqrt{\kappa_n \gamma})$, where ϑ_n and κ_n represent the number of the nearest neighbors and their distances. The poles of $\mathcal{H}(s)$ are then from the MT of $Q(\sqrt{x})$ and are not dependent on the ϑ_n and κ_n values. The poles are thus contributed by $\mathcal{G}(s)$ and $\mathcal{F}_X(1-s)$. These in general yield left-sided and right-sided poles, respectively, which in turn determine the asymptotics.

2. The first right-sided pole $\tilde{p}_0$ makes the dominant contribution to error probability performance as $\rho \to \infty$. The high-SNR average error probability (2.14) analyzed in [3] for fading channels further impaired by AWGN can thus be expressed in terms of MT as

$$\begin{aligned} G_d &= \tilde{p}_0, \\ G_c &= \lim_{s \to \tilde{p}_0} \left[(\tilde{p}_0 - s) G(s) F(1-s) \sum_n \vartheta_n \kappa_n^{-s} \right]^{-1/\tilde{p}_o}. \end{aligned} \tag{C.7}$$

   G_c and G_d are the array gain and diversity gain, respectively. As per AS3, $\mathcal{H}(s)$ contributes left-sided poles only. The diversity order is thus given by the first right-sided pole of $\mathcal{F}_X(1-s)$. Note that the monomial $f_X(x) \approx a(0)x^t$ corresponds to $\mathcal{F}_X(1-s)$ having a pole at $s = 1+t$. Thus, while [3] is derived from $f_X(x)$, our result is based on $\mathcal{F}_X(s)$.

To sum up, Proposition 2 states that the positive poles of $\mathcal{F}_X(1-s)$ describe the asymptotic of $P_e(\rho)$ as $\rho \to \infty$ whereas the negative poles of $\mathcal{F}_X(1-s)$ and $\mathcal{H}(s)$ together describe the asympotic $\rho \to 0^+$. The first positive pole of $\mathcal{F}_X(1-s)$ gives the diversity order. These asymptotics form the basis for the error probability UA, which will be developed subsequently. Specifically, only $b(0)$ and δ from the series corresponding to $\rho \to \infty$ and $c(l)$, $l = 0, 1, 2, \ldots, M_1$ from $\rho \to 0^+$ series are needed. Since $b(0)$ corresponds to the first right-sided pole $\tilde{p}_0$, we have

$$b(0) = a(0)\, H(\tilde{p}_0), \tag{C.8}$$

where $a(0) = \lim_{s\to\tilde{p}_0}[(\tilde{p}_0 - s)F(1-s)]$ is the residue of $\mathcal{F}_X(1-s)$ at $s = \tilde{p}_0$, which is also the coefficient of the monomial approximation to $f_X(x) = a(0)x^t$ considered in [3]. As per this monomial, $\tilde{p}_0 = t + 1$. As $b(0)$ and δ are closely related to $a(0)$ and t, either set of parameters may be used to develop the error probability UA.

If $\mathcal{F}_X(1-s)$ has positive poles only (this condition is satisfied for most of the popular fading models and diversity-combining systems in the absence of interference), it can be shown that the coefficients $c(l), l = 0, 1, 2, \ldots$ given by the first equality in (C.5) depend directly on the moments of X. This point will be verified by an example in the following section.

Although we focus on the use of MT to obtain these coefficients, they can also developed via the PDF or the moment generating function (MGF) of X. We briefly comment on these alternative approaches below.

1. **PDF**: $a(0)$ and t are given by the monomial expansion of $f_X(x)$ near 0. Similarly, by using the PDF $f(\beta)$, the moments $\mu_n = \int_0^\infty \beta^n f(\beta)d\beta$ can be easily obtained.

2. **MGF**: If MGF is readily available, it is fairly simple to extract $a(0)$ and t by the monomial expansion of $M_X(s)$ near $s = \infty$ [3]. Fortunately, the fractional moments are also simple to compute from the MGF [143]. Consider an N_r-branch MRC system in i.i.d. Rayleigh fading as an example. The MGF of X is $M_X(s) = (1+s)^{-N_r}$, which can be expanded for $s \to \infty$ as $M_X(s) = s^{-N_r} + O\big(s^{-(N_r+1)}\big)$, and hence, $a(0)$ and t are obtained to be $1/\Gamma(N_r)$ and $N_r - 1$, respectively [3].

   The fractional moments of X, $\mu_{l/2}$, $l = 1, 3, 5, \ldots$ can be computed by using [143] as

$$\mu_{l/2} = \mathbb{E}[X^{l/2}] = \Gamma(\lambda)^{-1}\int_0^\infty t^{\lambda-1}\zeta(-t)dt,$$

   where λ is chosen to be $1/2$ such that $n = l/2 + \lambda$ is a positive integer while satisfying $0 < \lambda < 1$; $\zeta(s) = \frac{d^n M_\beta(s)}{ds^n}$.

By using the above equation, $\mu_{l/2}$ can be obtained as

$$\mu_{l/2} = \frac{\Gamma(N_r+n)}{\Gamma(1/2)\Gamma(N_r)} \int_0^\infty y^{-1/2}(1+y)^{-(N_r+n)}\mathrm{d}y = \frac{\Gamma(N_r+l/2)}{\Gamma(N_r)},$$

where the last equality is obtained by using [144, eq. (3.191.3)].

C.3 Uniform Approximation

An error probability UA is a rational function that matches the asymptotics of $P_e(\rho)$ as $\rho \to 0^+$ and $\rho \to \infty$, simultaneously [145]. That is, if the UA is expanded into two series of ρ^{-n} and ρ^k, then those expansions will match the appropriate terms of (C.3).

Definition 2. A rational function $r(y)$ is given by

$$r(y) = \frac{p_0 + p_1 y + p_2 y^2 + \ldots + p_L y^L}{q_0 + q_1 y + q_2 y^2 + \ldots + q_K y^K}, \tag{C.9}$$

where L and K are are the degrees of the numerator and the denominator, respectively. To fit this rational function into $P_e(\rho)$ (C.2), the coefficients $p_0, p_1, \ldots p_L$ and $q_1, q_2, \ldots, q_K$ are determined from the asymptotics in (C.3). The values of L and K depend on the number of the low- and high-SNR terms used to construct $r(x)$. If $L < K$, the rational function is called proper, which is the case in our applications.

Proposition 2. *The UA for the error probability* $P_e(\rho)$ (C.2) *is given by*

$$P_e(\rho) = r(y) + \epsilon(y), \tag{C.10}$$

where $r(y)$ *is a rational function defined in* (C.9)*,* $y = \rho^\tau$*,* $K = L + \delta$*,* $L \geq 2$ *is an integer,* $p_0 = 1$ *and* $q_0 = 1/c(0)$*. The denominator coefficient vector* $\mathbf{q} = (q_1, q_2, \ldots, q_K)^T$ *is given by*

$$\mathbf{q} = -1/c(0)\mathbf{W}^{-1}\begin{pmatrix}\tilde{c}(1) & \tilde{c}(2) & \ldots & \tilde{c}(K-1) & \tilde{c}(K)\end{pmatrix}^T, \tag{C.11}$$

where $\tilde{c}(l) = c(l+L-2)$ *and* $\mathbf{W} = \{w_{ij}\}$*,* $i = 1, \ldots, K$*,* $j = 1, \ldots, K$ *with*

$$w_{ij} = \begin{cases} \tilde{c}(i-j) - b(0) & i = 1, 2; j = i + K - 2 \\ \tilde{c}(i-j) & \textit{otherwise.} \end{cases} \tag{C.12}$$

The numerator coefficient vector $\mathbf{p} = (p_1, p_2, \ldots, p_L)^T$ *is given by*

$$p_i = \begin{cases} c(i)/c(0) + \sum_{k=1}^{i} q_k c(i-k) & i = 1, \ldots L-2 \\ b(0)\, q_{K-j} & j = 0, 1; i = L-j. \end{cases} \tag{C.13}$$

The error term $\epsilon(y)$ *of* (C.10) *is* $O\left(y^{K+L-1}\right)$ *as* $y \to 0^+$ *and* $O\left(x^{-(\delta+1)}\right)$ *as* $x \to \infty$.

Proof. To construct UA, we require the rational function $r(y)$ in (C.9) to satisfy both the asymptotics in (C.3) simultaneously. Let us use only the first term of the asymptotic corresponding to $y \to \infty$. As $y \to \infty$, we find that

$$\frac{p_{L-1}y^{L-1} + p_L y^L}{q_{K-1}y^{K-1} + q_K y^K} = \frac{b(0)}{y^{K-L}}$$

if $p_{L-1} = b(0)\, q_{K-1}$ and $p_L = b(0)\, q_K$, where $K - L = \delta$. These conditions thus determine the values of p_i for $i = L-1, L$ as expressed in (C.13). To satisfy the asymptotic corresponding to $y \to 0^+$, we must have

$$\left(\sum_{l=0}^{\infty} c(l) y^l\right)\left(q_0 + \sum_{k=1}^{K} q_k y^k\right) = p_0 + \sum_{l=1}^{L} p_l y^l. \tag{C.14}$$

By comparing the coefficients of y^l on both sides of (C.14) for $l = L-1, L, \ldots, K+L-2$, we get

$$c(L-2+i)q_0 + \sum_{j=1}^{K} c(L-2+i-j)\, q_j = \begin{cases} p_{L-2+i} & i = 1, 2 \\ 0 & i = 3, \ldots K. \end{cases} \tag{C.15}$$

It follows from (C.14) that $c(0)q_0 = p_0$. Thus, if we set $p_0 = 1$, we get $q_0 = 1/c(0)$. After substituting for q_0, p_{L-1} and p_L, (C.15) can be given in matrix form (C.11). The solution of (C.11) completely determines the denominator of $r(y)$. Again, by the comparing the coefficients of y^i on both sides of (C.14) for $i = 1, 2, \ldots, L-2$, we get the values of p_i for $i = 1, 2, \ldots L-2$ as expressed in (C.13). □

Proposition 2 is a general result for average error probability, applicable to a variety of modulation schemes, fading channels and interference scenarios. The basic inputs required are τ, several coefficients $(c(l),\ l = 0, 1, 2, \ldots)$ of the $\rho \to 0^+$ series and the first coefficient $b(0)$ and δ of the $\rho \to \infty$ series.

We next demonstrate the UA approach to average error probability analysis of an N_r branch MRC diversity system in i.i.d. Rayleigh fading. We consider the scenario where the received signal is impaired mainly by AWGN, as well as the scenario with interference dominating the impairment, rather than noise.

C.3.1 Error Performance of N_r branch MRC in i.i.d. Rayleigh fading

Case 1: *Received signal impaired by noise*

For N_r branch MRC system, when no interference is present, and the performance is impaired mainly by AWGN, the receive SNR can be expressed as $\gamma = \rho X$, where ρ is the average receive SNR and X is a channel dependent RV, whose PDF is

$$f_X(x) = \frac{x^{N_r-1}e^{-X}}{(N_r-1)!}. \tag{C.16}$$

Its MT is $\mathcal{F}_X(s) = \frac{\Gamma(N_r+s-1)}{(N_r-1)!}$.Thus, $\mathcal{F}_X(1-s)$ has simple right-sided poles at $s = N_r, N_r+1, \ldots$. As per Proposition 1, these poles describe the high-SNR $P_e(\rho)$. Since the first pole is at $s = N_r$, the diversity order is N_r. For coherent modulations with generic $h(x) = Q\left(\sqrt{\kappa x}\right)$, $H(s)$ has simple poles at $s = 0, -1/2, -3/2, \ldots$. These poles describe the low-SNR expansion of $P_e(\rho)$. The non-integer poles of $H(s)$ indicate that the low-SNR expansion involves $\sqrt{\rho}$. We thus substitute $y = \sqrt{\rho}$ with $\tau = 1/2$. Then, $\delta = 2\tilde{p}_0$, and the necessary coefficients computed according to proposition 1 are as follows:

$$\begin{aligned} b(0) &= a\frac{2^{\tilde{p}_0-1}\Gamma(\tilde{p}_0+1/2)}{\tilde{p}_0\sqrt{\pi}\kappa^{\tilde{p}_0}} \\ c(l) &= \begin{cases} \frac{1}{2} & l = 0 \\ \dfrac{(-1)^{(l+1)/2}(\kappa/2)^{l/2}F(l/2+1)}{\sqrt{\pi}\,l\,\Gamma\left[(l+1)/2\right]} & l = 1, 3, \ldots \\ 0 & \text{otherwise.} \end{cases} \end{aligned} \tag{C.17}$$

where $\tilde{p}_0 = N_r$, $a = 1/\Gamma(N_r)$, and the moments $\mu_n = \mathcal{F}(n+1) = \Gamma(N_r + n)/\Gamma(N_r)$. For single branch ($N_r = 1$) case, the following simple UA can be obtained for coherent BPSK:

$$P_e(\rho) = \frac{1 + y + 0.5\,y^2}{2 + 4\,y + 5\,y^2 + 4\,y^3 + 2\,y^4} + \epsilon(y), \tag{C.18}$$

where $y = \sqrt{\rho}$. Note that the UA (C.18) matches the first three low-SNR terms and the first high-SNR term. Similar UAs for any other N_r can be readily derived. To test their accuracy, the UAs for the BER of BPSK modulation when $N_r = 1, 2, 4$ are plotted along with the exact result [71, Sec. 14.4], and the conventional high-SNR result [3] in Figure C.1. Notice that the UA coincides with the exact BER for the entire range $-10 \leq \rho < 30$ dB, while the high-SNR result diverges from the exact as the SNR decreases. Clearly, the UA provides an excellent approximation over the whole range of the SNR.

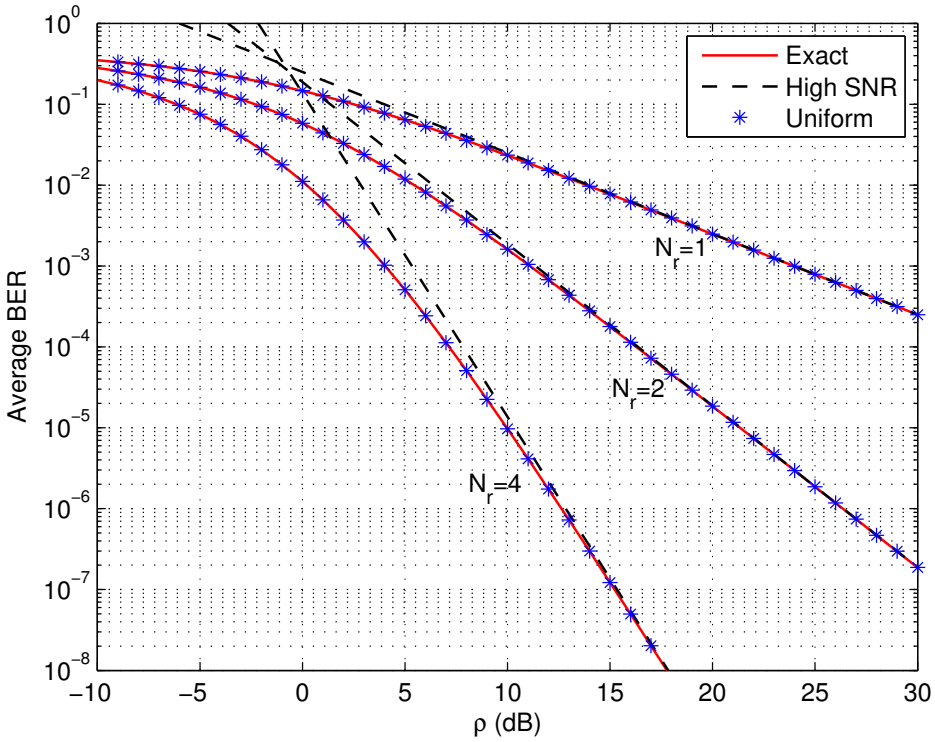

Figure C.1: The exact BER of MRC system, the high-SNR approximation [3] and the UA (C.10). In the UA, $L = 2$.

Case 2: *Received signal impaired by interference*

Let us consider an N_r branch MRC system in the presence of N_I co-channel interferers, with interference dominating the noise. The SIR in this case is given by

$$\gamma = \frac{\Omega_0 X_0}{\sum_{l=0}^{N_I} \Omega_l X_l} \tag{C.19}$$

where X_0 and $X_l, l = 1, 2, \ldots, N_I$ are the channel gains of the desired and N_I

interference links, respectively, with the corresponding average received powers Ω_0 and $\Omega_l, l = 1, 2, \ldots, N_I$. For the sake of demonstration purpose, we assume that all interferers have identical powers i.e. $\Omega_l = \Omega_I, (l = 1, 2, \ldots, N_I)$. Then, γ can then be expressed as $\gamma = \rho X$, where $\rho = \Omega_0/\Omega_I$ and $\beta = X_0/Z$, $Z = \sum_{l=1}^{N_I} X_l$. The MT of $f_X(x)$ is then given by

$$\mathcal{F}_X(s) = \mathcal{F}_{X_0}(s)\mathcal{F}_Z(2-s).$$

In Rayleigh fading, X_0 and Z are central chi square RVs with $2N_r$ and $2N_I$ degrees of freedom, respectively [146], and their MTs are $\mathcal{F}_{X_0}(s) = \Gamma(s+N_r-1)/\Gamma(N_r)$ and $\mathcal{F}_Z(s) = \Gamma(s+N_I-1)/\Gamma(N_I)$. Thus, we have

$$F_X(s) = \frac{\Gamma(s+N_r-1)\Gamma(1+N_I-s)}{\Gamma(N_r)\Gamma(N_I)}.$$

$\mathcal{F}_X(1-s)$ has positive poles at $s = N_r, N_r+1, \ldots$ and negative poles at $s = -N_I, -(N_I+1), \ldots$. Note that $\mathcal{F}_X(1-s)$ in this case has both positive and negative poles, whereas in the former cases, $\mathcal{F}_X(1-s)$ has only positive poles. As the first positive pole is at $s = N_r$, the diversity order is N_r. The negative poles of $\mathcal{F}_X(1-s)$ together with those of $\mathcal{H}(s)$ thus describe the asymptotic of $P_e(\rho)$ as $\rho \to \infty$. The asymptotic $\rho \to 0^+$ includes powers of $\sqrt{\rho}$ and thus requires that $\tau = 1/2$. Accordingly, from (C.5), we obtain the following coefficients:

$$b(0) = \frac{2^{Nr-1}\Gamma(N_I+N_r)\Gamma(N_r+1/2)}{\sqrt{\pi}N_r\kappa^{N_r}\Gamma(N_r)\Gamma(N_I)}$$

$$c(l) = \begin{cases} \frac{1}{2} & l = 0 \\ \dfrac{(-1)^{(l+1)/2}(\kappa/2)^{l/2}\Gamma(l/2+N_r)\Gamma(N_I-l/2)}{\sqrt{\pi}\,l\,\Gamma\left[(l+1)/2\right]\Gamma(N_r)\Gamma(N_I)} & l = 1, 3, \ldots \\ \dfrac{(-1)^{(l+2-2N_I)/2}(\kappa/2)^{l/2}\Gamma(l/2+N_r)\Gamma((1-l)/2)}{\sqrt{\pi}\,l\,\Gamma\left[(l+2-2N_I)/2\right]\Gamma(N_r)\Gamma(N_I)} & l = 2N_I, 2(N_I+1), \ldots \\ 0 & \text{otherwise.} \end{cases} \tag{C.20}$$

The UA for the average error rate $P_e(\rho)$ can now be readily computed by using Proposition 2. Note that the spatial distribution of the interfering nodes are not considered in this example. In Chapter 5, we derived error probability UA in the presence of interference, where the interfering nodes are spatially distributed according to a PPP.